CONTENTS

Page

INTENTIONALLY LEFT BLANK

TABLES

Page

TABLES (Continued)

Page

FIGURES

Page

FIGURES (Continued)

Page

FIGURES (Continued)

Page

INTENTIONALLY LEFT BLANK

2.3.6 Waste Package and Drip Shield Corrosion

[NUREG-1804, Section 2.2.1.2.2.3: AC 3, AC 4, AC 5; Section 2.2.1.3.1.3: AC 1(1) to (5), (7), AC 2, AC 3, AC 4, AC 5; Section 2.2.1.3.2.3: AC 1(1) to (5), AC 2; Section 2.2.1.3.3.3: AC 1(3), (6), (10), AC 2(5)]

This section addresses the requirements of proposed 10 CFR 63.114(a)(1) to (a)(7) and (b), regarding the abstraction of degradation of the Engineered Barrier System (EBS) in the total system performance assessment (TSPA). Section 2.3.6 also describes the models and analyses used to evaluate the performance of the waste package and the drip shield after closure. Specific acceptance criteria of NUREG-1804, Section 2.2.1.3.1.3, are addressed, as described below. Several potential failure mechanisms (e.g., hydrogen-induced cracking, localized corrosion due to dust deliquescence, and creep deformation) have been screened from further consideration and are listed in Section 2.2, Table 2.2-5. Mechanical degradation of the EBS due to seismic effects and rockfall is described in Section 2.3.4.

With regard to waste package and drip shield corrosion, this section presents:

- Data from the site and surrounding region pertinent to environmental conditions, laboratory testing, and the literature; uncertainties and variabilities in parameter values that have been used in the analyses; and alternative conceptual models that have been considered for use in the analyses
- Specific features, events, and processes (FEPs) that have been included in the analyses with technical bases for inclusion
- Specific degradation, deterioration, and alteration processes of the EBS that have been included in the analyses, and how they are affected by the in-drift environment
- Technical bases that have been provided for models used in the performance assessment
- Technical bases of several FEPs of interest that have been excluded from the performance assessment (note that FEPs that have been excluded are listed in Section 2.2, Table 2.2-5). Where a FEP has been included in the performance assessment for waste package degradation but the corresponding FEP for drip shield degradation has been excluded, the drip shield degradation process is presented herein for completeness.

The categories of information contained in this section, and the corresponding regulatory requirements and acceptance criteria (NUREG-1804) are provided in the table below. NUREG-1804, Section 2.2.1.3.1.3, Acceptance Criterion 1(6) is not referenced below because nuclear criticality is screened out as a scenario class in Section 2.2. With regard to NUREG-1804, Section 2.2.1.3.1.3, Acceptance Criterion 1(7), a peer review (Beavers et al. 2002) was performed in accordance with procedures that are consistent with NUREG-1297 (Altman et al. 1988a). The peer review evaluated the technical basis at that time for estimating the performance of waste packages and drip shields. The review served to focus the waste package and drip shield corrosion modeling and testing programs addressing key uncertainties, but was not directly used for model development. In addition, this section does not discuss the approach used for data qualification. However, scientific analyses, model development, and data qualification activities were conducted

in accordance with project procedures that comply with Quality Assurance Program requirements. The project procedures governing data qualification are consistent with NUREG-1298 (Altman et al. 1988b) in keeping with Acceptance Criterion 1(7). With regard to NUREG-1804, Section 2.2.1.3.1.3, Acceptance Criterion 3(5), an expert elicitation on waste package degradation was performed (CRWMS M&O 1998) to support the total system performance assessment for the viability assessment, but that information was not used in the current models.

SAR Section	Information Category	Proposed 10 CFR Part 63 Reference	NUREG-1804 Reference
2.3.6	Waste Package and Drip Shield Corrosion	63.114(a)(1) 63.114(a)(2) 63.114(a)(3) 63.114(a)(4) 63.114(a)(5) 63.114(a)(6) 63.114(a)(7) 63.114(b) 63.342(c)	Section 2.2.1.2.2.3: Acceptance Criterion 3 Acceptance Criterion 4 Acceptance Criterion 5 Section 2.2.1.3.1.3: Acceptance Criterion 1(1) Acceptance Criterion 1(2) Acceptance Criterion 1(3) Acceptance Criterion 1(4) Acceptance Criterion 1(5) Acceptance Criterion 1(7) Acceptance Criterion 2 Acceptance Criterion 3 Acceptance Criterion 4 Acceptance Criterion 5 Section 2.2.1.3.2.3: Acceptance Criterion 1(1) Acceptance Criterion 1(2) Acceptance Criterion 1(3) Acceptance Criterion 1(4) Acceptance Criterion 1(5) Acceptance Criterion 2 Section 2.2.1.3.3.3: Acceptance Criterion 1(3) Acceptance Criterion 1(6) Acceptance Criterion 1(10) Acceptance Criterion 2(5)
2.3.6.1	Summary and Overview	Not applicable	Not applicable
2.3.6.2	Implementation of the Waste Package and Drip Shield Corrosion Models in Total System Performance Assessment	63.114(a)(2) 63.114(a)(4) 63.114(a)(5) 63.114(a)(6) 63.114(b) 63.342(c)	Section 2.2.1.3.1.3: Acceptance Criterion 1(1) Acceptance Criterion 1(2) Acceptance Criterion 1(5) Section 2.2.1.3.3.3: Acceptance Criterion 1(10)

SAR Section	Information Category	Proposed 10 CFR Part 63 Reference	NUREG-1804 Reference
2.3.6.3	General Corrosion of the Waste Package Outer Barrier	63.114(a)(1) 63.114(a)(2) 63.114(a)(3) 63.114(a)(5) 63.114(a)(6) 63.114(a)(7) 63.114(b) 63.342(c)	Section 2.2.1.3.1.3: Acceptance Criterion 1(1) Acceptance Criterion 1(2) Acceptance Criterion 1(3) Acceptance Criterion 1(4) Acceptance Criterion 1(5) Acceptance Criterion 2 Acceptance Criterion 3(1) Acceptance Criterion 3(2) Acceptance Criterion 3(3) Acceptance Criterion 4 Acceptance Criterion 5 Section 2.2.1.3.2.3: Acceptance Criterion 1(1) Acceptance Criterion 1(2) Acceptance Criterion 1(3) Acceptance Criterion 1(4) Acceptance Criterion 1(5) Acceptance Criterion 2 Section 2.2.1.3.3.3: Acceptance Criterion 1(3) Acceptance Criterion 1(6) Acceptance Criterion 1(10) Acceptance Criterion 2(5)
2.3.6.4	Localized Corrosion of Waste Package	63.114(a)(1) 63.114(a)(2) 63.114(a)(3) 63.114(a)(5) 63.114(a)(6) 63.114(a)(7) 63.114(b) 63.342(c)	Section 2.2.1.3.1.3: Acceptance Criterion 1(1) Acceptance Criterion 1(2) Acceptance Criterion 1(3) Acceptance Criterion 1(4) Acceptance Criterion 1(5) Acceptance Criterion 2 Acceptance Criterion 3(1) Acceptance Criterion 3(2) Acceptance Criterion 3(3) Acceptance Criterion 4 Acceptance Criterion 5 Section 2.2.1.3.3.3: Acceptance Criterion 1(3) Acceptance Criterion 1(6) Acceptance Criterion 1(10)

SAR Section	Information Category	Proposed 10 CFR Part 63 Reference	NUREG-1804 Reference
2.3.6.5	Stress Corrosion Cracking of the Waste Package Outer Barrier	63.114(a)(1) 63.114(a)(2) 63.114(a)(3) 63.114(a)(5) 63.114(a)(6) 63.114(a)(7) 63.114(b) 63.342(c)	Section 2.2.1.3.1.3: Acceptance Criterion 1(1) Acceptance Criterion 1(2) Acceptance Criterion 1(3) Acceptance Criterion 1(4) Acceptance Criterion 1(5) Acceptance Criterion 2 Acceptance Criterion 3(1) Acceptance Criterion 3(2) Acceptance Criterion 3(3) Acceptance Criterion 3(4) Acceptance Criterion 4 Acceptance Criterion 5 Section 2.2.1.3.2.3: Acceptance Criterion 1(1) Acceptance Criterion 1(2) Acceptance Criterion 1(3) Acceptance Criterion 1(4) Acceptance Criterion 1(5) Acceptance Criterion 2 Section 2.2.1.3.3.3: Acceptance Criterion 1(3) Acceptance Criterion 1(6) Acceptance Criterion 1(10)
2.3.6.6	Early Failure of Waste Packages	63.114(a)(1) 63.114(a)(2) 63.114(a)(3) 63.114(a)(5) 63.114(a)(6) 63.114(a)(7) 63.114(b) 63.342(c)	Section 2.2.1.2.2.3: Acceptance Criterion 3 Acceptance Criterion 4 Acceptance Criterion 5 Section 2.2.1.3.1.3: Acceptance Criterion 1(1) Acceptance Criterion 1(2) Acceptance Criterion 1(3) Acceptance Criterion 1(4) Acceptance Criterion 1(5) Acceptance Criterion 2 Acceptance Criterion 3(1) Acceptance Criterion 3(2) Acceptance Criterion 3(3) Acceptance Criterion 3(4) Acceptance Criterion 4 Acceptance Criterion 5 Section 2.2.1.3.3.3: Acceptance Criterion 1(10)
2.3.6.7	Effects of Long-Term Thermal Aging and Phase Stability of Alloy 22	63.114(a)(1) 63.114(a)(2) 63.114(a)(3) 63.114(a)(5) 63.114(a)(6) 63.114(a)(7) 63.114(b) 63.342(c)	Section 2.2.1.3.1.3: Acceptance Criterion 1(1) Acceptance Criterion 1(2) Acceptance Criterion 1(3) Acceptance Criterion 1(4) Acceptance Criterion 2 Acceptance Criterion 3(1) Acceptance Criterion 3(2) Acceptance Criterion 3(3) Acceptance Criterion 4

SAR Section	Information Category	Proposed 10 CFR Part 63 Reference	NUREG-1804 Reference
2.3.6.8	Drip Shield Degradation	63.114(a)(1) 63.114(a)(2) 63.114(a)(3) 63.114(a)(5) 63.114(a)(6) 63.114(a)(7) 63.114(b) 63.342(c)	Section 2.2.1.2.2.3: Acceptance Criterion 3 Acceptance Criterion 4 Acceptance Criterion 5 Section 2.2.1.3.1.3: Acceptance Criterion 1(1) Acceptance Criterion 1(2) Acceptance Criterion 1(3) Acceptance Criterion 1(4) Acceptance Criterion 1(5) Acceptance Criterion 2 Acceptance Criterion 3(1) Acceptance Criterion 3(2) Acceptance Criterion 3(3) Acceptance Criterion 3(4) Acceptance Criterion 4 Acceptance Criterion 5 Section 2.2.1.3.2.3: Acceptance Criterion 1(1) Acceptance Criterion 1(2) Acceptance Criterion 1(3) Acceptance Criterion 1(4) Acceptance Criterion 1(5) Acceptance Criterion 2 Section 2.2.1.3.3.3: Acceptance Criterion 1(3) Acceptance Criterion 1(6)
2.3.6.9	Conclusions	Not applicable	Not applicable

In some instances, the acceptance criteria in the table above are addressed in multiple locations. For example, acceptance criteria in NUREG-1804, Section 2.2.1.3.1.3 are addressed in Sections 2.3.6 and 2.3.7 since the EBS includes waste packages, drip shields, and waste forms. Acceptance criteria in NUREG-1804, Section 2.2.1.3.3.3, are addressed by one or more of Sections 2.2, 2.3.3 to 2.3.7, 2.3.11, and 2.4, as described more fully in Section 2.3.5.

2.3.6.1 Summary and Overview

A major component of the strategy for safe disposal of nuclear waste is to isolate radionuclides from the environment in waste packages for extended time frames. In a multibarrier approach, the EBS works in association with and complements the natural barriers by preventing or substantially reducing the release rate of radionuclides from the waste and preventing or substantially reducing the rate of movement of radionuclides from the repository to the accessible environment. The waste package and drip shield are significant features of the EBS. A schematic of an emplacement drift showing waste packages and drip shields is shown in Figure 2.3.6-1. The primary purposes of the waste package are to contain the waste and to limit the transport of radionuclides. The purposes of the drip shield are to prevent seepage waters from contacting the waste package and to protect the waste package from rockfall.

The strategy in designing the waste package and in selecting the materials for its construction is to achieve a robust structure capable of withstanding a wide range of environmental scenarios that could develop in and around the waste package. Corrosion resistance is important to the long-term performance of waste packages and drip shields. The waste packages and drip shields are manufactured from highly corrosion-resistant metal alloys. The corrosion resistance of these alloys is attributed to the formation of a protective self-healing, passive layer. The alloys used to fabricate the waste packages and drip shields have excellent corrosion resistance over a wide range of aqueous solution compositions and temperatures. Based upon measurements of corrosion rates of the passive metals that comprise the waste package and drip shield, the waste packages and drip shields can remain intact with no penetrations due to general corrosion for durations of tens of thousands and even hundreds of thousands of years. While the waste package and drip shield alloys are resistant to stress corrosion cracking and localized corrosion, these corrosion modes may result in degradation of the features, so they are also analyzed.

The waste package consists of two concentric cylinders: an inner vessel of Stainless Steel Type 316 (UNS S31600, with further compositional restrictions as described in Section 1.5.2.7) designed for structural support, and a corrosion-resistant outer shell made of Alloy 22 (UNS N06022, a nickel-chromium-molybdenum alloy with further compositional restrictions as described in Section 2.3.6.7). The design and fabrication of the waste package is described in Section 1.5.2. The drip shield is an additional feature of the EBS, described in Section 1.3.4. The drip shield plates, which will be placed over the waste packages, are fabricated from Titanium Grade 7 (UNS R52400), a commercially available nearly pure titanium alloy containing a small addition of palladium to provide a higher degree of corrosion resistance. The structural components of the drip shield will be constructed using the higher-strength titanium alloy Titanium Grade 29 (UNS R56404), which has alloying elements aluminum and vanadium to provide the required strength and ruthenium to provide corrosion resistance. This titanium alloy is also highly corrosion resistant in a wide variety of chemical environments. The design and fabrication of the drip shield are described in Section 1.3.4.7.

2.3.6.1.1 Processes Contributing to EBS Barrier Capability

The waste package and drip shield corrosion models described in this section include characteristics of significant features and processes that contribute to the capability of the EBS, as described in Section 2.1.2.2 and Table 2.1-7. The waste package and drip shield features and some processes make significant contributions to the overall capability of the EBS.

Drip Shield—The following processes and characteristics of the drip shield are important to the capability of the EBS:

- **General Corrosion of Drip Shields**—General corrosion rates of titanium in a range of expected environmental conditions are sufficiently low that the drip shield will protect the waste package from rockfall and seepage water for extended time frames (Section 2.2, Table 2.2-1 FEP 2.1.03.01.0B). This process has been included in models of drip shield degradation presented in Section 2.3.6.8. Uncertainty in these corrosion rates has been modeled and accounted for. Thinning of the drip shield due to general corrosion is included in structural response models for seismic effects and rockfall in Section 2.3.4.

- **Localized Corrosion of Drip Shields**—Titanium is extremely resistant to localized corrosion due to its very passive film. Localized corrosion will not occur in repository environments and is excluded from TSPA (Section 2.2, Table 2.2-5, FEP 2.1.03.03.0B). The model for drip shield localized corrosion is presented in Section 2.3.6.8. Localized corrosion due to dust deliquescence is excluded from TSPA (Section 2.2, Table 2.2-5, FEP 2.1.09.28.0B).

- **Stress Corrosion Cracking of Drip Shields**—In the presence of residual stresses or sustained loading, titanium is potentially susceptible to stress corrosion cracking. Residual stresses and sustained loading are possible as a result of rockfall or seismically induced damage. Uncertainty exists in the stress state and threshold stress required for a stress corrosion crack to be initiated, and other uncertainties exist regarding the degree of propagation of any stress-induced crack of titanium. Due to the long time frames, stress corrosion cracking is modeled to be independent of the environment although the environments to support stress corrosion may not occur within the repository as modeled in Section 2.3.6.8. Although stress corrosion cracking is modeled to occur in the drip shield, the presence of cracks is an insufficient condition to affect the performance of the drip shield in preventing or substantially reducing the amount of water that could directly contact the waste package, as discussed in Section 2.3.6.8 and is excluded from TSPA (Section 2.2, Table 2.2-5, FEP 2.1.03.02.0B).

- **Early Failure of Drip Shields**—During fabrication and installation, a range of human factor errors could result in a drip shield being emplaced that has the potential for an early failure (Section 2.2, Table 2.2-1, FEP 2.1.03.08.0B). These potential errors are included in abstraction models (Section 2.3.6.8.4) used in the early failure scenario class of the TSPA as presented in Section 2.4.

- **Creep of Metallic Materials in the Drip Shield**—Titanium Grade 7, used for the drip shield plates, may undergo creep deformation at temperatures as low as room temperature when subjected to tensile stresses exceeding approximately 50% of the yield strength (SNL 2007a, Section 6.8.7). Titanium Grade 29, used for the drip shield structural supports, has significantly higher creep resistance than Titanium Grade 7 (SNL 2007a, Section 6.8.7). When the drip shield deforms through long-term creep, a confinement caused by rockfall rubble is developed which tends to inhibit further creep deformation. Creep of titanium resulting in instability (collapse) of the drip shield has been excluded from the performance assessment (Section 2.2, Table 2.2-5, FEP 2.1.07.05.0B). If creep occurs, it has the beneficial effect of decreasing the stress profile which in turn will reduce the rate of crack propagation. This beneficial effect has not been included in the stress corrosion cracking model (Section 2.2, Table 2.2-5, FEP 2.1.07.05.0B).

Waste Package—The following processes and characteristics of the waste package are important to the capability of the EBS:

- **General Corrosion of Waste Packages**—General corrosion rates of Alloy 22 in a range of expected environmental conditions are sufficiently low that the waste packages will protect the waste form for extended periods of time (Section 2.2, Table 2.2-1, FEP 2.1.03.01.0A). Uncertainty and variability in these corrosion rates has been included

in the model presented in Section 2.3.6.3. Waste package thinning due to general corrosion is accounted for in structural response models, as presented in Section 2.3.4.

- **Localized Corrosion of Waste Packages**—Localized corrosion mechanisms on the waste package surface are dependent on the thermal-hydrologic and thermal-chemical environment on the waste package surface (Section 2.2, Table 2.2-1, FEP 2.1.03.03.0A). Because localized corrosion due to dust deliquescence and condensation has been screened from TSPA (Section 2.2, Table 2.2-5, FEP 2.1.09.28.0A), localized corrosion is only possible in those cases where the drip shield fails to perform its function and certain aggressive incoming seepage is allowed to contact the waste package. This may occur where seismic ground motion is accompanied by fault displacement as described in Section 2.3.4. In the case of fault displacement, waste packages that are susceptible to localized corrosion have been modeled to have already experienced mechanical damage failure. Incoming seepage may also contact the waste package in the case of drip shield early failure, and is modeled to initiate localized corrosion (Section 2.4). TSPA assumes that an early failure waste package that has completely lost its containment function exists below the drip shield early failure. Uncertainty in the localized corrosion initiation and corrosion rate model is included in the model presented in Section 2.3.6.4.

- **Stress Corrosion Cracking of Waste Packages**—Stress corrosion cracking of Alloy 22 is modeled to occur as a result of residual stresses caused by mechanical impacts during mechanical degradation following seismic events, and possibly from residual stresses and undetected weld flaws in the closure lid (Section 2.2, Table 2.2-1, FEP 2.1.03.02.0A). Such stress cracks are sufficiently small and tight to allow only diffusive transport of radionuclides through the cracks (Section 2.2, Table 2.2-5, FEP 2.1.03.10.0A). Stress corrosion cracking is modeled to be independent of the environment although the environments to support stress corrosion may not occur within the repository as modeled in Section 2.3.6.5. Stress corrosion cracking models and data are presented in Section 2.3.6.5.

- **Early Failure of Waste Packages**—During fabrication, waste loading, and emplacement, a range of human factor errors could result in a waste package being emplaced that has the potential for an early waste package failure (Section 2.2, Table 2.2-1, FEP 2.1.03.08.0A). This possibility has been included in abstraction models used in the early failure scenario class of the TSPA as presented in Section 2.3.6.6.

2.3.6.1.2 Corrosion Test Environments and Relationship to In-Drift Chemical Environment

The waste packages and drip shields are manufactured from highly corrosion-resistant alloys. The objective of corrosion testing is to determine the corrosion behavior of these alloys over a broad range of environments that cover the expected in-drift chemical environment conditions. Environments beyond the expected conditions are also tested in order to examine the boundaries of corrosion resistance of the metals. The water chemistry of the in-drift chemical environments (brines) and their likelihood are discussed in Section 2.3.5.

As stated in the geochemical literature (e.g., Drever 1997) and discussed in Section 2.3.5.5, the three families of brines that result from evaporative concentration of dilute natural waters at the earth's surface are calcium chloride brines, carbonate brines, and sulfate brines (Figures 2.3.6-2 and 2.3.5-49). The type of brine that forms is a function of the chemical pathway the water follows as it evaporates. Chemical divides encountered as the water evaporates and solid phases precipitate lead to these three brine types, with all evaporating brines taking one of these pathways. These same three families of brines also apply to the brines formed by deliquescence, although brines formed by deliquescence are not expected to exhibit the same range of characteristics as brines formed from evaporative concentration of dilute natural waters at the earth's surface (SNL 2007b, Section 6.13.5.2).

The expected compositions of seepage into the repository include ambient waters and waters that have been modified by water–rock interactions, of the Na-K-Ca-Mg-CO_3-Cl-NO_3-SO_4-F system. More concentrated brines form by evaporative concentration of these waters on the waste package surface. Depending upon the temperature, partial pressure of carbon dioxide (pCO_2) in the drift, and the composition of the seepage, any of the three brines types can form (Section 2.3.5.5).

The test solutions utilized in corrosion testing supporting the corrosion models are related to these three families of natural brines. Solutions used in the corrosion tests are chosen based on two criteria. Either they are representative of the brines expected by evaporative concentration of seepage waters and deliquescent brines, or they provide information about material corrosion behavior over a broader range of conditions than those conditions believed to be representative. The brine types that are predicted to form in the repository are discussed in Section 2.3.5. Table 2.3.5-10 provides a correlation between the seepage waters and the corrosion testing solutions. The testing solution compositions of the three brine types are represented by the five standard test solutions provided in Table 2.3.6-1.

Corrosion test solutions corresponding to the calcium chloride brine family include: calcium chloride, calcium chloride plus calcium nitrate, simulated saturated water (SSW), and sodium chloride solutions. Corrosion test solutions corresponding to the carbonate brine family include simulated dilute water (SDW); simulated concentrated water (SCW); basic saturated water; and under certain circumstances, SSW and NaCl aqueous test solutions. Corrosion test solutions corresponding to the sulfate brine family include: simulated acidic water (SAW), SSW, and sodium chloride (SNL 2007b, Section 6.13.5.2). These test solutions provide the foundation for the corrosion testing activities supporting postclosure assessment of repository performance estimates in the TSPA model.

2.3.6.2 Implementation of the Waste Package and Drip Shield Corrosion Models in Total System Performance Assessment

[NUREG-1804, Section 2.2.1.3.1.3: AC 1(1), (2), (5); Section 2.2.1.3.3.3: AC 1(10)]

The TSPA model integrates the essential components of the conceptual and process models to simulate repository behavior. Sections 2.3.6.3 through 2.3.6.8 describe the waste package and drip shield degradation submodels of the TSPA, which are used to calculate time-dependent degradation due to general corrosion of the drip shields, as well as general corrosion, localized corrosion, and stress corrosion cracking of the waste packages. The numbers of early drip shield and waste package failures are also calculated. Figures 2.3.6-3 and 2.3.6-4 show the inputs and outputs for these

submodels and the relationship of these models to other TSPA model components. The waste package degradation submodel uses thermal-hydrologic and chemical environment parameters, corrosion rates, and other parameters (e.g., localized corrosion criteria, etc.) to produce outputs that describe the number and type (commercial spent nuclear fuel (SNF) or codisposal) of degraded waste packages. The submodel also estimates the average number and type (e.g., crack or patch) of penetrations per breached waste package. The waste form degradation and mobilization and the EBS flow and transport submodels use this information to calculate flow rates and diffusive transport areas through waste packages, degradation rates for the various waste forms, and the concentrations of radionuclide species available for transport. Figure 2.3.6-4 shows that for the drip shield, only general corrosion and early failure are included in the TSPA; other corrosion processes were evaluated and found to not occur or have insignificant impacts. Note that stress corrosion cracking of the drip shield in the absence of a seismic disruptive event is excluded from TSPA because the drip shield stresses are relieved during fabrication. The stresses resulting from drip shield emplacement error are accounted for in drip shield early failure (Section 2.3.6.8.4). Even if stress corrosion cracking were to occur due to rockfall, crack tortuosity and plugging would occur to preclude loss of drip shield function. Stress corrosion cracking and collapse of the drip shield as a result of seismic events is discussed in Section 2.3.4.

2.3.6.2.1 Summary of Features, Events, and Processes Included in Waste Package and Drip Shield Corrosion Models

This section describes in summary the conceptual models, relevant data, and models used to simulate and analyze waste package and drip shield corrosion. The approach used to treat each FEP included in this section is summarized in Table 2.3.6-2. Some excluded FEPs are described in this section. The complete set of both included and excluded FEPs is discussed in Section 2.2, Table 2.2-5. Screening decisions based on analysis of the FEPs to identify FEPs that should be included in and excluded from the TSPA analysis of postclosure performance are described in Section 2.2, Table 2.2-5. Those decisions related to waste package and drip shield corrosion are presented in Tables 2.2-2 and 2.2-5. The FEPs treated in the waste package and drip shield corrosion models are related to corrosion processes, microbial effects on corrosion, early failure of waste packages and drip shields due to defects, hydrogen-induced cracking, and the physical forms of waste packages and drip shields. As noted earlier, some excluded FEPs are described in Section 2.3.6 particularly where an FEP is included for the waste package, but the corresponding FEP is excluded for the drip shield.

2.3.6.2.2 Waste Package Degradation Processes

Several processes may result in degradation of the waste packages over time that could impact their functionality. Seismic effects, in-drift chemical environments, and volcanic effects are discussed in Sections 2.3.4, 2.3.5, and 2.3.11, respectively. Other processes are discussed in this section.

General Corrosion—As summarized below, passive general corrosion of the waste package outer corrosion barrier is included in the TSPA.

Passive general corrosion, referred to as “general corrosion” throughout, occurs uniformly across the waste package surface when the metal oxide passive film is stable. For the range of in-drift chemical environments, Alloy 22 is highly corrosion resistant and complete loss of passivity will

not occur (SNL 2007c, Section 6.4.3). Therefore, active general corrosion of the metal will not occur. Localized corrosion of the passive metal is analyzed as a separate degradation process.

General corrosion may occur in the presence or absence of water (aqueous corrosion and dry oxidation, respectively). The rate of dry oxidation has been demonstrated to be lower than the aqueous corrosion rate. Therefore, the higher corrosion aqueous corrosion rates are used even in the absence of water. The analysis of general corrosion is based on a conceptual understanding of the physical processes that occur, and review of experimental data and data uncertainty. The evaluation includes development of the numerical general corrosion model, assessment of model uncertainty, and abstraction and validation of the general corrosion model. The effect of microbially influenced corrosion is included as a multiplier to the general corrosion rates.

General aqueous corrosion is the uniform thinning of a metal or alloy due to electrochemical processes. The general corrosion rate for the waste package outer barrier is treated as temperature dependent and, for a given temperature, is assumed to be constant over time. This treatment is conservative because the general corrosion rate of metals and alloys tends to decrease with time (SNL 2007c, Section 6.4.3). General corrosion rates of the waste package outer barrier have been estimated based on experimental weight-loss measurements of Alloy 22 samples after a 5-year exposure in environments relevant to the repository (SNL 2007c, Section 6.4.3). In addition to long-term corrosion test results, general corrosion rates were also measured electrochemically to support the model for temperature dependence and to expand the range of experimental environments (SNL 2007c, Section 6.4.3).

General corrosion is modeled by dividing the waste package surface into subareas (referred to as patches with each patch having a surface area of ~231.5 cm^2) that are used to simulate the spatial variability of general corrosion across the waste package surface. The established patch size is approximately 4 times the size of the corrosion samples. The corrosion rate applied to a patch is statistically adjusted to be equivalent to sampling the corrosion rate cumulative distribution function 4 times and taking the highest rate (SNL 2008a, Section 6.3.5). This treatment is conservative for radionuclide release purposes because not all four samples within a patch would corrode at this highest rate. The waste packages have over a thousand patches, ensuring that the range of the corrosion rates is sampled (SNL 2008a, Section 6.3.5). In the seismic scenario (Section 2.3.4) where overall mechanical response is determined, the average patch corrosion rate is used to determine the average barrier thickness. The waste package is considered breached when one or more patches are penetrated. The model output (Section 2.4) consists of the percentage of breached waste packages versus time and the average number of patch penetrations per breached waste package versus time.

Two nominal waste package configurations (one for commercial SNF and one for codisposal waste packages) are considered for the corrosion analysis. The selected configurations adequately represent the various waste package configurations, including naval packages, that will be emplaced because the modeled waste packages include the range of waste package diameters and lengths and account for the majority of the waste package units.

The adequacy of the general corrosion model of the waste package outer barrier is established by comparing the corrosion rates and passive film stability of Alloy 22 to similar materials (SNL 2007c, Section 7.2.1). The general corrosion model predicts Alloy 22 general corrosion rates at the

50th, 95th, and 99.99th (a reasonable upper bound) percentiles at 25°C to be 1.13, 3.04, and 6.50 nm/yr using the medium level of uncertainty and the medium temperature dependence, respectively. Using the low level of uncertainty for the general corrosion rate distribution and the low temperature dependence, the 50th, 95th, and 99.99th percentile rates predicted by the model at 25°C are 4.02, 11.6, and 26.2 nm/year, respectively.

The modeled corrosion rates and passive film stability compare well to Alloy C (UNS N10002), a less corrosion resistant Ni-Cr-Mo alloy than Alloy 22, specimens exposed for 44 years to a marine environment at North Carolina's Kure Beach (i.e., with salt air and alternate wetting and drying, as well as the presence of surface deposits). Those specimens indicate that passivity was maintained over this exposure period as evidenced by the observation of a mirror-like surface finish after surface deposits were removed. Under the same conditions, the less corrosion resistant Alloy 600 exhibited a corrosion rate of 8 nm/yr after 36 years of exposure (SNL 2007c, Section 7.2.1). Section 2.3.6.3 provides more information on general corrosion.

Localized Corrosion—The localized corrosion model due to seepage onto the waste package is included in the TSPA.

Breakdown of the metal oxide passive film at discrete sites that leads to underlying metal dissolution is referred to as localized corrosion. This form of corrosion could penetrate the waste package much faster than general corrosion if the conditions for the initiation and propagation for localized corrosion are present and persist. Alloy 22 has a very stable passive film and was chosen specifically to resist localized corrosion in the in-drift chemical environment. However, under aggressive environmental exposure conditions, the passive films may break down locally, leading to localized corrosion of the underlying alloy. The development of localized corrosion on a given metal is dependent on several parameters, including surface temperature, and water chemistry on these surfaces.

The localized corrosion model for the waste package outer barrier consists of an initiation component and a propagation component (SNL 2007c, Section 6.4.4). Initiation requires breakdown of the passive film that can occur when an open-circuit corrosion potential, $E_{corr,}$ exceeds or equals a critical potential, $E_{critical}$ (SNL 2007c, Section 6.4.4; Farmer et al. 2000). The corrosion potential is defined as the open-circuit corrosion potential attained by a metallic sample immersed in a solution with no applied electrochemical driving force. The critical potential is defined as the potential above which the passive film may not reform if it is damaged and below which the passive film will reform (repassivate) if it is damaged. As demonstrated by experimental results, E_{corr} and $E_{critical}$ are functions of temperature, pH (E_{corr} only) and concentrations of chloride and nitrate ions. The localized corrosion model incorporates these functional dependencies for seepage water conditions only. Localized corrosion due to condensation and deliquescence in dust films has been excluded from the TSPA (Section 2.2, Table 2.2-5, FEP 2.1.09.28.0A and FEP 2.1.09.28.0B).

Corrosion rates may be enhanced where creviced geometries form on the waste package surface. The data used to develop the critical potential model were obtained with tight crevices formed for accelerated tests. The results are conservative in that these crevices are designed to be more severe than those on the waste package at the contact areas with the emplacement pallet or in areas where mineral deposits form due to evaporative concentration. To account for the possible increased

susceptibility of weld regions to localized corrosion, the majority of the test samples were from as-welded samples. The use of severely creviced samples is conservative because the initiation thresholds for Alloy 22, in terms of water chemistry and temperature, are lower for localized corrosion under creviced conditions (i.e., crevice corrosion) than for pitting corrosion (SNL 2007c, Section 6.4.4).

In the localized corrosion model, once localized corrosion initiates it continues, and the depth of penetration increases at a constant rate. This is conservative in that there are several processes and changing conditions that can cause the propagation rate to stifle (slow) or arrest (stop completely). A range of potential localized corrosion rates measured in highly aggressive environments is used to bound localized corrosion rates for the model.

The localized corrosion propagation rates for the waste package outer barrier are modeled to range from 12.7 to 1,270 μm/yr with a median value of 127 μm/yr (SNL 2007c, Section 6.4.4.7). The distribution is based on data that bound the propagation rates found in the literature for extremely aggressive solutions that cannot exist within the repository and thus is a conservative representation of localized corrosion rates of Alloy 22 for the exposure conditions expected in the repository. The entire variance in the propagation rate is due to uncertainty. Section 2.3.6.4 provides more information on localized corrosion. The area affected by localized corrosion is modeled as the area equal to the waste package area exposed to seepage.

Validation of the localized corrosion initiation model was accomplished by comparison to literature data and project data not used to develop the model. The results indicate that the Alloy 22 localized corrosion initiation model is accurate and conservative in that it tends to overpredict the occurrence of localized corrosion.

Validation of the localized corrosion propagation rate was accomplished by comparison of the propagation rates used in the model to propagation rates for similar, less corrosion-resistant alloys. The results indicate that the Alloy 22 localized corrosion propagation model predicts a range of rates consistent with experimental observations.

Stress Corrosion Cracking—As summarized below, stress corrosion cracking of the waste package is included in the TSPA.

The combined action of tensile stress and an environment that is favorable to stress corrosion cracking can lead to stress corrosion crack initiation and propagation. Not all corrosive environments will support stress corrosion cracking; instead, aggressive alloy-specific environments are necessary. Additionally, Alloy 22 is very resistant to stress corrosion cracking.

Stress corrosion cracking requires three simultaneous conditions: a susceptible material, critical environment, and sustained tensile stress. Alloy 22, the material used for the waste package outer barrier, is highly corrosion resistant but could be susceptible in the Yucca Mountain environment to stress corrosion cracking. Environments that could enable stress corrosion cracking are condensed layers of moisture, or bulk solutions from drips or seepage onto metal surfaces. Environmental conditions, which include temperature, dissolved oxygen, and ionic strength, could influence the stress corrosion cracking process. Due to the long time-frames of model application, the model

conservatively assumes that the waste package will undergo stress corrosion cracking if stress initiation conditions are met, regardless of the environment.

The stress corrosion cracking model is based on the slip dissolution and film rupture model for crack initiation and propagation. The stress corrosion cracking model establishes a threshold stress for the creation of stress corrosion cracks on smooth surfaces (referred to as incipient cracks) and establishes a stress intensity factor threshold for the initiation of crack growth. Weld flaws are also considered to propagate by stress corrosion cracking once the stress intensity factor threshold is satisfied.

The threshold stress, threshold stress intensity factor, and parameters associated with the slip dissolution and film rupture model are determined from experimental data developed for repository environments. The crack propagation rate is based on the stress intensity factor and Alloy 22 passive film properties.

The stress corrosion cracking model was validated by comparing measured crack growth rates reported in peer-reviewed literature with model predictions, as well as with a less conservative alternative conceptual model (SNL 2007a, Section 7.3). Furthermore, the model was also validated by comparing Alloy 22 slip dissolution and film rupture model predicted rates with subsequently developed experimentally measured Alloy 22 rates and demonstrating agreement (SNL 2007a, Section 7.3). For the empirical threshold stress intensity factor described in peer-reviewed literature, a conservative approach was used to establish a threshold stress intensity factor (K_{ISCC}) criterion. This criterion was established by extrapolating qualified Alloy 22 crack growth rate results experimentally obtained at higher stress intensity factor (K_I) values down to rates representative of the mean general corrosion rate where crack blunting occurs and cracks will not continue to grow. Section 2.3.6.5 provides more information on stress corrosion cracking.

Early Failure Due to Manufacturing or Handling-Induced Defects—As summarized below, early failure of the waste package is included in the TSPA.

An analysis evaluated the types of defects or imperfections that could occur in a waste package and potentially lead to its early failure and estimated a probability of occurrence for each. An early failure is defined as a through-wall penetration of a waste package, due to manufacturing- or handling-induced defects, at a time earlier than would be predicted by mechanistic degradation models for a defect-free waste package (SNL 2007d).

Only the Alloy 22 waste package outer corrosion barrier is considered for early failure treatment. Conservatively, no performance credit is applied for the ability of the stainless steel inner vessel or transportation, aging, and disposal (TAD) canister to preclude or limit water influx once the Alloy 22 outer corrosion barrier is breached. Within TSPA, early failure of a defective waste package is conservatively modeled to occur at the beginning of the postclosure period. This is conservative because the processes which would lead to waste package breach will not occur instantaneously even in the event of a defective waste package. Furthermore, the entire waste package surface area is treated as failed. This assumption is also conservative because the expected effect of early failure would be stress corrosion cracking, which results in cracks that are tight and of limited quantity. In fact, except for the early release scenario, the release of radionuclides through

waste package outer barrier stress corrosion cracks is modeled as diffusive release, as described in Section 2.3.7.12.

Several general types of manufacturing defects were considered as possible conditions that could lead to early waste package failure: weld flaws, base metal flaws, improper weld filler material, improper base metal, improper heat treatment, improper stress mitigation applications, improper weld-flux material, poor weld-joint design, contamination, mislocated welds, missing welds, administrative or operational errors, and handling damage (SNL 2007d, Section 6.2). As discussed in Section 2.3.6.6, analyses predict that potential early failures will occur in an average of slightly more than one out of the approximately 11,600 waste packages in the repository. Section 2.3.6.6 provides more information on early failure due to manufacturing defects.

Long-Term Thermal Aging—As summarized below, long-term thermal aging of the waste package is excluded from TSPA for all cases, including drift collapse (Section 2.2, Table 2.2-5, FEP 2.1.11.06.0A).

As described in Section 1.5.2, after fabrication the waste package outer barrier is solution annealed and quenched. This process is employed to minimize the formation of secondary phases within the Alloy 22 matrix. At intermediate temperatures (elevated temperatures below the solution anneal temperature), certain second intermetallic phases may precipitate from an annealed material leading to local depletion of elements, enrichment of elements, or both. If these locally precipitated phases are rich in elements beneficial to corrosion properties, locations in the base metal near the precipitates may be depleted in these same elements and the overall corrosion resistance of the material may be adversely affected.

For Alloy 22, the length of time for which phase stability is a concern is strongly dependent upon temperature. For temperatures above 650°C, an exposure time on the order of several tens of hours to approximately 100 hours can cause precipitation and phase instability that could compromise corrosion resistance. Modeling and analyses based upon project data and thermodynamic calculations indicate that, at 300°C, an exposure time of well over 1,000 years will not result in phase instability. At 200°C, thermal aging effects are not of concern for at least 10,000 years (BSC 2004a, Sections 6.6.4 and 8).

Upon emplacement, the temperature of the Alloy 22 waste package outer barrier will remain below approximately 200°C (Table 2.3.5-7 and Figure 2.3.5-33) except after drift collapse as described in Section 2.3.4. In the unlikely event of drift collapse in the first 90 years, the waste package outer barrier will be below approximately 300°C and after about 200 years would be below 200°C. With these conditions, the impact of thermal aging on the corrosion of Alloy 22 is insignificant (BSC 2004a, Section 8). Therefore, analyses indicate that degradation resulting from phase instability for Alloy 22 does not affect waste package performance for the drift collapse temperature profile (Section 2.2, Table 2.2-5, FEP 2.1.11.06.0A). Section 2.3.6.7 provides more information on long-term thermal aging.

2.3.6.2.3 Drip Shield Degradation Processes

Each of the above degradation processes, along with drip shield creep, is also discussed below as it relates to drip shield degradation. As identified earlier, the processes are analyzed for the potential

for degradation of the drip shield over time that could affect its functionality. Seismic effects on degradation of the drip shield are discussed in Section 2.3.4. In summary, drip shield general corrosion and early failure due to human error are included in TSPA. Stress corrosion cracking of the drip shield is excluded from TSPA (Section 2.2, Table 2.2-5, FEP 2.1.03.02.0B). Other drip shield degradation modes are also found to not occur or are found to have an insignificant impact as listed in Section 2.2, Table 2.2-5.

General Corrosion—General corrosion rates of the drip shield have been calculated based upon weight loss of Titanium Grade 7 samples after 2.5 years of exposure in repository-relevant environments (SNL 2007e, Section 6.1[a]). In addition, the model is validated using 5-year corrosion-rate data for Titanium Grade 16 (an alloy similar to Titanium Grade 7 with less palladium and thus less corrosion resistant), and other literature data on similar titanium alloys (SNL 2007e, Section 7.2[a]). The corrosion rates have been found to be independent of temperature for repository-relevant temperatures (SNL 2007e, Section 7.2.1[a]). Since the corrosion rate data was obtained at 60°C and 90°C and the drip shield temperature will be lower than 60°C for the majority of the postclosure period, if there was a temperature dependence, its lack of treatment is conservative. A solution dependent corrosion rate was observed with one solution resulting in higher corrosion rates than the rest. This effect is accounted for by treating the drip shield outer surface differently than the underside which will be exposed to relatively mild environments. Even the highest measured rate on both sides would not lead to failure of the drip shield for over 150,000 years (SNL 2007e, Section 6.1.5[a]). Microbially influenced corrosion was also evaluated and found to have no significant effect on either general or localized corrosion processes of titanium alloys under the exposure conditions in the repository (SNL 2007e, Section 6.7.2). The general corrosion rates for Titanium Grade 29 are based upon the corrosion rates for Titanium Grade 7 multiplied by a ratio of corrosion rates for Titanium Grade 29 and Titanium Grade 7 (SNL 2007e, Section 6.2[a]).

Localized Corrosion—The localized corrosion model is based on experimental measurements of key model parameters and validated through comparison of those measurements to corroborative data that have been published in the open scientific literature. The localized corrosion model does not predict crevice corrosion even at pH of 14 (SNL 2007e, Section 6.6.3). Given the exposure conditions expected in the repository, localized corrosion of titanium alloys is not considered possible and is, therefore, excluded from TSPA (Section 2.2, Table 2.2-5, FEP 2.1.03.03.0B) (SNL 2007e, Section 6.6).

Stress Corrosion Cracking—The drip shield will be fully stress-relief heat treated before emplacement (Section 1.3.4) and therefore will not be subjected to stress corrosion cracking in the absence of rockfall and seismic events. Mishandling and manufacturing defects are modeled as drip shield early failures (Section 2.3.6.8.4).

As modeled, stress corrosion cracking of Titanium Grade 7 could result from disruptive events (Section 2.3.4). Titanium Grade 7 specimens failed at applied stress ratios of about 1.1 to 1.4 times yield strength in constant load tests (SNL 2007a, Figure 4-1, Section 6.8.3). Although these constant load failures are the result of creep rupture rather than stress corrosion cracking, the failures are conservatively treated to result from stress corrosion cracking. This treatment is conservative because unlike constant load tests in the laboratory, stresses in the drip shield actually will be relieved through creep. In addition, a conservative threshold stress of 0.8 times the yield strength

was established based on these data and is used to evaluate response to seismic events in Section 2.3.4 (SNL 2007a, Section 6.8.3). For the higher strength Titanium Grade 29, a conservative stress corrosion cracking stress criterion of 0.5 times the yield strength is modeled based upon analysis of laboratory data and the observation that the non-ruthenium containing analogue, Titanium Grade 5 may be susceptible to stress corrosion cracking initiation in sodium chloride brines.

While stress corrosion cracking may occur in the event of seismic response to rockfall, stress corrosion cracking of the drip shield has been screened from TSPA because advective flow of water through the cracks is insignificant and will not affect repository performance (Section 2.2, Table 2.2-5, FEP 2.1.03.02.0B and 2.1.03.10.0B).

Early Failure Due to Manufacturing Defects—Early failure of the drip shield due to manufacturing and handling defects was considered (SNL 2007d, Sections 6.3 and 6.4). Despite the fact that the expected result of manufacturing error would be stress corrosion cracking, drip shield early failure is modeled as complete failure of the drip shield. Out of a total of approximately 11,600 drip shields, the number of early failed drip shields is modeled to average less than one drip shield.

Creep—Potential creep deformation of the drip shield under long-term loads resulting from the weight of the rock overburden following collapse of the emplacement drift was analyzed, assuming early drift collapse. The relatively low, long-term creep strain levels are less than levels where onset of creep rupture is expected and do not impact the drip shield seepage diversion function or the ability of the drip shield to protect the waste package from loads resulting from the rock overburden mass. Based on the relatively low, structurally acceptable creep strain calculated for conservative loading conditions, creep of the drip shield is excluded from the TSPA (Section 2.2, Table 2.2-5, FEP 2.1.07.05.0B).

Long-Term Thermal Aging—Experimental evidence indicates precipitation of deleterious phases will not occur in the drip shield materials under relevant repository conditions. Most of the drip shield will be fabricated with Titanium Grade 7. Intermetallic compounds have not been reported in Titanium Grade 7 with normal heat treatments, so phase instability caused by thermal processes (e.g., welding) will also be insignificant in the Titanium Grade 7. The drip shield structural support beam components will be fabricated with Titanium Grade 29, an alpha-beta alloy that is expected to remain stable under relevant repository conditions with proper fabrication and heat treatment controls (ASM International 1990, p. 628). Therefore, thermal aging and phase instability are not significant processes for drip shields and have been excluded from the TSPA (Section 2.2, Table 2.2-5, FEP 2.1.11.06.0B).

2.3.6.2.4 Total System Performance Assessment Treatment of Corrosion Uncertainty

The numerical models of each included corrosion or degradation process are incorporated directly in the TSPA model. Uncertainty in waste package degradation is analyzed with multiple realizations (SNL 2008a, Section 6.3.5). For each realization, values are sampled for the degradation parameters to reflect uncertainty in the corrosion behavior. Each realization is a complete simulation of a given number of waste packages explicitly considering variability in the degradation processes. Accordingly, the analysis provides the percentage of the total number of waste packages and drip

shields breached versus time. The average number of patch penetrations (capable of advective flow) and total crack penetration area (capable of diffusive transport) per breached waste package are reported as a group of degradation profile curves (resulting from the multiple realizations) that represent the potential range of the output parameters. For example, the waste package breach time profiles are reported with a group of curves representing the cumulative probability of waste package breach as a function of time. Waste package and drip shield degradation are discussed in greater detail in Section 2.4.1. The output from the numerical models is used as input for waste form degradation analysis and radionuclide release analysis from breached waste packages conducted within the TSPA model.

2.3.6.3 General Corrosion of the Waste Package Outer Barrier

[NUREG-1804, Section 2.2.1.3.1.3: AC 1(1) to (5), AC 2, AC 3(1) to (3), AC 4, AC 5; Section 2.2.1.3.2.3: AC 1(1) to (5), AC 2; Section 2.2.1.3.3.3: AC 1(3), (6), (10), AC 2(5)]

General corrosion occurs uniformly across the waste package surface when the metal oxide passive film is stable. When the passive film is tenacious and slow growing, general corrosion occurs slowly. For example, propagation of 7.5 nm/yr, the mean corrosion rate for creviced Alloy 22 samples at 60°C, is equivalent to over 130,000 years per millimeter of passive metal. Thus, because the metal surface is expected to remain passive, waste package lifetimes are expected to be extremely long. In aggressive environments, when the passive film may become unstable, localized corrosion can occur (Section 2.3.6.4).

The effects of general corrosion of the waste package outer barrier will, in part, determine the estimated time to waste package breach and is accounted for in Section 2.3.4 to reflect waste package thinning. General corrosion may occur in the presence or absence of water (aqueous corrosion and dry oxidation). The TSPA conservatively applies aqueous general corrosion degradation rates to the waste package for all repository conditions and discounts dry oxidation which is slower than aqueous corrosion. Analysis of general corrosion provided in this section includes a conceptual description, review of experimental data and data uncertainty, analysis of the general corrosion model and model uncertainty, and abstraction and validation of the general corrosion model.

2.3.6.3.1 Conceptual Description

[NUREG-1804, Section 2.2.1.3.1.3: AC 1(1) to (4)]

General aqueous corrosion is defined as the uniform thinning of the waste package outer barrier due to electrochemical processes. This thinning at extremely low rates results from the formation and slow dissolution of a protective, passive film on the metal surface. The passive film is self-forming and self-healing when the metal is exposed in air and to moisture. The passive film is expected to last for extremely long periods of time and if it were to crack or spall off it would heal in a short time span (SNL 2007c, Section 6.4). As long as the passive film remains stable, the general corrosion rates remain extremely low. When aggressive environments break down the passive film, localized corrosion may occur, as described in Section 2.3.6.4. Below a certain relative humidity threshold general corrosion would be expected to be only due to dry air oxidation which occurs more slowly than aqueous corrosion. It is conservatively assumed that aqueous corrosion occurs for all relative humidities and temperatures (SNL 2007c, Section 6.4.3).

The general corrosion rate is treated as temperature-dependent and, for a given temperature, is assumed to be constant over time. The treatment of the rate as time independent rate is conservative because the general corrosion rate of passive metals decreases with time (SNL 2007c, Section 6.4.3). As discussed later in this section, the lower corrosion rates with time are related to the development of a more protective passive film due to changes in its composition and structure over time. The effectiveness of the passive film is expected to be greater when the passive film has been formed over long time periods, allowing for a decrease in the film defect density (e.g., a decrease in the number of potential sites for localized attack).

As discussed in the following sections, general aqueous corrosion rates of the waste package outer barrier have been estimated based on weight-loss measurements of descaled Alloy 22 samples after a 5-year exposure to repository-relevant aqueous environments. The tests provide a source of corrosion data for Alloy 22 in environments relevant to the repository (SNL 2007c, Section 6.4.3). In addition to long-term corrosion test results, general corrosion rates were also measured electrochemically to determine the temperature dependence of Alloy 22 general corrosion (SNL 2007c, Section 6.4.3).

2.3.6.3.2 Data and Data Uncertainty

[NUREG-1804, Section 2.2.1.3.1.3: AC 2, AC 3(1) to (3)]

Data have been collected and analyzed to understand the extent of general corrosion expected on the waste package outer barrier. This section describes the long-term weight-loss measurements, temperature dependence, effects of microbial activity associated with general corrosion of the waste package, and data uncertainty.

2.3.6.3.2.1 Long-Term Weight-Loss Measurements

Long-term weight-loss measurements are used to determine the general corrosion rates of Alloy 22 samples in three Long-Term Corrosion Test Facility test solutions (SDW, SCW, and SAW). These test solutions are shown in Table 2.3.6-1 (DTN: LL040803112251.117). The temperature of the test solutions were controlled at either 60°C or 90°C, and the solutions were covered with a blanket of flowing air. Three types of Alloy 22 samples (U-bends, crevice samples, and weight-loss samples) were mounted on insulating racks and placed in the sample test solution tanks. Approximately half of the samples were submersed, half were located above the aqueous phase, and a limited number were at the waterline. Condensed water was present on samples located above the aqueous phase (SNL 2007c, Section 6.4.3).

The corrosion rate of Alloy 22 was determined in accordance with ASTM G 1-90, *Standard Practice for Preparing, Cleaning, and Evaluating Corrosion Test Specimens* (1999). Two types of test samples (weight-loss samples and crevice samples (SNL 2007c, Section 6.4.3.1.2)) were analyzed for general corrosion. Figures 2.3.6-5 and 2.3.6-6 show the corrosion rates determined for these two types of samples after an exposure period of slightly more than 5 years. Both types of samples were tested in both the vapor and the liquid phases. U-bend specimens were used in the assessment of stress corrosion cracking susceptibility.

After a 5-year exposure to each test condition, samples were removed from their test vessels to determine the corrosion rate by weight-loss measurements. Other samples were removed after

6-month, 1-year, and 2-year exposures. In all of the test conditions, the samples were covered with deposits, so the samples were cleaned before final weighing. Cleaning was carried out following practices detailed in ASTM G 1-90 (1999).

The mean corrosion rates for the weight-loss samples (approximately 60 samples) ranged from 0 to about 10 nm/yr (about 14 nm/yr at a 95% confidence level) as shown in Figure 2.3.6-5. However, no clear-cut water chemistry dependency was observed for these concentrated waters. The mean corrosion rates for the crevice samples, shown in Figure 2.3.6-6, ranged from 0 to about 16 nm/yr (about 24 nm/yr at a 95% confidence level). In most cases, the crevice samples exhibited corrosion rates approximately 2 to 5 times higher than the weight-loss samples in the same solutions (SNL 2007c, Section 6.4.3.2). Stereomicroscopic and scanning electron microscope observations of both weight-loss and crevice samples indicated little or no corrosion for Alloy 22 (SNL 2007c, Section 6.4.3.2). The machining grooves remained uniform and sharply defined throughout each sample. Crevice or localized corrosion was not visually observed in microscope examination of any of the tested samples; however, as described, the corrosion rates of the crevice samples were higher than those of the weight-loss samples. This may be attributed to the slightly different final polishing of the two sample types prior to exposure. In the case of the weight loss samples, both sides were polished, while only one surface of the creviced samples was polished. As a result, the creviced samples had not had the mill-annealed oxide film removed from one side prior to testing. After exposure, the final cleaning removed this film, in effect resulting in an overestimate of the corrosion rate for these samples (SNL 2007c, Section 6.4.3.2). Among the approximately 60 weight-loss and approximately 60 creviced samples, a maximum measured corrosion rate of about 24 nm/yr (at a 95% confidence level) was observed (SNL 2007c, Section 6.4.3.2).

For both the weight-loss and crevice samples, the corrosion rates were generally lower for samples exposed to vapor than for samples immersed in liquid, regardless of the test temperature or electrolyte solution (Figures 2.3.6-5 and 2.3.6-6). Note that the corrosion rate in the vapor phase at 90°C for SAW is higher than the corrosion rate in the bulk fluid, which may be due to the presence of HCl volatilized from the bulk fluid into the confined space in the partially enclosed vessel. The presence of carbonates in the SCW, leading to higher carbon dioxide in the gas phase, did not appear to influence the corrosion rate in the vapor as compared to the bulk fluid. Because the corrosion rates were so low and the temperature range (60°C to 90°C) was small in this study, a clear dependence on the temperature cannot be established for any set of these samples other than the weight loss specimens exposed in SCW aqueous conditions which are discussed in Section 2.3.6.3.3.1. Finally, for the weight-loss samples, the presence of welds appeared to have no deleterious effect on the corrosion rate. In fact, the nonwelded crevice samples exhibited slightly higher corrosion rates than welded crevice samples (SNL 2007c, Section 6.4.3.2).

Most of the uncertainties in the general corrosion rate of Alloy 22 have resulted from resolution of the sample weight-loss measurements due to the extremely low corrosion rates of Alloy 22 in the test solutions. The combined standard uncertainty is estimated to be approximately 0.18 nm/yr in the case of crevice samples and 0.31 nm/yr in the case of weight-loss samples (SNL 2007c, Section 6.4.3.3). These estimates correspond to 1σ.

Since the corrosion rates measured for crevice samples were larger than those for uncreviced samples (weight-loss samples), the corrosion rate distribution of the crevice samples was conservatively used for the base-case general corrosion rate of the waste package outer barrier (SNL

2007c, Section 6.4.3.2). Because only about 3% of the total variation in the measured general corrosion rate of the crevice samples is due to the measurement uncertainty, all (100%) of the measured variation is considered to be due to the variability in the general corrosion processes. Besides variability in the data, uncertainty in the curve fitting is also accounted for in the model.

2.3.6.3.2.2 Temperature Dependence

The use of a temperature dependence term is appropriate because the general corrosion (passive dissolution) of highly corrosion-resistant alloys such as Alloy 22 is governed by the transport properties of reacting species in the passive film and the rate of activation-controlled ion transfer at the film-solution interface, both of which are thermally activated processes (SNL 2007c, Section 6.4.3.4). The temperature dependence of the general corrosion rate is determined from short-term polarization-resistance data for Alloy 22 samples tested for a range of sample configurations, metallurgical conditions, and exposure conditions (temperature and water chemistry) (SNL 2007c, Section 6.4.3.4). Figure 2.3.6-7 shows the modeled temperature dependence of mill-annealed and as welded Alloy 22 corrosion rates measured by the polarization-resistance technique over the temperature range from 60°C to 100°C. Results were extrapolated down to 25°C and upwards to 200°C with the assumption that there is no change in mechanisms (SNL 2007c, Section 6.4.3.4). Sample configuration (multiple crevice assembly or prism crevice assembly), metallurgical conditions (mill-annealed or welded), and water chemistry within the range expected in the repository have no significant effect on the temperature dependence of the general corrosion rate. This is corroborated through data not used to develop the model, shown in Figure 2.3.6-8, which also included welded samples with aging.

The data from Figure 2.3.6-7 were combined to arrive at the Alloy 22 general corrosion rate temperature dependence term (C_1) discussed in Section 2.3.6.3.3.1. The uncertainty in the temperature dependence data is represented in the general corrosion model by variation in C_1.

2.3.6.3.2.3 Effect of Microbial Activity

Microbially influenced corrosion is the contribution to the corrosion of a metal or alloy due to the presence or activity, or both, of microorganisms. Microbially influenced corrosion most often occurs due to the increase in anodic or cathodic reactions due to the direct impact of microorganisms on the alloy or by indirect chemical effects on the surrounding solution. Microorganisms can affect the corrosion behavior of an alloy either by acting directly on the metal or through their metabolic products (SNL 2007c, Section 6.4.5).

Laboratory testing at room temperature with live organisms cultured from Yucca Mountain rock was used to evaluate the effect of microbiological processes on the corrosion behavior of the waste package outer barrier (SNL 2007c, Section 6.4.5). Using polarization-resistance measurements, it was shown that microbially influenced corrosion can increase the general corrosion rates of Alloy 22 by a factor of, at most, 2 (SNL 2007c, Section 6.4.5). Room temperature average corrosion rates for Alloy 22 in Yucca Mountain environments with microbes, and in sterile (no microbe) environments, are shown in Table 2.3.6-3.

The microbially influenced corrosion data were obtained using 12 strains of Yucca Mountain bacteria, including acid, slime, and sulfide producers, as well as iron-oxidizing bacteria. The growth

medium was supplemented with 0.5% glucose and 0.75% protease peptone in 100× concentrated simulated J-13 well water (Lian et al. 1999). Because the data were obtained in a nutrient-rich environment, the effects of microbial activity on corrosion rates in these tests are expected to be greater than they will be in the repository environment, which is expected to be limited by the factors discussed in Section 2.3.6.3.3.2. Therefore, the effects of data uncertainty are adequately and conservatively represented in the microbially influenced corrosion model.

Electrochemical corrosion rate results were also obtained on welded Alloy 22 samples exposed to 100× J-13 water plus 0.1% glucose at ambient temperature (SNL 2007c, Section 6.4.5). The testing was carried out in both Yucca Mountain microorganism-inoculated and sterile environments using the techniques of ASTM G 59-97, *Standard Test Method for Conducting Potentiodynamic Polarization Resistance Measurements* (1998). The tests were run for 70 to 125 days at room temperature. Testing was conducted at room temperature since the likelihood of achieving microbially influenced corrosion effects is expected to be greatest when the viability of microbes is high, rather than at elevated repository temperatures when microbes cannot thrive (SNL 2007c, Section 6.4.5; BSC 2004b, Section 7.1). Results show that the corrosion rates obtained for welded samples in nonsterile environments were only slightly higher than those in sterile environments (SNL 2007c, Section 6.4.5) and consistent with the enhancement factor of, at most, two obtained from the nonwelded sample data shown in Table 2.3.6-3. The data also show that the corrosion rates for welded samples are essentially the same as those for nonwelded samples (SNL 2007c, Section 6.4.5).

Overall, the corrosion rates from the electrochemical tests in microbial environments are so low that a temperature dependency for microbially influenced corrosion cannot be established. Since microbes are less likely to thrive at elevated temperatures, the use of a multiplier developed at room temperature is conservative and appropriate for all temperatures.

The treatment and analysis of the effect of microbial activity is based on testing results. The effect of microbial activity is not a different mode of corrosion but rather is an effect on the environment in contact with the metal surface, resulting in an increase in the observed general corrosion rate above that observed in sterile environments.

2.3.6.3.3 Model and Model Uncertainty

[NUREG-1804, Section 2.2.1.3.1.3: AC 1(1) to (5), AC 4; Section 2.2.1.3.3.3: AC 2(5)]

The model and model uncertainty developed for general corrosion of the waste package outer barrier and the effect of microbially influenced corrosion are discussed in this section.

2.3.6.3.3.1 General Corrosion Model

The general corrosion model is constructed using weight-loss corrosion data (from creviced samples) with a temperature dependence term. A cumulative distribution function is produced for use in the abstraction model and, ultimately, the TSPA model (Section 2.4).

The general corrosion rate is modeled by the Arrhenius relationship:

$$\ln(R_T) = C_0 - \frac{C_1}{T} \quad \text{(Eq. 2.3.6-1)}$$

where

R_T = the temperature dependent general corrosion rate in nanometers per year

T = the absolute temperature in Kelvin

C_0 = defined in Equation 2.3.6-2

C_1 = a constant (determined from experimental data with associated uncertainty) equaling the activation energy divided by the universal gas constant

$$C_0 = \ln(R_0) + \frac{C_1}{333.15} \quad \text{(Eq. 2.3.6-2)}$$

where

R_0 = the general corrosion rate at 60°C (333.15 K).

The 60°C and 90°C crevice sample corrosion rates were used to establish the general corrosion rate of the waste package outer barrier at 60°C (R_0) (SNL 2007c, Section 6.4.3). The data used to generate the cumulative distribution function and the resulting cumulative distribution function are shown in Figure 2.3.6-9. The data were fit to a Weibull distribution. A Weibull distribution with a scale factor of 8.141 nm/yr, shape factor of 1.476 is used to describe the corrosion rate distribution. Uncertainty due to fitting to the Weibull Distribution is accounted for by assigning three levels of uncertainty. The lowest 5% uncertainty level uses a scale parameter of 6.628 nm/yr and a shape parameter of 1.380. The highest 5% uncertainty uses 9.774 nm/yr and 1.578, respectively. The medium 90% uncertainty level uses the best fit values of 8.134 nm/yr and 1.476, respectively (SNL 2007c, Section 6.4.3). A 5%-90%-5% uncertainty partitioning was selected to ensure the general corrosion rate distributions are separated from each other and yet are sampled enough times to be meaningful (SNL 2007c, Section 6.4.3).

The temperature-dependence term (C_1) was determined from short-term polarization-resistance data (SNL 2007c, Section 6.4.3). The corrosion rate data for mill-annealed and as-welded Alloy 22 samples were used to estimate the temperature dependence of the waste package outer barrier general corrosion using the solution compositions shown in Table 2.3.6-4. The corrosion rates from the polarization-resistance measurements at various temperatures were used for a comparative analysis to extract the temperature dependence of the corrosion rates. The measurements were not

intended for obtaining the absolute values of the corrosion rate, but rather their relative rates for determination of temperature dependence. From applying data in Figure 2.3.6-7 to the Arrhenius relation of Equation 2.3.6-1, the temperature-dependence term (C_1) was determined to have a mean of 4905 K and a standard deviation of 1413 K using a linear mixed-effects statistical analysis approach. A normal distribution was used for the parameter in the regression analysis. According to the Arrhenius relation, C_1 equals E_a/R, where E_a is the activation energy (J/mol), and R is the universal gas constant (8.314 J/mol K). This temperature dependence corresponds to an activation energy of 40.78±11.75 kJ/mol (SNL 2007c, Section 6.4.3.4). The apparent activation energies for the individual solutions and solutions not used for model development are shown in Table 2.3.6-5. Note that the individual solution activation energies fall within the modeled range. The modeled apparent activation energies obtained through the linear mixed-effects approach were then compared to apparent activation energies obtained by comparing the general corrosion rates for weight loss coupons exposed at 60°C and 90°C in SCW for 5 years. These apparent activation energies ranged from a minimum of 5.67 kJ/mol to a maximum of 64.94 kJ/mol, with a mean value of 40.51 kJ/mol. A comparison of the two methodologies is shown in Figure 2.3.6-10. Based upon this comparison, the normal distribution was truncated between +2σ (64.28 kJ/mol) and –3σ (5.54 kJ/mol) (SNL 2007c, Section 6.4.3.4) to cover the range of observed activation energies from these equilibrated samples.

The Arrhenius relationship is used to predict the temperature-dependent general corrosion rate (R_T) from the general corrosion rate at 60°C (R_0) and the temperature-dependence term (C_1).

$$\ln(R_T) = \ln(R_0) + C_1\left(\frac{1}{333.15} - \frac{1}{T}\right) \qquad \text{(Eq. 2.3.6-3)}$$

The resulting distribution of the temperature dependent general corrosion rate (R_T) at 25°C, 60°C, 100°C, 150°C, and 200°C for the medium uncertainty level and the mean apparent activation energy is shown in Figure 2.3.6-11. The range of Alloy 22 corrosion rates using the range of uncertainty levels is shown in Figure 2.3.6-12.

The general corrosion model implemented in the TSPA models the general corrosion of the Alloy 22 waste package outer barrier as occurring uniformly over each subarea patch into which the waste package surface is divided. The model is conservatively independent of relative humidity and with a time invariant corrosion rate (SNL 2007c, Section 6.4.3).

In general, however, the corrosion rates of metals and alloys decrease with time. This decrease is shown in Figure 2.3.6-13 for the mean general corrosion rates of Alloy 22 after 0.5-, 1-, 2-, and 5-year exposures and for shorter exposure time results. The trend of decreasing general corrosion rate with time is consistent with the expected corrosion behavior of passive alloys, such as Alloy 22. This alternative conceptual modeling approach for time-dependent general corrosion behavior of the waste package outer barrier was not included in the TSPA model because the constant (time-independent) rate model is more conservative and bounds the general corrosion behavior of the waste package outer barrier after repository closure (SNL 2007c, Section 6.4.3). Since the long-term time-dependent rates are expected to be lower than the 5-year rates, the 5-year corrosion rates were conservatively selected for extrapolation over the repository time scale.

The existing data collected in both short-term electrochemical tests and long-term corrosion tests are given in *General Corrosion and Localized Corrosion of Waste Package Outer Barrier* (SNL 2007c). Exposure time ranged from 1 day to 5-plus years, the latter from the Long Term Corrosion Test Facility. The data are plotted for tests conducted at 90°C in Figure 2.3.6-13 (SNL 2007c, Figure 7-1). The data points from the Long Term Corrosion Test Facility in the figure represent the mean of a large number of weight-loss samples (58 for the 5-year weight loss data). The trend in Figure 2.3.6-13 clearly shows the decrease of the general corrosion rate with time. Thus, the current conservative approach for a constant (time-independent) general corrosion rate at a given temperature provides an additional level of confidence in the general corrosion model.

2.3.6.3.3.2 Microbially Influenced Corrosion

Microbial activity in the moisture on a surface can change the chemical composition of waters and solids in the environment. These alterations to the environment can affect the electrochemical reactions on a metal surface and the behavior of passive films on the metal and subsequently affect the corrosion behavior. Microbially influenced corrosion is not another mode of corrosion like pitting or crevice corrosion, but microbially influenced corrosion can affect each of these modes of corrosion.

The following environmental factors will severely limit microbial activities in the repository:

- Microbial incubation experiments have demonstrated that water availability is the primary limiting factor for microbial growth in the repository. The relative humidity and the liquid-water saturation degree in the repository are predicted to be low during the thermal pulse, thus further limiting microbial activities.

- Evaporation of seepage waters in the low relative humidity environment will result in brine solutions with ionic strengths higher than 10 molar, which is an environment in which only a few halophiles may be able to survive.

- An oxic environment will prevail in the repository over the growth-permissive high-humidity and cooler period hundreds of years after peak temperatures are reached, and, therefore, prevent the generation and accumulation of reduced inorganic species that are the prerequisite for autotrophic metabolism.

- The extremely low levels of phosphate and organic carbon are important limiting factors for microbial growth in the repository. The extremely low organic carbon supply in the repository will limit heterotrophic microbial activities.

Because of elevated temperatures, radiation fields, low humidity, and low nutrient supplies, the formation of biofilms in the drift is not expected. Due to the aforementioned environmental constraints, microbial activity in the repository will be limited, and its impacts on drift chemistry and subsequently the environment on the waste package will be insignificant (BSC 2004b, Section 7.1) and the effect on general corrosion rates is accounted for using the uncertain corrosion multiplier described below.

Microbially influenced corrosion is the contribution to the corrosion rate of a metal or alloy by the presence or activity, or both, of microorganisms (SNL 2007c, Section 6.4.5). Microbially influenced corrosion most often occurs due to the increase in anodic or cathodic reactions caused by the direct impact of microorganisms on the alloy or by indirect chemical effects on the surrounding solution. Microorganisms can affect the corrosion behavior of an alloy either through direct action on the metal or through their metabolic products. Microorganisms can act to trigger known corrosion modes that would not occur in the absence of the microbes (Jack 2002). Some types of aerobic bacteria may produce sulfuric acid by oxidizing reduced forms of sulfur (elemental, sulfide, sulfite), or certain fungi transform organic matter into organic acids (Fontana 1986, Section 8-10; Tatnall 1993, Chapter 1, pp. 7-9; Jones 1996, Table 11.3). It has been observed in laboratory testing with live organisms cultured from Yucca Mountain rock that nickel-based alloys, such as Alloy 22, are resistant to microbially influenced corrosion (Lian et al. 1999). The linear polarization resistance results, potentially sensitive to many types of redox processes, are not necessarily indicative of actual corrosion rates, and therefore the results may overstate the effect of microbes on corrosion. Other oxidation-reduction reactions at these low current levels in the test media could have significant contributions to the measured values. Because these tests utilized the strains of bacteria found in Yucca Mountain rock (e.g., 12 strains of Yucca Mountain bacteria including acid, slime, and sulfide producers, as well as iron-oxidizing bacteria), the testing results are appropriate for the Yucca Mountain environment.

For general corrosion of the waste package outer barrier, the effect of microbially influenced corrosion can be described as follows:

$$CR_{MIC} = CR_{st} \cdot f_{MIC} \qquad \text{(Eq. 2.3.6-4)}$$

where CR_{MIC} is the general corrosion rate in the presence of microorganisms, CR_{st} is the general corrosion rate of the alloy in the absence of microbially influenced corrosion, and f_{MIC} is the microbially influenced corrosion factor. If f_{MIC} is greater than 1, there is an enhancement (i.e., increase) of the general corrosion rate of the alloy as a consequence of the presence or activity of microorganisms (SNL 2007c, Section 6.4.5).

The microbially influenced corrosion factor, f_{MIC}, is calculated as the ratio of corrosion rates (microbes to sterile) from Table 2.3.6-3. The value of f_{MIC} for Alloy 22 in sterile media is set to 1 ($f_{MIC} = 1$), whereas the value of f_{MIC} for Alloy 22 in inoculated media is larger ($f_{MIC} = 2$). The f_{MIC} value of 2.0 is a conservative upper limit because this value was obtained under conditions for the microbes to thrive (room temperature, ample food in the form of 0.5% glucose and 0.75% protease peptone) and all current from the electrochemical tests was conservatively considered to be entirely due to metal oxidation. The microbially influenced corrosion factor f_{MIC} is modeled to be uniformly distributed between 1 and 2, and this distribution is due to variability related to the effect of microbially influenced corrosion on the corrosion rate. The microbially influenced corrosion factor is applied at the patch level when the relative humidity at the waste package outer corrosion barrier surface is above a threshold value of 75% to 90% (sampled uniformly) (SNL 2007c, Section 6.4.5).

Environmental factors that affect levels of bacterial growth include temperature and radiation. These factors, however, are closely related to relative humidity; as temperature and radiation

decrease in the repository, relative humidity is predicted to increase. At the same time, while there are some types of microorganisms that can survive the elevated temperatures (≥120°C) and high-radiation doses, if there is no available water, then microbial activity is completely prevented. Thus, because water availability is the primary limiting factor and this factor is coupled to other less critical limiting factors, water availability (as expressed by relative humidity) was used as the primary indicator of microbial activity (SNL 2007c, Section 6.4.5; BSC 2004b, Sections 6.4 and 7.1).

This relative humidity threshold range is based on the viability of microbes in repository conditions. The low value is set at the minimum value at which microbes can be active (75%), and the high value is the relative humidity at which most microbes can thrive (90%) (SNL 2007c, Section 6.4.5). This treatment is appropriate and conservative because the other factors, such as limited nutrient supplies, will limit microbial activity (SNL 2007c, Section 6.4.5).

2.3.6.3.4 Abstraction and Adequacy

[NUREG-1804, Section 2.2.1.3.1.3: AC 4, AC 5]

This section provides a summary of the model for general corrosion of the waste package outer barrier, and an explanation of how the adequacy of the model was established.

2.3.6.3.4.1 Abstraction for General Corrosion

Two nominal waste package configurations are considered. The first waste package configuration is referred to as the commercial SNF waste package configuration, which contains a TAD canister loaded with either 21 PWR or 44 BWR fuel rods. The second waste package configuration is the codisposal waste package configuration where the waste package length is considered to be the length of the 5 DHLW/DOE SNF Long waste package configuration (Section 1.5.2). For the purposes of corrosion analysis, these two waste package types represent the different waste package configurations since they cover the range of waste package outer barrier diameters and lengths and account for the majority of the waste packages (SNL 2008a, Section 6.3.5).

General corrosion is implemented in the TSPA model by dividing the waste package surface into subareas (referred to as patches, with each patch having a surface area of 231.5 cm^2), which are used to simulate variability of general corrosion across the waste package surface. Figure 2.3.6-14 shows a schematic representation of a waste package whose surface is divided into patches. The general corrosion model is applied at the patch level, such that each patch might have a different general corrosion rate. When one or more patches are penetrated, the waste package is considered to be breached. The model output (Section 2.4) consists of the percentage of breached waste packages versus time and the average number of patch penetrations per breached waste package versus time (SNL 2008a, Section 6.3.5).

To account for spatial variability observed in the weight loss experiments, the analysis uses a patch size (231.5 cm^2) that is 4 times the size of the crevice test sample. The general corrosion rates are adjusted to account for the change in scale using a methodology based on published literature (Aziz 1956; Shibata 1996). This adjustment is performed by adjusting the general corrosion rate distribution in a manner that effectively uses the highest of four sampled corrosion rates as the general corrosion rate of the waste package patch (SNL 2008a, Section 6.3.5). The approach is

conservative because only one-fourth of the patch actually corrodes at the maximum rate resulting in larger openings earlier than if the patch size were smaller. This information is used by Section 2.3.7 for modeling releases (SNL 2008a, Section 6.3.5). For each TSPA realization, a single general corrosion rate is applied to each patch term on the Alloy 22 waste package outer corrosion barrier to account for variation in the Alloy 22 general corrosion rate. The fitting uncertainty term is selected once per realization as is the temperature dependence. Spatial and temporal variability in the temperature of the repository lead to spatial and temporal variability in the Alloy 22 general corrosion rates (SNL 2008a, Section 6.3.5).

When the waste package is breached by any mechanism, the waste package general corrosion model is also applied to the inner surface of the waste package outer barrier (inside-out corrosion). The inside-out corrosion could cause penetrations by general corrosion in addition to those caused by outside-in general corrosion alone. Conservatively, no credit is taken for the ability of the stainless steel inner vessel or the TAD canister to limit water influx to the waste form after the waste package is breached (SNL 2008a, Section 6.3.5).

The effect of microbially influenced corrosion on the general corrosion of the waste package outer barrier is described in Section 2.3.6.3.3.2. Equation 2.3.6-4 defines a microbially influenced corrosion factor (f_{MIC}) that is a multiplier to the general corrosion rate. The microbially influenced corrosion factor is applied to the waste package outer barrier general corrosion rate when the relative humidity at the waste package outer barrier surface is equal to or above a uniformly distributed relative humidity range of 75% to 90% (SNL 2007c, Sections 6.4.5 and 7.1). The microbially influenced corrosion factor is sampled by the TSPA model as a stochastic value uniformly distributed between 1 and 2 (SNL 2007c, Section 6.4.5) on a patch to patch basis. The evaluation concluded that the relative humidity threshold equal to or above the range of 75% to 90% for microbially influenced corrosion is expected to lead to an overestimate of the microbially influenced corrosion effect, because other factors (such as elevated temperature, high radiation dose, and limited nutrient supplies) will also limit microbial activity. Additionally, microbial activity in the repository will have negligible impacts to in-drift chemistry (BSC 2004b, Section 7.1). Microbial activity, including microbially influenced corrosion, is expected to be minimal in the Yucca Mountain repository. Thus, this representation of the microbially influenced corrosion factor is conservative (SNL 2007c, Section 6.4.5).

2.3.6.3.4.2 Model Adequacy

Adequacy of the general corrosion model of the waste package outer barrier is established by comparing the corrosion rates and passive film stability of Alloy 22 to similar materials (SNL 2007c, Section 7). General corrosion behavior (passive corrosion) similar to that of Alloy 22 has been observed for other nickel–chromium–molybdenum alloys. For example, Alloy C, a nickel-chromium alloy, (UNS N10002, Cr~15%, Mo~16%, Fe~5%, W~3.5%, Ni-balance (SAE 1993)), is found to retain a very thin passive film, indicated by the mirror-like finish that remained after 44 years of exposure to a marine environment (an aggressive environment of salt air with alternate wetting and drying as well as the presence of surface deposits) (Baker 1988, p. 134, Table 6) at Kure Beach. More recent examination of samples from this alloy after more than 50 years of exposure indicates that the samples continue to maintain a mirror-like finish and passive behavior (McCright 1998, Figure ES-1). Under these same conditions, the less corrosion-resistant nickel-chromium Alloy 600 (UNS N06600, Cr~15%, Fe~8%, Ni-balance (SAE 1993)) exhibited a

corrosion rate of 8 nm/yr after 36 years of exposure, a long-term corrosion rate consistent with the model predictions for Alloy 22. In comparable test conditions, the corrosion rate of Alloy 22 is comparable to or less than Alloy C and much less than that of Alloy 600.

The general corrosion model predicts Alloy 22 general corrosion rates at the 50th, 95th, and 99.99th (a reasonable upper bound) percentiles at 25°C to be 1.13, 3.04, and 6.50 nm/yr, using the medium level of uncertainty and the medium temperature dependence respectively (Figure 2.3.6-12; SNL 2007c, Section 7.2.1).

The general corrosion model predicts 50th, 95th, and 99.99th percentile rates at 150°C for the medium level of uncertainty and the mean apparent activation energy to be 145 nm/yr, 392 nm/yr, and 839 nm/yr, respectively. These values are considerably higher than those expected (i.e., less than 120 nm/yr) for Alloy C-4 in the 5-year time frame. Thus, the Alloy 22 general corrosion rate model predictions are reasonable estimates of the general corrosion rate of Alloy 22 at elevated temperatures (e.g., 150°C) and are sufficiently accurate for their intended use (SNL 2007c, Section 7.2.1).

The 200°C general corrosion model predictions for the low level of uncertainty and the highest temperature dependence range for the 50th, 95th, and 99.99th percentile rates are 4.88, 14.1, and 31.8 μm/yr, respectively. These results are extremely high. This suggests that the model results beyond 150°C may be highly conservative. Other researchers have reported Alloy 22 general corrosion rates up to 9.4 μm/yr at temperatures between 150°C to 180°C (SNL 2007c, Section 7.2.1).

The temperature dependence of the general corrosion rate of Alloy 22 uses an apparent activation energy of 40.78 ± 11.75 kJ/mol (± σ) truncated at +2σ and −3σ (SNL 2007c, Section 6.4.3.4). The temperature dependence has been studied by other investigators. Scully et al. (2001, Table 4, Section 2.1) reported an activation energy of 20 to 50 kJ/mol for Alloy 22, while another study reported an activation energy of 32 kJ/mol (Lloyd et al. 2003). An activation energy of 19 kJ/mol was calculated for Alloy C-4 (UNS N06455) (EPRI 2002, Section 5.3.2). Another study estimated activation energies of 19.3 kJ/mol after 4 weeks exposure, increasing to 25.3 kJ/mol after 8 weeks of exposure (Hua and Gordon 2004). The activation energies observed in other studies are similar to the mean value used in the general corrosion model 40.78 kJ/mol and the modeled range of values of 5.53 kJ/mol to 64.28 kJ/mol, thus confirming the model adequacy (SNL 2007c, Section 7.2.1). The adequacy of the microbially influenced corrosion analysis also is supported by the fact that the base rates used in the development of the general corrosion rate term are based upon weight loss samples in nonsterile solutions which also contained some microbes. The MIC multiplier is applied to those rates as if they did not already reflect some microbially influenced corrosion (SNL 2007c, Section 8.1).

2.3.6.4 Localized Corrosion of Waste Package

[NUREG-1804, Section 2.2.1.3.1.3: AC 1(1) to (5), AC 2, AC 3(1) to (3), AC 4, AC 5; Section 2.2.1.3.3.3: AC 1(3), (6), (10)]

Localized corrosion is a phenomenon in which corrosion progresses at discrete sites or in a nonuniform manner. At least upon initiation, the propagation rate of localized corrosion is faster than that of general corrosion. In a passive metal such as Alloy 22, for localized corrosion to occur

the passive film first must be compromised to allow an aggressive environment to contact the bare metal surface. Localized corrosion includes both pitting and crevice corrosion. Pitting corrosion normally requires much harsher conditions for its initiation than crevice corrosion. For example, screening tests in aggressive environments show that the critical pitting corrosion temperature is much higher than the critical crevice corrosion temperature (SNL 2007c, Section 6.4.4). In addition, pitting corrosion has not been observed in Alloy 22 tests in the range of expected environments at Yucca Mountain. Pitting corrosion has only been observed in Alloy 22 tests in very concentrated calcium chloride brine environments (10 *M* chloride) and its probability of occurrence decreases with the presence of nitrate (SNL 2007c, Section 7.2.4). Because crevice corrosion requires less aggressive conditions to initiate than pitting corrosion, the localized corrosion model treats all localized corrosion as crevice corrosion, and the discussion below focuses on the electrochemical potential and environment needed for crevice corrosion to occur in the repository.

2.3.6.4.1 Conceptual Description

[NUREG-1804, Section 2.2.1.3.1.3: AC 1(1) to (4)]

Alloy 22 rapidly forms a stable oxide film (passive film) that impedes the rate of electrochemical reactions (SNL 2007c, Section 6.4.1). Under aggressive environmental exposure conditions, the passive films may break down locally leading to localized attack of the underlying alloy.

From a localized corrosion perspective, five time periods are identified for any waste package. Section 2.3.5 describes the time-temperature history for the repository and waste packages. These time periods are:

1. Emplacement of waste packages and preclosure ventilation

2. Heat-up after closure

3. Cooldown period where waste package surface and drift wall are above the boiling temperature of water

4. Cooldown period where waste package surface is above the boiling point of water and the drift wall temperature is below the boiling point of water (dripping and seepage possible) and localized corrosion may occur

5. Waste package environment evolves to more benign conditions where localized corrosion is less likely.

The times for these periods vary from waste package to waste package depending on thermal load and heat transfer in the drift and to the surrounding rock. Period 4 is the time period when waters from the rock can fall onto hot metal surfaces. In most instances, the drip shield will be intact during this period protecting the waste package from seepage water contact. Should the drip shield fail to perform its function, these seepage waters may form concentrated solutions on the waste package. The possibility of localized corrosion initiation is modeled below. As the temperature drops, the probability of localized corrosion initiation decreases.

The localized corrosion model for the waste package outer barrier consists of an initiation component and a propagation component (SNL 2007c, Section 6.4.4). Localized corrosion initiation requires that the open-circuit corrosion potential (E_{corr}) exceed or equal a critical potential ($E_{critical}$) (SNL 2007c, Section 6.4.4):

$$E_{corr} \geq E_{critical} \qquad \text{(Eq. 2.3.6-5)}$$

E_{corr} is the open-circuit corrosion potential attained by a metallic sample immersed in a solution with no applied electrochemical driving force. In this analysis, $E_{critical}$ is defined as the potential below which a passive film will be stable on a metal surface (i.e., the passive film will reform spontaneously if damaged) and above which the metal can undergo localized corrosion. Experimentally, $E_{critical}$ is measured by E_{rcrev} as shown in Figure 2.3.6-15. As demonstrated by the experimental results, E_{corr} and $E_{critical}$ are functions of temperature, pH, and concentrations of chloride and nitrate ions and are modeled with these functional dependencies. Once localized corrosion initiates, the rate of propagation is conservatively modeled as a constant rate. A constant rate is conservative because it does not take credit for processes or changing conditions that would cause the propagation rate to slow or stop completely (Section 2.3.6.4.3.2) (SNL 2007c, Section 6.4.4). Furthermore, this treatment is conservative because when E_{corr} is more positive than $E_{critical}$, it is presumed that all of the other requirements for crevice corrosion are present (i.e., it is presumed that there is a crevice tight enough for initiation on all waste package surfaces).

Crevice areas could form where the waste package outer barrier surface will be in contact with the emplacement pallet Alloy 22 surfaces (Section 1.3.4). In addition, mineral deposits could potentially form on the surface due to evaporative concentration of solutions contacting the waste package. Corrosion rates may be enhanced where creviced geometries form on the waste package surface. The data used to develop the critical potential model were obtained from samples with extremely tight crevices. The results are conservative in that these crevices are more severe than those that may potentially occur where the waste package contacts the emplacement pallet or in areas where mineral deposits form due to evaporative concentration. This approach also is conservative because the initiation thresholds for crevice corrosion of Alloy 22 in terms of water chemistry and temperature are lower than for pitting corrosion (SNL 2007c, Section 6.4.4).

2.3.6.4.2 Data and Data Uncertainty

[NUREG-1804, Section 2.2.1.3.1.3: AC 2, AC 3(1) to (3)]

The waste package outer barrier localized corrosion initiation model consists of the long-term steady–state corrosion potential model and the crevice repassivation potential model (SNL 2007c, Section 6.4.4). The bases for these models was a series of tests performed on Alloy 22 samples over a wide range of exposure environments. Included in the tests were a variety of electrolyte solution chemistries, exposure temperatures, sample geometries and configurations, and metallurgical conditions. The long-term steady–state corrosion potential model was constructed using data from relatively dilute (in terms of chloride and nitrate ion content) mixed ionic solutions (e.g., SAW and SCW, pure chloride solutions (up to about 12 mol/kg Cl^-), and mixed chloride (up to about 13 mol/kg Cl^-) and nitrate (up to about 2.6 mol/kg NO_3^-) solutions. The maximum temperature for any data point used in construction of the long-term steady–state corrosion potential model was

120°C (Table 2.3.6-6). The crevice repassivation potential model was constructed using a range of solutions, including solutions with high nitrate concentrations (up to 18 mol/kg NO_3^-) and chloride (up to 36 mol/kg Cl^-) at temperatures up to 120°C (Table 2.3.6-7).

2.3.6.4.2.1 Open-Circuit Corrosion Potential Data

To evaluate the localized corrosion susceptibility of the waste package outer barrier (SNL 2007c, Section 6.4.4), the model uses the corrosion potential (E_{corr}) of Alloy 22 under different environmental conditions and the uncertainty associated with the corresponding corrosion potential. Corrosion tests conducted on Alloy 22 crevice samples in SDW, SAW, and SCW solutions for over 5 years did not show the initiation of localized corrosion (SNL 2007c, Section 7.2.4).

Table 2.3.6-6 contains the corrosion potential data used to develop the corrosion potential model for Alloy 22. Several conclusions drawn from the data influence the development of the parametric model for localized corrosion initiation:

- At 90°C, the E_{corr} of Alloy 22 in multiionic acidic SAW is approximately +400 mV versus Ag/AgCl and the E_{corr} in multiionic alkaline SCW is approximately –190 mV versus Ag/AgCl. Ennoblement (i.e., the development of a more stable passive film) in simulated concentrated groundwaters is more pronounced under acidic conditions.

- The presence of silicate does not influence the E_{corr} of Alloy 22 in SAW at 90°C.

- Long-term E_{corr} is dependent on the amount of nitrate present and the ratio of nitrate to chloride. In 5 mol/L $CaCl_2$ + 0.05 mol/L $Ca(NO_3)_2$ at 90°C the E_{corr} of nonwelded samples average approximately +147 mV versus Ag/AgCl while in 1 mol/L $CaCl_2$ + 1 mol/L $Ca(NO_3)_2$ at 90°C the E_{corr} of nonwelded samples average approximately +330 mV versus Ag/AgCl.

- The dependence of long-term E_{corr} on pH is shown in Figure 2.3.6-16 where E_{corr} is seen to decrease as pH increases (SNL 2007c, Section 6.4.4) and is not affected by the presence of welds.

Data uncertainty is addressed through the statistical fitting of the data within the model and by using replicate samples for a given set of conditions and multiple sets of conditions (e.g., T, pH, NO_3^-, Cl^-) and multiple samples over a wide range of environments (SNL 2007c, Section 6.4.4). A comparison of the data and the E_{corr} model is shown in Figure 2.3.6-17.

2.3.6.4.2.2 Cyclic Polarization Data

To evaluate the localized corrosion susceptibility of the waste package outer barrier (SNL 2007c, Section 6.4.4), the model uses a critical potential ($E_{critical}$) for Alloy 22 under a range of environmental conditions (Table 2.3.6-7). While there are several criteria for determining $E_{critical}$, one conservative method is to use the crevice repassivation potential determined from cyclic potentiodynamic polarization tests. Thus, for this analysis, $E_{critical}$ is defined as the crevice repassivation potential (E_{rcrev}).

Cyclic potentiodynamic polarization is used to evaluate localized corrosion under a range of exposure conditions (e.g., temperature, solution composition) relevant to the repository environment. In these tests (shown schematically in Figure 2.3.6-15), the potential of the sample is progressively increased (scanned) positive from near the measured open-circuit corrosion potential into oxide film breakdown (current rises very rapidly), then the potential is scanned back toward the open-circuit corrosion potential. Note that for the comparison between materials shown in the figure, the test conditions were similar but not identical. When the oxide film is removed in the breakdown region, the oxide cannot reform until the potential reaches less positive potentials. The crevice repassivation potential (E_{rcrev}) is defined as the potential at which the reverse current crosses the forward current. The hysteresis on the return sweep is a qualitative indicator that localized corrosion has occurred during the test (however, not all tests initiate localized corrosion). This measure is inherently conservative, as the potential where breakdown initiates ($E_{breakdown}$ or E_{pit} which is a more positive potential) could also be used rather than using the crevice repassivation potential (E_{rcrev}) to define $E_{critical}$ (SNL 2007c, Section 6.4.4). Alloy 22 has a high resistance to localized corrosion, and tests conducted in many solutions do not show oxide film breakdown. In fact, few data exist from tests that do show localized corrosion under repository conditions. Thus, the crevice repassivation or breakdown potential cannot always be determined.

Schematic cyclic potentiodynamic polarization curves for three materials (Stainless Steel Type 316L, Alloy 22, and Titanium Grade 7) are shown in Figure 2.3.6-15. These curves show the trend in how the curves change with increasing localized corrosion resistance. The difference (ΔE) between the corrosion potential (E_{corr}) and the repassivation potential (E_{rcrev}) is labeled for Alloy 22. The magnitude of ΔE is a measure of the resistance to localized corrosion initiation (SNL 2007c, Section 6.4.4).

A series of the cyclic potentiodynamic polarization tests was performed for Alloy 22 samples over a range of exposure environments, including electrolyte solution chemistry and temperature (SNL 2007c, Section 6.4.4). Also included in the tests were a variety of sample geometries and configurations (e.g., multiple crevice assembly, rod, and disc) and varying metallurgical conditions (e.g., mill-annealed, as-welded, and as-welded plus thermally aged). The samples were held in solution for a minimum of 24 hours prior to testing (SNL 2007c, Section 6.4.4.2). Data were taken under aggressive conditions where a repassivation potential was observed. It was found that the crevice repassivation potential in solutions without nitrate ions was lower than in solutions with nitrate ions. Thus, nitrate is acting as an inhibitor to localized corrosion initiation. It was found that addition of nitrate ions to chloride solutions generally resulted in an increase in the crevice repassivation potential.

The above test data were obtained from as-welded samples with tightly creviced geometries. The samples included the weld, heat-affected zone, and base metal. In addition, data that did not show the occurrence of localized corrosion were excluded in the analysis. This is a conservative approach in that excluding data that did not show evidence of localized corrosion will skew the results in favor of localized corrosion initiation.

Data uncertainty is addressed through the statistical regression analysis of the data within the model, which provides for the coefficient uncertainties and the error terms, and by using replicate samples for a given environment and a wide range of environments (SNL 2007c, Section 6.4.4).

2.3.6.4.2.3 Localized Corrosion Propagation Rate Data

Upon the initiation of localized corrosion, the propagation depth is conservatively modeled using a constant rate. Due to the superior corrosion resistance of Alloy 22, few data exist for localized corrosion and propagation rates under repository conditions. Instead, a range of potential localized corrosion rates is determined for two highly aggressive environments: (1) 10 wt % $FeCl_3$ test solution (12.7 µm/yr) (Haynes International 1997a, p. 8) and (2) concentrated HCl solutions at elevated temperatures (where passive film is degraded), with corrosion rates between 127 and 1,270 µm/yr (Haynes International 1997b, p. 12). The use of an Alloy 22 corrosion rate of 12.7 µm/yr measured in a $FeCl_3$ solution containing about 2.1 *m* chloride ions at 75°C is a suitable analogue crevice solution for estimating the lower bound for metal dissolution (SNL 2007c, Section 6.4.4) because this represents a transpassive corrosion condition.

Data uncertainty is captured through sampling across the 2-order-of-magnitude spread in corrosion rates for various aggressive environments (SNL 2007c, Section 6.4.4.7).

2.3.6.4.3 Model and Model Uncertainty

[NUREG-1804, Section 2.2.1.3.1.3: AC 1(1) to (5), AC 4]

This section discusses the initiation and propagation components of the localized corrosion model.

2.3.6.4.3.1 Localized Corrosion Initiation Model

This section describes the initiation model development, model results, and model conservatisms.

2.3.6.4.3.1.1 Localized Corrosion Initiation Model Development

Localized corrosion initiates when the long-term corrosion potential E_{corr} is equal to or greater than the critical potential ($E_{critical}$). This is expressed mathematically as $\Delta E \le 0$, where $\Delta E = E_{critical} - E_{corr}$. The critical potential $E_{critical}$, defined as the crevice repassivation potential E_{rcrev}, is the potential below which the Alloy 22 surface undergoes spontaneous repassivation (i.e., E_{rcrev} in the following discussions is equivalent to $E_{critical}$ in prior sections) (SNL 2007c, Section 6.4.4).

Based on parametric analysis, the crevice repassivation potential, E_{rcrev}, is represented as a function of exposure parameters (SNL 2007c, Section 6.4.4.3.1):

$$E_{rcrev} = a_o + a_1 T + a_2 \ln[Cl^-] + a_3 \frac{[NO_3^-]}{[Cl^-]} + a_4 T \cdot [Cl^-] + \varepsilon_{rcrev} \qquad \text{(Eq. 2.3.6-6)}$$

The coefficients to be determined in this equation are a_0, a_1, a_2, a_3, and a_4; T is the temperature (°C), $[NO_3^-]$ is the molal nitrate concentration (moles per kilogram of water) and $[Cl^-]$ is the molal chloride concentration (moles per kilogram of water). The error term, ε_{rcrev}, represents data variance not explained by the fitting procedure.

The model coefficients were fit to the crevice repassivation potential data using regression analysis (SNL 2007c, Section 6.4.4). The value of the coefficients and their uncertainty (±1σ) from the fitting were determined to be: a_0 = 190.242 ± 18.373, $a_1 = -3.008 \pm 0.225$, $a_2 = -46.800 \pm 3.126$, $a_3 = 535.625 \pm 26.140$, and $a_4 = 0.061 \pm 0.010$. The error term, ε_{rcrev}, has a normal distribution with a mean of zero mV versus the saturated silver chloride electrode and a standard deviation of 45.055 mV versus saturated silver chloride electrode.

Variations in the crevice repassivation potential data for a given test condition are due to uncertainties associated with test procedures and to some randomness in the localized corrosion process (SNL 2007c, Section 6.4.4). Therefore, the entire variance of the model is attributed to uncertainty. The approach and criteria for obtaining the crevice repassivation potentials from the cyclic potentiodynamic polarization curves are conservative. Therefore, bounding the uncertainty of the model parameters to ±2σ is appropriate. Figure 2.3.6-18 provides a comparison of the model with truncation to the experimental data. The coefficient of determination R^2 is 0.829. An R^2 value of 0.829 indicates that the regression model fits the experimental data well.

A parametric model for the long-term steady-state corrosion potential of the Alloy 22 waste package outer barrier was developed (SNL 2007c, Section 6.4.4.5). This model is expressed as follows:

$$E_{corr} = c_o + c_1 T + c_2 pH + c_3 \frac{[NO_3^-]}{[Cl^-]} + c_4 T \frac{[NO_3^-]}{[Cl^-]} + c_5 pH \frac{[NO_3^-]}{[Cl^-]} + c_6 pH \ln[Cl^-] + \varepsilon_{corr} \quad \text{(Eq. 2.3.6-7)}$$

The estimated regression coefficients and their uncertainty (±1 standard deviation) are as follows: $c_0 = 1051.219 \pm 119.774$, $c_1 = -3.024 \pm 0.977$, $c_2 = -155.976 \pm 11.495$, $c_3 = -1352.040 \pm 252.224$, $c_4 = 10.875 \pm 1.890$, $c_5 = 137.856 \pm 23.158$, and $c_6 = -8.498 \pm 0.801$. The error term, ε_{corr}, is a term representing data variance that is not explained by the fitting procedure, and which has a normal distribution with a mean of zero mV saturated silver chloride electrode, and a standard deviation (referred to as s_{corr}) of 85.265 mV versus saturated silver chloride electrode. The entire variance is due to uncertainty, which is accounted for by sampling at ±2σ. Figure 2.3.6-17 provides a comparison between the truncated model and the experimental data. The coefficient of determination, R^2, is 0.872 demonstrating that the regression model fits the experimental data well.

Note that Equations 2.3.6-6 and 2.3.6-7, above, are based on parametric analysis and the equations do not suggest a functional form related to chemical or electrochemical processes. Temperature, pH, and molal concentrations were parameters of interest, and the parametric relationships that were developed as presented in these equations.

General Corrosion and Localized Corrosion of Waste Package Outer Barrier (SNL 2007c, Section 6.4.4) describes a number of experimental measurements of the long-term corrosion potential of Alloy 22 at various temperatures, pH values, and NO_3^- and Cl^- concentrations that were used to develop a model for the long-term corrosion potential (E_{corr}).

Because only nitrate ions are accounted for in the localized corrosion initiation model for the inhibitive effect, the model results for solutions with significant amounts of other potentially inhibitive ions, such as carbonate and sulfate (in addition to nitrate ions), are conservative (SNL 2007c, Section 8.3.1). The localized corrosion initiation model is developed using data from laboratory solutions that contained nitrate ions and that did not contain other potentially inhibitive ions such as carbonate and sulfate. The presence of other inhibitive ions in repository waters would be expected to result in a more benign environment than that which would be predicted by the localized corrosion initiation model.

The model results for the effects of the inhibitive nitrate anion, combined with the alkaline pH conditions of the typical carbonate waters in the repository, are consistent with the experimental observations of no localized corrosion susceptibility of Alloy 22 in similar waters (SNL 2007c, Section 8.3.1).

2.3.6.4.3.1.2 Localized Corrosion Initiation Model Results

The localized corrosion initiation model, as defined in Section 2.3.6.4.1, compares the long-term steady-state corrosion potential (E_{corr}) and the crevice repassivation potential ($E_{critical}$) or (E_{rcrev}) defined in Section 2.3.6.4.3.1.1 to determine whether localized corrosion will initiate.

Figures 2.3.6-19, 2.3.6-20, and 2.3.6-21 illustrate the effect of temperature and pH on the localized corrosion susceptibility of Alloy 22 in a 6 *m* chloride-based brine containing 1.8 *m* nitrate ions (NO_3/Cl ratio = 0.30). Figure 2.3.6-19 shows the model results at a pH of 7. Given that there is very little overlap of the prediction intervals, crevice corrosion initiation is expected to be a rare event under these exposure conditions. The mean crevice repassivation potential curve does not cross the mean long-term corrosion potential curve at any exposure temperature below 120°C. The +2σ long-term corrosion potential prediction interval crosses the −2σ crevice repassivation potential prediction interval at about 90°C. The +2σ long-term corrosion potential prediction interval crosses the −1σ crevice repassivation potential prediction interval at about 105°C. The greater the amount of overlap of the prediction intervals, the more probable is the initiation of crevice corrosion, meaning that at 110°C, crevice corrosion initiation is more probable than at 100°C. Crevice corrosion will not initiate at temperatures below about 90°C under these exposure conditions according to this model. As shown in Figure 2.3.6-20, with a decrease in pH to 5, the long-term open circuit potential at each temperature increases. The mean long-term corrosion potential crosses the mean crevice repassivation potential curve at about 95°C, and crevice corrosion initiation becomes more probable as temperature increases. As shown in Figure 2.3.6-21, with a further decrease of pH to a value of 4, the mean long-term corrosion potential crosses the mean crevice repassivation potential curve at about 50°C and the initiation of crevice corrosion is modeled to be probable over the entire temperature range from 30°C to 120°C (SNL 2007c, Section 6.4.4).

Figures 2.3.6-22 and 2.3.6-23 illustrate the effect of temperature and nitrate-ion concentration on the crevice corrosion susceptibility of Alloy 22 in a 6 *m* chloride-based brine at a pH of 4. Figure 2.3.6-22 shows the model results as a function of temperature, with a nitrate concentration of 3 m (NO_3/Cl ratio of 0.50). The mean long-term corrosion potential and crevice repassivation potential curves cross at about 80°C. The +1σ prediction interval long-term corrosion potential curve crosses the −1σ crevice repassivation potential prediction interval curve at about 53°C. In Figure 2.3.6-23, an increase of nitrate concentration to 6 m (NO_3/Cl ratio of 1.0) indicates that

crevice corrosion initiation is not expected below about 75°C and the mean long-term open circuit potential and crevice repassivation potential curves cross at about 102°C (SNL 2007c, Section 6.4.4.

Figures 2.3.6-24 and 2.3.6-25 illustrate the effect of chloride-ion concentration and pH on the localized corrosion susceptibility of Alloy 22 in a chloride-based brine with a nitrate-ion concentration of 3 *m* at a temperature of 90°C. Figure 2.3.6-24 shows the model results versus chloride-ion concentration for a solution with a pH of 7. Above a chloride concentration of about 7.5 *m*, the prediction intervals do not overlap, indicating that crevice corrosion initiation is not predicted to occur under these exposure conditions. The mean long-term corrosion potential and crevice repassivation potential curves cross at a chloride-ion concentration of about 1 *m*. The discontinuous change in slope at 3 m chloride is a consequence of constraining the nitrate ion-to-chloride-ion ratio to values at or below 1 in evaluating the models. There is also a change in slope at 20 *m* chloride, which is a consequence of constraining the chloride-ion concentration to values below 20 *m* in evaluating the models. Figure 2.3.6-25 show the model results at pH 4 and 90°C. The model predicts that the mean long-term corrosion potential and crevice repassivation potential curves cross at a chloride-ion concentration just below 5 *m*. A comparison between Figures 2.3.6-24 and 2.3.6-25 indicates that increases in chloride concentration decrease the likelihood of crevice corrosion initiation at pH 7 and increase the likelihood of crevice corrosion initiation at pH 4.

Figures 2.3.6-26 and 2.3.6-27 illustrate the localized corrosion susceptibility versus nitrate concentration. As shown in Figure 2.3.6-26 at 90°C, 6 *m* chloride-ion concentration, and a pH of 7, the -2σ prediction interval for the crevice repassivation potential and the $+2\sigma$ prediction interval for the long-term corrosion potential cross at a nitrate-ion concentration of about 2.5 *m*. Overall, given the very small amount of overlap between the prediction intervals, crevice corrosion initiation is not expected. As shown in Figure 2.3.6-27, for a 6 m chloride-ion solution at a pH of 4 at 90°C, the mean long-term corrosion potential and crevice repassivation potential curves cross at a nitrate-ion concentration of about 3.8 *m*. A comparison of Figures 2.3.6-26 and 2.3.6-27 indicates that, while increases in nitrate-ion concentration at pH 7 increase the likelihood of crevice corrosion initiation, at pH 4 increases in nitrate-ion concentrations decrease the likelihood of crevice corrosion initiation.

2.3.6.4.3.1.3 Conservatism for Localized Corrosion Initiation Model

Localized corrosion initiates when the passive film breaks down at local sites. Aggressive species (e.g., chloride ions) in solution facilitate localized attack at these sites. The localized corrosion initiation model uses the crevice repassivation potential as the critical potential (e.g., a majority of the data used in model development was collected from samples with crevice formers). Crevice repassivation potentials from short-term cyclic potentiodynamic polarization tests are a conservative measure of the critical potential for localized corrosion initiation of the waste package outer barrier because the initiation threshold for crevice corrosion in terms of water chemistry and temperature is lower than for pitting corrosion (Gdowski 1991, Section 3; Haynes International 1997b), which is another form of localized corrosion that may attack exposed surfaces. The chemical environment in a creviced region may be more aggressive than on an exposed surface due to metal ion hydrolysis in the creviced region leading to a decrease in pH (more acidic conditions). Electromigration of chloride ions (or other anions) into the crevice must occur to balance the charge

within the creviced region (Jones, D.A. 1996, pp. 220 to 222), increasing the severity of the solution in the creviced region unless the other ions are nitrate, sulfates or other inhibiting anions.

Crevices may form on the waste package surface at occluded regions, such as in between the waste package and the emplacement pallet Alloy 22 surfaces and potentially beneath mineral scales, corrosion products, and rocks. It is not expected that the entire waste package surface will be subjected to crevice-like conditions; therefore, application of the crevice repassivation potential model as a criterion for the initiation of localized corrosion to the area subjected to seepage, is conservative (SNL 2007c, Section 6.4.4).

An alternative method for the determination of critical potential would be to use the passive film breakdown potential (obtained from the forward scan of the cyclic potentiodynamic polarization tests). The breakdown potential could be considered as the potential where localized corrosion initiates under the conditions (sample and environment) examined. If the cyclic potentiodynamic polarization curve displays hysteresis (the reverse sweep current exceeds the forward sweep), this criterion would not account for the (often slow) kinetics of localized corrosion initiation and may not be appropriate for modeling the long time periods associated with repository performance. Furthermore, the breakdown potential is expected to be higher when the passive film has been formed over long time periods, allowing for a decrease in the film defect density (e.g., a decrease in the number of potential sites for localized attack) (Blackwood et al. 1988; Pan et al. 1997; SNL 2007c, Section 6.4.4).

The modeling approach did not incorporate a critical temperature below which no localized corrosion would occur, regardless of other conditions in the bulk chemical exposure environment. In fact, the empirical rules used to implement the corrosion initiation model (Section 2.3.6.4.4.1) include evaluation of corrosion initiation down to exposure temperatures as low as 20°C.

2.3.6.4.3.2 Localized Corrosion Propagation Model

When localized corrosion of the waste package outer barrier occurs, it is modeled as propagating into the waste package at a constant rate. This treatment is conservative because the localized corrosion rate tends to decrease with time and, in a number of metal/environment systems, to arrest shortly after initiation (Hunkeler and Boehni 1983; Marsh et al. 1991; Mughabghab and Sullivan 1989; Sharland et al. 1994; Ishikawa et al. 1994). While this arrest phenomena is seen in many systems, in other cases localized corrosion will continue. Results are presented here that demonstrate where stifling and arrest processes occurred with Alloy 22 in the given environments. The time-dependent alternative conceptual model is discussed in Section 2.3.6.4.3.2.2.

2.3.6.4.3.2.1 Localized Corrosion Constant Propagation Model

The localized corrosion propagation rates for the waste package outer barrier are modeled to range from 12.7 to 1,270 µm/yr with a median value of 127 µm/yr, as shown in Table 2.3.6-8 (SNL 2007c, Section 6.4.4). A loguniform distribution between the bounds was used for the localized corrosion propagation rate. Selection of this distribution was appropriate because the propagation rate values from the literature span 3 orders of magnitude. This distribution is based on data that bound those extreme propagation rates found in the literature and are a conservative representation of localized corrosion rates of Alloy 22 for the exposure conditions expected in the postclosure period. The

entire variance in the propagation rate is due to uncertainty. Although localized corrosion can be conservatively bounded by this distribution, it is expected that, once initiated, the localized corrosion propagation rate would decrease with increasing depth, as discussed in the alternative conceptual model (Section 2.3.6.4.3.2.2).

2.3.6.4.3.2.2 Alternative Conceptual Model for Time-Dependent Propagation Rate

An alternative conceptual model for localized corrosion propagation is a time-dependent growth law model. The growth law model can be developed based on a combination of electrochemical and corrosion exposure measurements. Many experiments demonstrate that the approach can be applied to pitting corrosion, which is another form of localized corrosion. Thus, a growth law model was considered as an alternative conceptual model.

A pitting model based on hemispherical pit growth yields a propagation law of the following form (CRWMS M&O 1998, Table 3-2; Hunkeler and Boehni 1983; McGuire et al. 1998, Section 5.2.8):

$$D = k \cdot t^n \qquad \text{(Eq. 2.3.6-8)}$$

where D is the depth of propagation, t is time, n is the time exponent, and k is a growth constant. The growth constant is dependent on the properties of the material, particularly its susceptibility to anodic dissolution in the acidic environment prevailing in a localized corrosion site. The time exponent, n, is about 0.5 for both diffusion-controlled (e.g., diffusion of metal ions out of the pit) and ohmically controlled (e.g., rate determined by the ohmic potential drop that develops in the electrolyte in the pit) pit growth (McGuire et al. 1998, Section 5.2.8; Vetter and Strehblow 1974). This growth law model was used in a separate analysis for the repository by the Electric Power Research Institute (EPRI 2002, Section 5.3.1).

The literature data available for less corrosion-resistant materials (Hunkeler and Boehni 1983; Marsh et al. 1991; Mughabghab and Sullivan 1989; Sharland et al. 1994; Ishikawa et al. 1994) clearly show that a propagation growth law of the form of Equation 2.3.6-8 is appropriate and that a value of n equal to 0.5, the theoretically predicted value, is justifiable. A key point regarding the materials discussed in the literature (e.g., iron, carbon steel, copper, and Titanium Grade 2 (UNS R50400)) is that they are materials that would be expected to undergo rapid localized corrosion propagation. If it is not stifled by the accumulation of corrosion product deposits or slow cathodic kinetics, propagation would be limited only by diffusive or ohmic effects, leading to a value of n approaching 0.5.

By contrast, for highly corrosion-resistant materials that are designed to resist localized corrosion, such as Alloy 22, additional metallurgical characteristics are important in determining the value of n. One example of such a metallurgical influence that is pertinent to the case of Alloy 22 is the ability of molybdenum to decrease the pitting current densities in stainless steels, possibly by reducing the active dissolution rate within the pit (Frankel 1998; Newman 1985). This prevents the critical pit or crevice chemistry needed to sustain propagation, leading to repassivation. In this situation, the n value in the growth law in Equation 2.3.6-8 effectively tends to 0. The depth of crevice propagation for Alloy 22 was electrochemically driven in extremely saline (5 mol/L LiCl)

solutions at 85°C and was limited to less than 100 μm, a finding that supports this repassivation claim (Kehler et al. 2001). The adoption of such a value assumes that metallurgical features, such as the influence of molybdenum on pits and crevices, will suppress propagation (SNL 2007c, Section 6.4.4.8.2).

The localized corrosion propagation model was selected for use in TSPA because it is more conservative than the growth law model. If implemented, the growth law model would result in longer time frames prior to waste package breach by localized corrosion (SNL 2007c, Section 6.4.4).

2.3.6.4.4 Abstraction and Adequacy

[NUREG-1804, Section 2.2.1.3.1.3: AC 4, AC 5]

2.3.6.4.4.1 Abstracted Model for Localized Corrosion

The abstracted model for localized corrosion addresses initiation, propagation, and the affected area.

Localized Corrosion Initiation—In order for localized corrosion to initiate, seepage water must contact the waste package. For intact or moderately degraded drifts, seepage water will not contact the waste package surface if the drift wall exposure temperature is above the boiling point of water (taken to be 100°C) in the drift (SNL 2007f, Sections 6.5.2 and 8.1). The waste package surface temperature is 120°C or below when the drift wall exposure temperature is 100°C or below (SNL 2008b, Figure 6.3-76[a] and 6.3-81[a]). For collapsed drifts, seepage water will not contact the waste package surface unless the temperature of the waste package surface is below the boiling point of water (SNL 2007f, Section 6.5.3). Therefore, the waste package outer barrier localized corrosion initiation model is only used to evaluate the potential for localized corrosion initiation due to seepage water contact (which can only occur when the waste package outer barrier surface temperature is below 120°C) (SNL 2007c, Section 6.4.4.6.6).

Therefore, when seepage water contacts the waste package, the following set of rules, based on the localized corrosion initiation model results, is used to implement that model (SNL 2007c, Sections 6.4.4.6.6, and 8.3.1):

- If localized corrosion is determined to initiate, then localized corrosion continues to occur regardless of changes in the bulk chemical exposure environment. This is conservative because as conditions become more benign crevice corrosion may cease. Furthermore, as corrosion continues, the crevice may open up and corrosion stifle.

- If the nitrate-to-chloride ion ratio in the environment exceeds 1.0, then evaluate E_{rcrev} and E_{corr} at a nitrate-to-chloride ion ratio of 1.0. This treatment is conservative because, at a given temperature and chloride-ion concentration, E_{rcrev} increases markedly with nitrate-ion concentration, while E_{corr} is less sensitive than E_{rcrev} to nitrate-ion concentration at lower pH values where crevice corrosion is more likely to initiate.

- If the molality of chloride ion in the environment exceeds 20 molal, then evaluate E_{rcrev} and E_{corr} at a molality of chloride ion of 20 molal. This treatment is conservative because,

at high chloride concentrations, the likelihood of crevice corrosion decreases with increasing chloride concentration.

- If the molality of chloride ion is less than 0.0005 molal, then evaluate E_{rcrev} and E_{corr} at a molality of chloride ion of 0.0005 molal. This treatment is conservative because allowing this term to approach zero would result in unrealistically high nitrate to chloride ratios, which would act to artificially reduce the likelihood of localized corrosion initiation.

- If the pH in the environment exceeds 10, then evaluate E_{corr} at a pH of 10. This treatment is conservative because E_{corr} decreases with increasing pH decreasing the likelihood of localized corrosion.

- If the pH in the environment is less than 1.9, then initiate localized corrosion. This treatment is conservative because localized corrosion will not occur in all environments with a pH less than 1.9.

Each of the above chemical limits has been determined to result in a conservative application of the localized corrosion model (SNL 2007c, Section 6.4.4.6.6). In addition to these rules, as discussed in Section 2.3.5, if seepage occurs at a relative humidity less than the predicted relative humidity of chloride or nitrate salt precipitation (~77%) (Section 2.3.5.5), then localized corrosion is initiated to account for the possibility of salt separation (SNL 2007c, Section 8.3.1).

Note, the salt separation aspects of localized corrosion initiation were not implemented.

Localized Corrosion Propagation—The localized corrosion propagation rate abstraction is discussed in Section 2.3.6.4.3.2.1. If aqueous brine chemistry causes the initiation of localized corrosion, then localized corrosion is modeled to continue to propagate regardless of changes in the bulk chemical exposure environment. This is a conservative modeling assumption that is implemented since no detailed model of the chemistry evolution of the crevice solution is available at this time.

Localized Corrosion Affected Area—If localized corrosion due to seepage brines occurs, the affected area is modeled as the wetted waste package surface underneath the breached portion of the drip shield (SNL 2007c, Section 6.4.4). This treatment is conservative, because the model is based upon samples with tight crevices, and only the area between the waste package and the emplacement pallet will be tightly creviced.

Brines produced from dust deposits onto the Alloy 22 waste package outer barrier will not generate a favorable environment for localized corrosion initiation and growth. If brine exists at elevated temperatures (>120°C), it will be benign, rather than corrosive, and initiation of localized corrosion and subsequent penetration of the waste package outer barrier are not expected. The quantity of brine at elevated temperatures is small, which hinders corrosion initiation and extent. Thus, the overall consequence of dust deliquescence on the localized corrosion of the waste package outer barrier will be insignificant. Therefore, localized corrosion of Alloy 22 due to dust deliquescence is excluded from TSPA (Section 2.2, Table 2.2-5, FEP 2.1.09.28.0A).

2.3.6.4.4.2 Localized Corrosion Model Adequacy

2.3.6.4.4.2.1 Localized Corrosion Initiation Model Adequacy

In the localized corrosion initiation model, localized corrosion of the waste package outer barrier occurs when the long-term steady–state open-circuit corrosion potential (E_{corr}) is equal to or greater than a critical potential. The crevice repassivation potential (E_{rcrev}) is used as the critical potential, that is, localized corrosion initiates when ΔE (defined as $E_{rcrev} - E_{corr}$) is less than or equal to zero (SNL 2007c, Section 6.4.4.1).

This conceptual model of localized corrosion initiation is recognized by the corrosion community and has appeared in numerous published studies: (Böhni 2000, Section B; Dunn, Cragnolino et al. 2000; Dunn, Yang et al. 2003; Frankel 1998; Frankel 2002; Frankel and Kelly 2002; and Beavers et al. 2002, Section 8.3). The following data, which were not used to develop the localized corrosion model, are used to demonstrate the model adequacy.

Measurements of the open-circuit corrosion potential of Alloy 22 under air-saturated conditions in a 6.2 mol/kg NaCl solution at 80°C for a period of 200 days were published (Jayaweera et al. 2003, pp. 9-18 to 9-22, Figure 9.13). The solution pH was maintained at 3 through HCl additions. This data was not used for model development. The measured corrosion potential at the end of the testing (200 days) ranged from −38 to 51 mV versus the saturated silver chloride electrode. For these exposure conditions, the mean value of the corrosion potential from the long-term steady–state corrosion potential model is 295 mV versus saturated silver chloride electrode, and $\pm 2\sigma$ values are 114 and 476. Although the lower bound of the model-predicted corrosion potentials is higher by about 63 mV, the model prediction is a reasonable match considering that the investigators indicated that the corrosion potential had likely not reached steady state (Jayaweera et al. 2003, p. 9-18). In addition, overestimates of the corrosion potential by the model are conservative because, for a given condition, the overestimates would result in narrower margins between the critical potential and corrosion potential (SNL 2007c, Section 7.2.2). These data and model predictions are shown in Table 2.3.6-9.

General Electric Global Research Center measured long-term corrosion potential (after about 915 days) of Alloy 22 compact tension specimens at 110°C in an aerated basic saturated water solution composed of 10.6 g Na_2CO_3 (anhydrous), 9.7 g KCl, 8.8 g NaCl, 0.2 g NaF, 13.6 g $NaNO_3$, 1.4 g Na_2SO_4 (anhydrous), and 4.1 g $Na_2SiO_3 \times 9H_2O$ dissolved in 55.3 g H_2O (Andresen et al. 2003, Table 1-4; pp 66 and 78). This data was not used for model development. The long-term corrosion potential was found to be between −99 to −89 mV versus saturated silver chloride electrode. The solution is calculated to have 5.08 *m* chloride ions and 2.89 *m* nitrate ions and a Pitzer pH value of 8.58. The long-term corrosion potentials predicted by the model using 4.62 *m* chloride ions, 2.82 *m* nitrate ions, and a pH of 8.58 at 110°C is −104 mV versus saturated silver chloride electrode (mean), 70 mV versus saturated silver chloride electrode (upper bound), and −279 mV versus saturated silver chloride electrode (lower bound). Using the calculated 5.08 m chloride-ion and 2.89 m nitrate-ion concentrations, these values change to −154 mV versus saturated silver chloride electrode (mean), 20 mV versus saturated silver chloride electrode (upper bound), and −328 mV versus saturated silver chloride electrode (lower bound). The long-term corrosion potentials predicted by the model are consistent with these measured values, providing confidence in the

accuracy of the long-term corrosion potential model (SNL 2007c, Section 7.2.2) and are shown in Table 2.3.6-9.

Two data points not used for model development were obtained. The experimentally determined crevice repassivation potentials for two specimens, (1) a measured crevice repassivation potential for specimen DEA3130 of −67 mV versus saturated silver chloride electrode was obtained in 1 *M* NaCl solution at 90°C, and (2) a measured crevice repassivation potential for specimen KE0416 of −77 mV versus saturated silver chloride electrode was obtained in 6 *m* NaCl + 0.9 *m* KNO_3 solution at 100°C (SNL 2007c, Section 7.2.3). As can be seen from Table 2.3.6-10, the predicted values from the crevice repassivation potential model are sufficiently accurate with respect to measured data not used to develop the model.

Model adequacy was also demonstrated by comparing the model predictions to a model published in the literature (Dunn et al. 2005). The DOE model provides results consistent with or below the Dunn crevice repassivation potential model for a wide range of compositions as demonstrated in Table 2.3.6-11 (SNL 2007c, Section 7.2.3). Project model adequacy was also demonstrated by comparing the model prediction for localized corrosion susceptibility in conjunction with the long-term steady–state corrosion potential model with relevant observations. Alloy 22 crevice samples were tested for over 5 years in three different solutions (SDW, SCW, and SAW). None of these creviced samples initiated localized corrosion after exposure for over 5 years (SNL 2007c, Section 7.2.4).

The localized corrosion initiation analysis results are summarized in Table 2.3.6-12. As indicated by the results in the table, the model is conservative in that it predicts the possibility of localized corrosion occurrence for the exposure conditions of the 5-year crevice samples, where no localized corrosion was observed for these 5-year crevice samples. The model is consistent with or conservative relative to experimental observations obtained from creviced samples used in long-term corrosion potential experiments and literature observations (SNL 2007c, Section 7.2.4). These results demonstrate that the localized corrosion initiation model (crevice repassivation potential model, in conjunction with the corrosion potential model) adequately predicts the localized corrosion susceptibility of Alloy 22 (SNL 2007c, Section 7.2). In addition, Table 2.3.6-13 provides a comparison of model predictions to long-term corrosion test observations for a wide range of environments. The model predictions are consistent with or overpredict the likelihood of localized corrosion initiation (SNL 2007c, Section 7.2.4).

Fabrication Related Effects—Two fabrication-related data sets related to surface stress mitigation and mockup tests were evaluated to support localized corrosion initiation model adequacy (SNL 2007c, Section 6.4.6). These evaluations consisted of quantitative comparisons of repassivation potentials obtained from samples with differing metallurgical conditions but exposed in similar chemical environments. The comparisons were performed in (1) 1 mol/L NaCl at 90°C, and (2) 6 mol/kg NaCl + 0.9 mol/kg KNO_3 at 100°C. The cyclic potentiodynamic polarization method (ASTM G 61-86 1998) was utilized to determine the crevice repassivation potential (SNL 2007c, Section 6.4.4.1). As shown below, fabrication related effects had no effect on the overall localized corrosion resistance of Alloy 22.

Surface Stress Mitigation—The weld region of the Alloy 22 waste package outer closure lid will be stress mitigated using low-plasticity burnishing (Section 1.9.2). Low-plasticity burnishing is a

process by which a high strength metallic ball is moved across the surface under load. It plastically deforms the surface layer of the material, resulting in compressive stresses. The purpose of the mitigation treatment is to eliminate surface tensile stresses that otherwise may be detrimental in the initiation and propagation of stress corrosion cracking. Low-plasticity burnishing was evaluated to determine if the surface treatment affects the resistance of Alloy 22 to initiation of localized corrosion.

The relative resistance of Alloy 22 to localized corrosion between the nonmitigated and the mitigated specimen surfaces was assessed by comparing the values of the crevice repassivation potential (E_{rcrev}) in two test solutions (1 mol/L NaCl at 90°C and 6 mol/L NaCl + 0.9 mol/L KNO_3 at 100°C). Test results demonstrate that the repassivation potential in these solutions was practically the same for both the welded and surface stress-mitigated samples and the nonmitigated samples (as-welded and mill-annealed). The same findings were reported previously (Fix et al. 2005). These results demonstrate that surface treatments, such as low-plasticity burnishing, do not decrease the resistance of Alloy 22 to crevice corrosion in either pure-chloride solutions or chloride-plus-nitrate solutions (SNL 2007c, Section 6.4.6, Figures 6-58 and 6-59).

Mockup Testing—Samples prepared from an Alloy 22 mockup waste container were tested to determine the anodic behavior and crevice repassivation potential (E_{rcrev}) in three electrolyte solutions (1 mol/L NaCl at 90°C, 6 mol/kg NaCl + 0.9 mol/kg KNO_3 at 100°C and 5 mol/L $CaCl_2$ at 90°C). The samples were fabricated from cores taken from the longitudinal weld seam of the full-diameter, quarter-length Alloy 22 mockup waste container outer barrier (Gordon 2002). The susceptibility of the samples to localized corrosion was assessed using the cyclic potentiodynamic polarization technique, with values of the repassivation potentials determined from the resulting polarization curves.

The repassivation potentials for the mockup samples were found to be the same or more positive than the repassivation potentials determined from as-welded prism crevice assembly samples and as-welded multiple crevice assembly samples and mill-annealed multiple crevice assembly samples prepared from other laboratory plates. Because the E_{corr} must exceed E_{rcrev} in order for localized corrosion to initiate, an increase in E_{rcrev} decreases the likelihood of initiating localized corrosion. These results demonstrate that fabrication processes involved in producing the mockup longitudinal weld seam do not decrease the resistance of Alloy 22 to crevice corrosion initiation in either pure-chloride solutions or chloride-plus-nitrate solutions (SNL 2007c, Section 6.4.6).

2.3.6.4.4.2.2 Localized Corrosion Propagation Model Adequacy

Validation of the localized corrosion propagation model was accomplished by comparison of the propagation rates used in the model to the propagation rates for similar, but less corrosion-resistant alloys such as Alloy C-276 (UNS N10276) and Alloy C-4 in aggressive solutions. The Alloy 22 average corrosion rate in a highly aggressive 10% ferric chloride localized corrosion test solution is about 12.7 µm/yr. The average corrosion rates of Alloy C-276 and Alloy C-4 (Ni–Cr–Mo alloys similar to Alloy 22) in the same test solution were 35.6 µm/yr and 508 µm/yr (Haynes International 1997a, p. 8). These values fall within the range of rates used for the Alloy 22 localized corrosion propagation model and also illustrate that Alloy 22 is more corrosion resistant than these other alloys. Smailos (1993) tested Alloy C-4 in two aggressive $MgCl_2$ based brines and one NaCl-based brine at 150°C for up to 18 months. It was found that localized corrosion (pitting) was observed in

these $MgCl_2$-based brines. Maximum pit depths between 300 and 900 µm were observed after 18 months of testing (Smailos 1993, Table III). These values correspond to pit propagation rates of between 200 and 600 µm/yr. These values fall within the range of rates used for the Alloy 22 localized corrosion propagation model. Pitting was not observed in the NaCl-based brine used in this study, which is expected to be more representative of repository conditions than $MgCl_2$-based brines, after 18 months of testing.

In addition, the localized corrosion propagation model assumes that, when it occurs, localized corrosion of the waste package outer barrier propagates at a constant rate. This assumption is conservative because the localized corrosion propagation rate decreases with time (SNL 2007c, Section 6.4.4).

Section 2.3.6.4.3.2.2 discussed the time-dependent growth law as an alternative conceptual model to the time-independent conservative model. That section showed that the rate of localized corrosion for many less corrosion-resistant metals follows a power law with a time exponent of about 0.5 consistent with a diffusion-controlled or ohmically controlled corrosion growth. For corrosion-resistant materials, the exponent effectively tends toward zero. As a consequence, the time-dependent growth law would result in longer time frames prior to waste package breach by localized corrosion than the time-independent growth law.

2.3.6.5 Stress Corrosion Cracking of the Waste Package Outer Barrier

[NUREG-1804, Section 2.2.1.3.1.3: AC 1(1) to (5), AC 2, AC 3(1) to (4), AC 4, AC 5; Section 2.2.1.3.2.3: AC 1(1) to (5), AC 2; Section 2.2.1.3.3.3: AC 1(3), (6), (10)]

Stress corrosion cracking is the process by which cracks initiate in a material under stress in the presence of a corrosive environment. Stress corrosion cracking may affect the time to waste package breach and possible diffusive releases. Analysis of stress corrosion cracking provided in this section includes a conceptual description, review of experimental data and data uncertainty, description of the model and model uncertainty, and abstraction and validation of the model.

Stress corrosion cracking of the waste package is addressed in three sections. Section 2.3.6.6 addresses stress corrosion cracking due to manufacturing defects (other than in the outer barrier weld region) that result in early waste package failure. Section 2.3.4 addresses stress corrosion cracking induced by seismic response and rockfall damage. This section, Section 2.3.6.5, establishes the residual stress threshold above which stress corrosion cracking may occur and addresses stress corrosion cracking of the waste package outer barrier closure weld regions.

2.3.6.5.1 Conceptual Description

[NUREG-1804, Section 2.2.1.3.1.3: AC 1(1) to (4)]

Stress corrosion cracking is the initiation and propagation of cracks due to three simultaneous conditions: a susceptible material, critical environment, and sustained tensile stress. Alloy 22, the material used for the waste package outer barrier, is highly resistant to stress corrosion cracking but may be susceptible to cracking in the Yucca Mountain environment and the stress conditions described in Section 2.3.6.5.2.3. Environmental conditions, which include temperature, dissolved oxygen, and ionic concentrations, may influence the stress corrosion cracking process. For modeling purposes, it is conservatively assumed that, regardless of the environment, the waste

package will undergo stress corrosion cracking if stress conditions are met (SNL 2007a, Section 5). This is a significant conservatism in light of the high corrosion resistance of Alloy 22 and the fact that only aggressive environments support stress corrosion cracking (SNL 2007a, Section 6.2).

The stress corrosion cracking model developed herein is based on the slip dissolution and film rupture model for crack initiation and propagation. The stress corrosion cracking model establishes a threshold stress for the creation of stress corrosion cracks on smooth surfaces (referred to as incipient cracks), and establishes a stress intensity factor threshold for the initiation of crack growth. Weld flaws are also considered to propagate by stress corrosion cracking once the stress intensity factor threshold criterion is exceeded. The threshold stress intensity factor is discussed in Section 2.3.6.5.3.2, and the determination of the weld-induced stress and stress intensity factor profiles through the waste package outer barrier is described in Section 2.3.6.5.2.3. The threshold stress, threshold stress intensity factor, and parameters associated with the slip dissolution and film rupture model are determined from experimental data developed for repository environments (SNL 2007a, Section 6.2.1).

In the stress corrosion cracking model, the crack propagation rate is based on the stress intensity factor and Alloy 22 passive film properties (SNL 2007a, Section 6.4.4). For the empirical threshold stress intensity factor, a conservative approach was used to establish a threshold stress intensity factor (K_{ISCC}) value by extrapolating qualified Alloy 22 crack growth rate results experimentally obtained at higher stress intensity factors (K_I) down to rates representative of the mean general corrosion rate where crack blunting occurs and crack growth arrests (SNL 2007a, Section 6.4.5).

2.3.6.5.2 Data and Data Uncertainty

[NUREG-1804, Section 2.2.1.3.1.3: AC 2, AC 3(1) to (4)]

Data have been collected and analyzed to characterize stress corrosion cracking of the Alloy 22 waste package outer barrier. This section describes the Alloy 22 data for threshold stress for crack initiation, crack growth rates, stress and stress intensity factor profiles of the welded regions, and weld flaw data.

2.3.6.5.2.1 Threshold Stress Criterion for Initiation of Stress Corrosion Cracking

It is generally observed that, for a given alloy, metallurgical condition, and environment and in the absence of cyclic stresses, initiation of stress corrosion cracking does not occur on a smooth surface (without sharp defects such as weld flaws) if the surface stress is below a threshold value defined as the threshold stress (ASM International 1987, Vol. 13, p. 276). This statement is valid for many conditions; however, in severe conditions not relevant to the repository, stress corrosion cracking can occur on smooth materials (e.g., in boiling $MgCl_2$) if sufficient stress is applied. This threshold stress is considered to apply for a wide range of environments, as described below.

2.3.6.5.2.1.1 Constant-Load Crack-Initiation Tests

To establish a threshold stress criterion for stress corrosion cracking initiation in Alloy 22, a series of tests under a variety of exposure conditions and sample configurations were conducted. These tests included constant-load crack-initiation tests performed on 120 Alloy 22 samples. The samples represent a range of different microstructures and metallurgical conditions, including annealed,

welded, thermally aged, and cold-worked samples. The inclusion of thermally aged samples accounts for possible effects of grain boundary segregation on SCC initiation. The samples were exposed for over 28,000 hours (approximately 3.2 years), or over 20,000 hours (approximately 2.3 years) for notched specimens, to a 105°C brine, basic saturated water (diluted to approximately 15% of full concentration), with a pH of approximately 10.3 at test temperature (SNL 2007a, Section 6.2.1) as shown in Figure 2.3.6-28. The time-to-failure (or total exposure time without failure) was determined at various applied stress ratios (applied stress to yield strength). Testing was conducted at an applied stress up to 2.1 times the yield strength of the as-received material and up to 2.0 times the yield strength of the welded material. These high stress ratios correspond to an applied stress of approximately 95% of the ultimate tensile strength of the Alloy 22 test material at 125°C. This demonstrates that Alloy 22 is highly resistant to stress corrosion cracking as no rupture of the metal was observed, including the as-welded state.

2.3.6.5.2.1.2 Slow Strain Rate Testing in Concentrated Brines

A series of slow strain rate tests were performed on Alloy 22 at 22°C to 120°C, and at a strain rate of 1.66×10^{-6} per second. The purpose of these tests was to provide information relevant to the susceptibility of Alloy 22 to stress corrosion cracking. Although slow strain rate testing does not give a direct measure of the threshold stress for stress corrosion cracking initiation, the absence of stress corrosion cracking at the open-circuit corrosion potential in tests in which specimens are pulled to failure at a low strain rate is consistent with Alloy 22 being highly resistant to stress corrosion cracking. These slow strain rate tests serve as an indication of whether or not certain ductile metals are susceptible to specific environmental conditions (SNL 2007a, Section 6.2.1).

These slow strain rate test results are summarized in Table 2.3.6-14. The tests cover a broad range of relevant, potentially aggressive environments in SAW, basic saturated water, SCW, and concentrated brines, including $CaCl_2$-type brines, with and without applied potential at pH as low as 3 (SNL 2007a, Section 6.2.1). Examination of the tabulated results indicates a high degree of stress corrosion cracking resistance at open-circuit corrosion potentials in all potentially relevant and aggressive test environments evaluated. However, there are some indications that stress corrosion cracking initiation may have occurred in SCW solution (about 1,000 times concentrated J-13 brine) with large applied anodic potentials (at between 200 to 400 mV versus Ag/AgCl, with a corresponding open-circuit corrosion potential between –76 to –241 mV versus Ag/AgCl). These results, in which the specimens are slowly pulled to the fracture stress, are consistent with the very low stress corrosion cracking susceptibility of Alloy 22 under potentially relevant conditions (SNL 2007a, Section 6.2.1).

2.3.6.5.2.1.3 U-Bend SCC Initiation Tests

Alloy 22 U-bend specimens containing residual stresses due to permanent deformation and applied restraint were exposed to a range of relevant aerated-brine environments (SDW, SCW, and SAW brines). Of the 52 samples examined, there was no evidence of stress corrosion cracking initiation after about 5 years of exposure (SNL 2007a, Section 6.2.1).

2.3.6.5.2.2 Weld Flaws and Incipient Cracks

Sixteen welded Alloy 22 specimen rings that represent the outer closure lid weld of a waste package were analyzed. The welds employed procedures, processes, and equipment similar to those that are anticipated to be used for waste package closure. Nondestructive examination, followed by metallographic examination, was used to accumulate information on weld flaws (Smith 2008). Seven weld flaws were identified using ultrasonic testing and confirmed by metallography. No flaws were found by metallography that were not found by ultrasonic testing, other than very small (~0.08 mm) gas pores (SNL 2007d, Section 4.1.2.2). Since these gas pores are small compared to the minimum flaw size for repair of 1.6 mm and do not have a radial orientation, they are not further considered. Several distributions were developed to characterize size, density, depth, and orientation of the weld flaws (SNL 2007d, Section 6.3.1).

For smooth surfaces, a crack length of 0.05 mm is the assumed initial size of the stress corrosion cracking cracks (Ford and Andresen 1988, p. 798). After the stress threshold is satisfied, this crack size is used within the model as the assumed initial size of incipient cracks (e.g., stress corrosion cracks formed on smooth surfaces) to determine whether the cracks grow or arrest (SNL 2007a, Section 6.3.3).

Weld flaw data (flaw density and size distributions) from nuclear piping welds (Khaleel et al. 1999) were also used to help determine the characteristics of flaws that could occur in the closure welds of the waste package (SNL 2007d, Section 6.3.1).

2.3.6.5.2.3 Stress and Stress Intensity Factor Profiles

The outer closure lid weld region will be stress mitigated to delay the initiation of stress corrosion cracking. Low-plasticity burnishing, which induces compressive stresses in the weld region, will be used for stress mitigation (Section 1.9.2). Low-plasticity burnishing can induce compressive hoop stresses to a minimum depth of 3 mm (SNL 2007a, Section 6.5.5). Stress corrosion cracking cannot occur in the absence of tensile stress; therefore, the stress-mitigated layer must corrode away prior to initiation of stress corrosion cracking.

The as-welded residual stress profiles for the waste package outer closure weld regions were determined using two-dimensional axisymmetric finite-element analysis methods (SNL 2007a, Section 6.5.3.3). The stress profile for the waste package outer closure weld region was modified to account for the effect of stress mitigation. The stress profiles as a function of depth were fit to a third order polynomial equation. The coefficients determined for the stress profiles are shown in Table 2.3.6-15.

Stress intensity factor profiles corresponding to these stress profiles were determined through the use of fracture mechanics analysis of an idealized crack geometry (a single edge cracked plate) with appropriate geometric correction factors. These are presented in Table 2.3.6-16.

Uncertainty in the stress and stress intensity factor profiles is introduced through a scaling factor sampled from a truncated (at $\pm 3\sigma$) normal distribution with a mean of zero and a standard deviation of 5% of the yield strength (SNL 2007a, Section 8.4.2). Residual stress profiles in stainless steel piping welds commonly display a sinusoidal variation around the circumference with a range of

about 34 MPa (5 ksi) about the mean stress. Thus, a sinusoidal variation around the circumference of the Alloy 22 waste package outer closure-lid welds was employed to capture this variability (SNL 2007a, Section 6.5.6).

2.3.6.5.2.4 Stress Corrosion Crack Growth Rates for Alloy 22

The stress corrosion cracking model uses a crack growth rate proportional to the stress intensity factor raised to a power, *n*, the repassivation slope (Section 2.3.6.5.3.2) (SNL 2007a, Section 6.4.4). The repassivation slope is a measure of the rate at which the passive film heals after rupture and crack advance. The repassivation slope is determined empirically by measuring the crack growth rate using fatigue pre-cracked compact tension fracture mechanics specimens exposed to relevant environments under known stress intensity factors. Alloy 22 compact tension specimens were tested at 110°C in concentrated basic saturated water mixed-salt environments. One such chemistry is shown as BSW-12 in Table 2.3.6-1.

Due to the resistance of Alloy 22 to stress corrosion cracking, cyclic loading was required in order to initiate and propagate pre-cracks in the compact tension specimens. The testing procedure included cyclic loading to initiate the pre-cracks, followed by long hold times at high constant load (SNL 2007a, Section 6.4.4). The data used as input for establishing the range of repassivation slope values for Alloy 22 are summarized in Table 2.3.6-17.

Based on this experimental approach and the corresponding calculated *n* values listed in Table 2.3.6-17, a normal distribution for *n* was constructed. The mean value and the standard deviation are 1.165 and 0.115, respectively. The lower and upper bounds of *n* at $\pm 2\sigma$ are 0.935 to 1.395, respectively (SNL 2007a, Section 6.4.4).

2.3.6.5.3 Model and Model Uncertainty

[NUREG-1804, Section 2.2.1.3.1.3: AC 1(1) to (5), AC 4]

This section describes the weld flaw analysis used as an input to the stress corrosion cracking model, the stress corrosion cracking model, and model results, and an alternative conceptual model. The stress corrosion cracking model for the waste package outer barrier includes: (1) threshold stress for nucleation of cracks; (2) the threshold stress intensity factor for initiation of crack growth; and (3) the crack growth rate itself.

2.3.6.5.3.1 Weld Flaw Analysis

Weld flaws in the closure-lid weld are possible sites for the initiation of stress corrosion crack growth. Weld flaws are generally larger than other surface defects and are conservatively modeled as maintaining their depth relative to the advancing general corrosion front (i.e., they are not removed by general corrosion processes) (SNL 2007a, Section 8.4). Therefore, the characteristics of flaws in the closure welds are important inputs to the waste package stress corrosion cracking analysis. The radially oriented flaws would be potentially driven by hoop stress, and residual stress analyses showed that the hoop stress is the dominant stress driving crack growth (SNL 2007a, Section 6.5.3). This section develops the weld flaw analysis for the Alloy 22 waste package outer barrier closure lid weld.

Weld flaw data (size, quantity, and orientation) were determined for the as-welded condition using the results from 16 closure weld rings. As described in Section 1.5.2, a nondestructive evaluation inspection technique will be applied to the closure welds and detected flaws above a threshold size will be repaired prior to low-plasticity burnishing. Recognizing that not all weld flaws will be detected during a nondestructive evaluation inspection, a probability of nondetection is modeled (SNL 2007d, Section 6.3.1).

The probability of nondetection of weld flaws as a function of size is based on experimental data for intergranular stress corrosion cracking in austenitic piping in the nuclear industry (Bush 1983, p. 13A.5.7). These results are based on experiments performed in the late 1970s, so they reflect detection capabilities that have since been improved upon. The probability distribution of the number of flaws before and after a nondestructive evaluation inspection and repair is summarized in Table 2.3.6-18.

The size distribution of nondetected weld flaws was estimated using statistical techniques consistent with U.S. Nuclear Regulatory Commission guidance (NRC 1983, Section 5.5.2; SNL 2007d, Section 6.3.1). The flaw size distribution before and after inspection and repair is summarized in Table 2.3.6-18.

The 16 closure weld rings were used to determine the orientation of weld flaws with respect to the hoop stress (the dominant stress driving crack growth). It was found that only a very small fraction (0.8%) of the weld flaws were oriented favorably (could result in crack growth) with respect to the hoop stress (i.e., were radial flaws) (SNL 2007d, Section 6.3.1.5).

The distributions for the number and size of weld flaws have uncertainty associated with them. These uncertainties are characterized in Table 2.3.6-18. The variation in the distributions for the number and size of weld flaws is a source of variability applied at the waste package level, as described in Section 2.4 (SNL 2008a, Section 6.3.5).

2.3.6.5.3.2 Stress Corrosion Cracking Model

The stress corrosion cracking model consists of the: (1) threshold stress criterion for nucleation of cracks on smooth surfaces; (2) threshold stress intensity factor criterion for initiation of crack growth; and (3) slip dissolution and film rupture model for crack growth rate, as follows:

1. Data for stress corrosion cracking initiation indicates little or no crack initiation for repository-relevant environments up to stress levels approaching the ultimate tensile strength (approximately 2 times the yield strength) for Alloy 22. For modeling purposes, the threshold stress criterion is conservatively taken to be 90% to 105% of the at-temperature yield strength (SNL 2007a, Section 6.2.2).

2. A threshold stress intensity factor criterion, K_{ISCC}, is used to determine if an initiated crack or weld flaw will propagate (SNL 2007a, Section 6.4.5). The K_{ISCC} concept (Jones and Ricker 1987; Sprowls 1987) has been widely used by engineers to assess the susceptibility of various materials to stress corrosion cracking. When the crack growth rate is equal to or less than the general corrosion rate, the stress intensity factor is decreased due to crack tip blunting, and therefore, the crack no longer propagates

(Andresen and Ford 1994, p. 62). Using the mean general corrosion rate of Alloy 22 and the repassivation slope distribution discussed earlier, the threshold stress intensity factor distribution shown in Table 2.3.6-19 is obtained.

3. The slip dissolution and film rupture model relates the crack growth rate to the periodic rupture of the metal oxide film, dissolution, and repassivation process at the crack tip. The velocity of crack advance is (SNL 2007a, Section 6.4.3):

$$V = \overline{A}\,(K_I)^{\overline{n}} \qquad \text{(Eq. 2.3.6-9)}$$

where

V	=	crack velocity, mm/s
$\overline{A}$	=	preexponential factor, mm/s/MPa(m)^{½})$^{\overline{n}}$
K_I	=	stress intensity factor, MPa(m)^{½}
$\overline{n}$	=	4 times the repassivation rate (or slope).

Parameters $\overline{A}$ and $\overline{n}$ are expressed in terms of the repassivation slope, n, as follows:

$$\overline{A} = 7.8 \times 10^{-2} n^{3.6} (4.1 \times 10^{-14})^n \qquad \text{(Eq. 2.3.6-10)}$$

and

$$\overline{n} = 4n \qquad \text{(Eq. 2.3.6-11)}$$

The parameter n is represented by a truncated normal distribution (at $\pm 2\sigma$) with a mean of 1.165 and a standard deviation of 0.115 (Section 2.3.6.5.2.4). The variation in the repassivation slope, n, is entirely due to uncertainty (SNL 2007a, Section 6.4.4 and 8.4.1).

Experimental data and model predictions for crack growth rates as a function of stress intensity factor are shown in Figure 2.3.6-29.

2.3.6.5.3.3 Alternative Conceptual Model

An alternative conceptual model for stress corrosion cracking propagation is the coupled environmental fracture model (Macdonald and Urquidi-Macdonald 1991; Macdonald et al. 1994), which is based on conservation of electrons involved in the corrosion process. The model incorporates the effects of oxygen concentration, flow rate, and the conductivity of the external environment and accounts for the effect of stress on crack growth. This model would result in lower crack propagation rates than the model used within the TSPA model (SNL 2007a, Section 6.4.6).

Comparison with experimental data (Ford and Andresen 1988, Figure 22) shows the crack growth rate predicted by the coupled environmental fracture model tends to be at the lower end of the experimental data range (Ford and Andresen 1988, Figure 22) and therefore, would be prone to underestimate the crack growth rate in comparison to other available models. For this reason, the coupled environmental fracture model was not included for further evaluation but was used only to corroborate the base-case slip dissolution-film rupture model, which more accurately represents crack growth rates.

2.3.6.5.4 Abstraction and Adequacy

[NUREG-1804, Section 2.2.1.3.1.3: AC 4, AC 5]

A summary of the model for waste package stress corrosion cracking and an explanation of how the model was validated are provided in this section.

2.3.6.5.4.1 Waste Package Stress Corrosion Cracking Abstraction and Uncertainty

Stress corrosion cracking is modeled to initiate at incipient flaws or weld flaws in the closure weld regions. As discussed in Section 2.3.6.3.4, the waste package surface is modeled as a collection of patches. Each waste package closure lid is represented by approximately 40 patches. Analyses (SNL 2007a, Section 6.6.1) indicate that the distance between two neighboring cracks would need to be greater than the plate thickness for the stress profile and stress intensity factor profile to be of sufficient magnitude to propagate both cracks through-wall. Therefore, there are about six through-wall cracks possible per waste package outer closure lid patch. It is conservatively modeled that when the first crack (due to a weld flaw) on a given patch penetrates the waste package, all possible through-wall cracks on that patch are considered to penetrate (SNL 2008a, Section 6.3.5[a]).

The dominant component of stress in the waste package outer barrier closure lid weld regions has been determined to be hoop stress, which promotes radially oriented crack growth. Therefore, only the hoop stress profile and the associated stress intensity factor profiles for radially oriented cracks are modeled (SNL 2007a, Section 6.5.6).

In the stress corrosion cracking model, incipient cracks are formed when the stress exceeds the threshold stress criterion for crack initiation. Weld flaws are already present and are not subject to the threshold stress criterion. If the stress intensity factor at the incipient crack or weld flaw tip exceeds the threshold stress intensity factor criterion, crack growth is allowed to occur. General corrosion depth is accounted for in determining the depth of the crack tip (SNL 2008a, Section 6.3.5).

The stress and stress intensity factor profiles in the waste package outer barrier closure weld regions are both variable and uncertain. Variability (angular variation) in the stress and stress intensity factor profiles for the outer lid closure weld region are shown in Figures 2.3.6-30 and 2.3.6-31, respectively. Uncertainty in the stress and stress intensity factor profiles for the outer lid closure weld region are shown in Figures 2.3.6-32 and 2.3.6-33, respectively.

The crack growth velocity is a function only of the repassivation slope (given the stress intensity factor at the crack tip depth). The repassivation slope is sampled once per TSPA realization of the

repository (e.g., the same value of n is used for each closure lid weld region) (SNL 2008a, Section 6.3.5).

2.3.6.5.4.2 Model Adequacy

Ford and Andresen (1988, pp. 789 to 800; Andresen and Ford 1994, pp. 61 to 70) have applied the stress corrosion cracking model to Stainless Steel Types 304 and 316L, Low Alloy Steel Types A533 and A508, and the nickel-based Alloys 600 (UNS N06600) and 182 (UNS W86182). They determined that the $\overline{A}$ versus $\bar{n}$ relationship used in the model was statistically valid for the chromium-containing, nickel-based Alloys 600 and 182 over a range of anionic impurity concentrations (Ford and Andresen 1988, Figure 10). Also, Andresen (1991, Figure 37) used the stress corrosion cracking model for the higher chromium content nickel-based alloy, Alloy 82 (UNS N06082). The chromium content range of Alloy 82 (18% to 22% chromium) overlaps the Alloy 22 (20% to 22.5% chromium) chromium content range. Experimental results (SNL 2007a, Section 6.4.4) indicate the crack growth rate of Alloy 22 exposed to relatively pure water (2 ppm O_2) at 288°C is consistent with that of other materials, such as Alloys 600 and 182 (Andresen, Young et al. 2002) and austenitic stainless steel (Andresen, Angeliu et al. 2002). These references provide support for the treatment of stress corrosion cracking of nickel-based Alloy 22 by the same fundamental mechanism as for these other nickel-based alloys.

The stress corrosion cracking model-predicted crack growth rates were also validated by comparison with crack growth rates collected using a similar method, the reversing direct current measurement technique on compact tension type fracture mechanics specimens not used for model development (Table 2.3.6-20). These data were found to lie within the span of model-predicted crack growth rates obtained by using the upper and lower bounding repassivation slopes (e.g., the $\pm 2\sigma$ values of n) or demonstrate lower crack growth rates than the model (Figure 2.3.6-34) (SNL 2007a, Section 7.3.2).

The stress corrosion cracking resistance of Alloy 22 is corroborated by results of high-magnification visual examination of U-bend specimens (both annealed and as-welded conditions) exposed for 5 years to relevant environments (SDW, SCW, and SAW) at 60°C and 90°C. These Alloy 22 U-bends showed no evidence of stress corrosion cracking initiation (SNL 2007a, Section 6.2.1).

Stress corrosion crack growth can occur at a rate such as that predicted by the slip dissolution-film rupture model only if the calculated stress intensity at any flaw of given dimensions of length and depth exceeds a threshold value known as K_{ISCC}. This criterion specifies an acceptable approach for the establishment of K_{ISCC} for Alloy 22 under environmental conditions relevant to the waste package (SNL 2007a, Section 7.3.4). Because there is no accepted theoretical basis for a priori or deterministic calculation of $K_{ISCC,}$ this parameter is determined by using crack growth rate versus applied stress intensity measurements. The measured values are then extrapolated to a conservative threshold value using the K_I dependence of crack growth rate explained in the validated slip dissolution-film rupture model. A conservative K_{ISCC} value was obtained by extrapolating crack growth rate versus K_I to a crack growth rate equal to the mean general corrosion rate at the alloy surface. The theoretical basis for this approach is that if the crack growth rate equals the rate at which the surface recedes due to general corrosion, then it is not possible to maintain a sharp crack

(the crack tip will blunt), and stress corrosion cracking is effectively arrested (SNL 2007a, Section 6.4.5).

The threshold stress is that value below which stress corrosion cracking does not initiate on a smooth metal surface. There is no firm accepted basis for calculating a threshold stress value for a given combination of material and environment (SNL 2007a, Section 7.3.4). Therefore, it is necessary to experimentally establish the threshold stress value. This has been accomplished by applying a safety factor on the minimum failure stress (or applied stress without failure) obtained from long-term, constant load stress corrosion tests. A safety factor of 2.0 is typically used in general engineering practice. For example, the American Society of Mechanical Engineers uses a reduction factor of 2 on the runout stress (endurance limit) for defining fatigue lifetime cycles (ASME 1969, p. 80). Thus, a safety factor of 2.0 used for the threshold stress is consistent with the American Society of Mechanical Engineers practice (SNL 2007a, Section 7.3.4).

Additionally, corroboration with available alternative conceptual models, such as the coupled environment fracture model for stress corrosion cracking, was considered for the validation of the base-case slip dissolution-film rupture model. It was concluded (SNL 2007a, Section 6.4.6) that both the slip dissolution-film rupture model and the coupled environmental fracture model are capable of predicting the crack growth rate for stress corrosion cracking (Section 2.3.6.5.3.3). However, the coupled environment fracture model appeared to have the tendency of underestimating the crack growth rate as compared to the slip dissolution-film rupture model when both models were applied to predict the crack growth rate for sensitized Stainless Steel Type 304 in the light water boiling water reactor environment. Comparison with experimental data (Ford and Andresen 1988) for crack propagation rate versus stress intensity factor for sensitized Stainless Steel Type 304 in fully aerated, high-purity water at elevated temperature indicated that the crack growth rate predicted by the coupled environmental fracture model, 3.2×10^{-9} cm/s at 20 MPa–$m^{0.5}$, tends to be at the lower end of the experimental data range (Macdonald and Urquidi-Macdonald 1991). For this reason, the coupled environmental fracture model was not included for further evaluation but only used to validate the base-case slip dissolution-film rupture model.

In summary, the stress corrosion cracking model was validated by comparing measured crack growth rates reported in peer-reviewed literature with model predictions, as well as with a less conservative alternative conceptual model, and by comparing Alloy 22 slip dissolution-film rupture model predicted rates with independently developed experimentally measured Alloy 22 rates and demonstrating agreement (SNL 2007a, Section 7.3). For the empirical threshold stress intensity factor described in peer-reviewed literature, a conservative approach was used to establish a threshold K_{ISCC} value by extrapolating the qualified Alloy 22 crack growth rate model from higher K_I values down to rates representative of the mean general corrosion rate where crack blunting occurs (SNL 2007a, Section 7.3).

2.3.6.6 Early Failure of Waste Packages

[NUREG-1804, Section 2.2.1.2.2.3: AC 3, AC 4, AC 5; Section 2.2.1.3.1.3: AC 1(1) to (5), AC 2, AC 3(1) to (4), AC 4, AC 5; Section 2.2.1.3.3.3: AC 1(10)]

Manufacturing and handling defects may result in the early failure of waste packages. Analysis of early failure provided in this section includes a conceptual description, review of experimental data

and data uncertainty, description of the analysis and uncertainty, and abstraction and adequacy of the abstraction.

The manufacturing and handling processes considered within this analysis are based on the waste package fabrication and handling processes described in Sections 1.2.4 and 1.5.2. These processes, including welding, post-weld stress mitigation, nondestructive examination, handling, and placement, will be controlled as described in Section 1.9.2.

2.3.6.6.1 Conceptual Description

[NUREG-1804, Section 2.2.1.3.1.3: AC 1(1) to (4)]

The purpose of this analysis is to evaluate the types of defects or imperfections that could occur in a waste package and potentially lead to its early failure and to estimate a probability of occurrence for each. An early failure is defined as the through-wall penetration of a waste package due to manufacturing- or handling-induced defects, at a time earlier than would be predicted by mechanistic degradation models for a defect-free waste package (SNL 2007d, Section 1).

The scope of this analysis is limited to the manufacturing- or handling-induced defects that might lead to the early failure of the waste package. Also, only the outer (Alloy 22) barrier for the waste package is investigated. No corrosion performance credit is taken for the structural (stainless steel) inner vessel of the waste package; therefore, it is not analyzed.

Within the TSPA, early failure of a defective waste package is conservatively modeled to occur at the time of repository closure (other than closure welds, which are modeled in Section 2.3.6.5). Waste package early failure is represented as loss of 100% of the surface area, even though it is expected that the radionuclide inventory would not be immediately available for transport because most through-wall penetrations, especially cracks from stress corrosion cracking, are tight and of limited length. Release through stress corrosion cracks in waste packages that are not subject to early failure is modeled as occurring through diffusive release, as described in Section 2.3.7.12.

Several general types of manufacturing defects were considered as possible mechanisms that could adversely affect waste package performance, including weld flaws, base metal flaws, improper weld material, improper base metal, improper heat treatment, improper low-plasticity burnishing, improper weld-flux material, poor weld-joint design, surface contamination, mislocated welds, missing welds, handling or installation damage, and administrative or operational error (SNL 2007d, Section 6.2). Flaws in waste package welds are discussed in detail in Section 2.3.6.5 in relation to their effect on stress corrosion cracking at the closure lid welds and are not included in this section (SNL 2007a, Section 6.5.3).

2.3.6.6.2 Data and Data Uncertainty

[NUREG-1804, Section 2.2.1.3.1.3: AC 2, AC 3(1) to (4)]

Data have been collected and analyzed to understand the possible extent of early failure of waste packages in the repository. This section describes possible defects identified from literature that could result in early failure of waste packages and data on the probability of occurrence.

2.3.6.6.2.1 Possible Defects Identified from Literature

This section presents a summary of the types of manufacturing defects from a literature review of various types of containers (SNL 2007d, Section 6.1). In addition to providing examples of the rates at which defective containers occur, this information provides insight into the various types of defects that can occur and the mechanisms that cause defects to propagate to failure. Literature information was investigated for the following types of containers to determine the types of defects and their probabilities (SNL 2007d, Section 6.1):

- Boilers and pressure vessels
- Nuclear fuel rods
- Underground storage tanks
- Radioactive cesium capsules
- Dry storage casks for SNF.

Table 2.3.6-21 briefly summarizes the information obtained from the literature search (SNL 2007d, Section 6.1.6) regarding the rates and causes of manufacturing defects in welded metallic containers. Eleven types of defects (SNL 2007d, Section 6.1.6) were identified through the literature:

- Weld flaws
- Base metal flaws
- Improper weld filler material
- Improper heat treatment
- Improper weld-flux material
- Poor weld-joint design
- Surface contamination
- Mislocated welds
- Missing welds
- Handling or installation damage
- Administrative or operational error.

Out-of-specification base metal defect was not identified in the literature search; only instances of improper weld material were found. Notwithstanding, it is reasonable to consider the possibility that base metal, as well as weld material, might be out of specification. Furthermore, improper stress relief (low-plasticity burnishing) for the closure weld could occur and is considered.

Thus, 13 types of defects, including an out-of-specification base metal defect and improper closure weld stress relief, are reviewed for their applicability to waste packages in Section 2.3.6.6.3.1.

2.3.6.6.2.2 Human Error Probability Data

Estimates of human error probabilities (Swain and Guttmann 1983) were used in the models to estimate defects in the waste packages. These probability estimates are considered to be accepted data because *PRA Procedures Guide, A Guide to the Performance of Probabilistic Risk Assessments for Nuclear Power Plants* (NRC 1983, Sections 4.1 and 4.5.7) recommends using these data to evaluate the probability of occurrence of human error in the conduct of probabilistic risk

assessments for nuclear power plants, and the waste package will be subjected to nuclear industry standards, as discussed in Section 1.9.2.

The human error probability data used are summarized in Table 2.3.6-22. The estimated human error probabilities (Swain and Guttmann 1983, pp. 2-18 and 2-19) are represented as a lognormal distribution. The nominal probability represents the median. The 5th percentile is calculated by dividing the median by error factors shown in Table 2.3.6-22, and the 95th percentile is calculated by multiplying the median by the error factors.

2.3.6.6.3 Analysis and Uncertainty

[NUREG-1804, Section 2.2.1.3.1.3: AC 1(1) to (5)]

Early failure of waste packages is modeled to account for the probability of such failure. This section provides the screening justifications for excluded defect types and how early failure probability is determined for the remaining defect types and describes the waste package early failure analysis. Uncertainty is accounted for through the use of the error factors summarized in Table 2.3.6-22, which provide for a range of probabilities for each of the human error types.

2.3.6.6.3.1 Evaluation of Defect Types

Of the general types of manufacturing defects identified in Section 2.3.6.6.2.1, the following types of defects have been evaluated and are eliminated from further consideration for the following reasons:

Weld Flaws—Since the waste package is solution annealed to remove welding stresses, only waste package closure weld flaws will act as possible stress corrosion cracking locations. Thus only waste package closure weld flaws are considered (SNL 2007d, Section 6.2.3; SNL 2007a, Section 6.3.4) and are modeled in Section 2.3.6.5.

Improper Weld-Flux Material—Improper weld-flux material is eliminated because the welding method to be employed for waste packages does not use weld-flux material (Section 1.9.2).

Poor Weld-Joint Design—Poor joint design can be eliminated from further consideration because of the significant development and testing effort for joints (Section 1.9.2).

Surface Contamination—The probability of waste package surface contamination that could affect waste package performance (e.g., chemical or organic) was also evaluated (SNL 2007d, Section 6.2.3). Stringent controls will be placed on waste package fabrication and handling to limit the amount and type of surface contamination (Section 1.9.2). The likelihood of this type of defect being undetected prior to emplacement would be significantly less than the more-dominant defect mechanisms, and on this basis is not further considered (SNL 2007d, Section 6.2.3).

Mislocated Welds—This defect is mainly applicable to very small, single-pass welds (e.g., fuel rod end caps). Mislocated welds are not expected for the large multipass welds on the waste packages due to their size, location, significant quality assurance requirements, inspection and extensive nondestructive evaluation, as described in Section 1.9.2. For large multipass welds, any significant mislocation of the electrode would cause the weld arc not to strike. This would be

immediately obvious to the operator and the control system for the automated welder (SNL 2007d, Section 6.2).

Missing Welds—The probability of missing welds does not warrant further consideration due to significant quality assurance requirements, inspections, and extensive nondestructive evaluations that will occur (SNL 2007d, Section 6.2) as described in Section 1.9.2. Extremely low fuel rod welding historical failure rates in the industry supports this conclusion (SNL 2007d, Section 6.1.2).

Administrative or Operational Error—Administrative and operational errors may occur, and provisions in drip shield and waste package fabrication and handling procedures and equipment design will be made to minimize these errors. Even after taking the planned precautions, these types of errors are still recognized, and the associated rates and consequences are included in the evaluations for the remaining defect modes. Therefore, these types of errors are not considered to be separate defect modes (SNL 2007d, Section 6.2.3).

The remaining types of defects are discussed in Section 2.3.6.6.3.2.

2.3.6.6.3.2 Determination of Early Failure Probability

The remaining types of defects (improper or out of specification base metal, improper heat treatment of the outer shell and outer lid, improper weld filler material, improper low-plasticity burnishing, handling or installation damage) are further analyzed (SNL 2007d, Section 6.3). Among these defects, improper heat treatment is the dominant process in terms of probability (SNL 2007d, Section 6.5).

The probability of defects occurring for each process type is quantified in the following sections. An event tree analysis was used to develop and quantify the probability of each of these event types (SNL 2007d, Section 6.3). An event tree example is shown in Figure 2.3.6-35.

2.3.6.6.3.2.1 Improper Base Metal Selection

The probability of improper base metal selection is based upon the probability of improper weld filler material which uses similar processes and procedures (SNL 2007d, Section 6.3.2).

New instrumentation, such as portable x-ray spectroscopy equipment, makes it possible to perform quick field measurements of material compositions. However, there is still the possibility that the technician in charge of this work fails to perform the operation correctly, and it is not detected by the supervisor or future quality checks.

A Monte Carlo sampling was performed on the fault tree and assigned probabilities to arrive at a distribution of the probability of defects due to improper base metal selection. Monte Carlo sampling is used to obtain the distribution characteristics resulting from variable events. The resulting mean, and median probabilities of improper base metal selection occurring and not being detected are 1.25×10^{-7} and 8.76×10^{-8} per waste package, respectively (SNL 2007d, Table 6-8).

2.3.6.6.3.2.2 Improper Weld Filler Material Selection

The probability of selecting improper weld filler material is evaluated based upon historical rates for selection of improper weld filler material in nuclear reactor vessels (SNL 2007d, Section 6.3.7).

A Monte Carlo sampling was performed on the resultant fault tree. The resulting mean and median probabilities of improper weld filler material selection occurring and not being detected are 1.25×10^{-7} and 8.76×10^{-8} per waste package, respectively (SNL 2007d, Table 6-8).

2.3.6.6.3.2.3 Improper Heat Treatment of Outer Corrosion Barrier

The processes and equipment that will be employed to perform the heat treatment during the fabrication of the waste package components are discussed in Section 1.5.2. The waste package outer barrier is solution annealed and quenched to remove residual stresses that may lead to stress corrosion cracking (Section 2.3.6.5), and to minimize precipitation that could lead to aging and phase stability issues (Section 2.3.6.7). Due to complexity and the time sensitive nature of the quench process, the movement of the heated shell to the quench tank and subsequent quenching is considered to be the most probable opportunity for potential error in the process. Therefore, the analysis of the heat treatment process focuses on this phase (SNL 2007d, Section 6.3.3).

While fabrication processes for the waste package outer corrosion barrier have not been finalized, full scale fabrication of prototypes have been performed that provide collaborative support for the assumptions concerning fabrication processes. As part of that fabrication process, a full-sized Alloy 22 prototype shell was furnace heated in an inverted position and subsequently tank quenched on both sides using two pipes for purging internal gases demonstrating the heat treatment process (SNL 2007d, Section 6.3.3).

The probability that the waste package outer corrosion barrier will be subjected to an improper heat treatment, without the error being detected prior to emplacement in the repository, is a combination of human error and process failure probabilities. Five events in the heat treatment process that could lead to an improper heat treatment without detection and rework are considered in this evaluation (SNL 2007d, Section 6.3.3) using the human error probabilities contained in Table 2.3.6-22:

- Failure to move the outer corrosion barrier from the heat treatment facility to the quench facility within the time constraint necessary to maintain the shell temperature.
- Whether or not the movement time is properly monitored. This event only has consequences if the movement time is not sufficiently short.
- Failure to quench the outer corrosion barrier according to the specifications for cooling.

- Whether or not the outer corrosion barrier quenching is properly monitored. This event only has consequences if the quenching operation is not successful.

- Whether or not a post-processing inspection of the log of the outer corrosion barrier heat treatment process detects whether the process was performed correctly or not. This event only has consequences if previous errors were undetected.

A Monte Carlo sampling was performed on the fault tree. Monte Carlo sampling is used to obtain the distribution characteristics resulting from variable events. The resulting mean and median probabilities of improper outer shell heat treatment occurring and not being detected are 7.7×10^{-5} and 4.25×10^{-5} per waste package, respectively (SNL 2007d, Table 6-8).

2.3.6.6.3.2.4 Improper Heat Treatment of Outer Lid

The waste package outer lid is solution annealed and quenched in a manner similar to the outer shell. Since the outer lid and outer shell operations are similar, the outer lid fault tree analyses are identical to the outer shell analyses presented in Section 2.3.6.6.3.2.3 (SNL 2007d, Section 6.3.4). However, as the events are independent of one another, they are separately analyzed.

A Monte Carlo sampling was performed on the fault tree. Monte Carlo sampling is used to obtain the distribution characteristics resulting from variable events. The resulting mean and median probabilities of improper outer lid heat treatment occurring and not being detected are 7.51×10^{-5} and 4.09×10^{-5} per waste package, respectively (SNL 2007d, Table 6-8).

2.3.6.6.3.2.5 Improper Low-Plasticity Burnishing

The processes and equipment that will be employed to perform low-plasticity burnishing of the outer lid weld are discussed in Section 1.2.4.2. A representative industry low-plasticity burnishing process was used to develop the events involved in the improper low-plasticity burnishing of the waste package outer lid (SNL 2007d, Section 6.3.5). The fault tree estimates probabilities that: (1) the equipment does not operate properly, and (2) it is not detected during operations or checking.

A Monte Carlo sampling was performed on the fault tree. Monte Carlo sampling is used to obtain the distribution characteristics resulting from variable events. The resulting mean and median probabilities of improper low-plasticity burnishing occurring and not being detected are 3.84×10^{-5} and 7.28×10^{-6} per waste package, respectively (SNL 2007d, Table 6-8).

2.3.6.6.3.2.6 Improper Handling

This section estimates the probability that a waste package is subjected to handling damage prior to or during its emplacement in the repository without the damage being detected. This analysis considers possible damage between receipt and final inspection at time of emplacement, including, but not limited to, possible damage associated with tilting to upright position, downending, placement on the pallet, and transportation to the underground. Handling damage is defined as any visible gouging or denting of the waste package surface that may jeopardize the performance of the Alloy 22 outer corrosion barrier (SNL 2007d, Section 6.3.6).

A Monte Carlo sampling was performed on the fault tree. Monte Carlo sampling is used to obtain the distribution characteristics resulting from variable events. The resulting mean and median probabilities of improper waste package handling causing damage and not being detected are 9.63×10^{-7} and 7.71×10^{-7} per waste package, respectively (SNL 2007d, Table 6-8).

2.3.6.6.3.2.7 Early Waste Package Failure Probability

Improper base material selection, improper heat treatment of the outer shell and lid, improper weld filler material, improper low-plasticity burnishing, or mishandling of the waste package might have adverse consequences on waste package performance (SNL 2007d, Section 6.2.3). The consequence common to these types of defects is an increased susceptibility to stress corrosion cracking. An evaluation to quantify the probability that a waste package is affected by at least one of these defect types was performed using Monte Carlo simulations. The resulting probabilities were then fit to a lognormal distribution. The resultant probability of early failure is evaluated by a lognormal distribution with a mean per waste package of 1.13×10^{-4} and an error factor of 8.17 (SNL 2007d, Section 6.5.1). This distribution has a mean, median, 5th percentile, and 95th percentile of 1.13×10^{-4}, 4.14×10^{-5}, 6.10×10^{-6}, and 4.07×10^{-4} per waste package, respectively. For the repository inventory of approximately 11,600 waste packages, this corresponds to slightly more than one waste package on average. These values are based on the waste package fabrication and handling processes described in Sections 1.2.4 and 1.5.2. and necessarily imply the failures are independent (e.g., common cause failures are not likely) (SNL 2007d, Section 6.3). Waste package fabrication and handling processes will be controlled as described in Section 1.9.2.

2.3.6.6.4 Abstraction and Adequacy

[NUREG-1804, Section 2.2.1.3.1.3: AC 4, AC 5]

A summary of the abstraction for early failure of waste packages and an explanation of the abstraction adequacy are provided in this section.

2.3.6.6.4.1 Abstraction

This section describes the abstraction for early failure of waste packages, which includes the number of waste package early failures and the consequence of the failures. The number of waste package early failures is abstracted consistent with Section 2.3.6.6.3.2.7. While the failure mechanisms are expected to result in enhanced probability of stress corrosion cracking, the waste packages are treated as completely failed at the time of repository closure (SNL 2007d, Section 6.5.2).

2.3.6.6.4.2 Abstraction Adequacy

A comparison of failure probabilities was performed with data from the industrial, power, and nuclear industries dealing with boilers, pressure vessels, nuclear fuel rods, underground storage tanks, radioactive cesium capsules, and SNF dry storage casks (Table 2.3.6-21).

One study (Doubt 1984, p. 7) examined data on 229 failures of pressure vessels constructed to Class I requirements of design codes recognized in the United Kingdom. The failures occurred in a population of 20,000 vessels (Smith and Warwick 1978). The vessels were all welded and forged

unfired pressure vessels with wall thicknesses greater than 9.5 mm and working pressures in excess of 725 kPa. External leakage or in-service rupture caused by preexisting defects in the weld or base metal or by incorrect material were identified in 17 instances (Doubt 1984, p. 7). Failures that were due to thermal or mechanical failure, corrosion, internal leaks, and part-through cracks found by visual examination or nondestructive examination were excluded. This yielded an estimated failure rate due to manufacturing defects of 8.5×10^{-4} per vessel (Doubt 1984, p. 7).

Another source of information on failures is available from the National Board of Boiler and Pressure Vessel Inspectors (1999). The board maintains records on all boilers and pressure vessels that carry a National Board–registered stamping. From 1919 to 1997, incident reports of over 27,600,000 registrations were filed. From 1992 to 1997, incident reports indicate the number of failures that have occurred as a result of various causes. For the category of faulty design or fabrication, the average incident rate is 83 per year. By taking the average incident rate per year, multiplying by the number of years in the study and dividing by the number of pressure vessels, a point estimate probability of 2.4×10^{-4} per vessel for failure due to fabrication or design defects can be calculated.

There is a large database detailing the number and causes of fuel-rod failures. Fuel-rod failure rates for both pressurized water reactor and boiling water reactor fuel have been documented (EPRI 1997). Failure rates through 1985 ranged from 2×10^{-4} to 7×10^{-4} per rod. As a result of vendor efforts to develop improved fuel designs addressing some of the causes of failure, the current range of failure rates is from 6×10^{-5} to 3×10^{-4} per rod. Another study (Yang 1997, p. 10) showed that there were a total of 10 handling-damage failures in a population of 21,810 pressurized water reactor discharged assemblies, which yields a rate of 4.6×10^{-4} per discharged assembly. In each case, only a few rods in each assembly were actually damaged. A summary of General Electric boiling water reactor experience shows the existence of only 47 manufacturing defect–related failures in 4,734,412 rods fabricated between 1974 and 1993 (Potts and Proebstle 1994, p. 92), which yields a rate of 9.9×10^{-6} per rod. In a study of boiling water reactor and pressurized water reactor fuel rods fabricated by Advanced Nuclear Fuels (Tschoepe et al. 1994, pp. 2 to 4), fuel rod failures related to manufacturing defects were 1.2×10^{-5}, 6.5×10^{-6}, and 8.2×10^{-6} for boiling water reactors, pressurized water reactors, and both types, respectively.

These results are similar to the predicted probabilities described in the early failure model discussed in Section 2.3.6.6.3.2.7. Of note is the fact that these results include historical errors that occurred before more recent improvements made in fabrication methods, processes, procedures, and human factors and is therefore conservative.

2.3.6.7 Effects of Long-Term Thermal Aging and Phase Stability of Alloy 22

[NUREG-1804, Section 2.2.1.3.1.3: AC 1(1) to (4), AC 2, AC 3(1) to (3), AC 4]

Long-term thermal aging is the process by which certain second phases may precipitate from the metal matrix. This aging could impact the long-term phase stability of Alloy 22. The precipitation of key elements that provide beneficial corrosion resistant properties may reduce the corrosion resistance of the bulk material. This precipitation could also adversely impact mechanical properties.

Thermal aging will not affect the corrosion behavior of Alloy 22 (Section 2.2, Table 2.2-5, FEP 2.1.11.06.0A). This section provides additional supporting information. Analysis of thermal aging provided in this section includes a conceptual description, review of experimental data and data uncertainty, and analysis of the thermal aging model and model uncertainty.

2.3.6.7.1 Conceptual Description

[NUREG-1804, Section 2.2.1.3.1.3: AC 1(1) to (4)]

The impact of thermal aging on the corrosion of Alloy 22 under expected repository conditions is not significant. Alloy 22 phase stability may be adversely affected by holding the material at intermediate temperatures (below the solution-annealing temperature) for extended periods of time. The length of time for which phase stability is of concern is strongly dependent upon temperature. For temperatures around 650°C, the time of exposure to cause precipitation is in the range of several tens of hours to approximately 100 hours. At 300°C, an exposure time of well over 1,000 years and, at 200°C, an exposure time of at least 10,000 years would be required before precipitation would be expected (BSC 2004a).

Upon emplacement, the temperature of the Alloy 22 waste package outer barrier will remain below approximately 200°C (Table 2.3.5-7 and Figure 2.3.5-33) for all but the unlikely drift collapse scenario described in Section 2.3.4 and the igneous intrusion scenario described in Section 2.3.11. In the unlikely event of drift collapse in the first 90 years, the waste package outer barrier would be below approximately 300°C and after about 200 years would be below approximately 200°C thereafter (Figure 2.3.4-98). For these conditions, the impact of thermal aging on the corrosion of Alloy 22 is insignificant and therefore has been excluded (BSC 2004a, Section 8). Degradation resulting from phase instability for Alloy 22 thus does not affect waste package performance for the drift collapse temperature profile. The waste package outer corrosion barriers are assumed to be completely failed in an igneous event and thus aging and phase stability is not an issue for the igneous intrusion scenario (Section 2.3.11).

The phase stability model considers three forms of thermal aging:

- Tetrahedrally close-packed phase and carbide precipitation in the base metal
- Tetrahedrally close-packed phase and carbide precipitation in welded regions
- Long-range ordering reactions.

Tetrahedrally close-packed phase and carbide precipitates that form in Alloy 22 are generally rich in chromium, molybdenum, or both (Raghavan et al. 1984) and may occur in the base metal and weld regions. Because these elements are responsible for the corrosion resistance of Alloy 22, precipitation of tetrahedrally close-packed phases and carbides, especially at grain boundaries, can lead to an increased susceptibility to localized corrosion in the alloy. These phases are brittle and also tend to embrittle the alloy (Summers et al. 1999). They are known to form in Alloy 22 at temperatures greater than approximately 600°C after an exposure time of more than 100 hours. The kinetics of this precipitation was determined for both the base metal and the weld-affected zone (BSC 2004a, Section 1).

The tetrahedrally close-packed phases P, μ, and σ are present in the weld metal in the as-welded condition. These phases are eliminated for the fabrication welds through solution heat treatment.

However, they may be present in the final closure welds, which are not solution-heat-treated. The planned stress mitigation technique low-plasticity burnishing (Section 1.2.4.2) will not result in an increase in aging and phase instability, as discussed in Section 2.3.6.4.4.

Long-range ordering results in very small and finely dispersed precipitates. Long-range ordering occurs relatively quickly in nickel–chromium–molybdenum alloys such as Alloy 22 at temperatures of approximately 450°C to 600°C but slows as the temperature is reduced. This ordering has been linked to an increased susceptibility of nickel–chromium–molybdenum alloys to stress corrosion cracking and hydrogen embrittlement (Tawancy et al. 1983). Analyses discussed in Section 2.3.6.7.3.1 provide information on the rate at which long-range ordering may occur in Alloy 22 under repository conditions.

2.3.6.7.2 Data and Data Uncertainty

[NUREG-1804, Section 2.2.1.3.1.3: AC 2, AC 3(1) to (3)]

Data have been collected and analyzed to understand the possible extent of second phase precipitation expected in the repository. This section describes the experimental results and the data uncertainty for these experiments.

2.3.6.7.2.1 Experimental Results

To measure the amount of tetrahedrally close-packed phase precipitation in Alloy 22 base metal and welds, area-fraction measurements (mathematically equivalent to volume fraction measurements) have been made using scanning electron microscope image analyses as a function of aging time and temperature (BSC 2004a, Section 6.6.5).

Figure 2.3.6-36 presents the area-fraction measurements of tetrahedrally close-packed precipitation for base metal as a function of time and temperature (BSC 2004a, Section 7.6). A power law fitted line is provided for the results at 760°C where multiple measurements were made. Tetrahedrally close-packed phases are seen to readily form at higher temperatures, 760°C to 800°C, in less than 1,000 hours. In general, as the temperature is decreased, the onset of tetrahedrally close-packed phase precipitation is delayed, and the slopes of trend lines at lower temperatures become shallower, indicating a slower rate of phase precipitation. The measurements presented here are consistent with model predictions discussed in Section 2.3.6.7.4, which indicate that formation of tetrahedrally close-packed phases from the face-centered cubic solid solution is not of concern for a time-temperature profile expected after repository closure.

Area-coverage measurements (linear-fraction measurements) on grain boundaries have also been performed using scanning electron microscope image analyses and are shown in Figure 2.3.6-37 (BSC 2004a, Section 6.6.5.1). These measurements are similar to the area-fraction measurements on base metal samples. The measurements give a quantitative measure of grain boundary precipitation kinetics. These results are consistent with the precipitation kinetics for base metals.

Because hardness increases with the amount of long-range ordering of precipitation, microhardness measurements are indicative of long-range ordering. This is analogous to precipitation in age-hardened alloys (Reed-Hill 1973). Figure 2.3.6-38 shows such microhardness (Hv) measurements made on Alloy 22 as a function of time and temperature. The data indicate that

long-range ordering is possible within the temperature range of approximately 450°C to 600°C, (BSC 2004a, Section 7.6), (below 450°C long-range ordering is not kinetically favored; above 600°C long range ordering is not thermodynamically stable and the precipitates will be incorporated back into the matrix.) This observation conforms to the critical order–disorder temperature of the computational model, which is about 596°C (BSC 2004a, Section 6.6.4.3).

Tetrahedrally close-packed phases are present in the interdendritic regions of the as-welded structure (Cieslak et al. 1986). After aging, the amount and size of tetrahedrally close-packed precipitates increase with both time and temperature up to 760°C. Nucleation of precipitates was also observed to form in some areas of these samples. The area fraction of precipitates is shown as a function of time and temperature in Figure 2.3.6-39. In the as-welded condition, there is approximately a 0.02 vol % tetrahedrally close-packed phase. The average activation energy calculated from the slopes of Arrhenius plots of these data is 241 kJ/mol, which is comparable to the values of 250 kJ/mol and 260 kJ/mol for base metal (Rebak et al. 2000). The measurements presented here are consistent with model predictions discussed in Section 2.3.6.7.4, which indicate that precipitate nucleation and growth in the welds will not occur for the time temperature profile after repository closure.

2.3.6.7.2.2 Data Uncertainty

Phase stability is studied at temperatures greater than those expected in the repository so that the rate at which phase changes occur can be measured (BSC 2004a, Section 7.5). Precipitation rates are measured as a function of temperature, and the functional relationship is extrapolated to the lower temperatures in the repository. The stability of the metallic structures for natural analogues (Section 2.3.6.7.3.3) suggests that no low-temperature mechanism exists with precipitation rates significantly greater than those predicted (BSC 2004a, Section 7.5). This conclusion provides confidence that the high-temperature mechanisms used to extrapolate kinetics are the same as the low-temperature mechanisms that will be experienced under repository conditions.

When experimentally determining the extent of phase precipitation, uncertainty in the experimental results is primarily due to measurement uncertainties in the image analysis process (BSC 2004a, Section 6.7.1.1). The measurement uncertainty in the area-fraction-coverage values is accounted for in the standard deviation and 95% confidence interval values for each series of measurements at a particular time and temperature. The standard deviations and 95% confidence intervals are computed using industry standard procedures (ASTM E 562-95 1995).

The aging and phase stability model predicts the extent, not the initiation, of phase precipitation as a function of time and temperature. Therefore, while volume-fraction data have large uncertainty at low volume percentages, data within this range have no effect on the aging and phase stability model results. The uncertainty in the range of relevance for this model application is acceptable, since sufficient precipitation has occurred to reduce measurement uncertainty (BSC 2004a, Section 6.7.1.1).

2.3.6.7.3 Model and Model Uncertainty

[NUREG-1804, Section 2.2.1.3.1.3: AC 1(1) to (4), AC 4]

This section discusses the thermodynamic model for the long-term thermal aging of Alloy 22, as well as an alternative conceptual model. A description of the natural analogues that were used to validate the model is also included.

2.3.6.7.3.1 Thermal Aging Model

Theoretical modeling was performed to determine the phase diagrams and other thermodynamic properties of the phases that form in Alloy 22. Theoretical modeling was also used to calculate the rate at which the relevant phase transformations occur (Turchi 2001).

The stability of binary (e.g., nickel–chromium, nickel–molybdenum, and molybdenum–chromium) and ternary (e.g., nickel–chromium–molybdenum) alloys was investigated. The study also focused on the role of additional solutes, such as silicon, carbon, cobalt, neodymium, tantalum, and tungsten, as well as focusing on stability, ordering, and precipitation in Alloy 22. Results indicate that the tetrahedrally close-packed phases (P and possibly μ) are stable at repository temperatures and will form if they are not kinetically inhibited (BSC 2004a, Sections 6.3.2 and 6.6.4). The phases that would be stable under repository conditions form at temperatures below approximately 800°C. Sigma (σ) phase has not been observed to form, but it is included in the model through mathematical treatment.

To simulate the kinetic transformations of Alloy 22 over long time periods, the model used a simplified ternary nickel–chromium–molybdenum alloy that can be considered a surrogate for Alloy 22 (BSC 2004a, Section 6.6.4.3). The nominal composition used was 21.1 wt % chromium, 13.5 wt % molybdenum, and the remainder was nickel. The surrogate was considered appropriate for computational simplification and use of available elemental database information. Some of the minor elements were combined with similarly functioning major elements in the surrogate. Three transformations were considered: the face-centered cubic matrix to the oP6-ordered phase, the face-centered cubic matrix to the P phase (the P phase is also used as a surrogate for the σ and μ phases), and the face-centered cubic matrix to the σ phase. The corresponding thermodynamic model-generated phase-fraction versus temperature diagrams are shown in Figure 2.3.6-40. By comparison, model-generated phase-fraction versus temperature property diagrams for Alloy 22 confirm, similar to the results for the ternary surrogate, that at equilibrium and low temperature a three-phase field, including the oP6 ordered phase, P phase, and σ phase and face-centered cubic phase should exist (BSC 2004a, Section 6.6.1.1, Figure 77).

In Figure 2.3.6-41, the time-temperature-transformation diagram associated with the face-centered cubic-to-oP6-ordered phase transformation of Ni–21.1Cr–13.5Mo is displayed with 2%, 10%, and 15% transformation rates (BSC 2004a, Section 6.6.4.3).

Similarly, the transformation of Ni–21.1Cr–13.5Mo from the face-centered cubic-based matrix to the P phase with 2%, 10%, and 15% transformation rates was predicted as a function of time and temperature (Figure 2.3.6-42). The results are comparable with the qualitative observations (Turchi 2001). Finally, the transformation of Ni–21.1Cr–13.5Mo from the face-centered cubic-based matrix

to the σ phase with 2%, 5%, and 10% transformation rates was predicted as a function of time and temperature (Figure 2.3.6-43).

Figures 2.3.6-41, 2.3.6-42, and 2.3.6-43 show that extrapolation of each curve to lower temperatures is consistent with the expectation that significant amounts (greater than 2%) of these phases out of the face-centered cubic-solid solution for expected time-temperature profiles will not form after repository closure (Figure 2.3.5-33) (BSC 2004a, Section 6.6.4.3).

Uncertainties in the modeling of phase stability occur due to measurement precision in the amount of the phases and the uncertainty in the database thermal-chemical values used to model the rate of phase precipitation. However, there is a large time and temperature margin between the maximum waste package surface temperature-time curves and the model (even in the event of seismic drift collapse shown in Section 2.3.4), demonstrating the model is adequate for excluding the effects of thermal aging and phase stability (Section 2.2, Table 2.2-5, FEP 2.1.11.06.0A).

2.3.6.7.3.2 Alternative Conceptual Model

The martensitic transformation reaction is an accepted mechanism for phase transformation in certain metallic alloys (BSC 2004a, Section 6.4). For this reason, it has been considered as an alternative conceptual model for the phase transformation for Alloy 22. However, in experimental results that span a wide range of temperatures and time periods, no martensite has been observed to form in Alloy 22 (BSC 2004a, Section 6.4). Due to its inherent characteristics (e.g., temperature-dependent reaction and extremely rapid formation times), if martensite were to form in Alloy 22, it would have been easily observed in the tests conducted to date. Since martensitic phase transformations have not been observed in Alloy 22, the alternative conceptual model using the martensitic transformation reaction has been eliminated from further consideration.

2.3.6.7.3.3 Natural Analogues

Awaruite is a naturally occurring ordered nickel–iron metallic mineral with an approximate stoichiometry of Ni_3Fe. It was first discovered in Awarua, New Zealand, but has also been found at various locations around the world (Krishnarao 1964, p. 443). Josephinite, a rock found in Josephine County, Oregon, contains larger grains of awaruite than other sources of awaruite. In some instances, josephinite also has a unique mixture of minerals that have been tied to changes in the local environment and to higher temperatures associated with hornblende diorite dikes from igneous intrusions (Dick 1974, p. 297; Göpel et al. 1990, p. 26). Using potassium–argon dating, the age of these dike intrusions has been calculated to be approximately 150 to 155 million years (Dick 1974, p. 292). Other nearby rocks also associated with the formation of josephinite have been dated, using lead isotopes, at 159 ±8 million years (Göpel et al. 1990, p. 24). Thus, the age of josephinite is on the order of 150 million years.

Some samples of josephinite contain taenite (the high-temperature, disordered, face-centered cubic matrix nickel–iron metallic phase), as well as awaruite. The composition and amount of each of these phases in the two-phase mixture have been substituted in the nickel–iron phase diagram, showing that the taenite and awaruite phases formed in the temperature range of 460°C down to about 400°C (Botto and Morrison 1976). The fact that the composition and amount of these phases correspond with the phase diagram at the higher temperatures indicates that no changes have

occurred at lower temperatures. Taenite will not form below about 350°C; α–iron and awaruite are the stable phases at ambient temperatures. The fact that taenite, not α–iron, is present in josephinite also indicates that no changes have occurred in the 150 million years since these samples formed. Although taenite may be metastable in josephinite, it is possible that kinetics are inhibiting the reaction. These observations lend credence to the modeling treatment of Alloy 22 that the same mechanisms that occur at high temperatures also occur at low temperatures and that no new low temperature mechanisms occur (BSC 2004a, Section 7.5).

2.3.6.7.4 Summary

[NUREG-1804, Section 2.2.1.3.1.3: AC 4]

A summary of the model for long-term thermal aging of Alloy 22 and the adequacy of the model are provided in this section. Analyses (BSC 2004a, Section 6.1.2) have conservatively assumed that aging and phase stability precipitation mechanisms that operate at higher temperatures also operate at much lower temperatures and that the phases seen at the higher temperatures are also stable and may form at the lower temperatures. Information from josephinite shows stability of metallic phases after exposure over millions of years at low temperatures (BSC 2004a, Section 7.5). This conclusion is fully consistent with model predictions and experimental observations of no low-temperature mechanism with rates greater than those predicted for lower temperatures extrapolated from high-temperature data. This observation provides confidence that the high-temperature mechanisms used to determine kinetics are the same as those that occur at lower temperatures (BSC 2004a, Section 7.5).

Long-range ordering occurs at lower temperatures than those for the tetrahedrally close-packed phases. However, the associated kinetics based on model predictions, transmission electron microscopy, and microhardness measurements support the expected lack of formation of the ordered phase of the Ni_2Cr-type at repository temperatures because the phase formation kinetics are primarily driven by thermally activated diffusion (BSC 2004a, Sections 6.3 and 6.6). Thus, alloys such as Alloy 22 homogenized (or annealed) at high temperatures and rapidly quenched should not display any deleterious phases. Computationally derived time-temperature-transformation curves at the lower temperatures that are expected in a repository, indicate that the formation of the P phase or oP6-ordered phase from the face-centered cubic solid solution will not occur (BSC 2004a, Section 6.6.4.3).

To minimize potential phase instabilities resulting from fabrication of the waste package outer barrier, a solution heat treatment and rapid water quench of the as-fabricated waste package will be implemented (Section 1.5.2). Therefore, no aging effects are expected for the as-fabricated waste package prior to emplacement, including fabrication welds. The outer closure welds are stress-mitigated through low-plasticity burnishing (Section 1.2.4.2); which results in a cold-worked outer surface. The resultant cold work may cause an increase in dislocation density, which in turn could cause an increase in diffusion rates (Porter and Easterling 1992; Tawancy et al. 1983). However, the resultant increase in kinetics due to cold working is insufficient to affect thermal aging and phase stability of Alloy 22 (SNL 2007c, Section 6.4.6). Furthermore, the depth of significant cold work is minimal, so even if the cold work resulted in accelerated aging, it would result only in a small depth of accelerated corrosion relative to the thickness of material in compression.

The computational phase kinetics results for the P phase for the ternary nickel–chromium–molybdenum alloy (a surrogate for Alloy 22) were compared with volume-fraction measurements on Alloy 22 base metal at temperatures of approximately 700°C and 750°C (BSC 2004a, Section 7.6). The computational phase kinetics results are used to construct the time-temperature-transformation diagrams for a particular phase. The P phase formation computational results were compared with the tetrahedrally close-packed volume-fraction measurements, as the P phase is the most likely to form at these temperatures and times (BSC 2004a, Sections 4.1.8 and 7.5). The comparison shows that the computational results are conservative compared to the measured data, even though the actual samples contained additional minor impurities (BSC 2004a, Section 7.5).

Model predictions and extrapolation of higher temperature results to lower temperatures show that formation of tetrahedrally close-packed or ordered phases in Alloy 22 base metal and annealed welds will not occur for repository conditions following closure (BSC 2004a, Section 6.6). On this basis, neither the waste package outer corrosion barrier base metal nor weld metal is subject to enhanced degradation due to the effects of thermal aging (BSC 2004a, Section 8; SNL 2007c, Section 6.4.6); thus, this process is not included in the TSPA model (Section 2.2, Table 2.2-5, FEP 2.1.11.06.0A). The model predictions and extrapolation are based upon the range of tested Alloy 22 compositions (BSC 2004a, Section 8). However, as the quantity of alloying elements are decreased within Alloy 22 the rate and likelihood of precipitation is reduced (Hu et al. 2005). Therefore, the model results are applicable to an Alloy 22 composition (UNS N06022), with the additional constraints as controlled by Section 1.9.2:

- Cr = 20.0 to 21.4 wt %
- Mo = 12.5 to 13.5 wt %
- Fe = 2.0 to 4.5 wt %
- W = 2.5 to 3.0 wt %.

This range of compositions is included in, but more restrictive than the UNS N06022 composition range:

- Cr = 20.0 to 22.5 wt %
- Mo = 12.5 to 14.5 wt %
- Fe = 2.0 to 6.0 wt %
- W = 2.5 to 3.5 wt %.

2.3.6.7.5 Effect of Aging and Phase Stability on Corrosion Behavior

To analyze the effects of thermal aging and phase stability on corrosion of Alloy 22, three metallurgical conditions of Alloy 22 were studied using the multiple crevice assembly samples: mill-annealed, as-welded, and as-welded plus thermally aged at 700°C for 173 hours. At these aged conditions, the grain boundaries were fully covered with tetrahedrally closed-packed phases, as would be expected based on the data presented in Figure 2.3.6-37, and some bulk precipitation also occurred as would be expected based on the data presented in Figure 2.3.6-36. The samples were tested (using electrochemical methods similar to those presented in Section 2.3.6.4.2) in 5 mol/L $CaCl_2$ and 5 mol/L $CaCl_2$ + 0.5 mol/L $Ca(NO_3)_2$ solutions at temperatures up to 120°C (SNL 2007c, Section 6.4.6). The $CaCl_2$-based brines were conservatively selected as they are more

aggressive than the NaCl- or KCl-based brines that are more likely to occur under repository conditions. After immersion in the test solution at open-circuit corrosion potential for 24 hours, the polarization resistance of the samples was measured. The corrosion rates from the polarization-resistance measurements were only for comparative analysis of the effects of thermal aging on corrosion of Alloy 22; the tests are not intended to obtain the absolute values of the corrosion rate.

Comparison of the calculated corrosion rates of the mill-annealed, as-welded, and as-welded plus thermally aged samples are shown in Figure 2.3.6-8 for 5 mol/L CaCl solutions (SNL 2007c, Section 6.4.6). The comparison in Figure 2.3.6-8 clearly shows that there is no significant or consistent increase in the corrosion rates above the mill-annealed samples at corresponding temperatures due to welding or thermal aging of the welded samples for the tested conditions.

Uncertainty results from the wide range of environmental conditions to which the materials will be subjected and the use of corrosion rates from the polarization-resistance measurements. The data indicate that the corrosion behavior of Alloy 22 is not significantly affected by metallurgical condition, and aged and welded materials typically demonstrate lower corrosion rates than those at corresponding temperatures for the base mill-annealed material. The observation that as-welded and as-welded plus thermal aging have no significant effect on corrosion rates relative to mill-annealed samples is consistent with published results (Brossia et al. 2001, Section 3.2.1.3, Figure 3-13; Rebak et al. 2002). Furthermore, comparison of the anodic passive current densities of the as-welded Alloy 22 samples to those of the base metal samples showed no significant effect of the welds on the passive corrosion behavior of the alloy (Brossia et al. 2001, Section 3.2.1.3, Figure 3-13).

Based on the thermal aging and phase stability analyses, which show that insignificant aging and phase instability would occur under the thermal conditions expected in the repository, the corrosion behavior of the waste package outer corrosion barrier are not expected to be deleteriously affected by aging and phase instability in the repository (Figure 2.3.6-8). Mechanical properties are not expected to be significantly affected since the predicted amount of secondary phase precipitation is small. Therefore, thermal aging and phase instability effects on the corrosion rate and mechanical properties of the waste package outer barrier are excluded from the TSPA model (Section 2.2, Table 2.2-5, FEP 2.1.11.06.0A). See Section 2.2, Table 2.2-5 for the list of additional FEPs excluded from waste package models.

2.3.6.8 Drip Shield Degradation

[NUREG-1804, Section 2.2.1.2.2.3: AC 3, AC 4, AC 5; Section 2.2.1.3.1.3: AC 1(1) to (5), AC 2, AC 3(1) to (4), AC 4, AC 5; Section 2.2.1.3.2.3: AC 1(1) to (5), AC 2; Section 2.2.1.3.3.3: AC 1(3), (6)]

Titanium alloy drip shields will be installed over the waste packages prior to repository closure (Section 1.3.4.7). The purpose of the drip shield is to divert any moisture that might seep from the drift walls around the waste packages to the drift floor. The drip shields also protect the waste packages from damage due to rockfall.

The drip shield plates will be made of Titanium Grade 7, and the structural supports will be made of the higher strength alloy Titanium Grade 29. The chemical compositions of Titanium Grades 7

and 29 are shown in Table 2.3.6-23 (ASTM B 265-02 2002). The table also contains the chemical composition of Titanium Grade 16, which is essentially identical to Grade 7, except that it contains less palladium (approximately 0.06 wt %) than Grade 7 (approximately 0.2 wt %) and is used as an analogue in some of the corrosion testing. As palladium is added to pure titanium to improve corrosion resistance, the corrosion performance of Titanium Grade 7 is superior to that of Titanium Grade 16 (Schutz 2003).

This section analyzes the same degradation modes for the drip shield under a range of conditions that were discussed for degradation of the waste package: (1) general corrosion, (2) localized corrosion, (3) stress corrosion cracking, (4) early failure, and (5) thermal aging and phase stability. In addition, titanium creep is also discussed. Section 2.3.4 covers drip shield degradation due to seismic response and drift collapse. The drip shield is modeled as having failed for igneous consequences in Section 2.3.11. Some of the degradation mechanisms that are applicable to the waste package do not result in loss of drip shield functionality and are only briefly discussed. For mechanisms that may result in degradation of the drip shield, this section provides a conceptual description, a review of experimental data and data uncertainty, analysis of the drip shield models and model uncertainty, and abstraction and validation of the models.

As described below, drip shield general corrosion is included in TSPA. Stress corrosion cracking of the drip shield as a result of seismic events is discussed in Section 2.3.4. Stress corrosion cracking of the drip shield (Section 2.2, Table 2.2-5, FEP 2.1.03.02.0B) is excluded from TSPA because advective flow through the resultant cracks (Section 2.2, Table 2.2-5, FEP 2.1.03.10.0B) will be insignificant. Drip shield early failure is included in TSPA. Other drip shield degradation processes (e.g. hydrogen-induced cracking) are found to not occur or are found to have an insignificant impact and are excluded from the TSPA (Section 2.2, Table 2.2-5).

2.3.6.8.1 General Corrosion

[NUREG-1804, Section 2.2.1.3.1.3: AC 1(1) to (5), AC 2, AC 3(1) to (3), AC 4, AC 5]

General corrosion may occur in the presence or absence of water (aqueous corrosion or dry oxidation, respectively). The TSPA model conservatively applies aqueous general corrosion of the drip shield for all repository conditions, even when the drip shield is dry. The effects of general corrosion on the drip shield determine the time to drip shield failure for the nominal scenario. Thinning of the drip shield due to general corrosion is also accounted for in the structural response calculations for the seismic scenario as discussed in Section 2.3.4. Analysis of general corrosion provided in this section includes a conceptual description, review of experimental data and data uncertainty, analysis of the general corrosion model and model uncertainty, and abstraction and validation of the general corrosion model.

2.3.6.8.1.1 Conceptual Description

[NUREG-1804, Section 2.2.1.3.1.3: AC 1(1) to (4)]

General corrosion is the uniform thinning of a material. The general corrosion rate of the drip shield is modeled to be constant with time. This treatment results in earlier drip shield failures than expected because the general corrosion rate of metals and alloys tends to decrease with time (SNL 2007e, Section 7.4.2). As discussed in the following sections, general corrosion rates of the drip

shield have been calculated based on weight loss of Titanium Grade 7 samples after a 2.5-year exposure to repository-relevant aqueous environments (SNL 2007e, Section 6.1[a]). In addition, the model is validated using 5-year corrosion-rate data for Titanium Grade 16, and other literature data on similar titanium alloys (SNL 2007e, Section 7.2[a]).

2.3.6.8.1.2 Data and Data Uncertainty

[NUREG-1804, Section 2.2.1.3.1.3: AC 2, AC 3(1) to (3)]

2.3.6.8.1.2.1 Weight-Loss Data

The general corrosion rates are calculated by using weight-loss data determined from long-term corrosion tests (Estill 1998). These tests employed two Titanium Grade 7 and Titanium Grade 16 sample types: weight-loss samples and creviced samples. Both types of samples were exposed to repository-relevant environments SAW, SCW, and SDW (Table 2.3.6-1). Corrosion rates calculated from crevice samples were slightly lower than those from weight-loss samples, Figure 2.3.6-44. Because the crevice sample corrosion rate is lower than the weight loss sample rate, only the weight loss data are used in the model (SNL 2007e, Section 6.1[a]). The weight loss sample data fall into three distinct groupings (Table 2.3.6-24). The corrosion rates for the 90°C SCW data which contains high concentrations of fluoride (F^-) are significantly higher than the rest of the data, and are used to represent the corrosion rate for the outside of the drip shield, which could be subjected to seepage conditions. For the underside of the drip shield the data set representing the more benign conditions were used. By performing its intended purpose, the outer surface is exposed to seepage environments whereas the inner surface of the intact drip shield may only experience water films due to condensation (SNL 2007e, Section 5.5). As a conservative simplification, the outer surface of the drip shield is assumed to be subjected to seepage conditions at all times, when in fact benign conditions should apply when seepage is not present.

Weight-loss data were obtained for a range of environments, including SDW, SCW, and SAW at 60°C and 90°C (SNL 2007e, Section 6.5). The treatment of these data is further discussed in Section 2.3.6.8.1.3.

General corrosion rates for Titanium Grade 7 based on weight-loss and crevice samples are shown as cumulative distribution functions in Figure 2.3.6-45. The highest measured rate is approximately 50 nm/yr. At this rate, even if applied to both the inner and outer surface of the drip shield, the drip shield plate would not be reduced to less than half of the original wall thickness of 15 mm for 75,000 years after repository closure. The corrosion rates for the majority of the test samples were below 20 nm/yr. Figure 2.3.6-46 shows the corrosion rate cumulative distribution functions of the 2.5-year weight-loss coupons binned into the benign condition (used to model the drip shield inner surface corrosion rate), intermediate conditions (SCW 60°C), and aggressive conditions (SCW 90°C, used to model the drip shield outer surface corrosion rate).

General corrosion rates of Titanium Grade 16 in SCW solution (which contains a significant concentration of fluoride (Table 2.3.6-1)) exposed for 5 years were also obtained (SNL 2007e, Section 7.4). The general corrosion rates for Titanium Grade 16 based on 5-year weight-loss samples and crevice samples in SDW and SCW are combined and shown in Figure 2.3.6-47. The 5-year weight-loss specimen data had a maximum value of about 58 nm/yr with most of the other values under 20 nm/yr (SNL 2007e, Section 7.4). The 5-year crevice specimen data show a

maximum value of about 77 nm/yr with most of the values below about 30 nm/yr. The Titanium Grade 16 data are used as corroborative information for the model based upon 2.5-year test data for the more corrosion resistant Titanium Grade 7.

Some parameter uncertainty arises from the fact that the corrosion rate is experimentally determined by comparing before-and-after specimen weights that are very close to each other, within the accuracy of the weight-loss measurement methodology. The corrosion rate values given in Figures 2.3.6-45 and 2.3.6-47 were derived from such measurements. Uncertainty in the data is accounted for by applying uncertainty to the mean corrosion rate, and by not including the negative weight loss data (SNL 2007e, Sections 6.1.6.[a] and 6.1.7[a]).

2.3.6.8.1.2.2 Microbially Influenced Corrosion Data

Corrosion handbooks and other literature reviews generally indicate that titanium alloys are immune to microbially influenced corrosion (Revie 2000, Chapter 47). The stability of the TiO_2 passive film formed on titanium alloys provides this immunity. While titanium is susceptible to biofouling in seawater solutions, the biofilm does not compromise the integrity of the TiO_2 passive film, and therefore, biofouled titanium maintains its resistance to localized corrosion processes (Revie 2000, Chapter 47). Furthermore, the production of nitrates, polythionates, thiosulfates, and oxygen associated with aerobic biologic activity does not significantly increase the corrosion rate of titanium alloys (Brossia et al. 2001, Section 4.1.3). Therefore, microbially influenced corrosion will not have a significant effect on either general or localized corrosion processes of titanium alloys under the exposure conditions in the repository (Section 2.2, Table 2.2-5, FEP 2.1.03.05.0B).

2.3.6.8.1.3 Model and Model Uncertainty

[NUREG-1804, Section 2.2.1.3.1.3: AC 1(1) to (5), AC 4]

The general corrosion rate of the drip shield is modeled separately for the inner surface and the outer surface to reflect the less corrosive environment present on the underside of the drip shield that is not subjected to seepage (SNL 2007e, Section 6.1.5[a]).

The general corrosion rate of the inner surface of the drip shield is determined by using the 2.5-year Titanium Grade 7 lower corrosion rate weight-loss samples to account for the benign conditions the underside of the drip shield will experience. This data is presented in Figure 2.3.6-46. For the inner surface, the mean corrosion rate is 5.15 nm/yr. The uncertainty of this mean value is characterized by a normal distribution with a standard deviation divided by the square root of the number of data points (25). The resulting normal uncertainty of the mean corrosion rate is a standard deviation of 0.83 nm/yr. The corrosion rate for benign conditions at the 99.9th percentile of the uncertain mean distribution is approximately 7.7 nm/yr (SNL 2007e, Sections 6.1.7[a] and 8.1[a]). The negative values of weight loss were conservatively removed from this calculation (SNL 2007e, Section 6.1.5[a]).

The uncertain mean general corrosion rate of the outer surface is represented by a Student *t*-distribution to the cumulative distribution function from the 2.5-year Titanium Grade 7 weight-loss samples using only the SCW 90°C data which was much more aggressive than the other exposure environments to account for seepage conditions. This data is presented in Figure 2.3.6-46. For the outer surface, the corrosion rate at the 50th percentile is approximately 46 nm/yr. The

uncertainty in this mean value is characterized by a Student *t*-distribution (a broader normal distribution) due to the limited number of data points (six), divided by the square-root of the number of data points. The resulting uncertainty of the mean corrosion rate has a standard deviation of about 2.9 nm/yr. The corrosion rate for aggressive environments at the 99.9th percentile of the mean distribution is approximately 53 nm/yr (SNL 2007e, Section 6.1.6[a]).

The model assumes the distribution of these rates is constant with time. This assumption is conservative because corrosion rates decrease with time (SNL 2007e, Section 6.1.8[a]).

The general corrosion rate of the Titanium Grade 29 drip shield structural support components has been estimated by comparing the corrosion rate of Titanium Grade 7 and Grade 29 for a variety of relevant environments shown in Table 2.3.6-25. (SNL 2007e, Section 6.2[a]). The ratios of these corrosion rates were used to create a distribution of rate multipliers that are applied to the Grade 7 rates in order to arrive at the Grade 29 rates (Figure 2.3.6-48). The corrosion rates for Titanium Grade 7 and Titanium Grade 29 are used in structural analyses as discussed in Section 2.3.4. The corrosion rate for Titanium Grade 29 is estimated by obtaining a Titanium Grade 7 corrosion rate for aggressive conditions, and multiplying that rate by a value sampled from the cumulative distribution function (approach 3) shown in Figure 2.3.6-48. The range of corrosion rate ratios is attributed to uncertainty. This approach is conservative because the corrosion rate used is for aggressive conditions, ratios below one are treated as equal to one, and the selected distribution (shown as approach 3 in Figure 2.3.6-48), provides higher corrosion rates for Titanium 29 than the two other possible distributions.

An alternative conceptual model was considered that used a parabolic time dependence for the general corrosion rate. This alternative conceptual model assumes that the increasing oxide layer thickness has an inhibiting effect on diffusion of oxidizing species to the underlying metal and thus has an inhibiting effect on corrosion. This model would be expected to be less conservative than the primary model previously described (SNL 2007e, Section 6.5.6). Much the same as the above alternative model, Figure 2.3.6-49 depicts the decreasing trends in general corrosion with time. Several important observations can be drawn from Figure 2.3.6-49. First, the corrosion rate of titanium alloys substantially decreases with time. Secondly, the 2.5-year maximum corrosion rate, obtained from Titanium Grade 7, is lower than the 5-year corrosion rate obtained from Titanium Grade 16. This observation confirms that the general corrosion resistance of Titanium Grade 7 is superior to that of Titanium Grade 16. Lastly, the difference between the corrosion rates obtained from the weight-loss samples and crevice samples diminishes at the prolonged exposure times, confirming the resistance to localized corrosion of titanium alloys in repository-relevant environments.

2.3.6.8.1.4 Drip Shield General Corrosion Model Abstraction

[NUREG-1804, Section 2.2.1.3.1.3: AC 4]

The drip shield general corrosion model abstraction includes a constant general corrosion rate with time. The drip shield general corrosion model abstraction is consistent with the model described in Section 2.3.6.8.1.1. The variation in the general corrosion rate of the drip shield is considered to be due only to uncertainty (spatial variability in the general corrosion rate is not modelled). For these reasons, unlike the waste packages, each drip shield is modeled as a single entity (inner and outer surface distributions) independent of repository environment. This treatment is appropriate because

the primary failure mode for drip shields is structural failure after accounting for drip shield thinning due to general corrosion as described in Section 2.3.4. For each realization, a single general corrosion rate is sampled from each general corrosion rate distribution (one for the inner surface and one for the outer surface). These are applied to all drip shields. Using this conceptual model for drip shield general corrosion, all drip shields in the repository fail by general corrosion at the same time for any given realization (SNL 2008a, Section 6.3.5).

2.3.6.8.1.5 General Corrosion Model Adequacy

[NUREG-1804, Section 2.2.1.3.1.3: AC 5]

Model adequacy is established by comparing model predictions to experimental measurements that have been published in the open scientific literature and project data not used to develop the model. Calculated corrosion rates can be compared to experimental measurements to confirm the calculated rates are reasonable (SNL 2007e, Sections 7.4 and 7.2[a]).

Using a combination of depth profiling by ion sputtering and x-ray photoelectron spectroscopy, measured over a 6-year exposure period, corrosion rates in the range of 0.5 to 4 nm/yr were observed on Titanium Grade 2 and Titanium Grade 7 samples in compacted clays saturated with saline solutions at 95°C (Mattsson and Olefjord 1990). These values are significantly less than the model results.

A range of experimental techniques were used that produced similar corrosion rates to rates obtained by weight change methods on Long-Term Corrosion Test Facility specimens, despite use of a wide range of exposure environments and temperatures (SNL 2007e, Sections 7.4 and 7.2.1[a]).

Similarly, an absence of a temperature dependence between 90°C and 200°C was observed in aggressive German Q-brines (NaCl 1.4%; KCl 4.7%; $MgCl_2$ 26.8%; $MgSO_4$ 1.4%; H_2O 65.7%; pH = 4.9 at 25°C) for an Alloy of Titanium with 0.2 wt % palladium (essentially Titanium Grade 7) over an exposure period of about 3.5 years (Smailos, Schwarzkopf, and Köster 1986; Smailos, Schwartzkopf, Köster et al. 1990; Smailos and Köster 1987).

The Titanium Grade 16 5-year corrosion data (not used for model development) show similar corrosion rates to those observed for 2.5-year model development data. The 5-year corrosion data help validate the use of the cumulative distribution functions based on 2.5-year data as reasonable when applied to longer time frames (SNL 2007e, Section 7.4.2). The Titanium Grade 16 general corrosion rates determined from weight-loss and crevice samples are shown in Figure 2.3.6-47. These 5-year Titanium Grade 16 data show similar corrosion rates as the 2.5-year Titanium Grade 7 data used within the model, demonstrating that the model is appropriate (SNL 2007e, Section 7.2.2[a]).

A 20-year atmospheric corrosion study was performed on a suite of titanium alloys (Covington and Schutz 1981). No evidence of corrosion of any significance was found. The closest analogue to Titanium Grade 7 or Titanium Grade 29 was essentially the same as Titanium Grade 29 (Ti-6Al-4V) without the corrosion-resistant ruthenium addition. The reported corrosion rates were up to about 25 nm/yr. The environments ranged from being near the ocean, to an industrial area, to a rural area, and therefore correspond best to the general corrosion model in benign conditions. For this less-corrosion-resistant titanium alloy to have such a low long-term general corrosion rate provides

strong qualitative support for both the drip shield general corrosion model as well as for the relative rate ratio used for Titanium Grade 29 general corrosion. No significant difference in corrosion rates of these samples was observed as a result of the different environments (SNL 2007e, Section 7.2.1[a]).

Other investigators have noted only a marginal increase in the corrosion of titanium alloys in very aggressive brine solutions (pH as low as 1 and as high as 14; chloride concentration on the order of 30% in solution) (Smailos and Köster 1987; Smailos, Schwartzkopf, and Köster 1990; Mattsson and Olefjord 1990; Kim and Oriani 1987).

2.3.6.8.2 Localized Corrosion

[NUREG-1804, Section 2.2.1.3.1.3: AC 1(1) to (4), AC 2(1) to (4), AC 3(1) to (3), AC 4, AC 5]

2.3.6.8.2.1 Conceptual Description

[NUREG-1804, Section 2.2.1.3.1.3: AC 1(1) to (4)]

Titanium forms stable oxide films (passive films) that impede the rate of electrochemical reactions. Under aggressive environmental exposure conditions, the passive films may break down locally leading to localized attack of the underlying metal. In the absence of extremely aggressive environments the passive film will be stable for long time frames and will heal itself in short time frames (SNL 2007e, Section 1.1).

The following localized corrosion data were generated based on this conceptual model. For relevant repository conditions, localized corrosion does not occur, and thus, the model is not implemented in the TSPA (Section 2.2, Table 2.2-5, FEP 2.1.03.03.0B).

2.3.6.8.2.2 Data

[NUREG-1804, Section 2.2.1.3.1.3: AC 2, AC 3(1) to (3)]

The cyclic polarization method has been used to determine the threshold potentials for titanium alloys in various test media relevant to the environments expected in the repository (SNL 2007e, Section 6.6). Relevant test environments include SDW, SCW, and SAW at 30°C, 60°C, and 90°C, as well as SSW at 100°C and 120°C. The chemical compositions of these test media are detailed in Table 2.3.6-1. The cyclic polarization measurements technique is based on ASTM G 5-94, *Standard Reference Test Method for Making Potentiostatic and Potentiodynamic Anodic Polarization Measurements* (1994). A representative cyclic polarization curve is shown in Figure 2.3.6-50. In general, complete passivity (no passive film breakdown) is shown by these curves between the corrosion potential and the point defined as the threshold potential, the potential at which the forward scan current density suddenly increases, which is used as the critical potential ($E_{critical}$) (SNL 2007e, Section 6.6).

Titanium Grade 16 crevice samples were immersed in SAW, SCW, and SDW at 60°C and 90°C for 1 year and in SAW, SCW, and SDW at 60°C and 90°C for 5 years. No localized corrosion attack was observed. Localized corrosion was not observed in cyclic polarization tests at temperatures up to 120°C (SNL 2007e, Sections 6.6.2 and 6.6.4).

The effect of Ca^{2+} and Mg^{2+} on general corrosion of Titanium Grade 7 at elevated temperatures is insignificant, as shown in Table 2.3.6-26. Therefore, environments containing Ca^{2+} and Mg^{2+} do not affect the stability of the passive film and thus do not promote the initiation of localized corrosion. For Titanium Grade 7 in 8 to 9 mol/L $CaCl_2$ and 9 mol/L $CaCl_2$ + 0.9 mol/L $Ca(NO_3)_2$ at 100°C and 150°C, ΔE (defined in Section 2.3.6.8.2.3) is in the range of 1.4 to 3.5 V (SNL 2007e, Section 6.6.5). This ΔE is well above the localized corrosion threshold of 0V and thus no localized corrosion will occur under these conditions.

2.3.6.8.2.3 Localized Corrosion Model

[NUREG-1804, Section 2.2.1.3.1.3: AC 4]

The localized corrosion model for the titanium drip shield states that localized corrosion occurs if the open-circuit corrosion potential (E_{corr}) exceeds, or is equal to, the threshold potential for breakdown of the passive film ($E_{critical}$) (Equation 2.3.6-5). This is similar to the initiation criterion for localized corrosion of Alloy 22.

In the case of titanium alloys, $E_{critical}$ is defined as the threshold potential where the current density in a cyclic polarization forward scan suddenly increases (SNL 2007e, Section 6.6.1), as shown in Figure 2.3.6-50. This definition is different from that for Alloy 22 which uses E_{rcrev}. The reason that the threshold potential was chosen for $E_{critical}$ for localized corrosion of titanium is that the crevice repassivation potentials were not always obtained in the cyclic potentiodynamic polarization tests performed on titanium alloys, due to the excellent resistance of titanium to localized corrosion (SNL 2007e, Section 6.6.1). Refer to Figure 2.3.6-50 for a general representation of these potentials.

In this model, localized corrosion would occur if E_{corr} is greater than or equal to $E_{critical}$. The difference between $E_{critical}$ and E_{corr} is defined as ΔE, which is a function of absolute temperature, T, solution pH, and the chloride ion concentration:

$$\Delta E = d_0 + d_1 \cdot T + d_2 \cdot \log(Cl^-) + d_3 \cdot pH + \varepsilon \qquad \text{(Eq. 2.3.6-12)}$$

where d_0, d_1, d_2, and d_3 are constants determined from fitting Equation 2.3.6-12 (SNL 2007e, Section 6.6.3). The model error term, ε, represents data variance not explained by the fitting procedure and has a normal distribution with a mean of zero and variance of 10,500. The median values of these parameters are: $d_0 = 2{,}050$, $d_1 = -1.17$, $d_2 = 14.1$, and $d_3 = -48.9$, respectively (SNL 2007e, Section 6.6.3).

Figure 2.3.6-51 contains plots of ΔE versus pH and temperature under constant chloride concentration and ΔE versus pH and chloride concentration under constant temperature using Equation 2.3.6-12. The figures taken together show that ΔE is significantly greater than zero over all ranges of pH, chloride concentration, and temperature, even at the $\pm 4\sigma$ confidence level which accounts for data uncertainty. A ΔE of several hundred millivolts is maintained even at very high pH. Localized corrosion of Titanium Grade 7 thus does not initiate in a repository-relevant environment even at pH values as high as 14 (SNL 2007e, Section 6.6.3.1).

The drip shield will have thick structural components constructed from high-strength Titanium Grade 29 (Section 1.3.4.7). The repository environment is not expected to cause localized corrosion of the Titanium Grade 29 structural components. The passive film on the Titanium Grade 29 structural support components is expected to remain stable under expected repository conditions. Localized corrosion of these structural support components is not included in the localized corrosion model (SNL 2007e, Section 6).

2.3.6.8.2.4 Localized Corrosion Model Adequacy

[NUREG-1804, Section 2.2.1.3.1.3: AC 5]

Model validation is accomplished by comparing experimental measurements of key model parameters to corroborative data that have been published in the open scientific literature and project data not used to develop the model. The model values would predict localized corrosion well before the literature data, thereby validating the model and demonstrating that it is conservative.

Published Titanium Grade 7 pitting potentials in concentrated NaCl solutions of approximately 5,200 to 9,600 mV versus Ag/AgCl (Schutz and Thomas 1987, Table 23) are greater than the threshold potential values (approximately 1,000 to 1,400 mV versus Ag/AgCl reference electrode) used to develop the model. Factors such as temperature, addition of alloying elements, and chloride ion concentration may shift the pitting potential slightly (Hua, Mon et al. 2004). Titanium Grade 5, which contains 6% aluminum and 4% vanadium, has a pitting potential of around 2 V versus Ag/AgCl. Given that the open-circuit corrosion potentials of titanium alloys under repository exposure conditions are expected to be around 0 mV (Hua, Mon et al. 2004), localized corrosion of titanium alloys is not considered to be possible for repository conditions (SNL 2007e, Section 6.6).

Tests also were performed for localized corrosion of Titanium Grade 7 in basic saturated water (BSW-12, which is 50,000 times more concentrated than J-13 well water by evaporation) for up to 8 weeks at temperatures from 60°C to 105°C (Hua, Sarver et al. 2002). No localized corrosion was observed. It was also noticed that the preexisting surface imperfections, possibly due to material processing, remained after 4 and 8 weeks of exposure (Hua and Gordon 2003). It was concluded that the observed weight losses were due to general corrosion only (Hua, Sarver et al. 2002).

No localized corrosion attack was observed in long-term corrosion tests for up to 5 years of exposure in repository-relevant environments (SNL 2007e, Section 6.6.4).

In addition, tests were performed for localized corrosion of Titanium Grade 7 and Titanium Grade 29 with both fresh (non-oxidized surfaces) and pre-oxidized surfaces in four different salt solutions: (1) 3.6 *m* $CaCl_2$ + 5.8 *m* KCL + 1.8 *m* KNO_3 + 2 *m* $NaNO_3$; (2) 7 *m* KCl + 1.8 *m* $NaNO_3$ + 1.2 *m* NaCl + 2.4 *m* Na_2SO_4; (3) 7.2 *m* KCl + 0.3 *m* KNO_3 + 3.3 *m* $NaNO_3$ + 2.1 *m* Na_2SO_4 + 0.2 *m* NaF; and (4) 5 *m* KCl + 2.8 *m* KNO_3 + 6.6 *m* $NaNO_3$ + 6.8 *m* Na_2SO_4 + 0.1 *m* NaF + 0.1 *m* NaBr. The cyclic potentiodynamic polarization tests show that the Titanium Grade 7 and Titanium Grade 29 alloys maintain passivity at potentials at least as high as 500 mV (vs Ag/AgCl) with no localized corrosion observed (MO0705SCCIGM06.000, Section 6).

2.3.6.8.3 Stress Corrosion Cracking of Drip Shield

The drip shield will be fully stress-relief-annealed before emplacement (Section 1.3.4.7). Drip shield fabrication and handling processes will be based on the process described in Section 1.3.4.7 and will be controlled as described in Section 1.9.2. Therefore, the drip shield is not expected to be subjected to stress corrosion cracking in the absence of seismic events and rockfall. Even if stress corrosion cracking of the drip shield were to occur, the cracks would have no effect as advective flow through cracks of the drip shield is excluded from TSPA (Section 2.2, Table 2.2-5, FEP 2.1.03.10.0B).

Stress corrosion cracking as a result of disruptive events is discussed in Section 2.3.4. The conceptual description for stress corrosion cracking of the drip shield is the same as that for Alloy 22, as discussed in Section 2.3.6.5. A threshold stress is established for use in Section 2.3.4. Failures of Titanium Grade 7 were observed at applied stress ratios of about 1.1 to 1.4 times the yield strength in constant load tests which were conservatively performed in fully immersed test conditions at 105°C (SNL 2007a, Figure 4-1). Some specimens failed relatively early (at less than or equal to 168 hours) at applied stresses above 110% of yield strength, but at 110% of yield strength, there was a mixture of failure and nonfailure times from about 200 hours for first failure to several thousand hours without failure. This is consistent with a threshold stress of somewhat less than 110% of yield strength and is estimated to be at the yield stress value (SNL 2007a, Section 6.8.3.1). However, subsequent control tests performed in air at the same temperature (105°C) exhibited failure times similar to those specimens tested in the brine environment, indicating that the specimen failures were likely due to creep rupture rather than stress corrosion (SNL 2007a, Section 6.8.3.1).

In developing a basis for a threshold stress criterion for stress corrosion cracking initiation for Titanium Grade 7, available literature indicates Titanium Grade 7 is extremely resistant (or immune) to stress corrosion cracking initiation in repository-relevant brine environments (SNL 2007a, Section 6.8.3.1.3). Consistent with the literature, DOE-conducted testing confirmed that no stress corrosion cracking initiation is observed over the full range of primary (constant-load) (Figure 2.3.6-28) and secondary (U-bend) stresses that were evaluated. The stress corrosion cracking initiation threshold stress criterion is set at 80% of the at-temperature yield strength. This criterion is based upon U-bend specimens tested for up to 2.5 years with surface stresses of 83% of yield strength and constant load tests that did not exhibit stress corrosion cracking initiation (SNL 2007a, Section 6.8.3.1.3).

As Titanium Grade 29 has a much higher creep strength (SNL 2007a, Section 6.8.3.2) than Titanium Grade 7, the threshold stress criterion for stress corrosion cracking initiation for Titanium Grade 29 is set at 50% of the yield strength or slightly less than one-half the maximum observed stress imposed without stress corrosion cracking initiation or creep rupture. This 50% of yield strength value is based upon 6-month, constant-load tests under very aggressive brine conditions at 210°C sour brine environment (a dearrated NaCl- and CaF_2-saturated solution containing approximately about 250,500 ppm chloride and 461 ppm fluoride ions and an overpressure of H_2S and a CO_2) and U-bends exposed to 165°C SCW brine for over 4 months (SNL 2007a, Section 6.8.3.2).

2.3.6.8.4 Drip Shield Early Failure

[NUREG-1804, Section 2.2.1.2.2.3: AC 3(1), AC 4(1), AC 5(1); Section 2.2.1.3.1.3: AC (1) to (5), AC 2, AC 3(1) to (4), AC 4, AC 5]

Manufacturing and handling defects may result in early failure of drip shields. Analysis of early failure provided in this section includes a conceptual description, review of experimental data and data uncertainty, a description of the analysis and uncertainty, and abstraction and adequacy of the abstraction.

The manufacturing and handling processes considered within this analysis are based upon drip shield fabrication and handling processes described in Section 1.3.4.7. These processes, including welding, stress relief heat treatment, nondestructive examination, handling and placement, will be controlled as described in Section 1.9.2. The approach followed to investigate the mechanisms that may lead to the early failure of the drip shield is similar to that performed for the waste package described in Section 2.3.6.6 (SNL 2007d, Sections 6.3 and 6.4).

2.3.6.8.4.1 Conceptual Description

[NUREG-1804, Section 2.2.1.3.1.3: AC 1(1) to (4)]

The purpose of this analysis is (1) to evaluate the types of defects or imperfections that could occur in a drip shield and potentially lead to its early failure; and (2) to estimate the probability of occurrence for each.

Within the TSPA, early failure of a defective drip shield is conservatively modeled to occur at the time of repository closure. Drip shield early failure is represented as loss of 100% of the functionality of the drip shield. The most likely effect of manufacturing defects would be early onset of stress corrosion cracking which has been screened from TSPA (Section 2.2, Table 2.2-5, FEP 2.1.03.02.0B). Consequently, it is extremely conservative to assume that 100% of the drip shield functionality is lost in the early failure scenario.

2.3.6.8.4.2 Data and Data Uncertainty

[NUREG-1804, Section 2.2.1.3.1.3:AC 2, AC 3(1) to (4)]

The data used for drip shield early failure are the same used for the waste package early failure described in Section 2.3.6.6.2 (SNL 2007d, Section 6.4). Uncertainty is accounted for through the use of the error factors summarized in Table 2.3.6-22, which provide for a range of probabilities for each of the human error types.

2.3.6.8.4.3 Analysis and Uncertainty

[NUREG-1804, Section 2.2.1.3.1.3: AC 1(1) to (5), AC 4]

Early failure of drip shields is modeled to account for the probability of such failure. This section provides the screening justifications for excluded defect types, and describes how early failure probability is determined for the remaining defect types. This section also provides a drip shield early failure analysis.

2.3.6.8.4.3.1 Evaluation of Defect Types

The general types of manufacturing defects identified in Section 2.3.6.6.2.1 were evaluated and eliminated from consideration for the following reasons:

Weld Flaws—Since the drip shield will be fully stress-relief-annealed (Section 1.3.4.7), weld flaws will not act as possible stress corrosion cracking locations. Thus, drip shield fabrication weld flaws are not further considered (SNL 2007d, Section 6.2.3).

Improper Weld-Flux Material—Improper weld-flux material is eliminated because the welding method to be employed for drip shields does not use weld-flux material (SNL 2007d, Section 6.2.3).

Poor Weld-Joint Design—Poor weld joint design can be eliminated from further consideration because of the significant development and testing effort for joints (SNL 2007d, Section 6.2.3).

Surface Contamination—The probability of drip shield surface contamination that could affect drip shield performance (e.g., chemical or organic) was also evaluated (SNL 2007d, Section 6.2.3). Stringent controls will be placed on drip shield package fabrication and handling to limit the amount and type of surface contamination (Section 1.3.4.7). The consequence of drip shield surface contamination is not significant from a corrosion standpoint (SNL 2007d, Section 6.2.3). On this basis, drip shield surface contamination with regard to early failure is not considered further.

Mislocated Welds—Mislocated welds are not expected for the large multipass welds on the drip shields due to their size, location, significant quality assurance requirements, inspection, and extensive nondestructive evaluation. For large multipass welds, any significant mislocation of the electrode would cause the weld arc not to strike. This would be immediately obvious to both the operator and the control system for the automated welder (SNL 2007d, Section 6.2.3).

Missing Welds—The probability of missing welds does not warrant further consideration due to significant quality assurance requirements, inspections, and extensive nondestructive evaluations that will occur (SNL 2007d, Section 6.2.3). Extremely low historic failure rates in the industry for fuel rod welding supports this conclusion (SNL 2007d, Section 6.1.2).

Improper Low-Plasticity Burnishing—The drip shield is not low-plasticity burnished, and therefore does not need to be considered for early failure.

Administrative or Operational Error—Administrative and operational errors may occur, and provisions in drip shield and waste package fabrication and handling procedures and equipment will be made to minimize these errors. Even after taking the planned precautions, these types of errors are still recognized, and the associated rates and consequences are included in the evaluations for the remaining defect modes. Therefore, these types of errors are not considered to be separate defect modes (SNL 2007d, Section 6.1.6).

The remaining types of defects are discussed in Section 2.3.6.8.4.3.2.

2.3.6.8.4.3.2 Determination of Early Failure Probability

The remaining types of defects (base metal flaws, improper weld filler material, improper heat treatment, improper handling and installation) were analyzed.

2.3.6.8.4.3.2.1 Base Metal Flaws

The frequency for occurrence for introducing base metal flaws in the drip shield material is based upon the same analysis used for waste package material in Section 2.3.6.6.3.2.1 (SNL 2007d, Section 6.4.1).

A Monte Carlo sampling was performed on the fault tree. Monte Carlo sampling is used to obtain the distribution characteristics resulting from variable events. The resulting mean and median probabilities of improper drip shield base material selection occurring and not being detected are 2.53×10^{-7} and 1.77×10^{-7} per drip shield, respectively (SNL 2007d, Table 6-8).

2.3.6.8.4.3.2.2 Improper Weld Filler Material

The frequency for occurrence for use of improper weld filler material in drip shield fabrication is based upon the same analysis used for waste package weld filler material in Section 2.3.6.6.3.2.2 (SNL 2007d, Section 6.4.3).

A Monte Carlo sampling was performed on the fault tree. Monte Carlo sampling is used to obtain the distribution characteristics resulting from variable events. The resulting mean and median probabilities of improper drip shield weld filler material selection occurring and not being detected are 2.53×10^{-7} and 1.77×10^{-7} per drip shield (SNL 2007d, Table 6-8).

2.3.6.8.4.3.2.3 Improper Heat Treatment

The frequency for occurrence of improper drip shield heat treatment is based upon a fault tree similar to that used for waste package outer shell heat treatment in Section 2.3.6.6.3.2.3, but is less complex because of the fewer steps involved in heat treatment for the drip shield compared to the waste package. (SNL 2007d, Section 6.4.2).

A Monte Carlo sampling was performed on the fault tree. Monte Carlo sampling is used to obtain the distribution characteristics resulting from variable events. The resulting mean and median probabilities of improper drip shield heat treatment occurring and not being detected are 3.23×10^{-6} and 5.33×10^{-7} respectively per drip shield (SNL 2007d, Table 6-8).

2.3.6.8.4.3.2.4 Improper Drip Shield Installation

The frequency for occurrence that a drip shield is improperly installed in the repository, leaving a gap between an adjacent drip shield, is considered. The probabilities used in the analyses are based upon whether or not the operator will notice and respond to the error, and whether a checker will recognized the error and respond.

A Monte Carlo sampling was performed on the fault tree. Monte Carlo sampling is used to obtain the distribution characteristics resulting from variable events. The resulting mean and median probabilities of improper drip shield installation occurring and not being detected are 4.36×10^{-9} and 6.76×10^{-10} respectively per drip shield (SNL 2007d, Table 6-8).

2.3.6.8.4.3.2.5 Early Drip Shield Failure Probability

Improper base metal selection, weld filler selection, improper heat treatment, and improper installation might have adverse consequences on drip shield performance (SNL 2007d, Sections 6.4.1, 6.4.2, 6.4.3 and 6.4.4). An evaluation to quantify the probability that a drip shield is affected by at least one of these defect types was performed using Monte Carlo simulations. The resulting probabilities were then fit to a lognormal distribution. The resultant probability of early failure is evaluated by a lognormal distribution, with a mean per drip shield of 2.21×10^{-6} and an error factor of 14 (SNL 2007d, Section 6.5.1). This distribution has a mean, median, 5th percentile, and 95th percentile of 2.21×10^{-6}, 4.3×10^{-7}, 7.86×10^{-8}, and 6.97×10^{-6} per drip shield, respectively. For approximately 11,600 drip shields, this corresponds to well less than one drip shield on average. These values are based on the drip shield fabrication and handling processes described in Section 1.3.4.7, and necessarily imply the failures are independent (e.g., common cause failures are not likely) (SNL 2007d, Section 6.3). Drip shield fabrication, handling, and installation will be controlled as described in Section 1.9.

2.3.6.8.4.4 Abstraction and Adequacy

[NUREG-1804, Section 2.2.1.3.1.3: AC 4, AC 5]

A summary of the abstraction for early failure of drip shields, and an explanation of the abstraction adequacy, are provided in this section.

2.3.6.8.4.4.1 Abstraction

This section describes the abstraction for early failure of drip shields, which includes the number of drip shield early failures and the consequence of the failures. The number of drip shield early failures is abstracted consistent with Section 2.3.6.8.4.3.2.5. While early failure of the drip shield is not expected to result in complete loss of functionality, the drip shields are treated as completely failed at the time of repository closure (SNL 2007d, Section 6.5.2).

2.3.6.8.4.4.2 Abstraction Adequacy

The same comparison used for waste package abstraction adequacy is applicable to the drip shield abstraction (see Section 2.3.6.6.4.2).

2.3.6.8.5 Creep Deformation

An important aspect of drip shield performance is the potential creep deformation under long-term applied loads. The only long-term load on the drip shield would be due to weight of the rock mass that would cover the drip shield following collapse of the emplacement drift. This rockfall could subject the drip shield to plastic deformation and mechanical damage due to the resulting stresses.

Because of the unlikely possibility of early drift collapse after waste emplacement, the time-dependent deformation and stability of the drip shield was analyzed for 10,000 years for Titanium Grade 7 (or its analogue, Titanium Grade 2) and Titanium Grade 29 (or its analogues, Titanium Grade 5 and 24) (BSC 2005, Section 5.6).

A situation where creep strain at any point within the drip shield reaches 10% is considered to collapse the drip shield, and creep rupture within the drip shield is inferred for any creep strain level exceeding 10%. Analyses indicate maximum total creep strain below 5% during the 10,000-year period for all portions of the drip shield (BSC 2005, Section 5.6).

These relatively low, long-term strain levels are much less than levels where onset of creep rupture is expected and do not impact the drip shield seepage diversion function or the ability to protect the waste package from loads resulting from the rock overburden mass. Based on the relatively low, structurally acceptable creep strain calculated for conservative loading conditions, creep of the titanium drip shield alloys is excluded from the TSPA on the basis of low consequence (Section 2.2, Table 2.2-5, FEP 2.1.07.05.0B).

2.3.6.8.6 Aging and Phase Stability

Because precipitation of deleterious phases will not occur in the drip shield materials under relevant repository conditions, aging and phase change are not possible drip shield degradation mechanisms (Section 2.2, Table 2.2-5, FEP 2.1.11.06.0B) for relevant repository conditions. Both Titanium Grades 7 and 16 (a less corrosion resistant alloy similar to Titanium Grade 7) are α-phase alloys with very small additions of palladium. The solubility of palladium in these materials is about 1 wt % at 400°C. The nominal concentrations of palladium in both Titanium Grades 7 and 16 are well below the solubility limit at this temperature (Gdowski 1997, pp. 1 to 8; Schutz 2003). Intermetallic compounds capable of being formed in this system have not been reported to occur in Titanium Grades 7 and 16 with normal heat treatments. The procedures and equipment that will be employed to perform heat treatment during fabrication of the drip shields have not been decided. Normal heat treatment temperatures and controls will be chosen to include the range of thermal conditions (e.g., temperatures) associated with the fabrication and welding of the drip shields. Welding and post-weld heat treatment will be controlled as described in Section 1.9.2 to ensure the repository is operated within the analytical bases established in the TSPA. Therefore, the effects of phase instability possibly caused by thermal processes (e.g., welding) on degradation of Titanium Grade 7 will be insignificant (Schutz 2003, pp. 1,043 to 1,057).

Part of the drip shield is fabricated from Titanium Grade 7. The thicker structural support beam components of the drip shield will be constructed using the higher-strength Titanium Grade 29, which has alloying elements aluminum and vanadium to provide the required structural strength in addition to palladium to provide corrosion resistance. Titanium Grade 29 is an alpha-beta alloy and is expected to remain stable with proper fabrication and heat treatment controls. Commercial alpha-beta titanium alloys are generally stable up to approximately 425°C for 1,000 hours or more (ASM International 1990, p. 628). Therefore, the Titanium Grade 29 structural support material is expected to remain stable at the maximum expected drip shield exposure temperatures under repository conditions of less than 200°C, or under drift collapse conditions of less than 300°C for about 200 years. Therefore, thermal aging and phase instability are excluded from TSPA.

2.3.6.9 Conclusions

2.3.6.9.1 Summary of Significant Processes for EBS Barrier Capability

The drip shield and waste package corrosion models described in this section include features and processes that contribute to the capability of the EBS, as described in Section 2.1.2.2. The drip shields and waste packages are significant features:

Waste Package—The following processes and characteristics of the waste package are important to the capability of the EBS:

- **General Corrosion of Waste Packages**—General corrosion rates of Alloy 22 in a range of likely environmental conditions are sufficiently low that the waste packages will last for long periods of time and are modeled within the TSPA. Thinning of the waste package due to general corrosion is accounted for in the structural response calculations presented in Section 2.3.4. General corrosion models are presented in Section 2.3.6.3.

- **Localized Corrosion of Waste Packages**—Localized corrosion mechanisms on the waste package surface are dependent on the thermal-hydrologic and thermal-chemical environment on the waste package surface. Localized corrosion is only possible in those cases where the drip shield fails to perform its function, incoming seepage is allowed to contact the waste package and certain aggressive environments are present. This may occur due to drip shield early failure or after considerable drip shield thinning due to general corrosion, as described in Section 2.3.6.4. Localized corrosion due to dust deliquescence is excluded from TSPA (Section 2.2, Table 2.2-5, FEP 2.1.09.28.0A)

- **Stress Corrosion Cracking of Waste Packages**—Stress corrosion cracking of Alloy 22 is modeled to occur as a result of mechanical degradation following seismic events and in the closure weld lid region for the nominal scenario. Such stress cracks are sufficiently small and tight to allow only diffusive transport of radionuclides through the cracks. Stress corrosion cracking models and data are presented in Section 2.3.6.5.

- **Early Failure of Waste Packages**—A range of human factor errors could result in a waste package being emplaced that has the potential for an early failure at a weld. This possibility has been included in abstraction models used in the early failure scenario class of the TSPA as presented in Section 2.3.6.6.

Drip Shield—The following processes and characteristics of the drip shield (Section 2.3.6.8) are potentially important to the capability of the EBS as discussed in Section 2.1:

- **General Corrosion of Drip Shields**—General corrosion rates of titanium in a range of likely environmental conditions are sufficiently low that the drip shields will perform for long periods of time and are modeled within the TSPA. Thinning of the drip shields due to general corrosion is accounted for in structural response modeling (see Section 2.3.4). This process has been included in models of drip shield degradation presented in Section 2.3.6.8.

- **Localized Corrosion of Drip Shields**—Titanium is extremely resistant to localized corrosion due to its passive film. Localized corrosion will not occur in repository environments. The model for drip shield localized corrosion is presented in Section 2.3.6.8. Localized corrosion due to dust deliquescence is excluded from TSPA (Section 2.2, Table 2.2-5, FEP 2.1.09.28.0B).

- **Stress Corrosion Cracking of Drip Shields**—The titanium drip shield is potentially susceptible to stress corrosion cracking. Uncertainty exists in the stress state and threshold stress required for a stress corrosion crack to be initiated, and other uncertainties exist regarding the degree of propagation of any stress-induced crack in titanium. Stress corrosion cracking is modeled to be independent of the environment although the environments to support stress corrosion may not occur within the repository. The presence of cracks will not affect the performance of the drip shield in preventing or substantially reducing the amount of water that could directly contact the waste package, and is excluded from TSPA (Section 2.2, Table 2.2-5, FEP 2.1.03.02.0B).

- **Early Failure of Drip Shield**—During fabrication and installation, a range of human factor errors could result in a drip shield being emplaced that has the potential for an early failure. This possibility is included in the early drip shield failure abstraction models used in the early failure scenario class of the TSPA (Section 2.4) and as discussed in detail in Section 2.3.6.8.]

- **Creep of Metallic Materials in the Drip Shield**—Titanium Grade 7 used for the drip shield plates may undergo creep deformation at temperatures as low as room temperature when subjected to tensile stresses exceeding approximately 50% of the yield strength (SNL 2007a, Section 6.8.7). Titanium Grade 29, which is used for the drip shield structural members, has significantly higher creep resistance (SNL 2007a, Section 6.8.3). The analyses of creep deformation of the drip shield includes the mechanical coupling of the drip shield deformation and its interaction with the surrounding rock rubble. When the drip shield deforms through long-term creep a reactive backpressure (a confinement caused by the rubble) is developed which tends to inhibit further creep deformation. Based on these analyses, creep of the drip shield titanium alloys has been excluded from the performance assessment (Section 2.2, Table 2.2-5, FEP 2.1.07.05.0B). Although not credited in the treatment of stress corrosion cracking of the drip shield titanium alloys, creep following any stress corrosion cracking has the beneficial effect of decreasing crack propagation.

2.3.6.9.2 Key Uncertainties Associated with Barrier Capability

Uncertainty in the characterization of the degradation of the drip shield and waste package arises from uncertainties in the models for the various environmental exposure conditions and degradation processes. The uncertainties in the TSPA abstractions include uncertainties in the data from the tests measuring degradation processes and rates, as well as uncertainties in the conceptual and numerical models used to analyze the processes. These uncertainties are incorporated probabilistically in the TSPA by using ranges of parameter values representing the chemical characteristics of fluids that can contact the drip shield and waste package and for the rates of the various degradation processes.

The ranges of parameters and process rates used in the performance model are based on the results of testing and analysis, as well as on the fundamental physical principles that apply.

The TSPA implementation of waste package degradation abstractions accounts for uncertainty by simulating the performance of several hundred waste packages. The effects of spatial and temporal variations in the exposure conditions across the repository are included by explicitly incorporating the relevant exposure condition histories described in Section 2.3.5 into the TSPA model. The exposure condition parameters that are considered to vary over the repository are temperature and relative humidity on the waste package outer surfaces.

In addition, variability in corrosion processes on a single waste package to account for sample to sample variability in corrosion rates used to develop the waste package corrosion model is represented by dividing the waste package outer surface area into subareas (i.e., patches) and stochastically sampling the degradation model parameter values for each patch. The use of patches explicitly represents the variability in degradation processes on a single waste package at a given time. Furthermore, every waste package in a given simulation is assigned different exposure conditions, thus addressing waste package–to–waste package variability.

In the TSPA model, uncertainty in waste package and drip shield degradation is analyzed with multiple realizations of the TSPA model.

Uncertainty in drip shield general corrosion rates is represented by two different corrosion rate distributions for the inner and outer surfaces of the drip shield. There is no variability in the drip shield general corrosion rate.

The general corrosion rate of the waste package outer surface is temperature dependent and includes variability and uncertainty components. Uncertainty in the general corrosion rate is contained in its temperature-dependent slope term, C_1 (Equation 2.3.6-1). The variability in the waste package rate results from R_0, the general corrosion rate distribution at 60°C (333.15 K), determined from the 5-year crevice geometry samples (Equation 2.3.6-2). Fitting uncertainty is accounted for with three separate Weibull distributions. In addition, spatial and temporal variability of the exposure temperature in the repository leads to spatial and temporal variability in the general corrosion rates used to model general corrosion of Alloy 22. The net result is that every patch on each waste package will have a different general corrosion rate that will vary with temperature.

Microbially influenced corrosion is represented by an enhancement factor applied to the general corrosion rate of the waste package outer surface when the relative humidity threshold is exceeded. The value for the threshold relative humidity above which microbially influenced corrosion takes place is uncertain and is sampled from a uniform distribution. Variability of the microbially influenced corrosion enhancement factor is sampled from a uniform distribution and applied to each waste package patch after the relative humidity threshold is reached.

The evaluation of waste package closure weld flaw sizes and number of flaws includes variability and uncertainty. The variation in weld flaw sizes is expressed as variability at the waste package level, given by a cumulative distribution function (SNL 2008a, Section 6.3.5). The variation in the number of weld defects is expressed as variability at the waste package level given by a Poisson distribution with an uncertain parameter (i.e., count per closure weld) (SNL 2008a, Section 6.3.5).

This parameter is a function of the flaw size and count parameters that are sampled as uncertain for each realization (SNL 2008a, Section 6.3.5).

The evaluation of stress corrosion cracking for the outer-closure lids includes variability and uncertainty. Variability is represented by the variation of the stress and stress intensity factor profiles with angle and depth. Uncertainty is expressed as the variation in stress and stress intensity profiles as a function of material yield strength. The epistemic uncertainty in the stress and stress intensity factor profiles is introduced through a scaling factor, z. The variations in the threshold stress and stress intensity factor distributions are entirely due to uncertainty. The uncertainty in crack growth rate is a function of the repassivation slope. The variation in the repassivation slope is entirely due to uncertainty.

The evaluation of early failed waste packages and drip shields accounts for both epistemic and aleatory uncertainty. Epistemic uncertainty in the probability of various errors which could lead to early failure (Table 2.3.6-22) results in distributions for the probability of a random waste package or drip shield failure. In a particular TSPA realization, the number of early failed waste packages and drip shields, the type of waste package affected and the location of each early failure are treated as aleatory uncertainties.

Fourteen uncertain coefficients in the waste package outer barrier localized corrosion initiation abstraction represent epistemic uncertainties in the underlying data. These coefficients correspond to the linear regression fitting parameters a_0, a_1, a_2, a_3, a_4, and ε_{rcrev} in Equation 2.3.6-6; and c_0, c_1, c_2, c_3 c_4, c_5, c_6, and ε_{corr} in Equation 2.3.6-7 associated with the crevice repassivation potential and the long-term steady-state corrosion potential.

2.3.6.9.3 Key Conservatisms in Models Used to Assess Barrier Capability

In addition to the parameter uncertainties above, a variety of uncertainties in the data from the tests measuring degradation and transport processes and uncertainties in the conceptual and numerical models used to analyze the processes are addressed by making bounding estimates and conservative assumptions in the waste package and drip shield degradation models described in this section. These assumptions generally lead to earlier waste package and drip shield failures resulting in earlier release times from the EBS. These assumptions include the following:

- **Early Failure of Waste Packages**—The entire surface area of an early failed waste package is considered to be completely failed, even though the failure mechanism would not be expected to impact the entire surface area. The main contributors to early waste package failure are the improper heat treatment of the waste packages and improper low-plasticity burnishing. Although the failure mechanisms are expected to involve stress corrosion cracking and possibly phase instability, the waste packages are conservatively treated as completely failed at the time of repository closure (SNL 2007d, Section 6.5.2). This conservatism in considering the entire surface area to be completely failed increases the area for radionuclide transport from the early failed waste packages. More information on early failure of waste packages is provided in Section 2.3.6.6.1.

- **Threshold Relative Humidity for General Corrosion Initiation on Waste Packages**—A relative humidity threshold for initiation of general corrosion of the waste packages is

modeled. A relative humidity threshold for the initiation of aqueous general corrosion clearly exists (ASM International 1987, p. 82), below which only slower dry oxidation would occur. However, there is insufficient information and data to quantify the aqueous general corrosion initiation threshold relative humidity for varying water chemistry conditions (SNL 2008a, Section 6.3.5). More information on threshold relative humidity for general corrosion initiation on waste packages is provided in Section 2.3.6.

General corrosion is initiated at the time of repository closure, leading to a conservative estimate of waste package corrosion. The use of a relative humidity threshold would delay the initiation of general corrosion (SNL 2008a, Section 6.3.5).

- **Stainless Steel Inner Vessel and TAD Canisters**—There is no corrosion credit taken for the use of a stainless steel inner vessel or TAD canister with regard to limiting water influx after the outer corrosion barrier is breached. Stainless steel is less corrosion resistant than the Alloy 22 used for the waste package outer corrosion barrier and may fail within a relatively short time after breach of the waste package outer corrosion barrier (SNL 2008a, Section 6.3.5). The stainless steel waste package inner vessel and TAD canister are expected to provide some performance benefit for waste containment and could potentially contribute to the reduction of the rate of radionuclide release after waste packages are breached (SNL 2007c, Section 6.3.3).

- **General Corrosion Rate of Waste Package Outer Corrosion Barrier**—The general corrosion rate of the waste package outer corrosion barrier at a given temperature is represented as being time independent. General corrosion rates of the waste package outer corrosion barrier actually decrease with time (SNL 2007c, Section 6.4.3.5.1). However, there is insufficient information and data to quantify the time dependence. This conservatism in considering the general corrosion rate as time independent is expected to result in the overestimation of waste package general corrosion rate (SNL 2007c, Figure 7-1). More information on the general corrosion rate of the waste package outer corrosion barrier is provided in Section 2.3.6.3.1.

- G**eneral Corrosion Rate Distribution for Waste Package Outer Corrosion Barrier**—Two sample types, weight-loss samples and creviced samples, are used for general corrosion weight-loss measurements. The general corrosion rate distribution for the waste package outer corrosion barrier is based on the weight loss of the creviced samples. General corrosion of creviced samples, however, is generally 2 to 5 times higher than for noncreviced samples (SNL 2007c, Section 6.4.3.2). Furthermore, the increased corrosion rates observed in the creviced samples are due to differences in sample preparation and not the crevice itself (SNL 2007c, Section 6.4.3.2). Use of the weight-loss samples would result in significantly lower corrosion rates. More information on general corrosion rate distribution for the waste package outer corrosion barrier is provided in Section 2.3.6.3.1.

- **General Corrosion Rate Distribution Adjustment for Patch Size**—The general corrosion rate distribution is conservatively adjusted for patch size. The patch size used in the TSPA model is a factor of 4 larger than the size of the crevice samples in the experiments that generated the data from which the general corrosion rate was derived.

The adjustment method is to effectively use the highest of four sampled values for the patch general corrosion rate (SNL 2008a, Section 6.3.5). The approach is conservative because it is probable that not all four samples from the Weibull distribution will have the highest rate (SNL 2008a, Section 6.3.5). More information on general corrosion rate distribution adjustment for patch size is provided in Section 2.3.6.3.4.

- **Waste Package Surface Area Subjected to Localized Corrosion**—No information is available regarding the spatial extent of the local environment exposure conditions on the waste package; therefore, the waste package surface area affected by localized corrosion due to seepage is based on the waste package surface area exposed to seepage (SNL 2007c, Section 8.3.1). This conservatism is expected to overestimate the area available for radionuclide transport from the waste packages. More information on waste package surface area subjected to localized corrosion is provided in Section 2.3.6.4.3.

- **Representation of the Critical Threshold Potential for Localized Corrosion**—The critical threshold potential ($E_{critical}$) is conservatively represented by the crevice repassivation potential (E_{rcrev}) determined from cyclic potentiodynamic polarization tests (SNL 2007c, Section 6.4.4.1). The chemical exposure conditions in creviced regions can be more severe than those in noncreviced regions (SNL 2007c, Section 1.2). This leads to the measurement of lower repassivation (critical) potentials in creviced versus noncreviced regions. More information on representation of the critical threshold potential for localized corrosion is provided in Section 2.3.6.4.3.

- **Crevice Corrosion**—The dominant form of localized corrosion is assumed to be crevice corrosion as opposed to pitting corrosion, which occurs on exposed surfaces away from the crevices. The initiation threshold for crevice corrosion, in terms of exposure conditions, is lower than that for pitting corrosion (SNL 2007c, Section 6.4.4). Additionally, crevice corrosion is applied to the entire waste package surface, although it is unlikely that crevice attack would occur over the entire surface area (SNL 2007c, Assumption 5.3). This conservatism in applying crevice corrosion to the entire waste package surface is expected to result in overestimation of the number of waste packages that experience localized corrosion. More information on crevice corrosion is provided in Section 2.3.6.4.1.

- **Localized Corrosion Rate of Waste Package Outer Corrosion Barrier**—The localized corrosion propagation rate for the waste package outer corrosion barrier is represented to propagate at a time-independent constant rate (SNL 2007c, Assumption 5.4). The localized corrosion propagation rate is known to actually decrease with increasing time (SNL 2007c, Section 6.4.4.8.2); however, there is insufficient information and/or data to quantify the time dependence. This conservatism in applying a constant localized corrosion rate is expected to result in the overestimation of the number of waste packages that fail due to localized corrosion. More information on the localized corrosion rate of the waste package outer corrosion barrier is provided in Section 2.3.6.4.1.

- **Effects of Inhibitive Anions**—No credit is taken in the localized corrosion initiation abstraction for the effects of inhibitive anions other than nitrate. For example, carbonate and sulfate ions can have an inhibitive effect on localized corrosion. However, there is

insufficient information and/or data to quantify the effect of inhibitive anions other than nitrate on localized corrosion initiation (SNL 2007c, Section 8.3.1). Localized corrosion initiation predictions for solutions with significant amounts of potentially inhibitive ions other than nitrate are thus expected to be conservative (SNL 2007c, Section 8.3.1), in that the model does not include the potential inhibitive effect of these other ions. More information on the effects of inhibitive anions is provided in Section 2.3.6.4.3.

- **Effect of Changing Chemical Environment on Localized Corrosion Propagation**—Once localized corrosion has been initiated, it is represented as continuing to propagate regardless of any changes in the bulk chemical exposure environment which potentially may lessen or halt the localized corrosion rate (SNL 2007c, Section 8.3.1). This conservatism is expected to result in the overestimation of the number of waste packages that fail due to localized corrosion. More information on the effect of changing chemical environment on localized corrosion propagation is provided in Section 2.3.6.4.3.

- **General Corrosion Rate of the Drip Shield**—The corrosion rates for general corrosion of the drip shield were overestimated by using time-independent rates that show no decrease in corrosion rate with time (SNL 2007e, Section 6.1.8[a]). More information on the general corrosion rate of the drip shield is provided in Section 2.3.6.8.1.5.

- **All Dripping Water Falls on Drip Shields**—All seepage into the drifts, not just the seepage above the drip shields, is assumed to fall on the drip shields. This conservative approach is taken to simplify the modeling approach and also because the uncertainty in the seepage locations is difficult to quantify (SNL 2007g, Section 5.1). This conservative approach will overestimate the seepage flux contacting the drip shield. More information on all dripping water falling on drip shields is provided in Section 2.3.7.12. This conservatism underestimates the barrier capability of the drip shield to divert water from the waste package. More information on how water that penetrates the drip shield falling on waste packages is provided in Section 2.3.7.12. This conservatism underestimates the contribution to barrier capability of the waste package and its ability to protect the waste from water and to limit its transport.

- **Dripping on the Waste Package**—All the dripping water that would penetrate a drip shield would be represented as falling on the crown of the waste package. This conservative approach is taken to simplify the modeling approach and also because the uncertainty in the seepage locations is difficult to quantify (SNL 2007g, Section 5.1). This conservatism would increase the flux through a breached drip shield and onto the waste packages as discussed in Section 2.3.7.12.

2.3.6.9.4 Summary of Key Abstraction Parameters Provided to TSPA and Consistency with Process Models

Figure 2.3.6-3 shows the information transfer among the principal model components for the TSPA nominal scenario class. The waste package and drip shield degradation model component, shown on Figure 2.3.6-4, includes submodels for drip shield degradation and waste package degradation.

Waste package and drip shield corrosion are incorporated in the TSPA in a manner consistent with the underlying process models and analyses as described in Section 2.3.6.

The waste package general corrosion abstraction (Section 2.3.6.3.4.1) provides the TSPA waste package and drip shield degradation model component with parameters for waste package patch size, cumulative distribution functions for Alloy 22 general corrosion rates, temperature dependent corrosion rates, and enhancement factor for microbially influenced corrosion.

The waste package localized corrosion abstraction (Section 2.3.6.4.4.1) provides the TSPA waste package and drip shield degradation model component with expressions for the crevice repassivation potential and the long-term steady-state corrosion potential and an algorithm for evaluation of localized corrosion initiations under a range of repository-relevant exposure conditions. The abstraction also provides a range of localized corrosion rates (Table 2.3.6-8) for use once localized corrosion has been initiated. TSPA treats the entire waste package surface as affected, when the model output states that the affected area is limited to the wetted surface area. This simplification is conservative, in that it over-estimates the affected area.

The waste package stress corrosion cracking abstraction (Section 2.3.6.5.4.1) provides the TSPA waste package and drip shield degradation model component with parameters for evaluation of the waste package closure weld including: stress corrosion cracking threshold stress and stress intensity criteria, weld flaw sizes and numbers, variation of the stress and stress intensity factor profiles with angle and depth, crack growth rate, and repassivation slope.

The waste package early failure abstraction (Section 2.3.6.6.4.1) provides the TSPA waste package and drip shield degradation model component with a distribution representing the probability of a defective waste package due to improper base metal, improper weld filler material, improper heat treatment, improper low-plasticity burnishing, or mishandling.

The drip shield general corrosion abstraction (Section 2.3.6.8.1.4) provides the TSPA waste package and drip shield degradation model component with cumulative distribution functions of corrosion rates for the inner and outer surfaces of the drip shield.

The drip shield early failure abstraction (Section 2.3.6.8.4.4.1) provides the TSPA waste package and drip shield degradation model component with a distribution representing the probability of a defective drip shield due to improper base metal, improper weld filler, improper heat treatment, or mishandling.

2.3.6.10 General References

Altman, W.D.; Donnelly, J.P.; and Kennedy, J.E. 1988a. *Peer Review for High-Level Nuclear Waste Repositories: Generic Technical Position.* NUREG-1297. Washington, D.C.: U.S. Nuclear Regulatory Commission. TIC: 200651.

Altman, W.D.; Donnelly, J.P.; and Kennedy, J.E. 1988b. *Qualification of Existing Data for High-Level Nuclear Waste Repositories: Generic Technical Position.* NUREG-1298. Washington, D.C.: U.S. Nuclear Regulatory Commission. TIC: 200652.

Andresen, P.L. 1991. "Fracture Mechanics Data and Modeling of Environmental Cracking of Nickel-Base Alloys in High Temperature Water." *Corrosion 91, The NACE Annual Conference and Corrosion Show, March 11–15, 1991, Cincinnati, Ohio*, Paper No. 44, Houston, Texas: National Association of Corrosion Engineers. TIC: 255507.

Andresen, P.L.; Angeliu, T.M.; Young, L.M.; Catlin, W.R.; and Horn, R.M. 2002. "Mechanisms and Kinetics of SCC in Stainless Steels." *Tenth International Conference on Environmental Degradation of Materials in Nuclear Power Systems–Water Reactors, August 5–9, 2001, Lake Tahoe, Nevada.* Houston, Texas: NACE International. TIC: 252999.

Andresen, P.L. and Ford, F.P. 1994. "Fundamental Modeling of Environment Cracking for Improved Design and Lifetime Evaluation in BWRs." *International Journal of Pressure Vessels and Piping, 59* (1–3), 61–70. New York, New York: Elsevier. TIC: 247388.

Andresen, P.L.; Kim, Y.J.; Emigh, P.W.; Catlin, G.M.; and Martiniano, P.J. 2003. *GE GRC Final Report.* BSC PO 2450-100-PO-10508. Las Vegas, Nevada: Bechtel SAIC Company. ACC: MOL.20040520.0076.

Andresen, P.L.; Young, L.M.; Emigh, P.W.; and Horn, R.M. 2002. "Stress Corrosion Crack Growth Rate Behavior of Ni Alloys 182 and 600 in High Temperature Water." *Corrosion/2002, 57th Annual Conference & Exposition, April 7–11, 2002, Denver, Colorado*, Paper No. 02510. Houston, Texas: NACE International. TIC: 255502.

ASM International 1987. *Corrosion*. Volume 13 of *ASM Handbook*. Formerly 9th Edition, Metals Handbook. Materials Park, Ohio: ASM International. TIC: 240704.

ASM International 1990. *Properties and Selection: Nonferrous Alloys and Special-Purpose Materials*. Volume 2 of *ASM Handbook*. Formerly Tenth Edition, *Metals Handbook.* Materials Park, Ohio: ASM International. TIC: 241059.

ASME (American Society of Mechanical Engineers) 1969. *Criteria of the ASME Boiler and Pressure Vessel Code for Design by Analysis in Sections III and VIII, Division 2*. New York, New York: American Society of Mechanical Engineers. TIC: 254727.

ASTM B 265-02. 2002. *Standard Specification for Titanium and Titanium Alloy Strip, Sheet, and Plate.* West Conshohocken, Pennsylvania: American Society for Testing and Materials. TIC: 254000.

ASTM E 562-95. 1995. *Standard Test Method for Determining Volume Fraction by Systematic Manual Point Count*. Philadelphia, Pennsylvania: American Society for Testing and Materials. TIC: 253834.

ASTM G 1-90. 1999. *Standard Practice for Preparing, Cleaning, and Evaluating Corrosion Test Specimens*. West Conshohocken, Pennsylvania: American Society for Testing and Materials. TIC: 238771.

ASTM G 5-94. 1994. *Standard Reference Test Method for Making Potentiostatic and Potentiodynamic Anodic Polarization Measurements*. Philadelphia, Pennsylvania: American Society for Testing and Materials. TIC: 231902.

ASTM G 59-97. 1998. *Standard Test Method for Conducting Potentiodynamic Polarization Resistance Measurements.* West Conshohocken, Pennsylvania: American Society for Testing and Materials. TIC: 249897.

ASTM G 61-86. 1998. *Standard Test Method for Conducting Cyclic Potentiodynamic Polarization Measurements for Localized Corrosion Susceptibility of Iron-, Nickel-, or Cobalt-Based Alloys*. West Conshohocken, Pennsylvania: American Society for Testing and Materials. TIC: 246716.

Aziz, P.M. 1956. "Application of the Statistical Theory of Extreme Values to the Analysis of Maximum Pit Depth Data for Aluminum." *Corrosion, 12* (10), 35–46. Houston, Texas: National Association of Corrosion Engineers. TIC: 241560.

Baker, E.A. 1988. "Long-Term Corrosion Behavior of Materials in the Marine Atmosphere." *Degradation of Metals in the Atmosphere, Proceedings of the Symposium on Corrosion of Metals, Philadelphia, Pennsylvania, 12–13 May 1986*, Dean, S.W. and Lee, T.S., eds. ASTM STP 965, 125–144. Philadelphia, Pennsylvania: American Society for Testing and Materials. TIC: 224019.

Beavers, J.A.; Devine, T.M., Jr.; Frankel, G.S.; Jones, R.H.; Kelly, R.G.; Latanision, R.M.; and Payer, J.H. 2002. *Final Report, Waste Package Materials Performance Peer Review Panel, February 28, 2002*. Las Vegas, Nevada: Waste Package Materials Performance Peer Review Panel. ACC: MOL.20020614.0035.

Benhardt, H.C.; Eide, S.A.; Held, J.E.; Olsen, L.M.; and Vail, R.E. 1994. *Savannah River Site Human Error Data Base Development for Nonreactor Nuclear Facilities (U).* WSRC-TR-93-581. Aiken, South Carolina: Westinghouse Savannah River Company, Savannah River Site. ACC: MOL.20061201.0160.

Blackwood, D.J.; Peter, L.M.; and Williams, D.E. 1988. "Stability and Open Circuit Breakdown of the Passive Oxide Film on Titanium." *Electrochimica Acta, 33* (8), 1143–1149. New York, New York: Pergamon Press. TIC: 248517.

Böhni, H. 2000. "Localized Corrosion of Passive Metals." *Uhlig's Corrosion Handbook*, Chapter 10. Revie, R.W., ed. 2nd Edition. New York, New York: John Wiley & Sons. TIC: 248360.

Botto, R.I. and Morrison, G.H. 1976. "Josephinite: A Unique Nickel-Iron." *American Journal of Science, 276* (3), 241–274. New Haven, Connecticut: Yale University, Kline Geology Laboratory. TIC: 249797.

Brossia, C.S.; Browning, L.; Dunn, D.S.; Moghissi, O.C.; Pensado, O.; and Yang, L. 2001. *Effect of Environment on the Corrosion of Waste Package and Drip Shield Materials*. CNWRA 2001–2003. San Antonio, Texas: Center for Nuclear Waste Regulatory Analyses. TIC: 252324.

BSC (Bechtel SAIC Company) 2004a. *Aging and Phase Stability of Waste Package Outer Barrier.* ANL-EBS-MD-000002 REV 02. Las Vegas, Nevada: Bechtel SAIC Company. ACC: DOC.20041005.0003.

BSC 2004b. *Evaluation of Potential Impacts of Microbial Activity on Drift Chemistry.* ANL-EBS-MD-000038 REV 01. Las Vegas, Nevada: Bechtel SAIC Company. ACC: DOC.20041118.0005.

BSC 2005. *Creep Deformation of the Drip Shield*. CAL-WIS-AC-000004 REV 0A. Las Vegas, Nevada: Bechtel SAIC Company. ACC: DOC.20050830.0007.

Bush, S.H. 1983. *Reliability of Nondestructive Examination*. NUREG/CR-3110. Volume 3. Washington, D.C.: U.S. Nuclear Regulatory Commission. TIC: 218323.

Cieslak, M.J.; Headley, T.J.; and Romig, A.D., Jr. 1986. "The Welding Metallurgy of Hastelloy Alloys C-4, C-22, and C-276." *Metallurgical Transactions A, 17A* (11), 2035–2047. Warrendale, Pennsylvania: Metallurgical Society of AIME. TIC: 233952.

Covington, L.C. and Schutz, R.W. 1981. "Resistance of Titanium to Atmospheric Corrosion." *Corrosion/81, International Corrosion Forum, April 6–10, 1981, Toronto, Ontario, Canada*, 113/1–113/7. Houston, Texas: National Association of Corrosion Engineers. TIC: 248534.

CRWMS M&O (Civilian Radioactive Waste Management Systems Management & Operating Contractor) 1998. *Waste Package Degradation Expert Elicitation Project*. Rev. 1. Las Vegas, Nevada: CRWMS M&O. ACC: MOL.19980727.0002.

Dick, H.J.B. 1974. "Terrestrial Nickel–Iron from the Josephine Peridotite, Its Geologic Occurrence, Associations, and Origin." *Earth and Planetary Science Letters, 24* (2), 291–298. Amsterdam, The Netherlands: North-Holland. TIC: 249849.

Doubt, G. 1984. *Assessing Reliability and Useful Life of Containers for Disposal of Irradiated Fuel Waste*. AECL-8328. Chalk River, Ontario, Canada: Atomic Energy of Canada Limited. TIC: 227332.

Drever, J.I. 1997. "Evaporation and Saline Waters." Chapter 15 of *The Geochemistry of Natural Waters: Surface and Groundwater Environments*. 3rd Edition. Upper Saddle River, New Jersey: Prentice Hall. TIC: 246732.

Dunn, D.S.; Cragnolino, G.A.; and Sridhar, N. 2000. "An Electrochemical Approach to Predicting Long-Term Localized Corrosion of Corrosion-Resistant High-Level Waste Container Materials." *Corrosion, 56* (1), 90–104. Houston, Texas: NACE International. TIC: 254836.

Dunn, D.S.; Pensado, O.; and Cragnolino, G.A. 2005. "Performance Assessment of Alloy 22 as a Waste Package Outer Barrier." *Corrosion/2005, 60th Annual Conference & Exposition, 1945-2005, April 3-7, 2005, George R. Brown Convention Center, Houston, Texas*. Paper No. 05588. Houston, Texas: NACE International. TIC: 257165.

Dunn, D.S.; Yang, L.; Pan, Y.-M.; and Cragnolino, G.A. 2003. "Localized Corrosion Susceptibility of Alloy 22." *Corrosion/2003, 58th Annual Conference & Exposition, March 16–20, 2003, San Diego, California*, Paper No. 03697. Houston, Texas: NACE International. TIC: 254387.

EPRI (Electric Power Research Institute) 1997. *The Technical Basis for the Classification of Failed Fuel in the Back-End of the Fuel Cycle*. EPRI TR-108237. Palo Alto, California: Electric Power Research Institute. TIC: 236839.

EPRI 2002. *Evaluation of the Proposed High-Level Radioactive Waste Repository at Yucca Mountain Using Total System Performance Assessment, Phase 6*. EPRI TR-1003031. Palo Alto, California: Electric Power Research Institute. TIC: 252239.

Estill, J.C. 1998. "Long-Term Corrosion Studies." Section 2.2 of *Engineered Materials Characterization Report*. McCright, R.D., ed. UCRL-ID-119564 Volume 3 Rev. 1.1. Livermore, California: Lawrence Livermore National Laboratory. ACC: MOL.19981222.0137.

Farmer, J.; McCright, D.; Gdowski, G.; Wang, F.; Summers, T.; Bedrossian, P.; Horn, J.; Lian, T.; Estill, J.; Lingenfelter, A.; and Halsey, W. 2000. "General and Localized Corrosion of Outer Barrier of High-Level Waste Container in Yucca Mountain." *Transportation, Storage, and Disposal of Radioactive Materials, 2000, Presented at the 2000 ASME Pressure Vessels and Piping Conference, Seattle, Washington, July 23–27, 2000*, Hafner, R.S., ed. PVP-*408*, 53–69. New York, New York: American Society of Mechanical Engineers. TIC: 251259.

Fix, D.V.; Yilmaz, A.; Wong, L.L.; Estill, J.C.; and Rebak, R.B. 2005. "Effect of Surface Stress Mitigation on the Corrosion Behavior of Alloy 22." *Corrosion/2005, 60th Annual Conference & Exposition, 1945–2005, April 3–7, 2005, George R. Brown Convention Center, Houston, Texas*, Paper No. 05606, Houston, Texas: NACE International. TIC: 257165.

Fontana, M.G. 1986. *Corrosion Engineering*. 3rd Edition. New York, New York: McGraw-Hill. TIC: 240700.

Ford, F.P. and Andresen, P.L. 1988. "Development and Use of a Predictive Model of Crack Propagation in 304/316L, A533B/A508 and Inconel 600/182 Alloys in 288°C Water." *Environmental Degradation of Materials in Nuclear Power Systems—Water Reactors, Proceedings of the Third International Symposium, Traverse City, Michigan, August 30–September 3, 1987*, Theus, G.J. and Weeks, J.R., eds. 789–800. Warrendale, Pennsylvania: Metallurgical Society. TIC: 247505.

Frankel, G.S. 1998. "Pitting Corrosion of Metals, A Review of the Critical Factors." *Journal of the Electrochemical Society, 145* (6), 2186–2198. Pennington, New Jersey: Electrochemical Society. TIC: 254587.

Frankel, G.S. 2002. "Localized Corrosion Phenomenology and Controlling Parameters." Section 6 of *Waste Package Materials Performance Peer Review, A Compilation of Special Topic Reports*. Wong, F.M.G. and Payer, J.H., eds. Las Vegas, Nevada: Waste Package Materials Performance Peer Review Panel. ACC: MOL.20020731.0138.

Frankel, G.S. and Kelly, R.G. 2002. "Passivity-Induced Ennoblement." Section 11 of *Waste Package Materials Performance Peer Review, A Compilation of Special Topic Reports*. Wong, F.M.G. and Payer, J.H., eds. Las Vegas, Nevada: Waste Package Materials Performance Peer Review Panel. ACC: MOL.20020731.0138.

Gdowski, G.E. 1991. *Survey of Degradation Modes of Four Nickel-Chromium-Molybdenum Alloys*. UCRL-ID-108330. Livermore, California: Lawrence Livermore National Laboratory. ACC: NNA.19910521.0010.

Gdowski, G.E. 1997. *Degradation Mode Survey Candidate Titanium—Base Alloys for Yucca Mountain Project Waste Package Materials*. UCRL-ID-121191, Rev. 1. Livermore, California: Lawrence Livermore National Laboratory. ACC: MOL.19980120.0053.

Göpel, C.; Manhès, G.; and Allègre, C.J. 1990. "U-Pb Isotope Systematics in Josephinites and Associated Rocks." *Earth and Planetary Science Letters, 97* (1/2), 18–28. Amsterdam, The Netherlands: Elsevier. TIC: 249851.

Gordon, G.M. 2002. "F.N. Speller Award Lecture: Corrosion Considerations Related to Permanent Disposal of High-Level Radioactive Waste." *Corrosion, 58* (10), 811–825. Houston, Texas: NACE International. TIC: 256497.

Haynes International 1997a. *Hastelloy Alloy C-276*. Kokomo, Indiana: Haynes International. TIC: 238832.

Haynes International 1997b. *Hastelloy C-22 Alloy*. Kokomo, Indiana: Haynes International. TIC: 238121.

Hu, H.; Turchi, P.E.A.; and Wong, F. 2005. *Computational Modeling of Phase Stability in Alloy 22 Over a Range of Chemical Compositions for the Yucca Mountain Project*. UCRL-MI-212471. Livermore, California: Lawrence Livermore National Laboratory. ACC: LLR.20070627.0002.

Hua, F. and Gordon, G. 2003. "On Apparent Bi-Linear Corrosion Rate Behavior of Ti Grade 7 in Basic Saturated Water (BSW-12) Below and Above 80°C." *Corrosion/2003, 58th Annual Conference & Exposition, March 16–20, 2003, San Diego, California*, Paper No. 03687. Houston, Texas: NACE International. TIC: 254248.

Hua, F. and Gordon, G. 2004. "Corrosion Behavior of Alloy 22 and Ti Grade 7 in a Nuclear Waste Repository Environment." *Corrosion, 60*, (8), 764–777. Houston, Texas: NACE International. TIC: 256354.

Hua, F.; Mon, K.; Pasupathi, V.; Gordon, G.; and Shoesmith, D. 2004. "Corrosion of Ti Grade 7 and Other Ti Alloys in Nuclear Waste Repository Environments—A Review." *Corrosion/2004, 59th Annual Conference & Exposition, March 28–April 1, 2004, New Orleans*, Paper No. 04689. Houston, Texas: NACE International. TIC: 255943.

Hua, F.; Sarver, J.; Jevec, J.; and Gordon, G. 2002. "General Corrosion Studies of Candidate Container Materials in Environments Relevant to Nuclear Waste Repository." *Corrosion/2002,*

57th Annual Conference & Exposition, April 7–11, 2002, Denver, Colorado, Paper No. 02530. Houston, Texas: NACE International. TIC: 252067.

Hunkeler, F. and Boehni, H. 1983. "Pit Growth Measurements on Stainless Steels." *Passivity of Metals and Semiconductors, Proceedings of the Fifth International Symposium on Passivity, Bombannes, France, May 30–June 3, 1983*, Froment, M., ed. 655–660. New York, New York: Elsevier. TIC: 236283.

Ishikawa, H.; Honda, A.; and Sasaki, N. 1994. "Long Life Prediction of Carbon Steel Overpacks for Geological Isolation of High-Level Radioactive Waste." *Life Prediction of Corrodible Structures*. Parkins, R.N., ed. *1*, 454–483. Houston, Texas: NACE International. TIC: 254834.

Jack, T.R. 2002. "Biological Corrosion Failures." In *Failure Analysis and Prevention*, Volume 11, 881–898 of *ASM Handbook*. Materials Park, Ohio: ASM International. TIC: 258293.

Jayaweera, P.; Priyantha, N.; Macdonald, D.D.; Engelhard, G.; and Davydov, A. 2003. *Deterministic Prediction of Localized Corrosion Damage to Alloy C-22 HLNW Canisters*. SRI Project 10333. Menlo Park, California: SRI International. TIC: 253900.

Jones, D.A. 1996. *Principles and Prevention of Corrosion*. 2nd Edition. Upper Saddle River, New Jersey: Prentice Hall. TIC: 241233.

Jones, R.H. and Ricker, R.E. 1987. "Stress-Corrosion Cracking." In *Corrosion,* Volume 13, 145–163 of *Metals Handbook*. 9th Edition. Metals Park, Ohio: ASM International. TIC: 209807.

Kehler, B.A.; Ilevbare, G.O.; and Scully, J.R. 2001. "Crevice Corrosion Stabilization and Repassivation Behavior of Alloy 625 and Alloy 22." *Corrosion, 57* (12), 1042–1065. Houston, Texas: NACE International. TIC: 254305.

Khaleel, M.A.; Chapman, O.J.V.; Harris, D.O.; and Simonen, F.A. 1999. "Flaw Size Distribution and Flaw Existence Frequencies in Nuclear Piping." *Probabilistic and Environmental Aspects of Fracture and Fatigue: The 1999 ASME Pressure Vessels and Piping Conference*. PVP-386, 127–144. New York, New York: American Society of Mechanical Engineers. TIC: 245621.

Kim, Y.J. and Oriani, R.A. 1987. "Brine Radiolysis and its Effect on the Corrosion of Grade 12 Titanium (1)." *Corrosion, 43* (2), 92–97. Houston, Texas: National Association of Corrosion Engineers. TIC: 246022.

Krishnarao, J.S.R. 1964. "Native Nickel-Iron Alloy, Its Mode of Occurrence, Distribution and Origin." *Economic Geology, 59* (3), 443–448. Lancaster, Pennsylvania: Economic Geology Publishing. TIC: 249850.

Lian, T.; Martin, S.; Jones, D.; Rivera, A.; and Horn, J. 1999. "Corrosion of Candidate Container Materials by Yucca Mountain Bacteria." *Corrosion 99, 54th Annual Conference and Expo, San Antonio, Texas, April 25–30, 1999*, Paper No. 476. Houston, Texas: NACE International. TIC: 245833.

LL040803112251.117. Target Compositions of Aqueous Solutions Used for Corrosion Testing. Submittal date: 08/14/2004.

Lloyd, A.C.; Shoesmith, D.W.; McIntyre, N.S.; and Noël, J.J. 2003. "Effects of Temperature and Potential on the Passive Corrosion Properties of Alloys C22 and C276." *Journal of the Electrochemical Society, 150* (4), B120–B130. New York, New York: Electrochemical Society. TIC: 255963.

Macdonald, D.D. and Urquidi-Macdonald, M. 1991. "A Coupled Environment Model for Stress Corrosion Cracking in Sensitized Type 304 Stainless Steel in LWR Environments." *Corrosion Science, 32* (1), 51–81. New York, New York: Pergamon Press. TIC: 254386.

Macdonald, D.D.; Urquidi-Macdonald, M.; and Lu, P.-C. 1994. "The Coupled Environmental Fractural Model—A Deterministic Method for Calculating Crack Growth Rates." *Corrosion 94, The Annual Conference and Corrosion Show*, Paper No. 246, Houston, Texas: NACE International. TIC: 254388.

Marsh, G.P.; Taylor, K.J.; and Harker, A.H. 1991. *The Kinetics of Pitting Corrosion of Carbon Steel Applied to Evaluating Containers for Nuclear Waste Disposal*. SKB TR-91-62. Stockholm, Sweden: Svensk Kärnbränsleförsörjning AB. TIC: 206582.

Mattsson, H. and Olefjord, I. 1990. "Analysis of Oxide Formed on Ti During Exposure in Bentonite Clay-I. The Oxide Growth." *Werkstoffe und Corrosion, 41* (7), 383–390. Weinheim, Germany: VCH Verlagsgesellschaft mbH. TIC: 246290.

McCright, R.D. 1998. *Corrosion Data and Modeling, Update for Viability Assessment*. Volume 3 of *Engineered Materials Characterization Report*. UCRL-ID-119564, Rev. 1.1. Livermore, California: Lawrence Livermore National Laboratory. ACC: MOL.19980806.0177.

McGuire, R.; Vlasity, J.; Kessler, J.; Long, A.; Childs, S.; Ross, B.; Schwartz, F.; Shoesmith, D.; Kolar, M.; Apted, M.; Zhou, W.; Sudicky, E.; Smith, G.; Kozak, M.; Salter, P.; Klos, R.; Venter, A.; Stenhouse, M.; Watkins, B.; and Little, R. 1998. *Alternative Approaches to Assessing the Performance and Suitability of Yucca Mountain for Spent Fuel Disposal*. EPRI TR-108732. Palo Alto, California: Electric Power Research Institute. TIC: 248813.

MO0705SCCIGM06.000. Final Report for FY06: Stress Corrosion Crack Initiation & Growth Measurements in Environments Relevant to High Level Nuclear Waste Packages. Submittal date: 05/14/2007.

Mughabghab, S.F. and Sullivan, T.M. 1989. "Evaluation of the Pitting Corrosion of Carbon Steels and Other Ferrous Metals in Soil Systems." *Waste Management, 9* (4), 239–251. Elmsford, New York: Pergamon Press. TIC: 254591.

National Board of Boiler and Pressure Vessel Inspectors 1999. "Incident Reports." Columbus, Ohio: National Board of Boiler and Pressure Vessel Inspectors. TIC: 245629.

Newman, R.C. 1985. "The Dissolution and Passivation Kinetics of Stainless Alloys Containing Molybdenum—I. Coulometric Studies of Fe–Cr and Fe–Cr–Mo Alloys." *Corrosion Science, 25* (5), 331–339. New York, New York: Elsevier. TIC: 254590.

NRC (U.S. Nuclear Regulatory Commission) 1983. *PRA Procedures Guide, A Guide to the Performance of Probabilistic Risk Assessments for Nuclear Power Plants*. NUREG/CR-2300. Two volumes. Washington, D.C.: U.S. Nuclear Regulatory Commission. TIC: 205084.

Pan, J.; Leygraf, C.; Thierry, D.; and Ektessabi, A.M. 1997. "Corrosion Resistance for Biomaterial Applications of $Ti0_2$ Films Deposited on Titanium and Stainless Steel by Ion-Beam-Assisted Sputtering." *Journal of Biomedical Materials Research, 35*, 309–318. New York, New York: John Wiley & Sons. TIC: 253215.

Payer, J.H. 2004. *Corrosion Resistance of Alloy 22*. Presented to: Nuclear Waste Technical Review Board, May 18-19, 2004. Washington, D.C.: U.S. Department of Energy, Office of Civilian Radioactive Waste Management. ACC: MOL.20040629.0421.

Porter, D.A. and Easterling, K.E. 1992. "Diffusion along Dislocations." Section 2.7.2 of *Phase Transformations in Metals and Alloys*. 2nd Edition. 102–103. New York, New York: Chapman & Hall. TIC: 254148.

Potts, G.A. and Proebstle, R.A. 1994. "Recent GE BWR Fuel Experience." *Proceedings of the 1994 International Topical Meeting on Light Water Reactor Fuel Performance, West Palm Beach, Florida, April 17–21, 1994*, 87–95. La Grange Park, Illinois: American Nuclear Society. TIC: 243043.

Raghavan, M.; Mueller, R.R.; Vaughn, G.A.; and Floreen, S. 1984. "Determination of Isothermal Sections of Nickel Rich Portion of Ni–Cr–Mo System by Analytical Electron Microscopy." *Metallurgical Transactions A, 15A* (5), 783–792. New York, New York: Metallurgical Society of American Institute of Mining, Metallurgical, and Petroleum Engineers. TIC: 240057.

Rebak, R.B.; Edgecumbe Summers, T.S.; Lian, T.; Carranza, R.M.; Dillman, J.R.; Corbin, T.; and Crook, P. 2002. "Effect of Thermal Aging on the Corrosion Behavior of Wrought and Welded Alloy 22." *Corrosion/2002, 57th Annual Conference & Exposition, April 7–11, 2002, Denver, Colorado.* Paper No. 02542. Houston, Texas: NACE International. TIC: 254582.

Rebak, R.B.; Summers, T.S.E.; and Carranza, R.M. 2000. "Mechanical Properties, Microstructure and Corrosion Performance of C-22 Alloy Aged at 260°C to 800°C." *Scientific Basis for Nuclear Waste Management XXIII, Symposium held November 29–December 2, 1999, Boston, Massachusetts.* Smith, R.W. and Shoesmith, D.W., eds. *608*, 109–114. Warrendale, Pennsylvania: Materials Research Society. TIC: 0249052.

Reed-Hill, R.E. 1973. *Physical Metallurgy Principles*. Second Edition. 797–801. New York, New York: D. Van Nostrand Company. TIC: 237154.

Revie, R.W., ed. 2000. *Uhlig's Corrosion Handbook*. 2nd Edition. New York, New York: John Wiley & Sons. TIC: 248360.

SAE (Society of Automotive Engineers) 1993. *Metals & Alloys in the Unified Numbering System.* 6th Edition. Warrendale, Pennsylvania: Society of Automotive Engineers. TIC: 243414.

Sawyer, D.T. and Roberts, J.L., Jr. 1974. "II. Reference Electrodes." *Experimental Electrochemistry for Chemists*. 34–60. New York, New York: John Wiley & Sons. TIC: 254739.

Schutz, R.W. 2003. "2003 F.N. Speller Award Lecture: Platinum Group Metal Additions to Titanium: A Highly Effective Strategy for Enhancing Corrosion Resistance." *Corrosion, 59* (12), 1043–1057. Houston, Texas: NACE International. TIC: 255969.

Schutz, R.W. and Thomas, D.E. 1987. "Corrosion of Titanium and Titanium Alloys." In *Corrosion,* Volume 13, pages 669–706 of *ASM Handbook*. Formerly 9th Edition, *Metals Handbook*. Materials Park, Ohio: ASM International. TIC: 240704.

Scully, J.R.; Ilevbare, G.; and Marks, C. 2001. *Passivity and Passive Corrosion of Alloys 625 and 22*. SEAS Report No. UVA/527653/MSE01/103. Charlottesville, Virginia: University of Virginia, School of Engineering & Applied Science. TIC: 248056.

Sharland, S.M.; Naish, C.C.; Taylor, K.J.; and Marsh, G.P. 1994. "An Experimental and Modelling Study of the Localized Corrosion of Carbon Steel Overpacks for the Geological Disposal of Radioactive Waste." *Life Prediction of Corrodible Structures*. Parkins, R.N., ed. *1*, 402–418. Houston, Texas: NACE International. TIC: 254835.

Shibata, T. 1996. "Statistical and Stochastic Approaches to Localized Corrosion." *Corrosion, 52* (11), 813–830. Houston, Texas: NACE International. TIC: 236691.

Smailos, E. 1993. "Corrosion of High-Level Waste Packaging Materials in Disposal Relevant Brines." *Nuclear Technology, 104*, 343–350. La Grange Park, Illinois: American Nuclear Society. TIC: 249836.

Smailos, E. and Köster, R. 1987. "Corrosion Studies on Selected Packaging Materials for Disposal of High Level Wastes." *Materials Reliability in the Back End of the Nuclear Fuel Cycle, Proceedings of a Technical Committee Meeting, Vienna, 2–5 September 1986*, IAEA TECHDOC-421, 7–24. Vienna, Austria: International Atomic Energy Agency. TIC: 252877.

Smailos, E.; Schwarzkopf, W.; and Köster, R. 1986. "Corrosion Behaviour of Container Materials for the Disposal of High-Level Wastes in Rock Salt Formations." *Nuclear Science and Technology.* EUR 10400. Luxembourg, Luxembourg: Commission of the European Communities. TIC: 248245.

Smailos, E.; Schwarzkopf, W.; Köster, R.; Fiehn, B.; and Halm, G. 1990. *Corrosion Testing of Selected Packaging Materials for Disposal of High-Level Waste Glass in Rock Salt Formations*. KfK 4723. Karlsruhe, Germany: Kernforschungszentrum Karlsruhe GmbH. TIC: 215124.

Smith, D. 2008. *Weld Flaw Evaluation and Nondestructive Examination Process Comparison Results for High-Level Radioactive Waste Package Manufacturing Program*. TDR-EBS-ND-000007 REV 02. Las Vegas, Nevada: Bechtel SAIC Company. ACC: ENG.20081017.0006.

Smith, T.A. and Warwick, W.A. 1978. "Survey of Defects in Pressure Vessels Built to High Standards of Construction." *The Annual Winter Meeting of the American Society of Mechanical Engineers, San Francisco, California, December 10–15, 1978*. PVP-PB-032, 21–53. New York, New York: American Society of Mechanical Engineers. TIC: 244550.

SNL (Sandia National Laboratories) 2007a. *Stress Corrosion Cracking of Waste Package Outer Barrier and Drip Shield Materials*. ANL-EBS-MD-000005 REV 04. Las Vegas, Nevada: Sandia National Laboratories. ACC: DOC.20070913.0001.

SNL 2007b. *Engineered Barrier System: Physical and Chemical Environment.* ANL-EBS-MD-000033 REV 06. Las Vegas, Nevada: Sandia National Laboratories. ACC: DOC.20070907.0003.

SNL 2007c. *General Corrosion and Localized Corrosion of Waste Package Outer Barrier.* ANL-EBS-MD-000003 REV 03. Las Vegas, Nevada: Sandia National Laboratories. ACC: DOC.20070730.0003.

SNL 2007d. *Analysis of Mechanisms for Early Waste Package/Drip Shield Failure*. ANL-EBS-MD-000076 REV 00. Las Vegas, Nevada: Sandia National Laboratories. ACC: DOC.20070629.0002.

SNL 2007e. *General Corrosion and Localized Corrosion of the Drip Shield*. ANL-EBS-MD-000004 REV 02 ADD 01. Las Vegas, Nevada: Sandia National Laboratories. ACC: DOC.20070807.0004.

SNL 2007f. *Abstraction of Drift Seepage.* MDL-NBS-HS-000019 REV 01 ADD 01. Las Vegas, Nevada: Sandia National Laboratories. ACC: DOC.20070807.0001.

SNL 2007g. *EBS Radionuclide Transport Abstraction*. ANL-WIS-PA-000001 REV 03. Las Vegas, Nevada: Sandia National Laboratories. ACC: DOC.20071004.0001.

SNL 2008a. *Total System Performance Assessment Model /Analysis for the License Application*. MDL-WIS-PA-000005 REV 00 ADD 01. Las Vegas, Nevada: Sandia National Laboratories. ACC: DOC.20080312.0001.

SNL 2008b. *Multiscale Thermohydrologic Model*. ANL-EBS-MD-000049 REV 03 ADD 02. Las Vegas, Nevada: Sandia National Laboratories. ACC: DOC.20080201.0003.

Sprowls, D.O. 1987. "Evaluation of Stress-Corrosion Cracking." In *Corrosion*, Volume 13, 245–282 of *Metals Handbook*. 9th Edition. Metals Park, Ohio: ASM International. TIC: 209807.

Summers, T.S.E.; Wall, M.A.; Kumar, M.; Matthews, S.J.; and Rebak, R.B. 1999. "Phase Stability and Mechanical Properties of C-22 Alloy Aged in the Temperature Range 590 to 760°C for 16,000 Hours." *Scientific Basis for Nuclear Waste Management XXII, Symposium held November 30–December 4, 1998, Boston, Massachusetts*, Wronkiewicz, D.J. and Lee, J.H., eds. *556*, 919–926. Warrendale, Pennsylvania: Materials Research Society. TIC: 246426.

Swain, A.D. and Guttmann, H.E. 1983. *Handbook of Human Reliability Analysis with Emphasis on Nuclear Power Plant Applications Final Report*. NUREG/CR-1278. Washington, D.C.: U.S. Nuclear Regulatory Commission. TIC: 246563.

Tatnall, R.E. 1993. Introduction to *A Practical Manual on Microbiologically Influenced Corrosion*. Kobrin, G., ed. Pages 1–9. Houston, Texas: NACE International. TIC: 246992.

Tawancy, H.M.; Herchenroeder, R.B.; and Asphahani, A.I. 1983. "High-Performance Ni–Cr–Mo–W Alloys." *Journal of Metals, 35* (6), 37–43. Warrendale, Pennsylvania: The Minerals, Metals & Materials Society. TIC: 245100.

Tschoepe, E., III; Lyle, F.F., Jr.; Dancer, D.M.; Interrante, C.G.; and Nair, P.K. 1994. *Field Engineering Experience with Structural Materials*. San Antonio, Texas: Center for Nuclear Waste Regulatory Analyses. TIC: 244536.

Turchi, P.E.A. 2001. "Delivery of Property Diagram (Phase Fraction Versus Temperature) of Alloy 22 at Its Nominal Composition." Memorandum from P.E.A. Turchi (BSC) to file, May 21, 2001, PROJ.05/01.051, with enclosure. ACC: MOL.20010522.0158.

Vetter, K.J. and Strehblow, H.H. 1974. "Pitting Corrosion in an Early Stage and its Theoretical Implications." *Localized Corrosion, U.R. Evans Conference on Localized Corrosion, December 6–10, 1971, Williamsburg, Virginia*. International Corrosion Conference Series, NACE-3, 240–251. Houston, Texas: National Association of Corrosion Engineers. TIC: 254803.

Yang, R.L. 1997. "Meeting the Challenge of Managing Nuclear Fuel in a Competitive Environment." *Proceedings of the 1997 International Topical Meeting on LWR Fuel Performance, Portland, Oregon, March 2–6, 1997*, 3–10. La Grange Park, Illinois: American Nuclear Society. TIC: 232556.

INTENTIONALLY LEFT BLANK

Table 2.3.6-1. Target Composition of Standard Test Solutions Based on J-13 Well Water

Ion	SDW (mg/L)	SCW (mg/L)	SAW (mg/L)	SSW (mg/L)	BSW-12 (mg/L)
K^+	3.4×10^1	3.4×10^3	3.4×10^3	1.42×10^5	6.762×10^4
Na^+	4.09×10^2	4.09×10^4	3.769×10^4	4.87×10^5	1.0586×10^5
Mg^{2+}	1	<1	1.00×10^3	0	0
Ca^{2+}	5×10^{-1}	<1	1.00×10^3	0	0
F^-	1.4×10^1	1.4×10^3	0	0	1.331×10^3
Cl^-	6.7×10^1	6.7×10^3	2.425×10^4	1.28×10^5	1.313×10^5
NO_3^-	6.4×10^1	6.4×10^3	2.30×10^4	1.313×10^6	1.395×10^5
SO_4^{2-}	1.67×10^2	1.67×10^4	3.86×10^4	0	1.392×10^4
HCO_3^-	9.47×10^2	7×10^4	0	0	0
Si	27 (60°C); 49 (90°C)	27 (60°C); 49 (90°C)	27 (60°C); 49 (90°C)	0	0
pH	9.8 to 10.2	9.8 to 10.2	2.7	5.5 to 7	12

NOTE: pH measured for actual solutions at room temperature. BSW-12 denotes the specific pH of the water. For certain experiments, the pH of basic saturated water is altered by addition of NaOH.
BSW = basic saturated water.

Source: DTN: LL040803112251.117.

Table 2.3.6-2. FEPs Included in Section 2.3.6

FEP Number and FEP Name	Description	Summary of Technical Approach for FEP Inclusion
2.1.03.01.0A General corrosion of waste packages	General corrosion may contribute to waste package failure.	General corrosion of waste packages is modeled as uniform thinning of the waste package outer barrier (Section 2.3.6.3). The general corrosion model is constructed around weight-loss corrosion data (Section 2.3.6.3.2) with a temperature-dependent term (Section 2.3.6.3.3). The general corrosion rate is represented as constant versus time under a given temperature. General corrosion is modeled by dividing the waste package surface into subareas (patches) that are used to simulate variability across the barrier surfaces (Section 2.3.6.3.4).
2.1.03.01.0B General corrosion of drip shields	General corrosion may contribute to drip shield failure.	General corrosion of the drip shield is modeled as uniform thinning of the drip shield (Section 2.3.6.8.1). The general corrosion rate is modeled as constant with time and temperature (Section 2.3.6.8.1) and constructed around weight-loss data determined from long-term corrosion tests (Section 2.3.6.8.1). The general corrosion of the drip shield is modeled separately for the inner surface and the outer surfaces to reflect the less corrosive environment that will be present on the underside of the drip shield (Section 2.3.6.8.1). Each drip shield is modeled as a single entity with no spatial variability (Section 2.3.6.8.1). A corrosion rate ratio multiplier is used to determine the corrosion rate for the Titanium Grade 29 drip shield structural support material from the corrosion rates for the Titanium Grade 7 (Section 2.3.6.8.1).
2.1.03.02.0A Stress corrosion cracking of waste packages	Waste packages may become wet at specific locations that are stressed, leading to stress corrosion cracking. The possibility of stress corrosion cracking under dry conditions or due to thermal stresses is also addressed as part of this FEP.	Stress corrosion cracking of waste packages is modeled as the initiation and propagation of cracks due to three simultaneous conditions: a susceptible material, critical environment, and sustainable tensile stress (Section 2.3.6.5.1). The threshold stress, threshold stress intensity factor, and parameters associated with the slip dissolution/film rupture crack growth model are determined from experimental data developed for repository environments (Section 2.3.6.5.2). Stress corrosion cracking of the waste package closure weld region is modeled to initiate at incipient flaws or weld flaws in the closure weld region. Each waste package closure lid is represented as a collection of approximately 40 patches. It is conservatively modeled that, when the first crack on a given patch penetrates through-wall, all possible through-wall cracks on that patch are considered to penetrate through-wall (Section 2.3.6.5.4).

Table 2.3.6-2. FEPs Included in Section 2.3.6 (Continued)

FEP Number and FEP Name	Description	Summary of Technical Approach for FEP Inclusion
2.1.03.03.0A Localized corrosion of waste packages	Localized corrosion (pitting or crevice corrosion) could enhance degradation of the waste packages.	Localized corrosion of waste packages is modeled by an initiation component and a propagation component which progress at discrete sites, (e.g., in a nonuniform manner) (Section 2.3.6.4.1). Localized breakdown at defect sites of the passive film is modeled with data from tests over a wide range of exposure conditions using a cyclic potentiodynamic polarization technique (Section 2.3.6.4.2). Upon initiation of localized corrosion, the propagation depth is modeled using a constant rate (Section 2.3.6.4.3.2) and a distribution function to address uncertainty ranges found in the literature (Section 2.3.6.4.3.2). The area affected by localized corrosion resulting from seepage brines is modeled as the entire waste package surface area underneath the breached portion of the drip shield (Section 2.3.6.4.4.1).
2.1.03.05.0A Microbially influenced corrosion of waste packages	Microbial activity may either directly (e.g., direct enhancement of the dissolution rate) or indirectly (e.g., through the formation of chemical species which in turn support increased metal oxidation) enhance the corrosion rate of the waste package, leading to an acceleration of the corrosion rate beyond the levels anticipated based upon the bulk environment to which it is exposed.	Microbially influenced corrosion of waste packages can enhance corrosion rates of Alloy 22 by, at most, a factor of 2 (Section 2.3.6.3.3.2). Microbially influenced corrosion is modeled in TSPA as an enhancement factor uniformly distributed between 1 and 2. The factor is applied at the patch level to the general corrosion rate when the relative humidity at the waste package outer corrosion barrier surface is equal to or above a threshold value of 70% to 90% (Section 2.3.6.3.3.2).
2.1.03.08.0A Early failure of waste packages	Waste packages may fail prematurely because of manufacturing defects, improper sealing, or other factors related to quality control during manufacture and emplacement.	Early failure of waste packages due to manufacturing or handling-induced defects is modeled based on possible defects identified from literature and human error probability data (Section 2.3.6.6.2). The waste packages are treated as breached at the time of repository closure (Section 2.3.6.4.4.1).
2.1.03.08.0B Early failure of drip shields	Drip shields may fail prematurely because of manufacturing defects, improper sealing, or other factors related to quality control during manufacture and emplacement.	Early failure of drip shields due to manufacturing or handling-induced defects is modeled based on possible defects identified from literature and human error probability data (Section 2.3.6.8.4.2). The drip shields are treated as failed at the time of repository closure (Section 2.3.6.8.4.2).

Table 2.3.6-2. FEPs Included in Section 2.3.6 (Continued)

FEP Number and FEP Name	Description	Summary of Technical Approach for FEP Inclusion
2.1.03.11.0A Physical form of waste package and drip shield	The specific forms of the various drip shields, waste packages, and internal waste containers that are proposed for the Yucca Mountain repository can affect long-term performance. Waste package form may affect container strength through the shape and dimensions of the waste package and affect heat dissipation through waste package volume and surface area. Waste package and drip shield materials may affect physical and chemical behavior of the disposal area environment. Waste package and drip shield integrity will affect the releases of radionuclides from the disposal system. Waste packages may have both local effects and repository-scale effects. All types of waste packages and containers, including commercial SNF, DOE SNF, and DOE HLW, should be considered.	Effects of the physical form of waste packages and drip shields on long-term performance are included by considering several nominal waste package configurations (Section 2.3.6.3.4.1). Two nominal waste package configurations are considered to represent the waste package configurations for commercial SNF, DOE-owned HLW and DOE-owned SNF (long and short waste packages) and Naval short and long packages. They cover the range of waste package lengths and outer barrier thickness, and waste package diameters, and account for the majority of the waste package units (Section 2.3.6.3.4.1).

NOTE: HLW = high-level radioactive waste.

Table 2.3.6-3. Alterations in Corrosion Rates and Potential Associated Microbial Degradation

Tested Sample Initial Condition	Average Corrosion Rate (μm/yr)
Alloy 22 + Yucca Mountain Microbes	0.022
Sterile Alloy 22	0.011

Source: SNL 2007c, Table 6-16.

Table 2.3.6-4. Solutions Used to Determine Temperature-Dependence of Alloy 22 General Corrosion

Solution	Solution Description	Number of Measurements	Nitrate Molality	Chloride Molality
F1	1 *m* NaCl + 0.05 *m* KNO_3	46	0.05	1
F2	1 *m* NaCl + 0.15 *m* KNO_3	33	0.15	1
F3	1 *m* NaCl + 0.5 *m* KNO_3	28	0.5	1
F4	3.5 *m* NaCl + 0.175 *m* KNO_3	33	0.175	3.5
F5	3.5 *m* NaCl + 0.525 *m* KNO_3	43	0.525	3.5
F6	3.5 *m* NaCl + 1.75 *m* KNO_3	22	1.75	3.5
F7	6 *m* NaCl + 0.3 *m* KNO_3	73	0.3	6
F8	6 *m* NaCl + 0.9 *m* KNO_3	69	0.9	6
F9	6 *m* NaCl + 3 *m* KNO_3	33	3.0	6

Source: SNL 2007c, Table 6-8.

Table 2.3.6-5. Apparent Activation Energies of Alloy 22 for Individual Solutions

Solution	Solution Description	Temperature Range (°C)	Activation Energy (kJ/mol)
F1	1 *m* NaCl + 0.05 *m* KNO_3	60 to 100	58.06
F2	1 *m* NaCl + 0.15 *m* KNO_3	60 to 100	45.22
F3	1 *m* NaCl + 0.5 *m* KNO_3	60 to 100	47.58
F4	3.5 *m* NaCl + 0.175 *m* KNO_3	60 to 100	50.63
F5	3.5 *m* NaCl + 0.525 *m* KNO_3	60 to 100	35.86
F6	3.5 *m* NaCl + 1.75 *m* KNO_3	60 to 100	28.46
F7	6 *m* NaCl + 0.3 *m* KNO_3	60 to 100	26.00
F8	6 *m* NaCl + 0.9 *m* KNO_3	60 to 100	43.24
F9	6 *m* NaCl + 3 *m* KNO_3	60 to 100	31.96
G1	4 *M* NaCl	45 to 105	7.69
G2	4 *M* NaCl + 0.04 *M* Na_2SO_4	45 to 105	51.03
G3	4 *M* NaCl + 0.4 *M* Na_2SO_4	45 to 105	45.84
K1	12 *m* $CaCl_2$ + 6 *m* $Ca(NO_3)_2$	100 to 150	35.61
L1	5 *M* $CaCl_2$	30 to 120	28.07

NOTE: Experimental results for solutions F1 through F9 were used in the linear mixed effects model shown in Figure 2.3.6-7 to arrive at the modeled apparent activation energy range. The apparent activation energies shown in this table are for the individual solutions. The results for solutions other than F1 through F9 were not used for model development. L2 a solution containing 5 *M* CaCl2 + 0.5 *M* $Ca(NO_3)_2$ displayed a negative temperature dependence, but is excluded from consideration because a negative temperature dependence is unrealistic, and is contrary to literature observations of the behavior of Alloy 22 (SNL 2007c, Section 6.4.3.4).

Source: SNL 2007c, Tables 6-9 and 6-10.

Table 2.3.6-6. Corrosion Potential Data Used in Model Development

Specimen Type	Material Condition	Solution	T (°C)	Calculated Pitzer pH	[Cl] (*m*)	[NO_3] (*m*)	NO_3/Cl	E_{corr} (mV vs Ag/AgCl)	Immersion Days
PCA	ASW	5*m* $CaCl_2$ + 5*m* $Ca(NO_3)_2$	120	5.17	10.00	10.00	1.00	482	723
PCA	ASW	5*m* $CaCl_2$ + 5*m* $Ca(NO_3)_2$	120	5.17	10.00	10.00	1.00	483	723
PCA	ASW	5*m* $CaCl_2$ + 5*m* $Ca(NO_3)_2$	120	5.17	10.00	10.00	1.00	483	723
PCA	ASW	5*m* $CaCl_2$ + 5*m* $Ca(NO_3)_2$	120	5.17	10.00	10.00	1.00	483	723
Rod	ASW	5*m* $CaCl_2$ + 5*m* $Ca(NO_3)_2$	120	5.17	10.00	10.00	1.00	447	723
Rod	ASW	5*m* $CaCl_2$ + 5*m* $Ca(NO_3)_2$	120	5.17	10.00	10.00	1.00	453	723
PCA	ASW	5*m* $CaCl_2$ + 5*m* $Ca(NO_3)_2$	100	5.28	10.00	10.00	1.00	263	729
PCA	ASW	5*m* $CaCl_2$ + 5*m* $Ca(NO_3)_2$	100	5.28	10.00	10.00	1.00	244	729
PCA	ASW	5*m* $CaCl_2$ + 5*m* $Ca(NO_3)_2$	100	5.28	10.00	10.00	1.00	234	729
PCA	ASW	5*m* $CaCl_2$ + 5*m* $Ca(NO_3)_2$	100	5.28	10.00	10.00	1.00	215	729
Rod	ASW	5*m* $CaCl_2$ + 5*m* $Ca(NO_3)_2$	100	5.28	10.00	10.00	1.00	173	729
Rod	ASW	5*m* $CaCl_2$ + 5*m* $Ca(NO_3)_2$	100	5.28	10.00	10.00	1.00	190	729
PCA	ASW	3.5*m* NaCl + 0.175*m* KNO_3 + 0.7*m* $MgSO_4$	80	5.56	3.50	0.175	0.05	31	735
PCA	ASW	3.5*m* NaCl + 0.175*m* KNO_3 + 0.7*m* $MgSO_4$	80	5.56	3.50	0.175	0.05	27	735
Rod	ASW	3.5*m* NaCl + 0.175*m* KNO_3 + 0.7*m* $MgSO_4$	80	5.56	3.50	0.175	0.05	38	735
Rod	ASW	3.5*m* NaCl + 0.175*m* KNO_3 + 0.7*m* $MgSO_4$	80	5.56	3.50	0.175	0.05	2	735
PCA	ASW	1*M* NaCl + 0.15*M* KNO_3	90	5.76	1.00	0.15	0.15	–114	741

Table 2.3.6-6. Corrosion Potential Data Used in Model Development (Continued)

Specimen Type	Material Condition	Solution	T (°C)	Calculated Pitzer pH	[Cl] (*m*)	[NO_3] (*m*)	NO_3/Cl	E_{corr} (mV vs Ag/AgCl)	Immersion Days
PCA	ASW	1*M* NaCl + 0.15*M* KNO_3	90	5.76	1.00	0.15	0.15	–119	741
PCA	ASW	1*M* NaCl + 0.15*M* KNO_3	90	5.76	1.00	0.15	0.15	–63	741
PCA	ASW	1*M* NaCl + 0.15*M* KNO_3	90	5.76	1.00	0.15	0.15	–120	741
Rod	ASW	1*M* NaCl + 0.15*M* KNO_3	90	5.76	1.00	0.15	0.15	–40	741
Rod	ASW	1*M* NaCl + 0.15*M* KNO_3	90	5.76	1.00	0.15	0.15	–35	741
PCA	ASW	1*M* NaCl + 0.15*M* KNO_3	75	5.72	1.00	0.15	0.15	–82	749
PCA	ASW	1*M* NaCl + 0.15*M* KNO_3	75	5.72	1.00	0.15	0.15	–114	749
PCA	ASW	1*M* NaCl + 0.15*M* KNO_3	75	5.72	1.00	0.15	0.15	–119	749
PCA	ASW	1*M* NaCl + 0.15*M* KNO_3	75	5.72	1.00	0.15	0.15	–112	749
Rod	ASW	1*M* NaCl + 0.15*M* KNO_3	75	5.72	1.00	0.15	0.15	–110	749
Rod	ASW	1*M* NaCl + 0.15*M* KNO_3	75	5.72	1.00	0.15	0.15	–108	749
Rod	ASW	5*M* $CaCl_2$	90	4.00	11.99	0.00	0.00	–30	650
Rod	ASW	5*M* $CaCl_2$	90	4.00	11.99	0.00	0.00	–4	650
PCA	ASW	3.5*m* NaCl + 0.175*m* KNO_3	100	5.61	3.50	0.175	0.05	–131	252
PCA	ASW	3.5*m* NaCl + 0.175*m* KNO_3	100	5.61	3.50	0.175	0.05	–154	252
PCA	ASW	3.5*m* NaCl + 0.175*m* KNO_3	100	5.61	3.50	0.175	0.05	–137	252
PCA	ASW	3.5*m* NaCl + 0.175*m* KNO_3	100	5.61	3.50	0.175	0.05	–123	252
PCA	ASW	3.5*m* NaCl + 0.525*m* KNO_3	100	5.60	3.50	0.525	0.15	–152	256
PCA	ASW	3.5*m* NaCl + 0.525*m* KNO_3	100	5.60	3.50	0.525	0.15	–153	256
PCA	ASW	3.5*m* NaCl + 0.525*m* KNO_3	100	5.60	3.50	0.525	0.15	–155	256

Table 2.3.6-6. Corrosion Potential Data Used in Model Development (Continued)

Specimen Type	Material Condition	Solution	T (°C)	Calculated Pitzer pH	[Cl] (*m*)	[NO_3] (*m*)	NO_3/Cl	E_{corr} (mV vs Ag/AgCl)	Immersion Days
PCA	ASW	3.5*m* NaCl + 0.525*m* KNO_3	100	5.60	3.50	0.525	0.15	–154	256
PCA	ASW	6*m* NaCl + 0.9*m* KNO_3	100	5.41	6.00	0.90	0.15	–83	265
PCA	ASW	6*m* NaCl + 0.9*m* KNO_3	100	5.41	6.00	0.90	0.15	–72	265
PCA	ASW	6*m* NaCl + 0.3*m* KNO_3	100	5.43	6.00	0.30	0.05	–129	280
PCA	ASW	6*m* NaCl + 0.3*m* KNO_3	100	5.43	6.00	0.30	0.05	–140	280
PCA	ASW	6*m* NaCl + 0.3*m* KNO_3	100	5.43	6.00	0.30	0.05	–123	280
PCA	ASW	6*m* NaCl + 0.3*m* KNO_3	100	5.43	6.00	0.30	0.05	–130	280
Rod	MA	5*M* $CaCl_2$ + 0.5*M* $Ca(NO_3)_2$	90	2.97	12.59	1.26	0.10	482	463
Rod	MA	5*M* $CaCl_2$ + 0.5*M* $Ca(NO_3)_2$	90	2.97	12.59	1.26	0.10	482	463
Rod	MA	5*M* $CaCl_2$ + 0.5*M* $Ca(NO_3)_2$	90	2.97	12.59	1.26	0.10	481	463
Rod	ASW	5*M* $CaCl_2$ + 0.5*M* $Ca(NO_3)_2$	90	2.97	12.59	1.26	0.10	82	463
Rod	ASW	5*M* $CaCl_2$ + 0.5*M* $Ca(NO_3)_2$	90	2.97	12.59	1.26	0.10	47	463
Rod	ASW	5*M* $CaCl_2$ + 0.5*M* $Ca(NO_3)_2$	90	2.97	12.59	1.26	0.10	28	463
Rod	MA	5*M* $CaCl_2$	120	3.93	11.99	0.00	0.00	–164	497
Rod	MA	5*M* $CaCl_2$	120	3.93	11.99	0.00	0.00	–56	497
Rod	MA	5*M* $CaCl_2$	120	3.93	11.99	0.00	0.00	–39	497
Rod	ASW	5*M* $CaCl_2$	120	3.93	11.99	0.00	0.00	22	497
Rod	ASW	5*M* $CaCl_2$	120	3.93	11.99	0.00	0.00	166	497
Rod	ASW	5*M* $CaCl_2$	120	3.93	11.99	0.00	0.00	–19	497
Rod	MA	BSW	105	8.61	4.62	2.82	0.61	–97	256

Table 2.3.6-6. Corrosion Potential Data Used in Model Development (Continued)

Specimen Type	Material Condition	Solution	T (°C)	Calculated Pitzer pH	[Cl] (*m*)	[NO_3] (*m*)	NO_3/Cl	E_{corr} (mV vs Ag/AgCl)	Immersion Days
Rod	MA	BSW	105	8.61	4.62	2.82	0.61	–124	256
Rod Halar Coated	MA	BSW	105	8.61	4.62	2.82	0.61	–231	256
Rod Halar Coated	MA	BSW	105	8.61	4.62	2.82	0.61	–198	256
Rod	ASW	BSW	105	8.61	4.62	2.82	0.61	–211	256
Rod	ASW	BSW	105	8.61	4.62	2.82	0.61	–208	256
Rod Halar Coated	ASW	BSW	105	8.61	4.62	2.82	0.61	–252	256
Rod Halar Coated	ASW	BSW	105	8.61	4.62	2.82	0.61	–214	256
Rod	MA	4*M* NaCl	90	5.55	4.40	0.00	0.00	–170	328
Rod	MA	4*M* NaCl	90	5.55	4.40	0.00	0.00	–165	328
Rod	MA	4*M* NaCl	90	5.55	4.40	0.00	0.00	–175	328
Rod	ASW	4*M* NaCl	90	5.55	4.40	0.00	0.00	–133	328
Rod	ASW	4*M* NaCl	90	5.55	4.40	0.00	0.00	–84	328
Rod	ASW	4*M* NaCl	90	5.55	4.40	0.00	0.00	–83	328
Rod	MA	SAW - w/out silicate	90	1.93	0.76	0.39	0.52	389	375
Rod	MA	SAW - w/out silicate	90	1.93	0.76	0.39	0.52	389	375
Rod	MA	SAW - w/out silicate	90	1.93	0.76	0.39	0.52	387	375
Rod	ASW	SAW - w/out silicate	90	1.93	0.76	0.39	0.52	395	375

Table 2.3.6-6. Corrosion Potential Data Used in Model Development (Continued)

Specimen Type	Material Condition	Solution	T (°C)	Calculated Pitzer pH	[Cl] (*m*)	[NO_3] (*m*)	NO_3/Cl	E_{corr} (mV vs Ag/AgCl)	Immersion Days
Rod	ASW	SAW - w/out silicate	90	1.93	0.76	0.39	0.52	394	375
Rod	ASW	SAW - w/out silicate	90	1.93	0.76	0.39	0.52	394	375
Rod	MA	SCW	90	9.98	0.21	0.11	0.52	–191	394
Rod	MA	SCW	90	9.98	0.21	0.11	0.52	–173	394
Rod	MA	SCW	90	9.98	0.21	0.11	0.52	–160	394
Rod	ASW	SCW	90	9.98	0.21	0.11	0.52	–133	394
Rod	ASW	SCW	90	9.98	0.21	0.11	0.52	–207	394
Rod	ASW	SCW	90	9.98	0.21	0.11	0.52	–163	394
Rod	MA	5*M* $CaCl_2$ + 0.5*M* $Ca(NO_3)_2$	90	2.97	12.59	1.26	0.10	188	693
Rod	MA	5*M* $CaCl_2$ + 0.5*M* $Ca(NO_3)_2$	90	2.97	12.59	1.26	0.10	75	693
Rod	MA	5*M* $CaCl_2$ + 0.5*M* $Ca(NO_3)_2$	90	2.97	12.59	1.26	0.10	113	693
Rod	ASW	5*M* $CaCl_2$ + 0.5*M* $Ca(NO_3)_2$	90	2.97	12.59	1.26	0.10	232	558
Rod	ASW	5*M* $CaCl_2$ + 0.5*M* $Ca(NO_3)_2$	90	2.97	12.59	1.26	0.10	275	558
Rod	MA	5*M* $CaCl_2$ + 0.05*M* $Ca(NO_3)_2$	90	4.03	11.70	0.12	0.01	253	704
Rod	MA	5*M* $CaCl_2$ + 0.05*M* $Ca(NO_3)_2$	90	4.03	11.70	0.12	0.01	57	704
Rod	MA	5*M* $CaCl_2$ + 0.05*M* $Ca(NO_3)_2$	90	4.03	11.70	0.12	0.01	92	704
Rod	ASW	5*M* $CaCl_2$ + 0.05*M* $Ca(NO_3)_2$	90	4.03	11.70	0.12	0.01	176	561
Rod	ASW	5*M* $CaCl_2$ + 0.05*M* $Ca(NO_3)_2$	90	4.03	11.70	0.12	0.01	214	561
Rod	MA	1*M* $CaCl_2$ + 1*M* $Ca(NO_3)_2$	90	6.39	2.62	2.58	0.99	321	622
Rod	MA	1*M* $CaCl_2$ + 1*M* $Ca(NO_3)_2$	90	6.39	2.62	2.58	0.99	324	622

Table 2.3.6-6. Corrosion Potential Data Used in Model Development (Continued)

Specimen Type	Material Condition	Solution	T (°C)	Calculated Pitzer pH	[Cl] (*m*)	[NO_3] (*m*)	NO_3/Cl	E_{corr} (mV vs Ag/AgCl)	Immersion Days
Rod	MA	1*M* $CaCl_2$ + 1*M* $Ca(NO_3)_2$	90	6.39	2.62	2.58	0.99	321	622
Rod	MA	1*M* $CaCl_2$ + 1*M* $Ca(NO_3)_2$	90	6.39	2.62	2.58	0.99	316	622
Rod	ASW	1*M* $CaCl_2$ + 1*M* $Ca(NO_3)_2$	90	6.39	2.62	2.58	0.99	360	457
Rod	ASW	1*M* $CaCl_2$ + 1*M* $Ca(NO_3)_2$	90	6.39	2.62	2.58	0.99	341	457
Rod	MA	4.5 years LTCTF SAW	90	2.72	0.77	0.37	0.49	387	834
Rod	MA	4.5 years LTCTF SAW	90	2.72	0.77	0.37	0.49	381	834
Rod	MA	4.5 years LTCTF SAW	90	2.72	0.77	0.37	0.49	374	834
Rod	MA	4.5 years LTCTF SAW	90	2.72	0.77	0.37	0.49	382	834
Rod	MA	4.5 years LTCTF SAW	90	2.72	0.77	0.37	0.49	384	834
Rod	MA	4.5 years LTCTF SAW	90	2.72	0.77	0.37	0.49	373	834
Rod	MA	4.5 years LTCTF SAW	90	2.72	0.77	0.37	0.49	377	834
Rod	MA	4.5 years LTCTF SAW	90	2.72	0.77	0.37	0.49	382	834
Rod	MA	SAW	90	2.38	1.39	0.40	0.29	400	876
Rod	MA	SAW	90	2.38	1.39	0.40	0.29	400	876
Rod	MA	SAW	90	2.38	1.39	0.40	0.29	397	876
Rod	MA	SAW	90	2.38	1.39	0.40	0.29	399	876
Rod	MA	SAW	90	2.38	1.39	0.40	0.29	388	525
Rod	MA	SAW	90	2.38	1.39	0.40	0.29	389	525
Rod	MA	SAW	90	2.38	1.39	0.40	0.29	385	525
Rod	MA	SAW	90	2.38	1.39	0.40	0.29	387	525

Table 2.3.6-6. Corrosion Potential Data Used in Model Development (Continued)

Specimen Type	Material Condition	Solution	T (°C)	Calculated Pitzer pH	[Cl] (*m*)	[NO_3] (*m*)	NO_3/Cl	E_{corr} (mV vs Ag/AgCl)	Immersion Days
Rod	MA	SAW - LTCTF Origin Vessel 26	25	2.02	0.77	0.37	0.49	266	846
Rod	MA	SAW - LTCTF Origin Vessel 26	25	2.02	0.77	0.37	0.49	254	846
Rod	MA	SAW - LTCTF Origin Vessel 26	25	2.02	0.77	0.37	0.49	238	846
Prev tested U-bend	ASW	SDW - LTCTF Origin Vessel 30	90	9.41	3.30×10^{-3}	9.73×10^{-4}	0.29	101	1,089
Untested U-bend	ASW	SDW - LTCTF Origin Vessel 30	90	9.41	3.30×10^{-3}	9.73×10^{-4}	0.29	110	1,089
Prev tested U-bend	ASW	SDW - LTCTF Origin Vessel 29	60	9.30	3.30×10^{-3}	9.73×10^{-4}	0.29	55	1,089
Untested U-bend	ASW	SDW - LTCTF Origin Vessel 29	60	9.30	3.30×10^{-3}	9.73×10^{-4}	0.29	32	1,089
Prev tested U-bend	MA	BSW	105	8.61	4.62	2.82	0.61	62	729
Untested U-bend	ASW	BSW	105	8.61	4.62	2.82	0.61	5	729
Prev tested U-bend	ASW	SCW - LTCTF Origin Vessel 28	90	10.04	0.21	0.12	0.56	–24	1,089
Untested U-bend	ASW	SCW - LTCTF Origin Vessel 28	90	10.04	0.21	0.12	0.56	–61	1,089
Prev tested U-bend	ASW	SAW - LTCTF Origin Vessel 26	90	2.72	0.77	0.37	0.49	290	1,102
Untested U-bend	ASW	SAW - LTCTF Origin Vessel 26	90	2.72	0.77	0.37	0.49	372	1,102
Prev tested U-bend	ASW	SAW - LTCTF Origin Vessel 25	60	2.39	0.77	0.37	0.49	374	1,089

Table 2.3.6-6. Corrosion Potential Data Used in Model Development (Continued)

Specimen Type	Material Condition	Solution	T (°C)	Calculated Pitzer pH	[Cl] (*m*)	[NO_3] (*m*)	NO_3/Cl	E_{corr} (mV vs Ag/AgCl)	Immersion Days
Untested U-bend	ASW	SAW - LTCTF Origin Vessel 25	60	2.39	0.77	0.37	0.49	406	1,089

NOTE: ASW = as-welded; BSW = basic saturated water; MA = mill-annealed, nonwelded specimen; PCA = prism crevice assembly.

Source: SNL 2007c, Appendix VIII.

Table 2.3.6-7. Crevice Repassivation Potential Data Used in Model Development

Sample Type	Material Condition	Solution	Temperature (°C)	Calculated Pitzer pH	[Cl] molal	[NO_3] molal	NO_3/Cl molal ratio	E_{rcrev} (mV vs. SSC)
PCA	ASW	0.0005 *M* NaCl	60	6.51	5.00×10^{-4}	0.00	0.00	339
PCA	ASW	0.0005 *M* NaCl	90	6.21	5.00×10^{-4}	0.00	0.00	214
PCA	ASW	0.005 *M* NaCl	60	6.51	5.80×10^{-3}	0.00	0.00	359
PCA	ASW	0.05 *M* NaCl	60	6.51	0.05	0.00	0.00	161
PCA	ASW	0.5 *M* NaCl	60	6.45	0.51	0.00	0.00	61
MCA	MA	1 *M* NaCl	60	6.45	1.02	0.00	0.00	84
MCA	MA	1 *M* NaCl	60	6.45	1.02	0.00	0.00	28
MCA	MA	1 *M* NaCl	90	6.16	1.02	0.00	0.00	–24
MCA	MA	1 *M* NaCl	90	6.16	1.02	0.00	0.00	–126
MCA	MA	1 *M* NaCl	90	6.16	1.02	0.00	0.00	–109
MCA	MA	1 *M* NaCl	90	6.16	1.02	0.00	0.00	–42
PCA	ASW	1 *M* NaCl	90	6.16	1.02	0.00	0.00	–104
PCA	ASW - LPB	1 *M* NaCl	90	6.16	1.02	0.00	0.00	–134
PCA	ASW - LSP	1 *M* NaCl	90	6.16	1.02	0.00	0.00	–114
MCA	MA	1 *M* NaCl	90	6.16	1.02	0.00	0.00	–45
PCA	ASW - Mockup	1 *M* NaCl	90	6.16	1.02	0.00	0.00	–54
PCA	ASW - Mockup	1 *M* NaCl	90	6.16	1.02	0.00	0.00	–52
MCA	MA	1.25 *M* NaCl	60	6.44	1.29	0.00	0.00	48
MCA	MA	1.25 *M* NaCl	60	6.44	1.29	0.00	0.00	23

Table 2.3.6-7. Crevice Repassivation Potential Data Used in Model Development (Continued)

Sample Type	Material Condition	Solution	Temperature (°C)	Calculated Pitzer pH	[Cl] molal	[NO_3] molal	NO_3/Cl molal ratio	E_{rcrev} (mV vs. SSC)
MCA	MA	1.25 *M* NaCl	90	6.14	1.29	0.00	0.00	–33
MCA	MA	1.25 *M* NaCl	90	6.14	1.29	0.00	0.00	–65
PCA	ASW	4 *M* NaCl	60	6.25	4.40	0.00	0.00	–52
MCA	MA	4 *M* NaCl	60	6.25	4.40	0.00	0.00	–116
MCA	MA	4 *M* NaCl	60	6.25	4.40	0.00	0.00	–107
MCA	MA	4 *M* NaCl	60	6.25	4.40	0.00	0.00	–50
MCA	MA	4 *M* NaCl	60	6.25	4.40	0.00	0.00	–69
MCA	MA	4 *M* NaCl	75	6.10	4.40	0.00	0.00	–140
MCA	MA	4 *M* NaCl	75	6.10	4.40	0.00	0.00	–140
MCA	MA	4 *M* NaCl	75	6.10	4.40	0.00	0.00	–157
PCA	MA	4 *M* NaCl	75	6.10	4.40	0.00	0.00	–118
MCA	MA	4 *M* NaCl	75	6.10	4.40	0.00	0.00	–148
MCA	MA	4 *M* NaCl	90	5.97	4.40	0.00	0.00	–161
MCA	MA	4 *M* NaCl	90	5.97	4.40	0.00	0.00	–168
MCA	MA	4 *M* NaCl	90	5.97	4.40	0.00	0.00	–160
MCA	MA	4 *M* NaCl	90	5.97	4.40	0.00	0.00	–165
MCA	MA	4 *M* NaCl	105	5.85	4.40	0.00	0.00	–157
MCA	MA	4 *M* NaCl	105	5.85	4.40	0.00	0.00	–168
MCA	MA	4 *M* NaCl	105	5.85	4.40	0.00	0.00	–119
MCA	MA	4 *M* NaCl	105	5.85	4.40	0.00	0.00	–142

Table 2.3.6-7. Crevice Repassivation Potential Data Used in Model Development (Continued)

Sample Type	Material Condition	Solution	Temperature (°C)	Calculated Pitzer pH	[Cl] molal	[NO_3] molal	NO_3/Cl molal ratio	E_{rcrev} (mV vs. SSC)
PCA	ASW	3 *m* KCl + 3 *m* NaCl + 3 *m* KNO_3 + 3 *m* $NaNO_3$ (+ 0.0001 *m* HCl)	110	3.19	6.00	6.00	1.00	330
PCA	ASW	3 *m* KCl + 3 *m* NaCl + 3 *m* KNO_3 + 3 *m* $NaNO_3$ (+ 0.0001 *m* HCl)	110	3.19	6.00	6.00	1.00	413
PCA	ASW	4 *m* $CaCl_2$	110	4.41	8.00	0.00	0.00	–243
PCA	ASW	4 *m* KCl + 4 *m* NaCl	110	5.76	8.00	0.00	0.00	–223
PCA	ASW	4 *m* KCl + 4 *m* NaCl	110	5.76	8.00	0.00	0.00	–210
PCA	ASW	4 *m* KCl + 4 *m* NaCl + 0.4 *m* KNO_3 + 0.4 *m* $NaNO_3$	90	5.89	8.00	0.80	0.10	–82
PCA	ASW	4 *m* KCl + 4 *m* NaCl + 0.4 *m* KNO_3 + 0.4 *m* $NaNO_3$	90	5.89	8.00	0.80	0.10	–80
PCA	ASW	4 *m* KCl + 4 *m* NaCl + 0.4 *m* KNO_3 + 0.4 *m* $NaNO_3$	110	5.76	8.00	0.80	0.10	–50
PCA	ASW	4 *m* KCl + 4 *m* NaCl + 0.4 *m* KNO_3 + 0.4 *m* $NaNO_3$	110	5.76	8.00	0.80	0.10	–103
PCA	ASW	4 *m* KCl + 4 *m* NaCl + 0.4 *m* KNO_3 + 0.4 *m* $NaNO_3$ (+ 0.0001 *m* HCl)	110	3.36	8.00	0.80	0.10	–106
PCA	ASW	4 *m* KCl + 4 *m* NaCl + 0.8 *m* KNO_3 + 0.8 *m* $NaNO_3$	110	5.76	8.00	1.60	0.20	–44
MCA	ASW	5 *M* $CaCl_2$	30	4.55	11.99	0.00	0.00	–57
PCA	ASW	5 *M* $CaCl_2$	60	4.20	11.99	0.00	0.00	–65
PCA	ASW	5 *M* $CaCl_2$	60	4.20	11.99	0.00	0.00	–64
MCA	ASW	5 *M* $CaCl_2$	45	4.36	11.99	0.00	0.00	24

Table 2.3.6-7. Crevice Repassivation Potential Data Used in Model Development (Continued)

Sample Type	Material Condition	Solution	Temperature (°C)	Calculated Pitzer pH	[Cl] molal	[NO_3] molal	NO_3/Cl molal ratio	E_{rcrev} (mV vs. SSC)
MCA	ASW	5 *M* $CaCl_2$	60	4.20	11.99	0.00	0.00	–88
MCA	ASW	5 *M* $CaCl_2$	60	4.20	11.99	0.00	0.00	–48
MCA	ASW	5 *M* $CaCl_2$	60	4.20	11.99	0.00	0.00	–47
MCA	MA	5 *M* $CaCl_2$	60	4.20	11.99	0.00	0.00	18
MCA	MA	5 *M* $CaCl_2$	60	4.20	11.99	0.00	0.00	22
MCA	MA	5 *M* $CaCl_2$	60	4.20	11.99	0.00	0.00	–27
MCA	MA	5 *M* $CaCl_2$	60	4.20	11.99	0.00	0.00	–2
MCA	MA	5 *M* $CaCl_2$	60	4.20	11.99	0.00	0.00	29
MCA	MA	5 *M* $CaCl_2$	75	4.08	11.99	0.00	0.00	–147
MCA	MA	5 *M* $CaCl_2$	75	4.08	11.99	0.00	0.00	–138
PCA	ASW	5 *M* $CaCl_2$	75	4.08	11.99	0.00	0.00	–138
PCA	ASW	5 *M* $CaCl_2$	75	4.08	11.99	0.00	0.00	–137
MCA	MA	5 *M* $CaCl_2$	75	4.08	11.99	0.00	0.00	–128
MCA	ASW	5 *M* $CaCl_2$	75	4.08	11.99	0.00	0.00	–126
MCA	ASW	5 *M* $CaCl_2$	75	4.08	11.99	0.00	0.00	–125
MCA	MA	5 *M* $CaCl_2$	75	4.08	11.99	0.00	0.00	–121
MCA	MA	5 *M* $CaCl_2$	75	4.08	11.99	0.00	0.00	–119
MCA	ASW	5 *M* $CaCl_2$	75	4.08	11.99	0.00	0.00	–117
MCA	MA	5 *M* $CaCl_2$	75	4.08	11.99	0.00	0.00	–115
MCA	MA	5 *M* $CaCl_2$	75	4.08	11.99	0.00	0.00	–97

Table 2.3.6-7. Crevice Repassivation Potential Data Used in Model Development (Continued)

Sample Type	Material Condition	Solution	Temperature (°C)	Calculated Pitzer pH	[Cl] molal	[NO_3] molal	NO_3/Cl molal ratio	E_{rcrev} (mV vs. SSC)
MCA	MA	5 *M* $CaCl_2$	75	4.08	11.99	0.00	0.00	–93
MCA	MA	5 *M* $CaCl_2$	75	4.08	11.99	0.00	0.00	–88
MCA	MA	5 *M* $CaCl_2$	75	4.08	11.99	0.00	0.00	–77
MCA	MA	5 *M* $CaCl_2$	75	4.08	11.99	0.00	0.00	–19
MCA	MA	5 *M* $CaCl_2$	75	4.08	11.99	0.00	0.00	–8
MCA	MA	5 *M* $CaCl_2$	75	4.08	11.99	0.00	0.00	42
MCA	ASW	5 *M* $CaCl_2$	90	4.00	11.99	0.00	0.00	–189
PCA	MA	5 *M* $CaCl_2$	90	4.00	11.99	0.00	0.00	–189
PCA	ASW	5 *M* $CaCl_2$	90	4.00	11.99	0.00	0.00	–184
MCA	MA	5 *M* $CaCl_2$	90	4.00	11.99	0.00	0.00	–183
MCA	MA	5 *M* $CaCl_2$	90	4.00	11.99	0.00	0.00	–183
MCA	ASW	5 *M* $CaCl_2$	90	4.00	11.99	0.00	0.00	–175
PCA	ASW	5 *M* $CaCl_2$	90	4.00	11.99	0.00	0.00	–172
PCA	MA	5 *M* $CaCl_2$	90	4.00	11.99	0.00	0.00	–168
MCA	ASW	5 *M* $CaCl_2$	90	4.00	11.99	0.00	0.00	–164
MCA	ASW	5 *M* $CaCl_2$	90	4.00	11.99	0.00	0.00	–161
MCA	MA	5 *M* $CaCl_2$	90	4.00	11.99	0.00	0.00	–143
MCA	MA	5 *M* $CaCl_2$	90	4.00	11.99	0.00	0.00	–133
MCA	MA	5 *M* $CaCl_2$	90	4.00	11.99	0.00	0.00	–129
MCA	MA	5 *M* $CaCl_2$	90	4.00	11.99	0.00	0.00	–85

Table 2.3.6-7. Crevice Repassivation Potential Data Used in Model Development (Continued)

Sample Type	Material Condition	Solution	Temperature (°C)	Calculated Pitzer pH	[Cl] molal	[NO_3] molal	NO_3/Cl molal ratio	E_{rcrev} (mV vs. SSC)
MCA	MA	5 *M* $CaCl_2$	90	4.00	11.99	0.00	0.00	–35
MCA	MA	5 *M* $CaCl_2$	90	4.00	11.99	0.00	0.00	–8
PCA	ASW - Mockup	5 *M* $CaCl_2$	90	4.00	11.99	0.00	0.00	–73
PCA	ASW - Mockup	5 *M* $CaCl_2$	90	4.00	11.99	0.00	0.00	–169
MCA	MA	5 *M* $CaCl_2$	105	3.95	11.99	0.00	0.00	–195
MCA	MA	5 *M* $CaCl_2$	105	3.95	11.99	0.00	0.00	–185
MCA	MA	5 *M* $CaCl_2$	120	3.93	11.99	0.00	0.00	–216
MCA	MA	5 *M* $CaCl_2$	120	3.93	11.99	0.00	0.00	–198
PCA	ASW	5 *M* $CaCl_2$	120	3.93	11.99	0.00	0.00	–190
PCA	ASW	5 *M* $CaCl_2$	120	3.93	11.99	0.00	0.00	–186
MCA	ASW	5 *M* $CaCl_2$	120	3.93	11.99	0.00	0.00	–183
MCA	ASW	5 *M* $CaCl_2$	120	3.93	11.99	0.00	0.00	–179
MCA	MA	5 *M* $CaCl_2$	120	3.93	11.99	0.00	0.00	–178
MCA	MA	5 *M* $CaCl_2$	120	3.93	11.99	0.00	0.00	–164
MCA	ASW	5 *M* $CaCl_2$	120	3.93	11.99	0.00	0.00	–161
MCA	ASW	10 *m* $CaCl_2$	100	3.67	20.00	0.00	0.00	–197
MCA	ASW	10 *m* $CaCl_2$	100	3.67	20.00	0.00	0.00	–183
MCA	ASW	1 *m* NaCl + 0.05 *m* KNO_3	60	6.45	1.00	0.05	0.05	94
MCA	ASW	1 *m* NaCl + 0.05 *m* KNO_3	80	6.25	1.00	0.05	0.05	25
MCA	ASW	1 *m* NaCl + 0.05 *m* KNO_3	80	6.25	1.00	0.05	0.05	–52

Table 2.3.6-7. Crevice Repassivation Potential Data Used in Model Development (Continued)

Sample Type	Material Condition	Solution	Temperature (°C)	Calculated Pitzer pH	[Cl] molal	[NO_3] molal	NO_3/Cl molal ratio	E_{rcrev} (mV vs. SSC)
MCA	ASW	1 *m* NaCl + 0.05 *m* KNO_3	100	6.08	1.00	0.05	0.05	–118
MCA	ASW	1 *m* NaCl + 0.05 *m* KNO_3	100	6.08	1.00	0.05	0.05	–122
PCA	ASW	1 *m* NaCl + 0.05 *m* KNO_3	100	6.08	1.00	0.05	0.05	–86
PCA	ASW	1 *m* NaCl + 0.05 *m* KNO_3	100	6.08	1.00	0.05	0.05	–81
PCA	ASW	1 *m* NaCl + 0.05 *m* KNO_3	100	6.08	1.00	0.05	0.05	–64
PCA	ASW	1 *m* NaCl + 0.15 *m* KNO_3	80	6.25	1.00	0.15	0.15	68
MCA	ASW	1 *m* NaCl + 0.15 *m* KNO_3	100	6.08	1.00	0.15	0.15	–65
MCA	ASW	3.5 *m* NaCl + 0.175 *m* KNO_3	60	6.30	3.50	0.175	0.05	–6
MCA	ASW	3.5 *m* NaCl + 0.175 *m* KNO_3	60	6.30	3.50	0.175	0.05	–73
MCA	ASW	3.5 *m* NaCl + 0.175 *m* KNO_3	80	6.10	3.50	0.175	0.05	–77
MCA	ASW	3.5 *m* NaCl + 0.175 *m* KNO_3	80	6.10	3.50	0.175	0.05	–85
MCA	ASW	3.5 *m* NaCl + 0.175 *m* KNO_3	100	5.94	3.50	0.175	0.05	–132
MCA	ASW	3.5 *m* NaCl + 0.175 *m* KNO_3	100	5.94	3.50	0.175	0.05	–104
MCA	ASW	3.5 *m* NaCl + 0.525 *m* KNO_3	100	5.94	3.50	0.525	0.15	–85
MCA	MA	3.5 *m* NaCl + 0.525 *m* KNO_3	100	5.94	3.50	0.525	0.15	–88
MCA	MA	3.5 *m* NaCl + 0.525 *m* KNO_3	100	5.94	3.50	0.525	0.15	–3
MCA	ASW	3.5 *m* NaCl + 0.525 *m* KNO_3	100	5.94	3.50	0.525	0.15	–96
MCA	ASW	6 *m* NaCl + 0.3 *m* KNO_3	60	6.15	6.00	0.3	0.05	–18
MCA	MA	6 *m* NaCl + 0.3 *m* KNO_3	80	5.96	6.00	0.3	0.05	–114
MCA	MA	6 *m* NaCl + 0.3 *m* KNO_3	80	5.96	6.00	0.3	0.05	–107

Table 2.3.6-7. Crevice Repassivation Potential Data Used in Model Development (Continued)

Sample Type	Material Condition	Solution	Temperature (°C)	Calculated Pitzer pH	[Cl] molal	[NO_3] molal	NO_3/Cl molal ratio	E_{rcrev} (mV vs. SSC)
MCA	ASW	6 *m* NaCl + 0.3 *m* KNO_3	80	5.96	6.00	0.3	0.05	–95
MCA	ASW	6 *m* NaCl + 0.3 *m* KNO_3	80	5.96	6.00	0.3	0.05	–97
MCA	ASW	6 *m* NaCl + 0.3 *m* KNO_3	100	5.80	6.00	0.3	0.05	–88
MCA	ASW	6 *m* NaCl + 0.3 *m* KNO_3	100	5.80	6.00	0.3	0.05	–120
PCA	ASW	6 *m* NaCl + 0.3 *m* KNO_3	100	5.80	6.00	0.3	0.05	–93
PCA	ASW	6 *m* NaCl + 0.3 *m* KNO_3	100	5.80	6.00	0.3	0.05	–61
MCA	MA	6 *m* NaCl + 0.3 *m* KNO_3	100	5.80	6.00	0.3	0.05	–88
MCA	MA	6 *m* NaCl + 0.3 *m* KNO_3	100	5.80	6.00	0.3	0.05	–79
MCA	MA	6 *m* NaCl + 0.9 *m* KNO_3	80	5.97	6.00	0.90	0.15	–52
MCA	MA	6 *m* NaCl + 0.9 *m* KNO_3	80	5.97	6.00	0.90	0.15	–27
MCA	ASW	6 *m* NaCl + 0.9 *m* KNO_3	80	5.97	6.00	0.90	0.15	26
MCA	MA	6 *m* NaCl + 0.9 *m* KNO_3	100	5.81	6.00	0.90	0.15	–85
MCA	MA	6 *m* NaCl + 0.9 *m* KNO_3	100	5.81	6.00	0.90	0.15	–89
MCA	ASW	6 *m* NaCl + 0.9 *m* KNO_3	100	5.81	6.00	0.90	0.15	–85
MCA	ASW	6 *m* NaCl + 0.9 *m* KNO_3	100	5.81	6.00	0.90	0.15	–39
PCA	ASW - Mockup	6 *m* NaCl + 0.9 *m* KNO_3	100	5.81	6.00	0.90	0.15	–75
PCA	ASW - Mockup	6 *m* NaCl + 0.9 *m* KNO_3	100	5.81	6.00	0.90	0.15	–74
MCA	ASW	10 *m* $CaCl_2$ + 0.5 *m* $Ca(NO_3)_2$	100	3.89	20.00	1.00	0.05	–41
MCA	ASW	10 *m* $CaCl_2$ + 0.5 *m* $Ca(NO_3)_2$	100	3.89	20.00	1.00	0.05	–39
MCA	ASW	10 *m* $CaCl_2$ + 1.5 *m* $Ca(NO_3)_2$	100	4.38	20.00	3.00	0.15	18

Table 2.3.6-7. Crevice Repassivation Potential Data Used in Model Development (Continued)

Sample Type	Material Condition	Solution	Temperature (°C)	Calculated Pitzer pH	[Cl] molal	[NO_3] molal	NO_3/Cl molal ratio	E_{rcrev} (mV vs. SSC)
PCA	ASW	10 *m* $CaCl_2$ + 5 *m* $Ca(NO_3)_2$	100	5.39	20.00	10.00	0.50	76
PCA	ASW	10 *m* $CaCl_2$ + 5 *m* $Ca(NO_3)_2$	100	5.39	20.00	10.00	0.50	83
PCA	ASW	10 *m* $CaCl_2$ + 5 *m* $Ca(NO_3)_2$	100	5.39	20.00	10.00	0.50	87
MCA	ASW	10 *m* $CaCl_2$ + 5 *m* $Ca(NO_3)_2$	100	5.39	20.00	10.00	0.50	105
PCA	ASW	10 *m* $CaCl_2$ + 5 *m* $Ca(NO_3)_2$	100	5.39	20.00	10.00	0.50	179

NOTE: ASW = as-welded; *m* = molality; *M* = molarity; MA = mill-annealed; MCA = multiple crevice assembly; PCA = prism crevice assembly; SSC = saturated silver chloride electrode.

Source: SNL 2007c, Appendix IX.

Table 2.3.6-8. Bounding Rates for Localized Corrosion for Alloy 22 (Distribution)

Percentile	Localized Corrosion Rate (μm/yr)
0th	12.7
50th	127
100th	1,270

Source: SNL 2007c, Table 6-15.

Table 2.3.6-9. Summary of Model Validation Analysis for the Corrosion Potential Model

Test Condition and Data Source	Measured E_{corr} (mV_{SHE})	Measured E_{corr} (mV_{SSC})[a]	Environmental Condition Inputs to Model Calculation	E_{corr} Model	
				Mean (mV_{SSC})	Bounds (mV_{SSC})
Alloy 22 in 6.2 *m* NaCl, 80°C, nominal pH of 3 (Jayaweera et al. 2003, pp. 9-18 to 9-22, Figure 9.13)	160 to 250	–39 to 51	6.2 *m* [Cl], 80°C, pH 3	295	114 (Lower) 476 (Upper)
Alloy 22 in basic saturated water at 110°C (Andresen et al. 2003, Table 1-4; pp. 66 and 78)	100 to 110	–99 to –89	4.62 *m* [Cl], 2.82 *m* [NO_3], 110°C, pH 8.58	–104	–279 (Lower) 70 (Upper)
Alloy 22 in basic saturated water at 110°C (Andresen et al. 2003, Table 1-4; pp. 66 and 78)	100 to 110	–99 to –89	5.08 *m* [Cl], 2.89 *m* [NO_3], 110°C, pH 8.58	–154	–328 (Lower) 20 (Upper)

NOTE: [a]At 25°C, the SSC reference electrode is 199 mV more noble than the standard hydrogen electrode (Sawyer and Roberts 1974, pp. 39 to 45, Table 2 4).

Source: SNL 2007c, Table 7-2.

Table 2.3.6-10. Summary of Model Validation Analysis for Crevice Repassivation Potential Model

Exposure Environment	Measured E_{rcrev} (mV_{SSC})	Environmental Condition Inputs to Model Calculation	E_{rcrev} Model	
			Mean (mV_{SSC})	Bounds (mV_{SSC})
1 M NaCl at 90°C	–67	1.02 *m* [Cl], 0 *m* [NO_3], pH 6.16, 90°C	–76	15 (Upper) –167 (Lower)
6 *m* NaCl + 0.9 *m* KNO_3 at 100°C	–77	6 *m* [Cl], 0.9 *m* [NO_3], pH 5.81, 100°C	–77	13 (Upper) –168 (Lower)

Source: SNL 2007c, Table 7-3.

Table 2.3.6-11. Alternate Model Comparison to Crevice Repassivation Potential Model

Exposure Environment	[Cl] molal	[NO_3] molal	pH	E_{Dunn} (mV_{SSC})	E_{rcrev} Model	
					Mean (mV_{SSC})	Bounds (mV_{SSC})
1 *M* NaCl at 80°C	1.02	0	6.25	294	–46	44 (Upper) –137 (Lower)
4 *M* NaCl at 120°C	4.4	0	5.75	–282	–208	–116 (Upper) –300 (Lower)
5 *M* $CaCl_2$ at 105°C	11.99	0	4.00	–155	–165	–174 (Upper) –256 (Lower)
5 *M* $CaCl_2$ + 0.05 *M* $Ca(NO_3)_2$ at 120°C	11.70	0.12	3.96	–237	–195	–103 (Upper) –286 (Lower)
5 *M* $CaCl_2$ + 0.5 *M* $Ca(NO_3)_2$ at 105°C	12.59	1.26	3.15	645	–110	–19 (Upper) –201 (Lower)
1 *M* $CaCl_2$ + 1 *M* $Ca(NO_3)_2$ at 120°C	2.62	2.58	5.82	544	331	434 (Upper) 228 (Lower)

Source: SNL 2007c, Table 7-4.

Table 2.3.6-12. Comparison of Model Prediction for Localized Corrosion Susceptibility with Experimental Observations of Alloy 22 Crevice Samples Tested for Over 5 Years

Long-Term Immersion Test Results					Model Results		
Exposure Environment	**Crevice Corrosion Observation**	**pH**	**[Cl] (molal)**	**[NO_3] (molal)**	**Mean ΔE (mV vs. SSC)**	**Lower Bound ΔE (mV vs. SSC)**	**Upper Bound ΔE (mV SSC)**
SDW, 90°C	No	9.41	3.30×10^{-3}	9.73×10^{-4}	304	18	590
SCW, 90°C	No	10.04	0.21	0.12	373	101	646
SAW, 90°C	No	2.72	0.77	0.37	–168	–435	98

NOTE: SSC = saturated silver chloride electrode.

Source: SNL 2007c, Table 7-5.

Table 2.3.6-13. Comparison of Long-Term Corrosion Test Observations to Model Predictions

Solution	Immersion Days	Cell#	T(°C)	Creviced Geometry	Crevice Corrosion	Rod Geometry	Pitting Corrosion	Modeled ΔE		
								Lower Bound	Mean	Upper Bound
5 *m* $CaCl_2$ + 5 *m* $Ca(NO_3)_2$	723	33	120	4	0	2	0	–398	–116	166
5 *m* $CaCl_2$ + 5 *m* $Ca(NO_3)_2$	729	32	100	4	0	2	0	–184	93	370
3.5 *m* NaCl + 0.175 *m* KNO_3 + 0.7 *m* $MgSO_4$	735	31	80	4	2	2	0	–227	38	303
1 *M* NaCl + 0.15 *M* KNO_3	741	30	90	4	0	2	0	–202	62	325
1 *M* NaCl + 0.15 *M* KNO_3	749	29	75	4	0	2	0	–185	80	344
5 *M* $CaCl_2$	650	28	90	4	4	2	0	–466	–201	63
3.5 *m* NaCl + 0.175 *m* KNO_3	252	25	100	4	0	0	0	–225	39	304
3.5 *m* NaCl + 0.525 *m* KNO_3	256	24	100	4	0	0	0	–223	41	305
6 *m* NaCl + 0.9 *m* KNO_3	265	23	100	4	2	0	0	–236	28	291
6 *m* NaCl + 0.3 *m* KNO_3	280	22	100	4	0	0	0	–239	26	290
5 *M* $CaCl_2$ + 0.5 *M* $Ca(NO_3)_2$	463	21	90	6	6	6	0	–597	–332	–66
5 *M* $CaCl_2$	497	20	120	6	6	6	0	–462	–191	79
BSW	256	19	105	0	0	8	0	15	284	554
4 *M* NaCl	328	18	90	0	0	6	0	–233	31	295
SAW w/o Silicate	375	17	90	0	0	6	0	–485	–216	52
SCW	394	16	90	0	0	6	0	124	394	665
5 *M* $CaCl_2$ + 0.5 *M* $Ca(NO_3)_2$	693	15	90	0	0	6	1	–597	–332	–66
5 *M* $CaCl_2$ + 0.05 *M* $Ca(NO_3)_2$	704	14	90	0	0	6	1	–458	–194	70

Table 2.3.6-13. Comparison of Long-Term Corrosion Test Observations to Model Predictions (Continued)

Solution	Immersion Days	Cell#	T(°C)	Creviced Geometry	Crevice Corrosion	Rod Geometry	Pitting Corrosion	Modeled ΔE		
								Lower Bound	Mean	Upper Bound
1 *M* $CaCl_2$ + 1 *M* $Ca(NO_3)_2$	622	13	90	0	0	6	0	–93	186	465
4.5 years LTCTF SAW	834	10	90	0	0	8	0	–435	–168	98
SAW	876	9	90	0	0	8	0	–587	–322	–57
SAW - LTCTF Vessel 26	846	7-2	25	0	0	3	0	–178	106	390
SDW - LTCTF Vessel 30	1,089	6	90	0	0	2	0	18	304	590
SDW - LTCTF Vessel 29	1,089	5	60	0	0	2	0	107	393	678
BSW	729	4	105	1	0	1	0	15	284	554
SCW - LTCTF Vessel 28	1,089	3	90	0	0	2	0	101	373	646
SAW - LTCTF Vessel 26	1,102	2	90	0	0	2	0	–435	–168	98
SAW - LTCTF Vessel 25	1,089	1	60	0	0	2	0	–312	–42	228
Data below is from cells not used for long-term corrosion potential model development										
1 *m* NaCl + 0.05 *m* KNO_3	223	27	100	4	0	0	0	–218	47	312
1 *m* NaCl + 0.15 *m* KNO_3	230	26	100	4	0	0	0	–217	47	312
5 *M* $CaCl_2$	894	8	120	0	0	5	5	–462	–191	79
SCW - LTCTF Vessel 27	218	7-1	60	0	0	2	0	281	559	837

NOTE: Variations in solution composition (e.g., between the SAW solution compositions in cells 2, 9, 10, and 17) can lead to variations in the calculated ΔE values. BSW = basic saturated water; LTCTF = Long-Term Corrosion Test Facility.

Source: SNL 2007c, Table 7-6

Table 2.3.6-14. Slow Strain Rate Test Results for Annealed Alloy 22

Specimen ID	Test Environment	Temperature (°C)	E_{corr} (mV vs. Ag/AgCl)	$E_{Applied}$ (mV vs. Ag/AgCl)	Time to Failure of the Specimen (hours)	Maximum Stress (MPa)	Reduction in Area (%)	Observation
012	Air	22	None	None	124	786	74	Ductile necking
040	Air	22	None	None	123	813	70	Ductile necking
098	1*M* NaCl at pH = 6.9	90	–104	+400	74[a]	660	76	No SCC
123	4*M* NaCl at pH = 6.2	98	–323	+349	127	762	80	No SCC
091	1*M* NaF at pH = 9.2	85	133	E_{corr}	112	756	67	No SCC
130	1*M* NaF at pH = 7.6	90	–244	+400	112	727	67	Incipient SCC
004	8.5*M* $CaCl_2$ at pH ~ 6	120	–140 to –180	E_{corr}	127	752	71	No SCC
013	1% $PbCl_2$ at pH ~ 4 Aerated	95	—	E_{corr}	126	765	72	No SCC
015	SAW at pH ~3	63	–7 to +360	E_{corr}	118	758	79	No SCC
016	SAW at pH ~3 + 0.005% $Pb(NO_3)_2$	76	–6 to +370	E_{corr}	124	772	74	No SCC
017	SAW at pH ~3 + 0.005% $Pb(NO_3)_2$	76	0 to +350	E_{corr}	125	772	74	No SCC
003	SAW at pH ~3 + 0.005% $Pb(NO_3)_2$	95	–90 to +400	E_{corr}	118	752	85	No SCC
127	BSW at pH ~13 – $[NO_3 + SO_4]$[b]	98	–240 to –220	E_{corr}	123	745	72	No SCC
124	BSW at pH ~13 – $[NO_3 + SO_4]$[b]	105	–330	+100	120	745	78	No SCC
122	BSW at pH ~13 – $[NO_3 + SO_4]$[b]	98	–245	+200	122	752	72	No SCC
120	BSW at pH ~13	105	–323	+400	99	745	74	No SCC
119	BSW at pH ~13	105	–301	+400	118	745	75	No SCC
115	BSW at pH ~13 - $[NO_3]$[b]	105	–335	+400	115	752	77	No SCC
129	BSW at pH ~13 - $[SO_4^{2-}]$[b]	105	–314	+400	119	731	82	No SCC

Table 2.3.6-14. Slow Strain Rate Test Results for Annealed Alloy 22 (Continued)

Specimen ID	Test Environment	Temperature (°C)	E_{corr} (mV vs. Ag/AgCl)	$E_{Applied}$ (mV vs. Ag/AgCl)	Time to Failure of the Specimen (hours)	Maximum Stress (MPa)	Reduction in Area (%)	Observation
125	SSW at pH ~6	100	–154	+400	113	717	71	No SCC
020	SCW at pH ~9 to 10	22	–109	+400	116	800	85	No SCC
133	SCW at pH ~9 to 10	22	–128	+400	124	798	80	No SCC
032	SCW at pH ~9 to 10	50	–129	+400	110	757	75	Incipient SCC
134	SCW at pH ~9 to 10	65	–217	+400	97	684	59	SCC
112	SCW at pH ~9 to 10	73	–93	+400	91	697	71	SCC
021	SCW at pH ~9 to 10	73	–172	+400	90	665	64	SCC
033	SCW at pH ~9 to 10	86	–169	+400	76	642	44	SCC
113	SCW at pH ~9 to 10	75	–200	+317	116	765	63	Incipient SCC
030	SCW at pH ~9 to 10	85	–182	+300	98	725	65	SCC
020	SCW at pH ~9 to 10	22	–109	+291	116	800	85	No SCC
023	SCW at pH ~9 to 10	73	–224	+200	DNB	DNB	72	Incipient SCC
025	SCW at pH ~9 to 10	73	–172	+200	116	776	80	Incipient SCC
029	SCW at pH ~9 to 10	89	–144	+200	112	678	73	Incipient SCC
026	SCW at pH ~9 to 10	73	–241	+100	120	764	79	No SCC
037	SCW at pH ~9 to 10	22	–76	E_{corr}	DNB	DNB	32	No SCC

Table 2.3.6-14. Slow Strain Rate Test Results for Annealed Alloy 22 (Continued)

Specimen ID	Test Environment	Temperature (°C)	E_{corr} (mV vs. Ag/AgCl)	$E_{Applied}$ (mV vs. Ag/AgCl)	Time to Failure of the Specimen (hours)	Maximum Stress (MPa)	Reduction in Area (%)	Observation
034	SCW at pH ~9 to 10	90	–143	E_{corr}	129	712	80	No SCC

NOTE: [a]Short time to failure due to crevice corrosion at coating interface.
[b]Basic saturated water without the presence of nitrate or sulfate, or both.
DNB = did not break-equipment stoppage; SCC = stress corrosion cracking.

Source: SNL 2007a, Table 6-2.

Table 2.3.6-15. Hoop Stress Profile Coefficients for the Plasticity Burnished Naval Long and TAD Waste Package Outer Barrier Closure Lid

Stress Coefficient	Unit	Section A-A		Section B-B		Conversion Factors	Unit	Section A-A		Section B-B	
		Radial Stress	Hoop Stress	Radial Stress	Hoop Stress			Radial Stress	Hoop Stress	Radial Stress	Hoop Stress
A_0	ksi	–90.179	–75.293	–82.228	–72.008	1 ksi = 6.894757 MPa	MPa	–621.762	–519.127	–566.942	–496.478
A_1	ksi/in.	772.46	853.48	695.42	817.86	1 ksi/in. = 0.271447 MPa/mm	MPa/mm	209.682	231.675	188.770	222.006
A_2	ksi/in.^{2}	–1,646.7	–1,626	–1,470.7	–1,542	1 ksi/in.^{2} = 0.010687 MPa/mm^2	MPa/mm^2	–17.598	–17.377	–15.717	–16.479
A_3	ksi/in.^{3}	994.72	922.37	881.5	859.56	1 ksi/in.^{3} = 0.000421 MPa/mm^3	MPa/mm^3	0.419	0.388	0.371	0.362

NOTE: Section A-A is through the root of the outer lid closure weld and perpendicular to the outside surface of the outer lid. Section B-B is through the inside edge of the weld. The last four columns are converted to metric units by using the conversion factors shown in the middle column.

Source: SNL 2007a, Table 6-14.

Table 2.3.6-16. Stress and Stress Intensity Factor Profiles for the Plasticity-Burnished Naval Long and TAD Waste Package Outer Lid

Distance from Outer Surface (mm)	Single-Edge Cracked Plate (Radial Stress)		Elliptical (Hoop Stress)	
	Sx (MPa)	K-Sx (MPa√m)	Sx (MPa)	K-Sx (MPa√m)
0.4064	–539.4256	–17.9483	–427.8182	–9.4403
0.8128	–462.7335	–22.6622	–342.0932	–13.0870
1.2192	–391.5169	–24.5417	–261.7957	–15.7063
1.6256	–325.6071	–24.7639	–186.7694	–17.7655
2.0320	–264.8353	–23.8426	–116.8581	–19.4500
2.4384	–209.0327	–22.0731	–51.9054	–20.8568
2.8448	–158.0308	–20.2774	8.2447	–18.7051
3.2512	–111.6606	–18.1813	63.7487	–16.1168
3.6576	–69.7535	–15.6533	114.7627	–13.1794
4.0640	–32.1407	–12.7494	161.4431	–9.9714
4.4704	1.3465	–9.5133	203.9461	–6.5568
4.8768	30.8769	–5.9794	242.4278	–2.9886
5.2832	56.6192	–2.2008	277.0447	0.6173
5.6896	78.7421	1.8491	307.9530	4.2344
6.0960	97.4145	6.1848	335.3088	7.9070
6.5024	112.8050	10.7787	359.2686	11.6084
6.9088	125.0823	15.6038	379.9885	15.3153
7.3152	134.4154	20.6344	397.6247	19.0077
7.7216	140.9727	26.0005	412.3336	22.6634
8.1280	144.9232	32.1659	424.2715	26.2705
8.5344	146.4356	38.7572	433.5945	29.8352
8.9408	145.6786	45.7646	440.4589	33.3463
9.3472	142.8209	53.1787	445.0210	36.7941
9.7536	138.0313	60.9899	447.4371	40.1706
10.1600	131.4785	69.1883	447.8633	43.4690
10.5664	123.3313	75.7990	446.4560	46.7415
10.9728	113.7585	82.6202	443.3715	49.9358

Table 2.3.6-16. Stress and Stress Intensity Factor Profiles for the Plasticity-Burnished Naval Long and TAD Waste Package Outer Lid (Continued)

Distance from Outer Surface (mm)	Single-Edge Cracked Plate (Radial Stress)		Elliptical (Hoop Stress)	
	Sx (MPa)	K-Sx (MPa√m)	Sx (MPa)	K-Sx (MPa√m)
11.3792	102.9286	89.6163	438.7659	53.0484
11.7856	91.0106	96.7504	432.7956	56.0768
12.1920	78.1732	103.9864	425.6167	59.0194
12.5984	64.5850	111.2875	417.3856	61.8761
13.0048	50.4149	119.6266	408.2586	64.7048
13.4112	35.8315	128.5514	398.3918	67.4665
13.8176	21.0037	137.7290	387.9415	70.1443
14.2240	6.1001	147.1219	377.0640	72.7415
14.6304	–8.7104	156.6950	365.9156	75.2627
15.0368	–23.2592	166.4143	354.6525	77.7130
15.4432	–37.3775	180.0773	343.4309	80.0499
15.8496	–50.8966	198.4291	332.4072	82.2619
16.2560	–63.6477	217.8863	321.7376	84.3998
16.6624	–75.4621	238.4456	311.5782	86.4731
17.0688	–86.1710	260.1082	302.0855	88.4922
17.4752	–95.6056	282.8795	293.4157	90.4686
17.8816	–103.5974	311.7154	285.7250	92.6432
18.2880	–109.9774	357.0449	279.1696	95.5196
18.6944	–114.5770	404.2907	273.9059	98.4483
19.1008	–117.2274	453.3914	270.0901	101.4484
19.5072	–117.7599	504.2920	267.8784	104.5400
19.9136	–116.0057	556.9519	267.4272	107.7446
20.3200	–111.7961	611.3402	268.8926	111.0842

Source: SNL 2007a, Table 6-16.

Table 2.3.6-17. Determination of the Slip-Dissolution Film-Rupture Model Parameters for Alloy 22

Specimen	Test Conditions	Hold Time (hrs)	Tested Stress Intensity Factor (MPa$\sqrt{m}$)	Measured Crack Growth Rate (mm/s)[a]	Calculated *n* Value
C153	110°C BSW (20% Cold-worked)	Constant load	30	5.0×10^{-10}	1.119
C144	110°C BSW (Mill-annealed)	1	30	10^{-11}	1.392
C152	110°C BSW (Mill-annealed)	24	45	4.0×10^{-10}	1.281
C200	110°C BSW (Mill-annealed + Aged 700°C/175 hr)	Constant load	24.2	6.0×10^{-10}	1.041
C263	150°C SCW (As-welded)	24	40	1.2×10^{-9}	1.151
C264	150°C SCW (As-welded)	2.5	40	1.3×10^{-9}	1.145
C265	150°C SCW (As-welded + TCP)	1	40	2.0×10^{-9}	1.111
C266	150°C SCW (As-welded + LRO)	1	40	3.0×10^{-9}	1.080

NOTE: [a]Crack growth rate of 10^{-11} mm/s is used to represent test results where cracking appeared to cease propagating (i.e., the growth rate seemed to approach zero).
BSW = basic saturated water; LRO = long-range ordering; SCW = simulated concentrated water; TCP = tetrahedrally close-packed.

Source: SNL 2007a, Table 6-6.

Table 2.3.6-18. Main Characteristics of Flaws in Waste Package Outer Barrier Closure Weld

	Weld Flaw Size[a] (mm)			Probability of Number of Flaws[b]		
	Mean	**5th percentile**	**95th percentile**	**0**	**1**	**2 or more**
Before Ultrasonic Testing Inspection	4.8	0.23	15.2	0.585	0.303	0.112
After Ultrasonic Testing Inspection and Weld Repair	1.0	0.072	2.6	0.844	0.140	0.015

NOTE: [a]Flaw sizes are given with two significant figures.
[b]Probability values on number of flaws are rounded to give a total of 1.
For information only; do not use in calculations.

Source: SNL 2007d, Table 6-6.

Table 2.3.6-19. Threshold Stress Intensity Factor Distribution for Alloy 22

	Standard Deviation (SD)	***n* Value (n_{Mean} ± *i*SD, i = 0, 1, and 2)**	**'K_{ISCC}' Value (MPa$\sqrt{m}$)**
n_{Mean} = 1.165	–2	0.935	1.96
n_{SD} = 0.115	–1	1.050	3.83
V_{gcMean} = 7.23 nm/yr	0	1.165	6.62
	1	1.280	10.45
	2	1.395	15.38

NOTE: V_{gcMean} is the mean general corrosion rate of the Alloy 22 samples exposed for 5 years at 60°C and 90°C exposure samples.

Source: SNL 2007a, Table 6-8.

Table 2.3.6-20. Crack Growth Rates in Alloy 22 Compact Tension Specimens

Specimen ID	**Test Solution**	**Nominal Test Temperature (°C)**	**Average Stress Intensity (MPa•$m^{1/2}$)**	**Crack Growth Rate (mm/s)**
DCT-13	BSW	100	45.13	2.12×10^{-9}
DCT-14	BSW	100	44.88	4.23×10^{-9}
DCT-16	BSW	100	46.38	1.41×10^{-9}
DCT-18	SAW	94	45.07	2.12×10^{-10}
DCT-19	SAW	94	45.08	1.41×10^{-11}
DCT-20	SCW	95	45.11	4.23×10^{-10}
DCT-21	SCW	95	44.68	2.82×10^{-11}
DCT-22	SCW	95	44.37	4.94×10^{-12}

NOTE: BSW = basic saturated water.

Source: SNL 2007a, Table 7-3.

Table 2.3.6-21. Summary of Defect-Related Failures in Various Welded Metallic Containers

Container Type	Information on Failure	Types of Defects Leading to Early Failure
Boilers and Pressure Vessels	17 out of 20,000 pressure vessels that were less than 40 years old as of 1976 failed due to manufacturing defects (dominant cause was fatigue growth of weld flaws). Stainless steel cladding on some reactor coolant system components for two nuclear units (different fabricators) cracked due to surface contamination remaining from transport or fabrication.	• Weld flaws • Base metal flaws • Improper weld material • Improper heat treatment • Improper weld flux • Poor weld-joint design • Contaminants.
Nuclear Fuel Rods (PWR and BWR)	Undetected manufacturing defect-related failure rate approximately 1 rod per 100,000. Overall failure rates in the range of 2 to 7 rods per 10,000 before 1985, 0.6 to 3 rods per 10,000 from 1985 to 1997.	• Weld flaws • Base metal flaws • Mislocated welds • Contamination • Missing welds • Improper weld material • Handling damage.
Underground Storage Tanks	Fraction of population initially failed due to manufacturing or handling defects in the range of 0.04% to 0.0003%.	• Handling or installation damage • Weld flaws.
Radioactive Cesium Capsules	One failure out of 1,600 capsules.	• Administrative error resulting in unanticipated operating environment.
Dry Storage Casks for SNF	Four out of 19 Sierra Nuclear VSC-24 casks found to have cracked closure welds during postweld inspection (dye-penetrant and helium leak test only).	• Weld flaws • Base metal flaws • Contamination.

NOTE: BWR = boiling water reactor; PWR = pressurized water reactor.

Source: SNL 2007d, Table 6-2.

Table 2.3.6-22. Estimates of Human Error Probabilities

Item	Description	Nominal (Median) Probability	Error Factor	Expected (Mean) Probability	Source:
1	Failure to use written test or calibration procedure	0.05	5	8.1×10^{-2}	Swain and Guttmann 1983, Item 6 of Table 20-6
2	Error of commission in reading and recording quantitative information from un annunciated digital readout (less than 4 digits)	0.001	3	1.25×10^{-3}	Swain and Guttmann 1983, Item 2 of Table 20-10
3	Error of commission in check-reading[a] analog meter with difficult-to-see limit marks, such as scribe lines	0.002	3	2.50×10^{-3}	Swain and Guttmann 1983, Item 3 of Table 20-11
4	Selection of wrong control on a panel from an array of similar-appearing controls identified by labels only	0.003	3	3.75×10^{-3}	Swain and Guttmann 1983, Item 2 of Table 20-12
5	Improperly mate a connector (this includes failures to seat connectors completely and failure to test locking features of connectors for engagement)	0.003	3	3.75×10^{-3}	Swain and Guttmann 1983, Item 13 of Table 20-12
6	Checker failure to detect error made by others during routine tasks	0.1	5	1.6×10^{-1}	Swain and Guttmann 1983, Item 1 of Table 20-22
7	Failure to complete change of state of a component if a switch must be held down until completion	0.003	3	3.75×10^{-3}	Swain and Guttmann 1983, Item 10 of Table 20-12
8	Checking routine tasks with alerting factors	0.05	5	8.1×10^{-2}	Swain and Guttmann 1983, Item 3 of Table 20-22
9	Failure of administrative control	1.9×10^{-4}	10	5×10^{-4}	Benhardt et al. 1994, Table 4, Item 1 (routine, repetitive circumstances)
10	Failure to respond to a compelling signal	0.0011	10	0.003	Benhardt et al. 1994, Table 4, Item 2 (few competing signals)

NOTE: [a]Check-reading means reference to a display merely to see if the indication is within allowable limits; no quantitative reading is taken.

Table 2.3.6-23. Chemical Composition of Relevant Titanium Grades

ASTM Grade	UNS	N	C	H	O	Fe	Al	V	Pd	Ru	Residual (each)	Residual (total)
12	R53400	0.03	0.08	0.015	0.25	0.30	—	—	—	—	0.2 to 0.4 Molybdenum	0.6 to 0.9 Nickel
2	R50400	0.03	0.08	0.015	0.25	0.30	—	—	—	—	0.1	0.4
7	R52400	0.03	0.10	0.015	0.25	0.30	—	—	0.12 to 0.25	—	0.1	0.4
16	R52402	0.03	0.08	0.015	0.25	0.30	—	—	0.04 to 0.08	—	0.1	0.4
5	R56400	0.05	0.08	0.015	0.20	0.40	5.5 to 6.75	3.5 to 4.5	—	—	0.1	0.4
23	R56407	0.03	0.08	0.0125	0.13	0.25	5.5 to 6.5	3.5 to 4.5	—	—	0.1	0.4
24	R56405	0.05	0.08	0.015	0.20	0.40	5.5 to 6.75	3.5 to 4.5	0.04 to 0.08	—	0.1	0.4
9	R56320	0.03	0.08	0.015	0.15	0.25	2.5 to 3.5	2.0 to 3.0	—	—	0.1	0.4
28	R56323	0.03	0.08	0.015	0.15	0.25	2.5 to 3.5	2.0 to 3.0	—	0.08 to 0.14	0.1	0.4
29	R56404	0.03	0.08	0.015	0.13	0.25	5.5 to 6.5	3.5 to 4.5	—	0.08 to 0.14	0.1	0.4

Source: Reorganized from ASTM B 265-02 2002, Table 2.

Table 2.3.6-24. Titanium Grade 7 General Corrosion Rates from Weight-Loss Geometry Coupons Exposed for 2.5 Years

Aggressive Condition (SCW Aqueous at 90°C) (nm/yr)	Intermediate Condition (SCW Aqueous at 60°C) (nm/yr)	Benign Condition (Remainder Data) (nm/yr)
43.57	2.92	2.88
43.63	11.83	2.89
43.75	14.83	2.89
46.29	17.64	2.90
49.46	23.37	2.91
49.70	26.30	2.92
		2.94
		2.94
		2.94
		2.94
		2.94
		2.95
		2.95
		2.96
		2.96
		2.96
		5.77
		5.84
		5.87
		5.88
		5.88
		5.90
		14.49
		14.59
		17.64

Source: SNL 2007e, Table 6-4[a].

Table 2.3.6-25. Chemical Composition of the Test Solutions Used to Obtain Relative Corrosion Rates for Titanium Grade 29 and Titanium Grade 7 (Molal)

ID	Temp. (°C)	pH	$CaCl_2$	KCl	KNO_3	$NaNO_3$	NaCl	Na_2SO_4	NaF	NaBr
TS-1	150	4.9	3.6	5.8	1.8	2	0	0	0	0
TS-2	120	7.3	0	7	0	1.8	1.2	2.4	0	0
TS-3	120	9.0	0	7.2	0.3	3.3	0	2.1	0.2	0
TS-4	150	9.7	0	5	2.8	6.6	0	6.8	0.1	0.1

Source: SNL 2007e, Table 6-7[a].

Table 2.3.6-26. General Corrosion Rates of Titanium Grade 7 in Selected Test Media Containing High Concentrations of Chlorides of Ca^{2+}, Mg^{2+}, and Fe^{3+} Ions at Elevated Temperature

Test Medium	Temperature	Corrosion Rate (nm/yr)
62% $CaCl_2$	150°C	None Detected or Insignificant
10% and 30% $FeCl_3$	Boiling	None Detected or Insignificant
Saturated $MgCl_2$	Boiling	None Detected or Insignificant

Source: Schutz and Thomas 1987, Appendix 2.

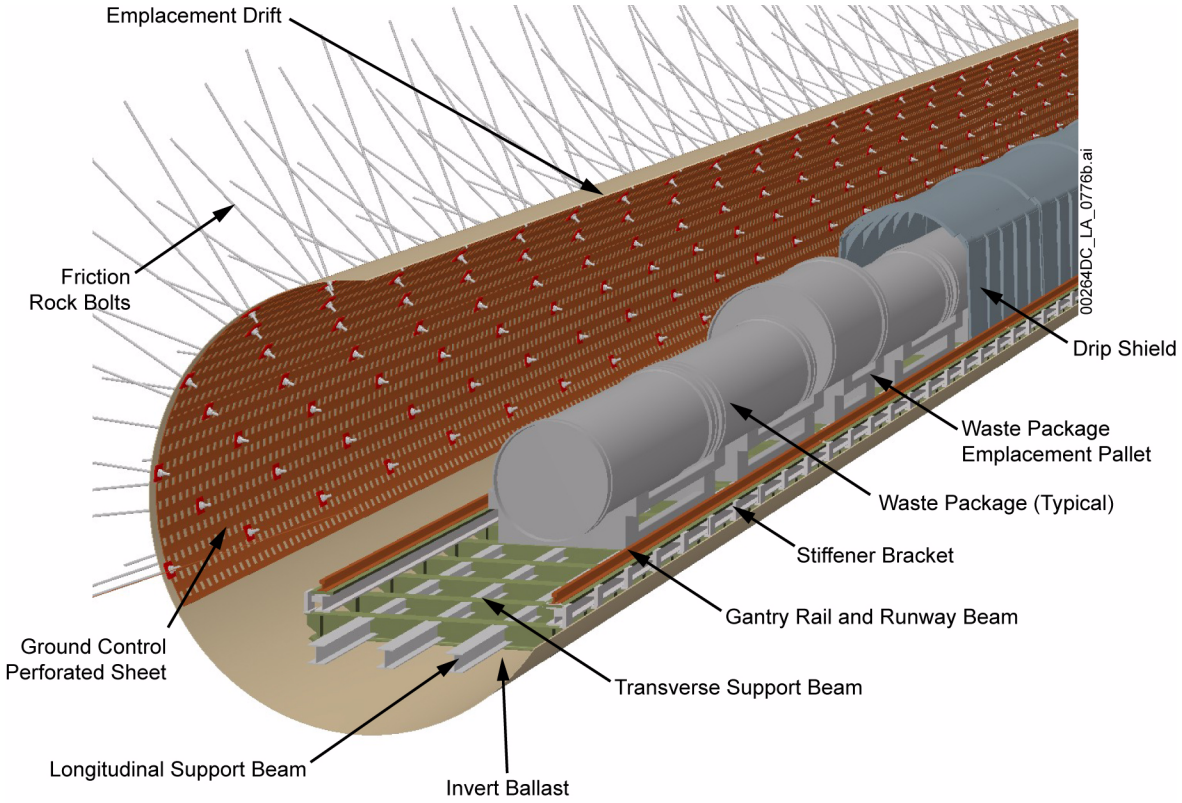

Figure 2.3.6-1. Schematic of an Emplacement Drift Showing Waste Packages and Drip Shields

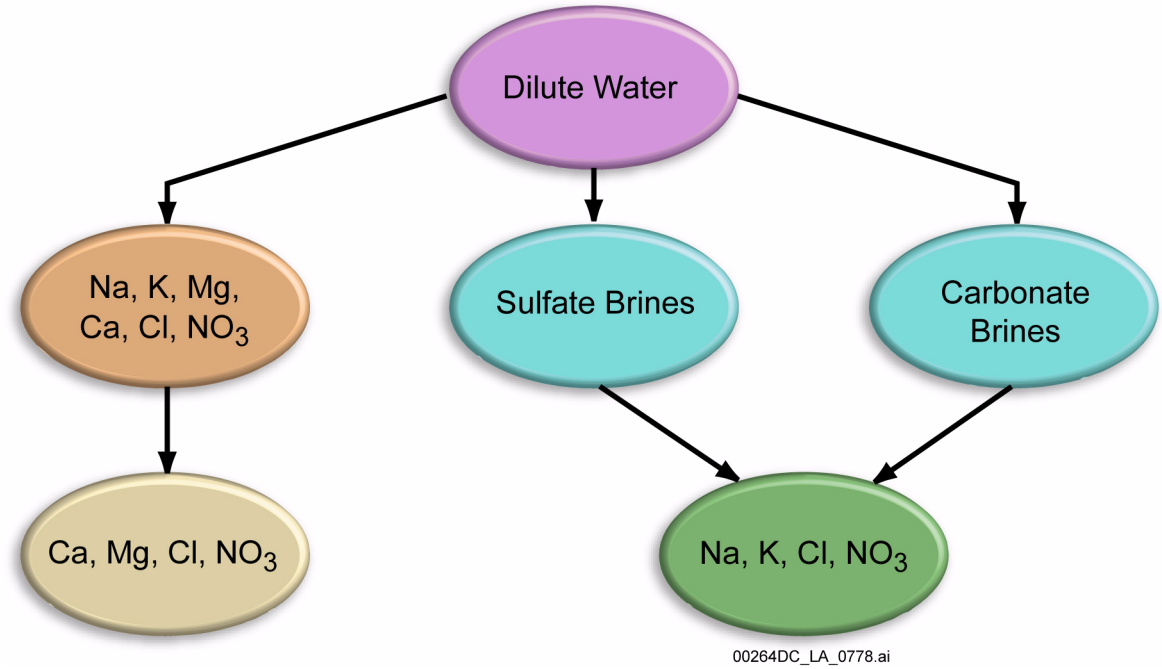

Figure 2.3.6-2. Expected Aqueous Solution Types

NOTE: Dilute waters are transformed to different types of brines, depending on their composition, through the processes of evaporation and mineral precipitation. The figure shows the dominant component assemblages produced by evaporation.

Source: Payer 2004, p. 52.

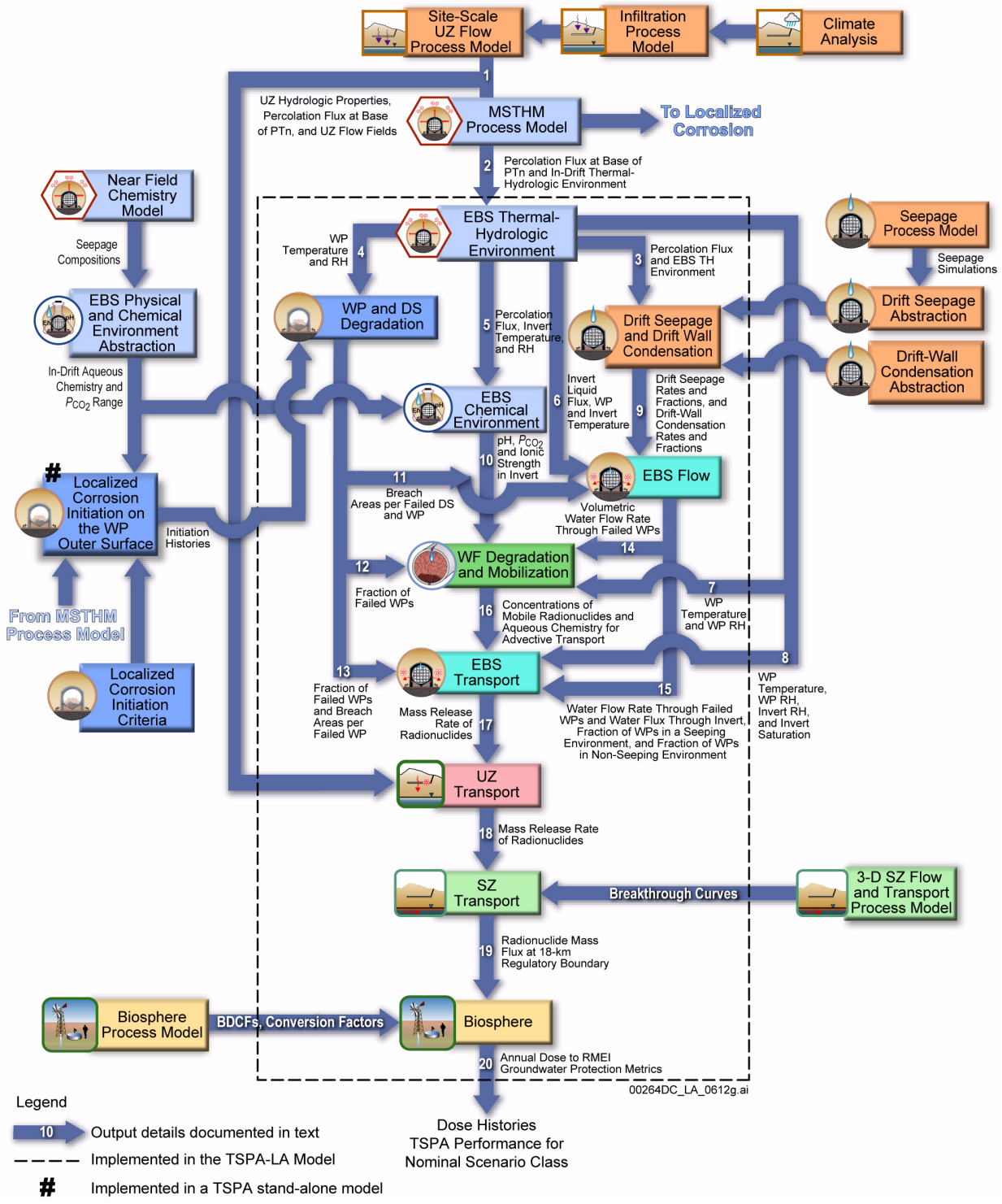

Figure 2.3.6-3. Information Transfer Between the Principal Model Components of the TSPA Nominal Scenario Class

NOTE: For details about outputs and information transfer shown on this figure, see Section 2.4.2.3.2.1.
DS = drip shield; LC = localized corrosion; PA = performance assessment; RH = relative humidity; RMEI = reasonably maximally exposed individual; SZ = saturated zone; TH = thermal-hydrologic; THC = thermal-hydrologic-chemical; UZ = unsaturated zone; WF = waste form; WP = waste package.

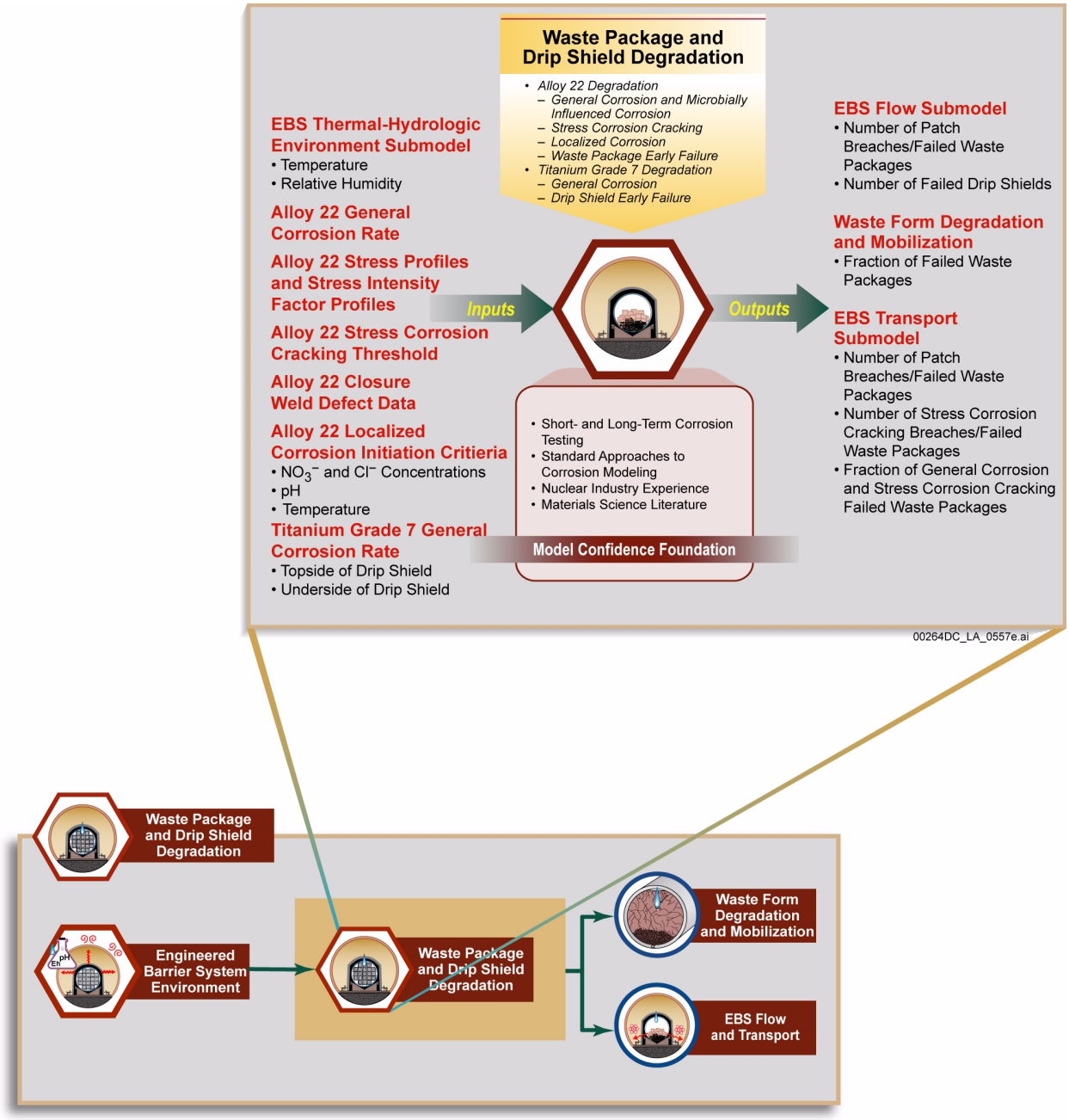

Figure 2.3.6-4. Inputs, Outputs, and Basis for Model Confidence for the Waste Package and Drip Shield Degradation Submodel for Early Failure and Nominal Scenario Classes

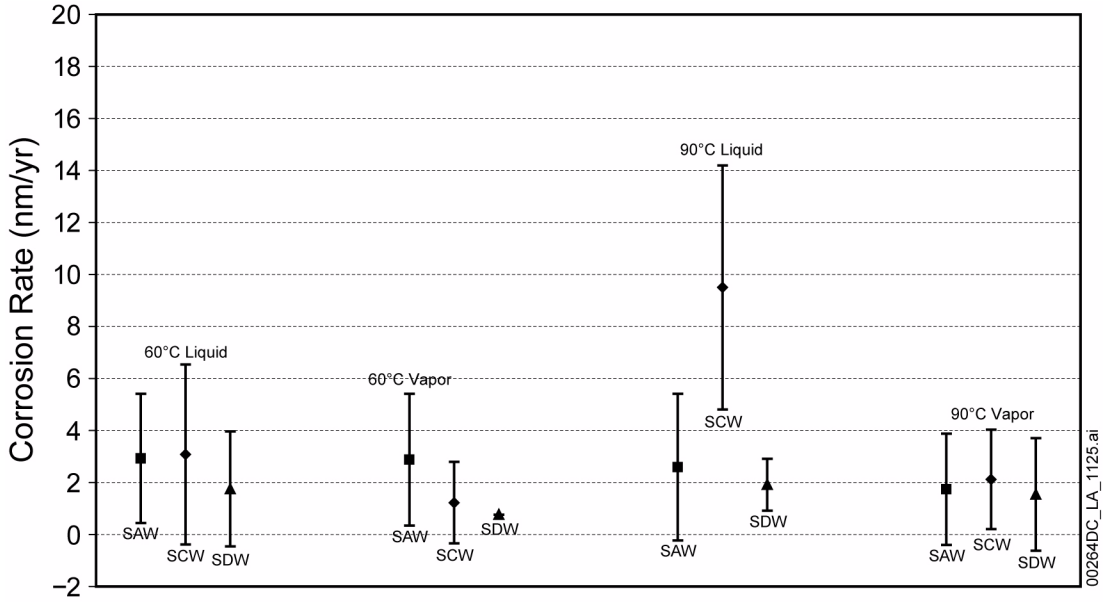

Figure 2.3.6-5. Mean Corrosion Rates for Alloy 22 Weight-Loss Samples in Simulated Acidified Water, Simulated Concentrated Water, and Simulated Dilute Water

NOTE: Error bars are at a 95% confidence level. Rates are for samples exposed for slightly more than 5 years.

Source: SNL 2007c, Figure 6-10.

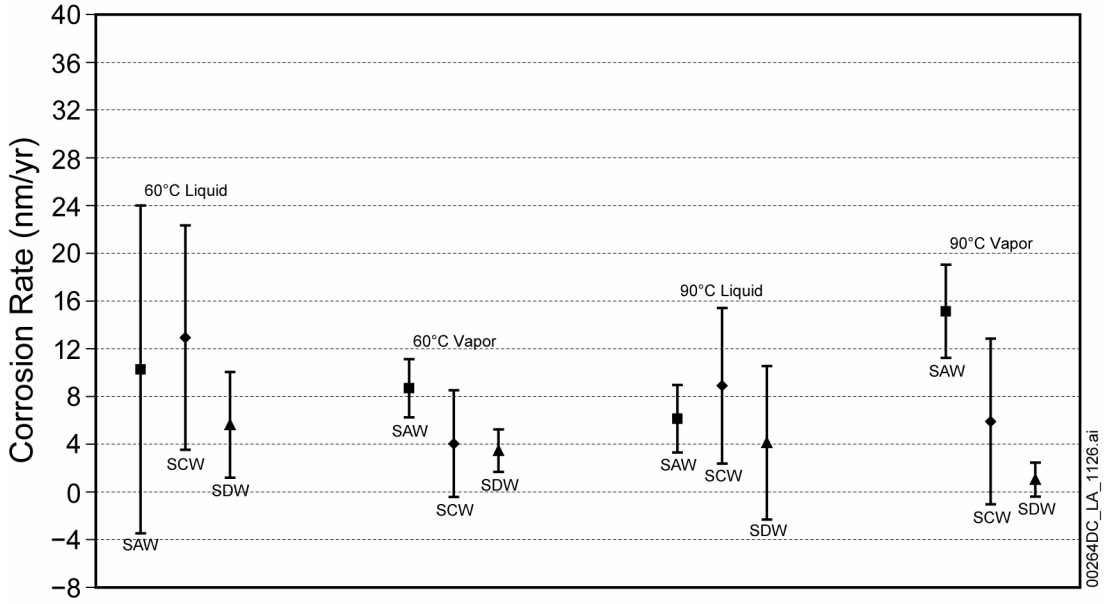

Figure 2.3.6-6. Mean Corrosion Rates for Alloy 22 Crevice Samples in Simulated Acidified Water, Simulated Concentrated Water, and Simulated Dilute Water

NOTE: Error bars are at a 95% confidence level. Rates are for samples exposed for slightly more than 5 years.

Source: SNL 2007c, Figure 6-11.

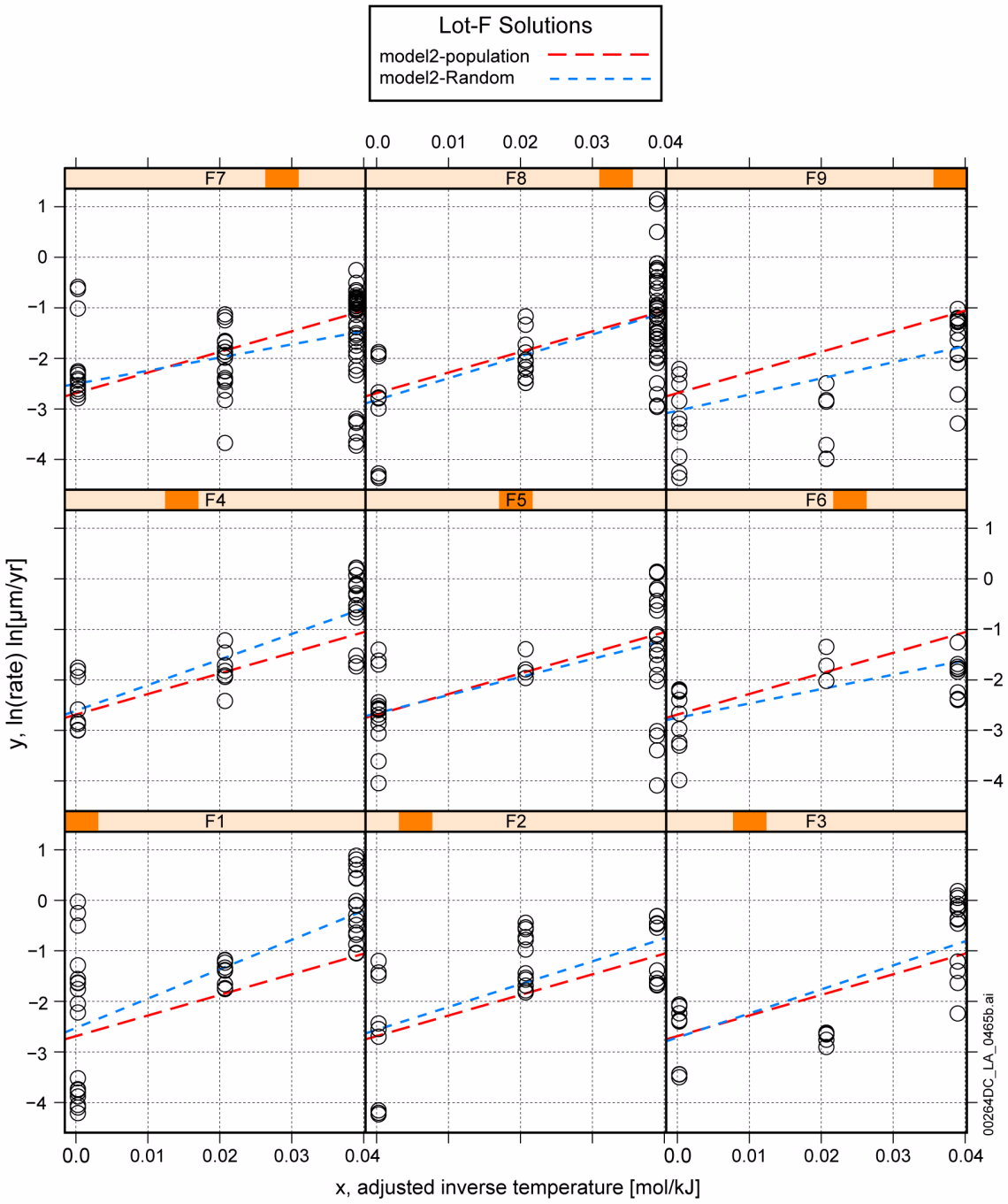

Figure 2.3.6-7. Alloy 22 Corrosion Rates Obtained by Linear Polarization Resistance Measurements in Nine Aqueous Environments Covering a Range of Nitrate and Chloride Ion Concentrations

NOTE: The red-dashed line represents the median C_1 for the population fixed-effects model and is the same for all 9 environments. The blue dashed line represents the linear mixed-effects model adjusted by the random effects in each solution. Solutions F1 through F9 are described in Table 2.3.6-4. The adjusted inverse temperature (x axis variable) for temperatures of 60°C, 80°C, and 100°C, values are approximately 0, 0.020, and 0.039 mol/kJ.

Source: SNL 2007c, Figure 6-25.

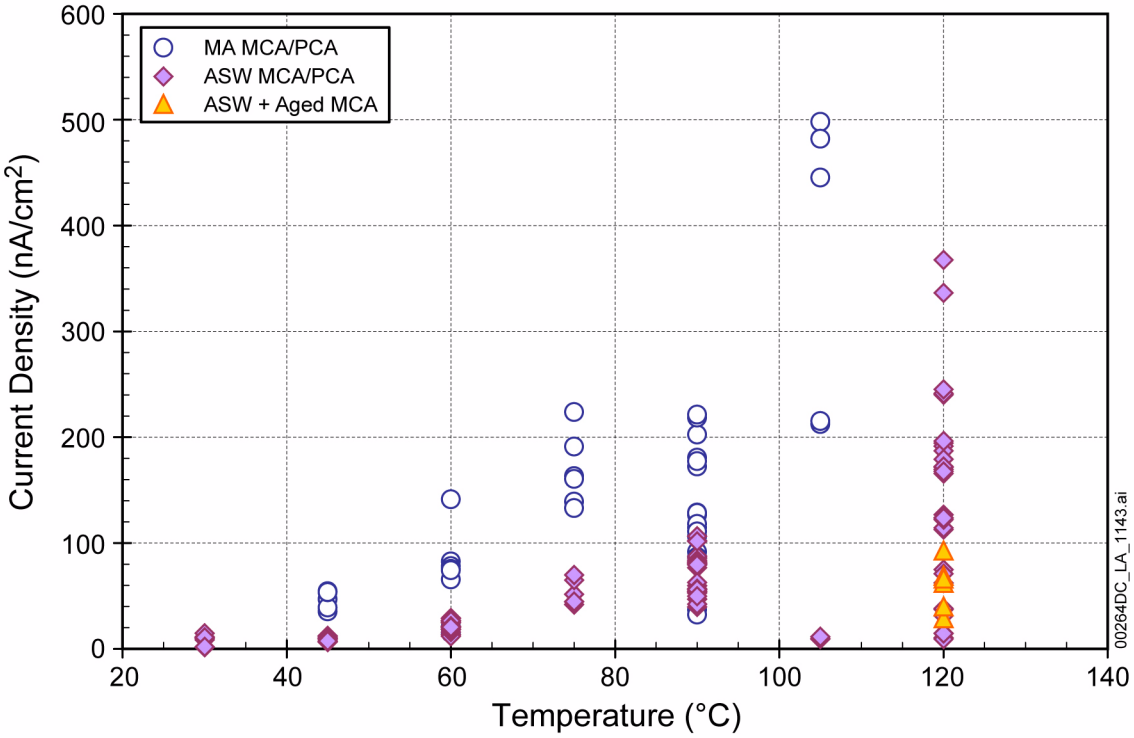

Figure 2.3.6-8. Comparison of Alloy 22 Corrosion Rates from Polarization Resistance Measurements of Mill-Annealed, As-Welded, and As-Welded Plus Aged Alloy 22 Multiple Crevice Assembly and Prism Crevice Assembly Samples in 5 *M* $CaCl_2$ Brines at Varying Temperatures

NOTE: Current density is proportional to corrosion rate.

Source: SNL 2007c, Figure 6-56.

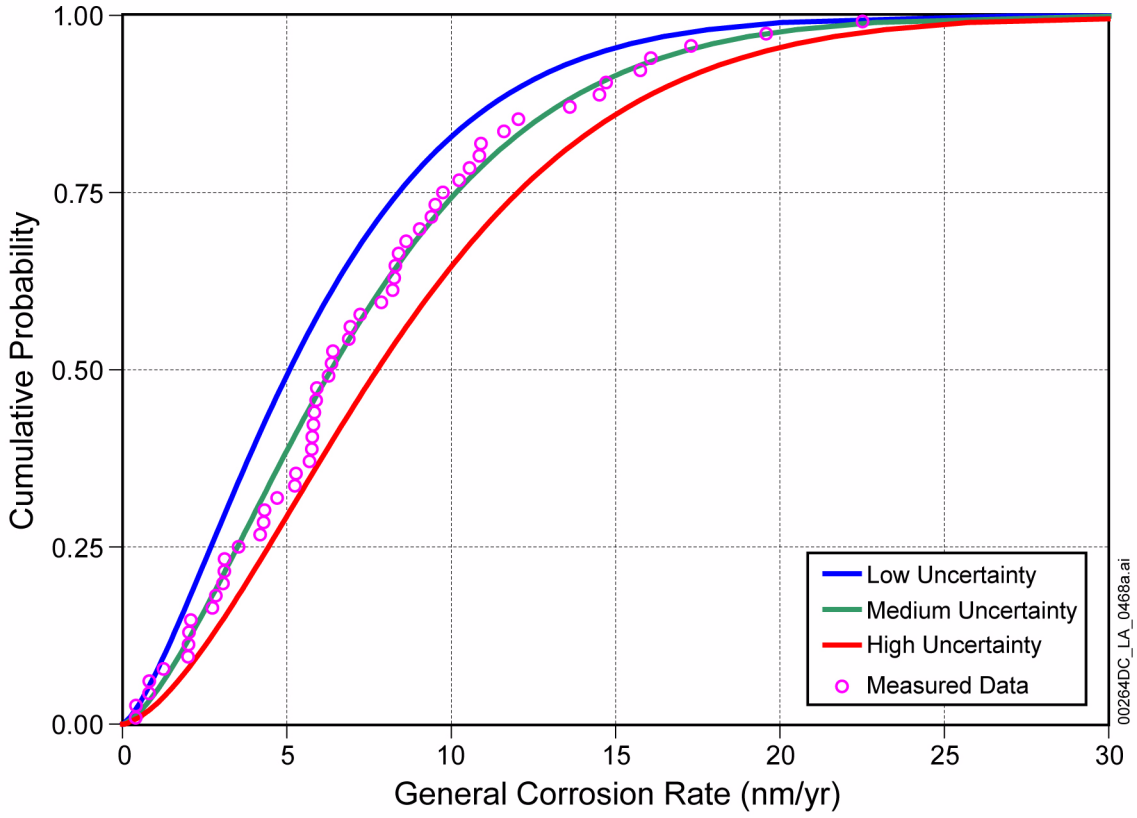

Figure 2.3.6-9. Cumulative Distribution Function of the Alloy 22 General Corrosion Rate at 60°C Including Low, Medium, and High Uncertainty Levels Resulting from Fitting of 5-Year Exposed Creviced Sample Data

NOTE: The medium uncertainty level is sampled 90% of the time, and the high and low uncertainty levels are each sampled 5% of the time.

Source: SNL 2007c, Figure 6-23.

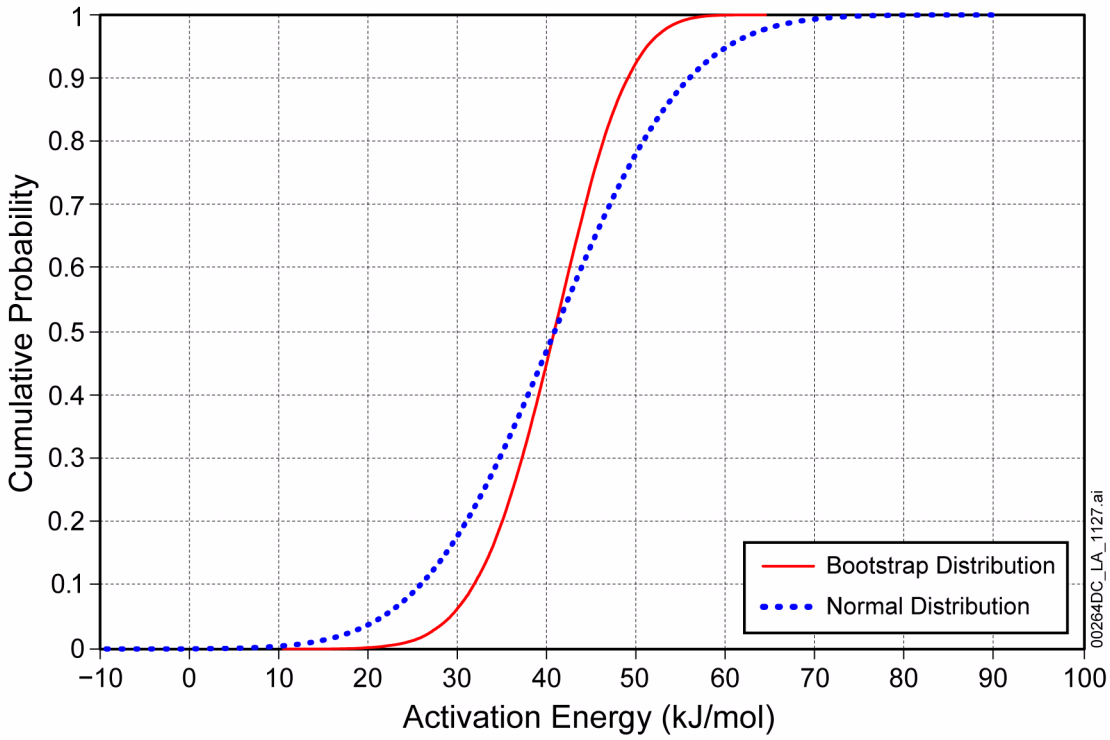

Figure 2.3.6-10. Comparison of Temperature Dependence Obtained by Polarization Resistance (Normal Distribution) and Analysis of Weight-Loss Samples Exposed for 5 Years to SCW 60°C and 90°C (Bootstrap Distribution)

Source: SNL 2007c, Appendix VII.

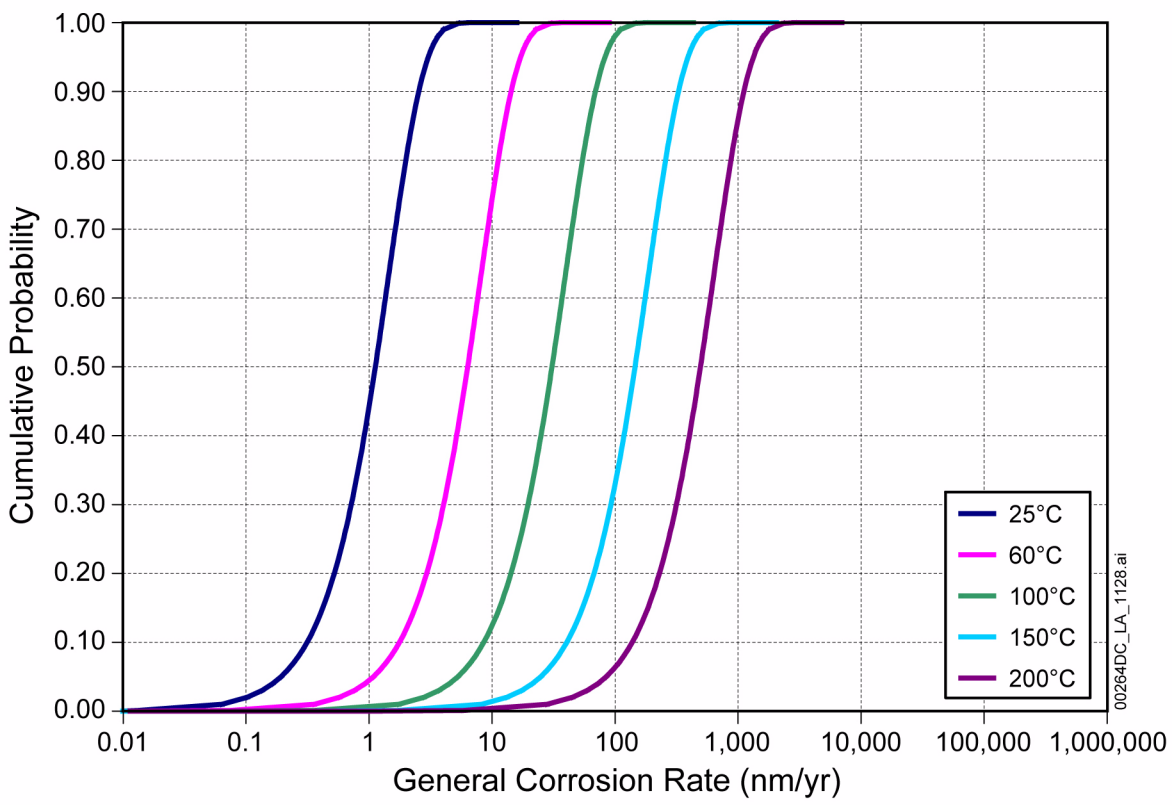

Figure 2.3.6-11. Calculated Model Outputs of the Base-Case Temperature-Dependent General Corrosion Model with the Medium Uncertainty Level for R_o and the Mean Apparent Activation Energy of 40.78 kJ/mol at 25°C, 60°C, 100°C, 150°C, and 200°C

Source: SNL 2007c, Figure 6-26.

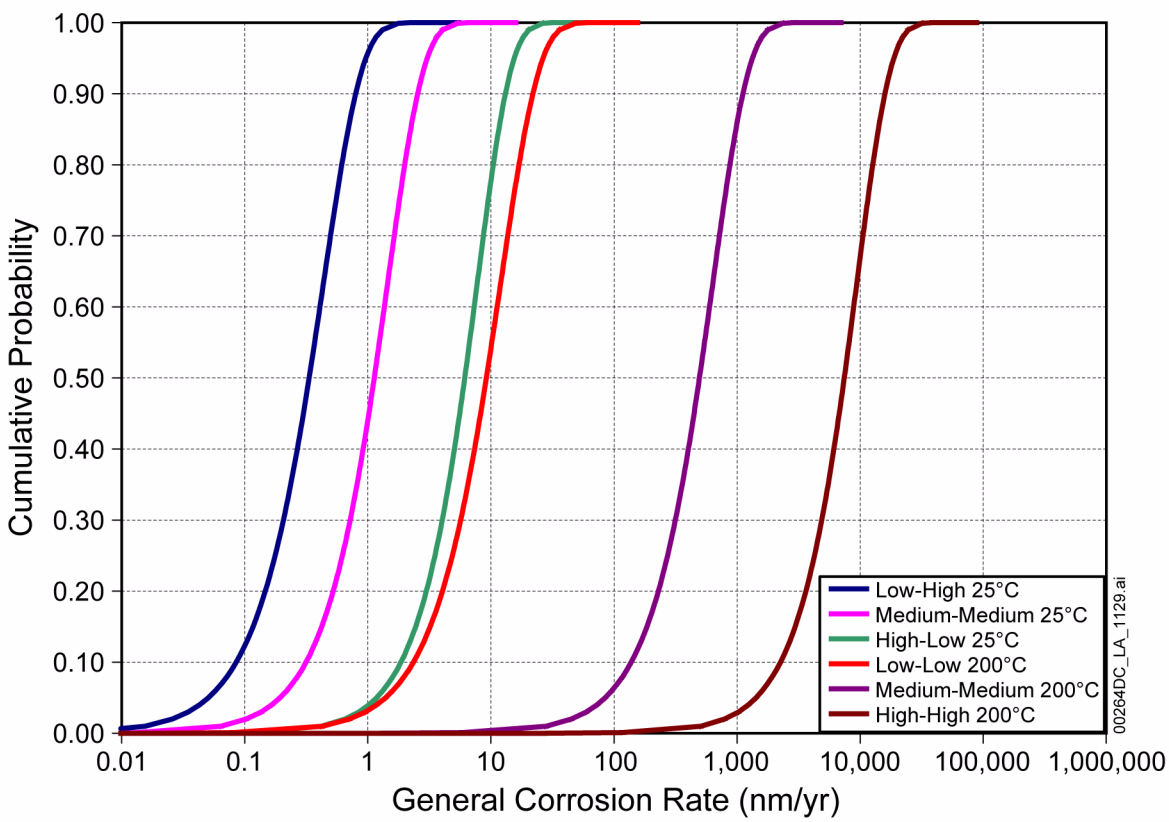

Figure 2.3.6-12. Calculated Model Outputs of the Base-Case Temperature-Dependent General Corrosion Model with Uncertainty Levels and Apparent Activation Energies Designed to Span the Range of Possible Values at 25°C and 200°C

NOTE: Low-high refers to the lower bound activation energy and high uncertainty level, while high-low refers to the upper bound activation energy and low uncertainty level.

Source: SNL 2007c, Figure 6-27.

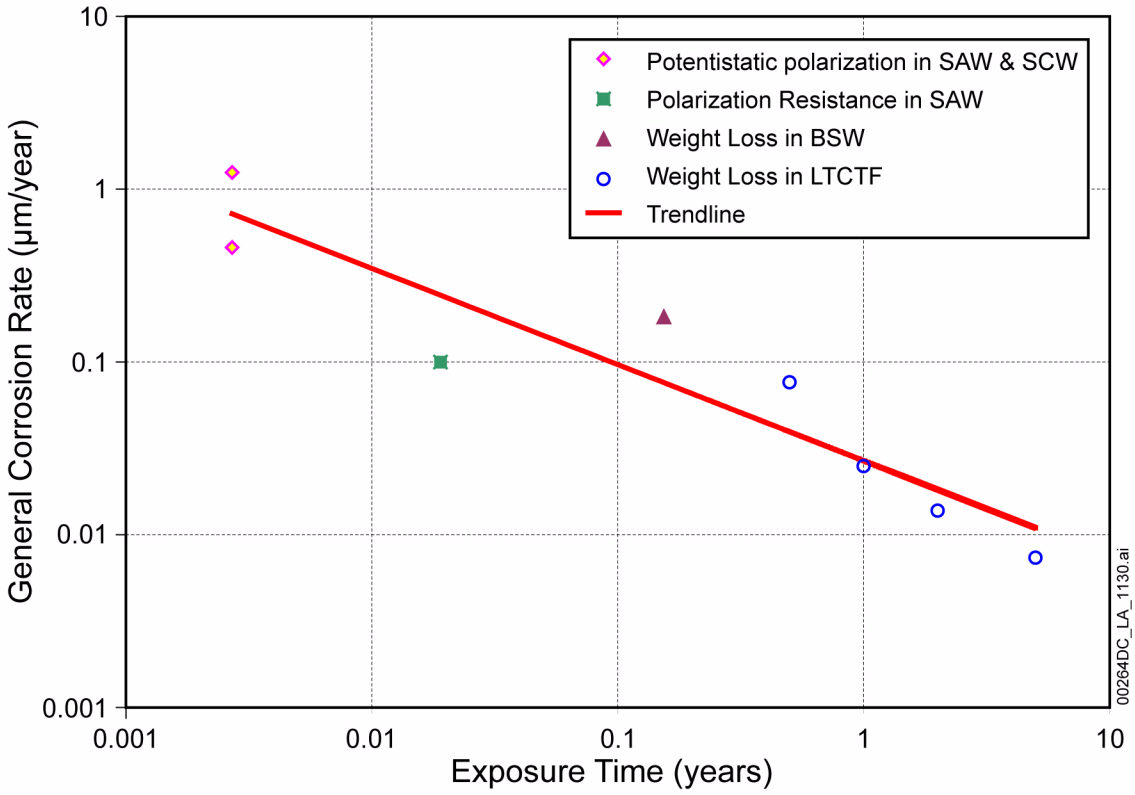

Figure 2.3.6-13. Decrease of Mean General Corrosion Rate of Alloy 22 with Time at 90°C

NOTE: Trend line was obtained by a linear regression fit.
BSW = basic saturated water. LTCTF = Long Term Corrosion Test Facility.

Source: SNL 2007c, Figure 7-1.

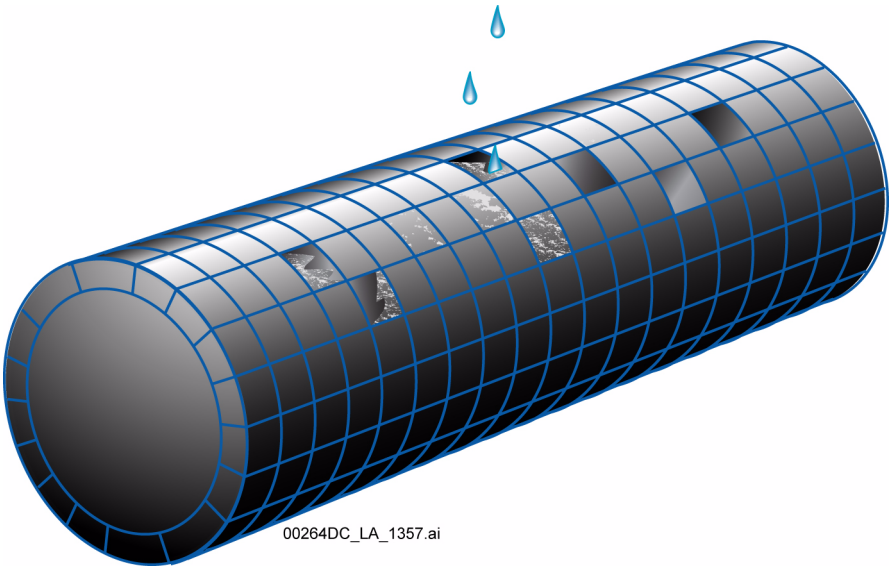

Figure 2.3.6-14. Schematic Representation of Waste Package Patches

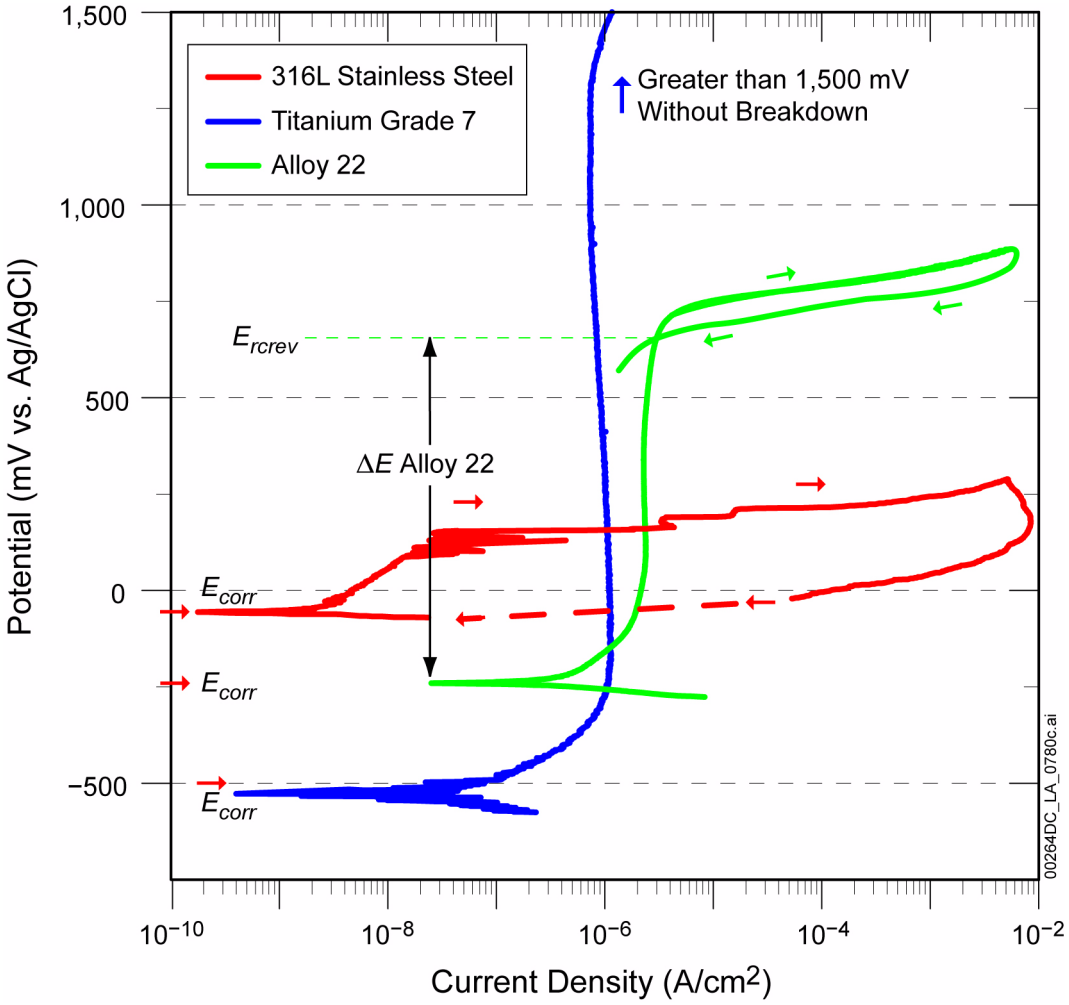

Figure 2.3.6-15. Schematic Cyclic Potentiodynamic Polarization Curves for Stainless Steel Type 316L, Alloy 22, and Titanium in High-Chloride Solutions

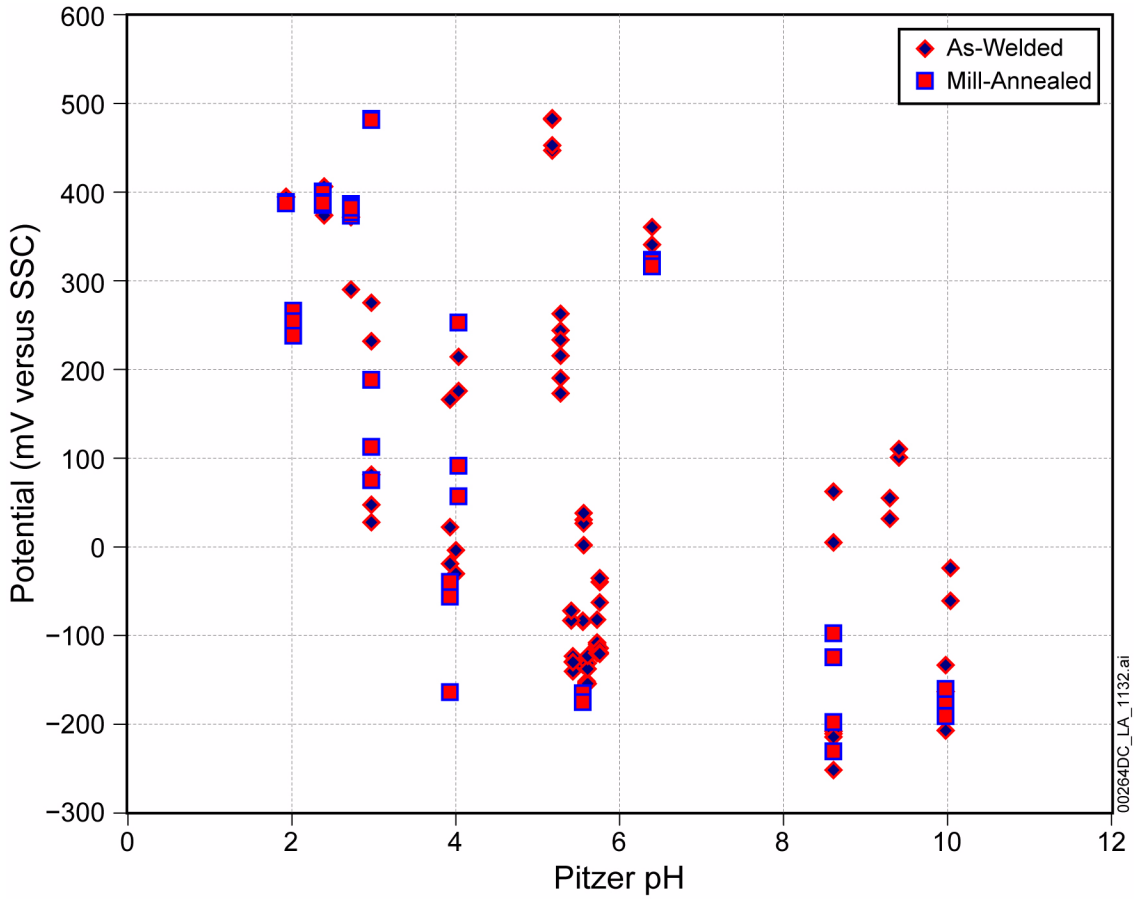

Figure 2.3.6-16. Long-Term Open-Circuit Corrosion Potential versus pH of Alloy 22 Samples with Differing Sample Configurations and Metallurgical Conditions

NOTE: SSC = saturated silver chloride electrode.

Source: SNL 2007c, Figure 6-40.

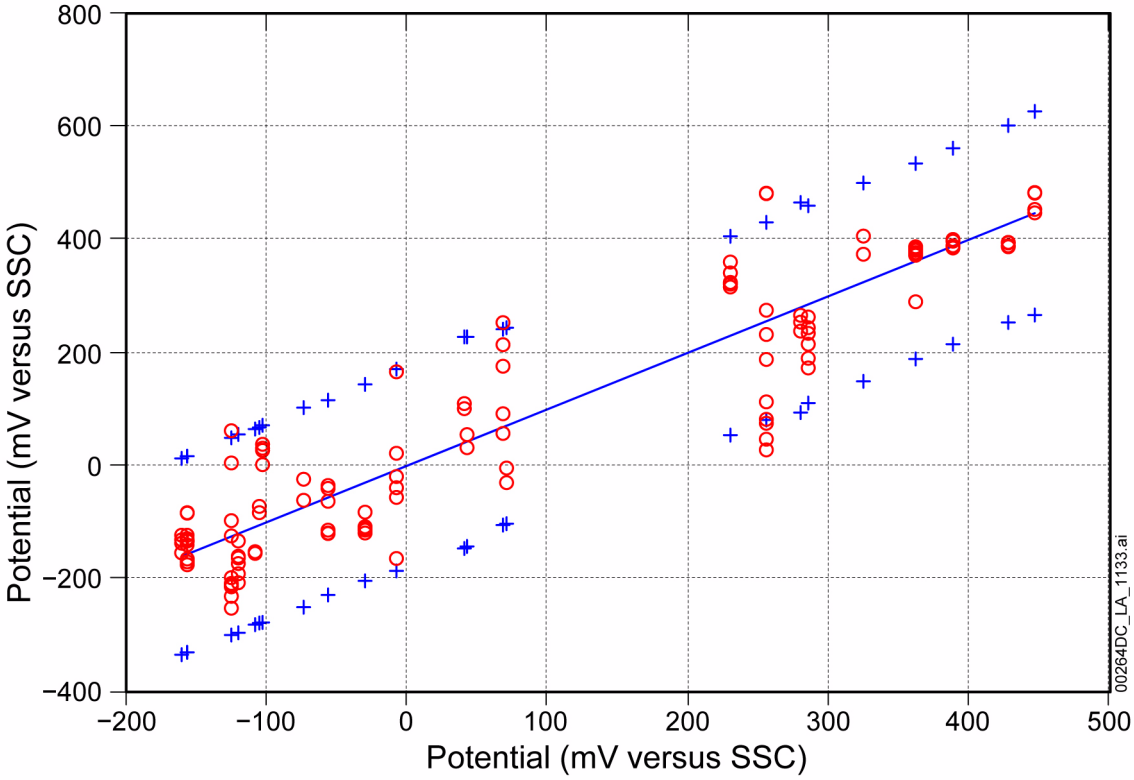

Figure 2.3.6-17. Model Prediction and Experimental Data for Alloy 22 Long-Term Corrosion Potential (E_{corr})of the Waste Package Outer Barrier

NOTE: The horizontal axis is the long-term corrosion potential predicted by the model while the vertical axis is either the measured long-term corrosion potential for the measured data points (circles) or the ±2 standard deviation prediction intervals represented by plus signs, or the mean model prediction represented by the solid line. SSC = saturated silver chloride electrode.

Source: SNL 2007c, Figure 6-41.

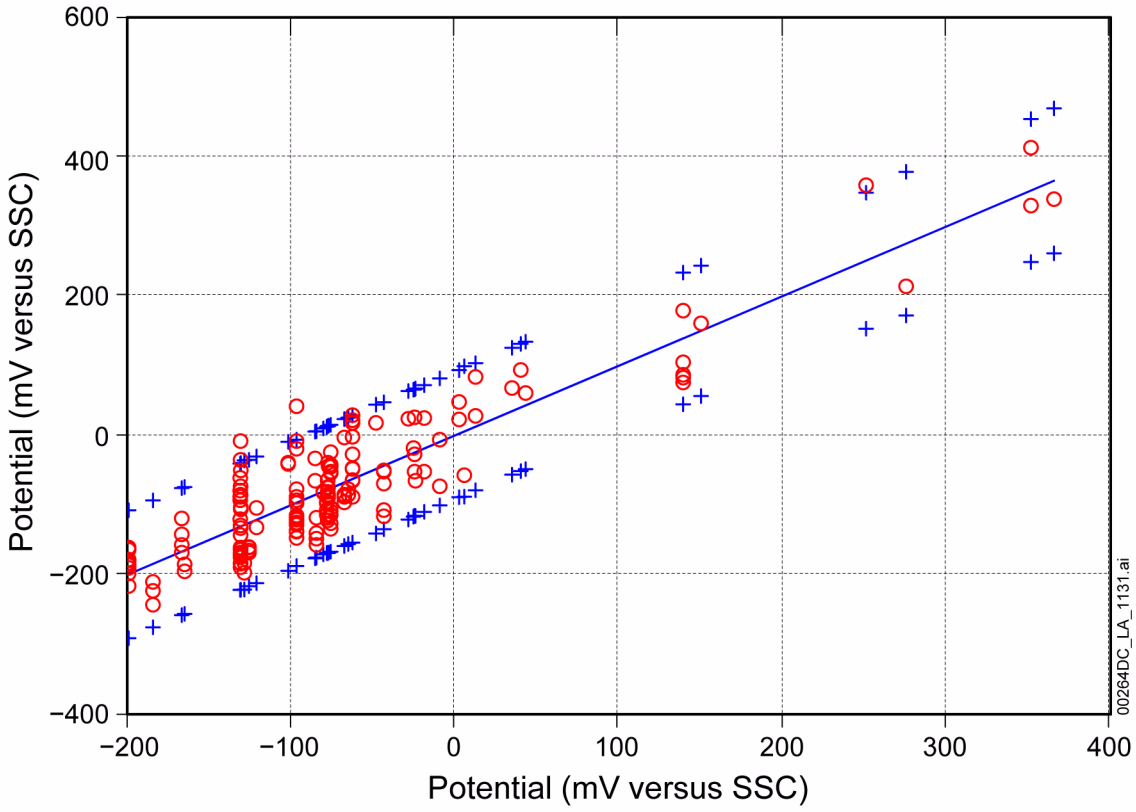

Figure 2.3.6-18. Model Predictions and Experimental Data for the Alloy 22 Crevice Repassivation Potential of the Waste Package Outer Barrier

NOTE: The horizontal axis is the crevice repassivation potential predicted by the model while the vertical axis is either the measured repassivation potential for the measured data points represented by circles, or the ±2 standard deviation prediction intervals represented by plus signs, or the mean model prediction represented by the solid line.
SSC = saturated silver chloride electrode.

Source: SNL 2007c, Figure 6-34.

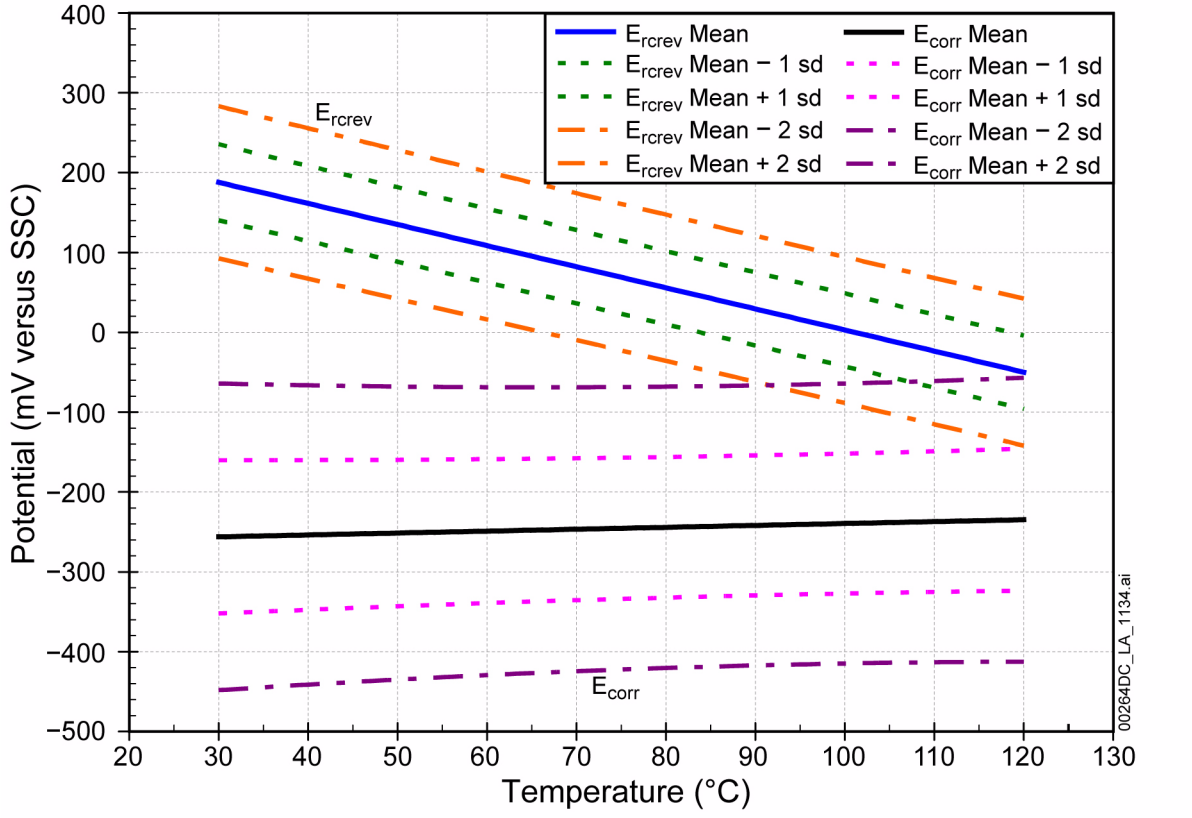

Figure 2.3.6-19. Alloy 22 Localized Corrosion Initiation Model Results as a Function of Temperature with a pH of 7

NOTE: Figure shows E_{rcrev} and E_{corr} versus temperature for 6 *m* chloride, with a pH of 7, and 1.8 *m* nitrate (with a NO_3/Cl ratio of 0.30).
SD = standard deviation; SSC = saturated silver chloride electrode.

Source: SNL 2007c, Figure 6-42.

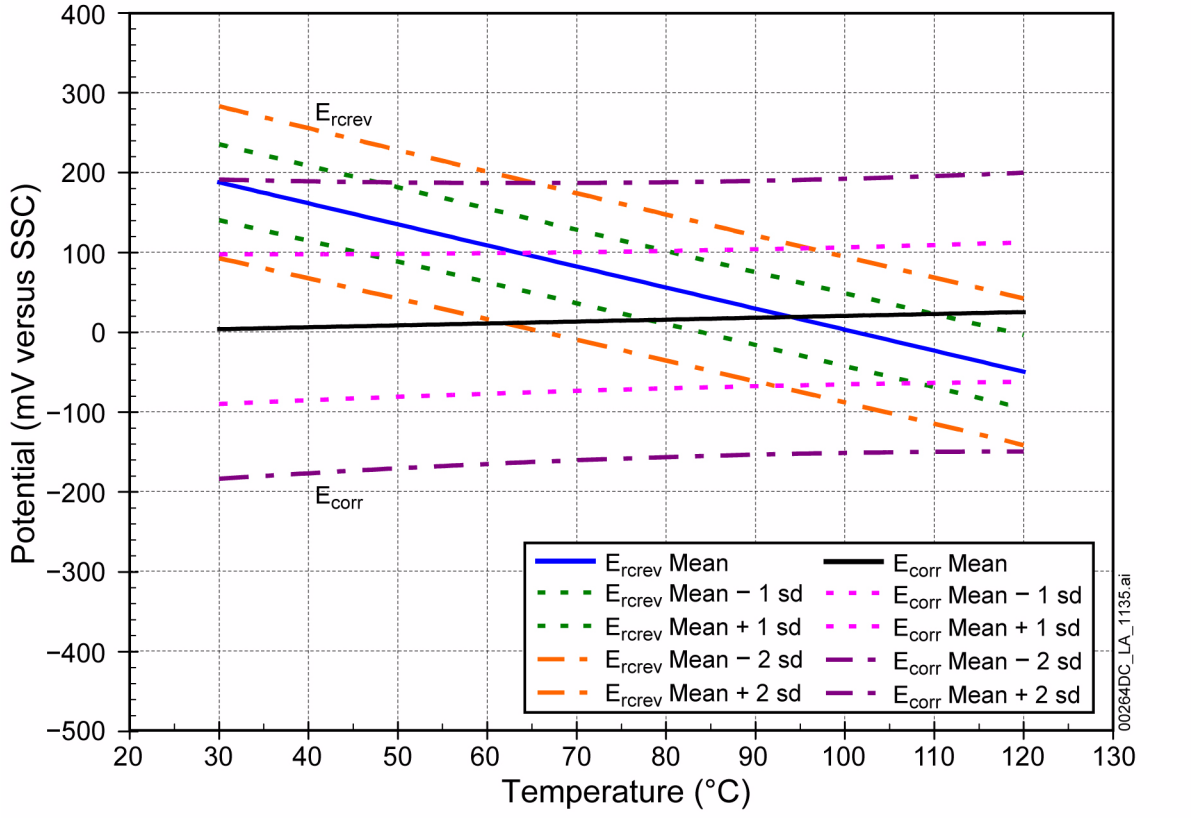

Figure 2.3.6-20. Alloy 22 Localized Corrosion Initiation Model Results as a Function of Temperature with a pH of 5

NOTE: Figure shows E_{rcrev} and E_{corr} versus temperature for 6 *m* chloride, with pH of 5, and 1.8 *m* nitrate (with a NO_3/Cl ratio of 0.30).
SD = standard deviation; SSC = saturated silver chloride electrode.

Source: SNL 2007c, Figure 6-43.

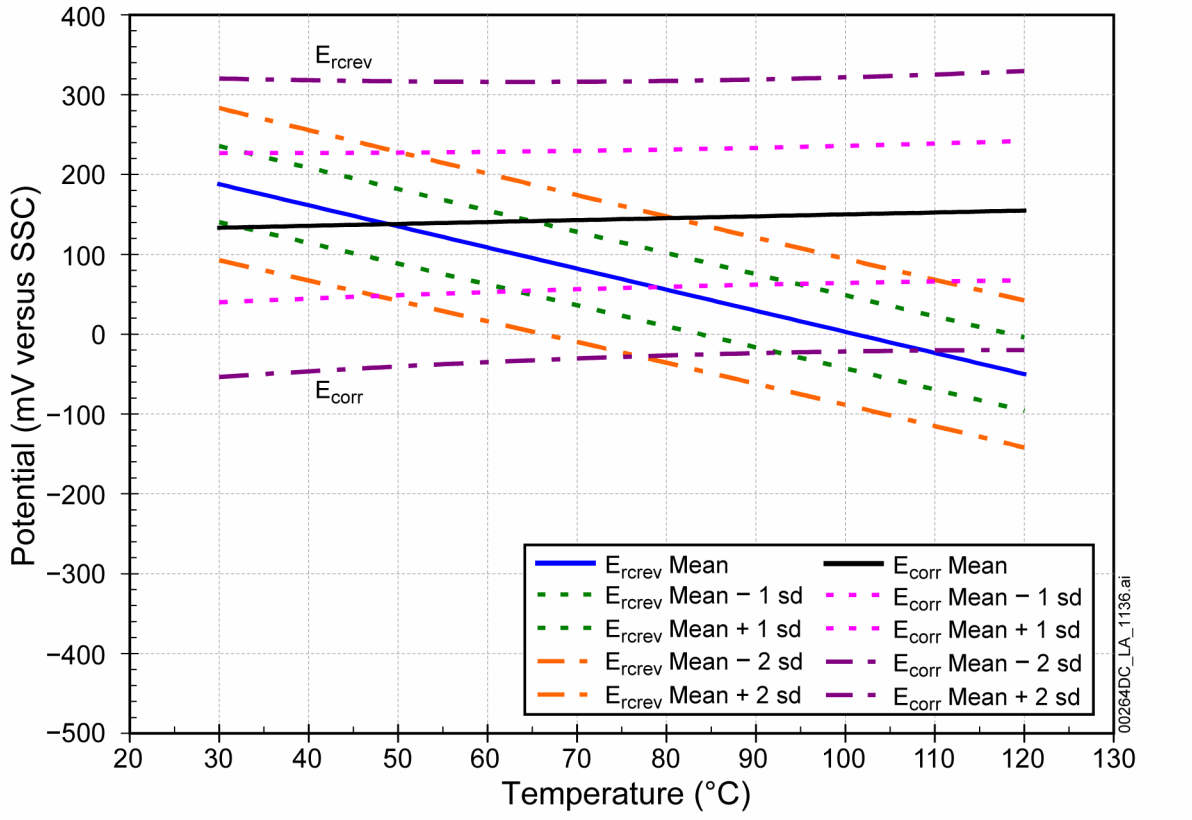

Figure 2.3.6-21. Alloy 22 Localized Corrosion Initiation Model Results as a Function of Temperature with a pH of 4

NOTE: Figure shows E_{rcrev} and E_{corr} versus temperature for 6 *m* chloride, with pH of 4, and 1.8 *m* nitrate (with a NO_3/Cl ratio of 0.30).
SD = standard deviation; SSC = saturated silver chloride electrode.

Source: SNL 2007c, Figure 6-44.

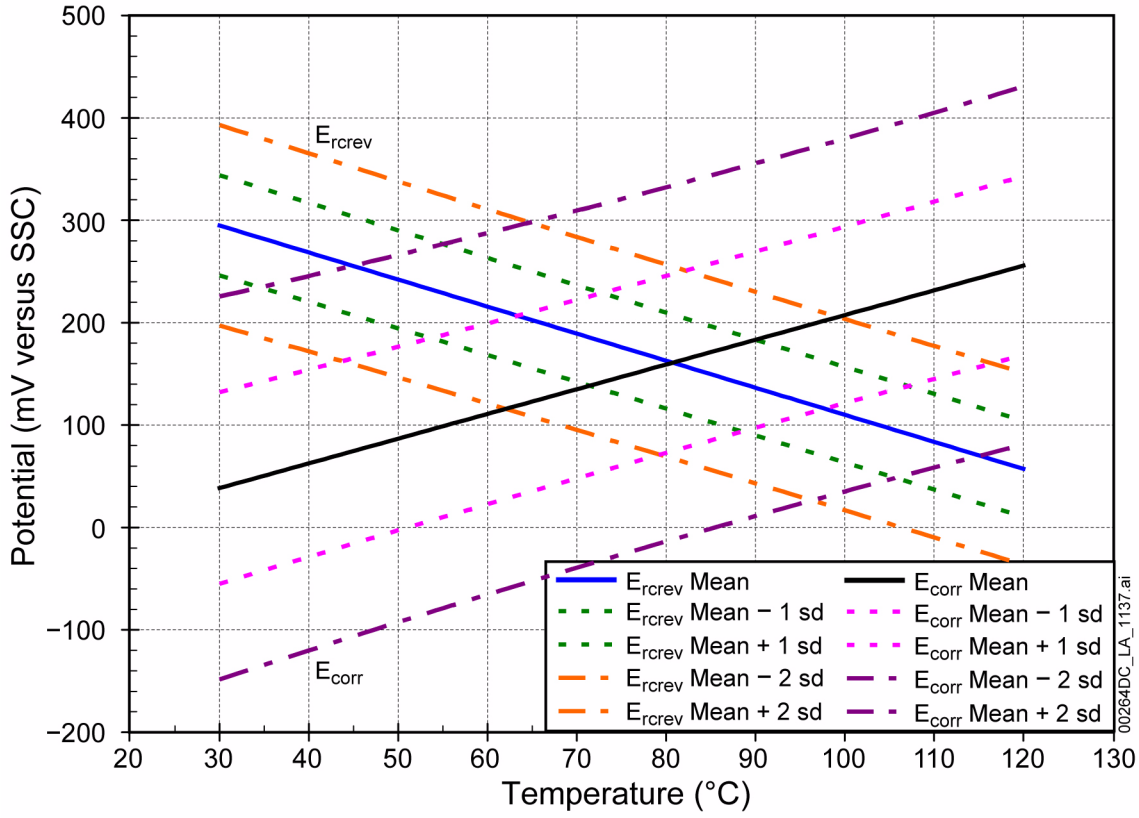

Figure 2.3.6-22. Alloy 22 Localized Corrosion Initiation Model Results as a Function of Temperature for 3 *m* Nitrate

NOTE: Figure shows E_{rcrev} and E_{corr} versus temperature for 6 *m* chloride, with pH of 4, and 3 *m* nitrate (with a NO_3/Cl ratio of 0.50).
SD = standard deviation; SSC = saturated silver chloride electrode.

Source: SNL 2007c, Figure 6-45.

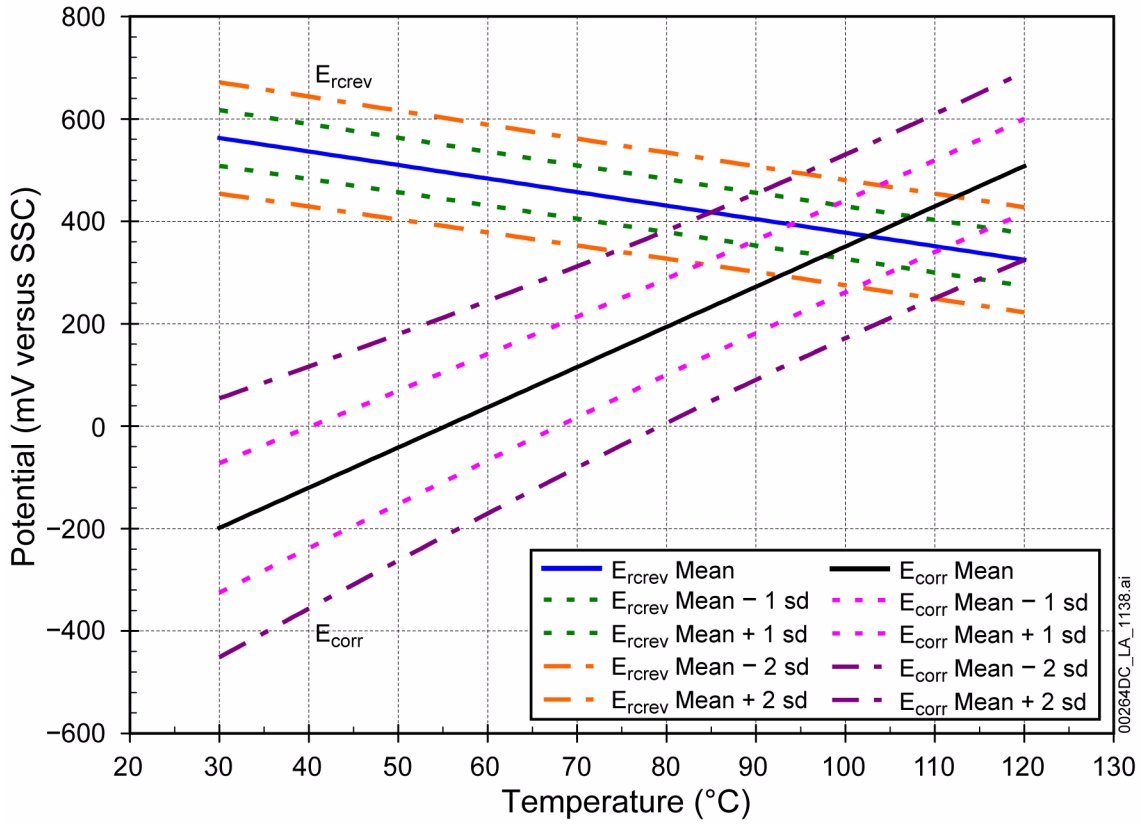

Figure 2.3.6-23. Alloy 22 Localized Corrosion Initiation Model Results as a Function of Temperature for 6 *m* Nitrate

NOTE: Figure shows E_{rcrev} and E_{corr} versus temperature for 6 *m* chloride, with a pH of 4, and 6 *m* nitrate (with a NO_3/Cl ratio of 1.00).
SD = standard deviation; SSC = saturated silver chloride electrode.

Source: SNL 2007c, Figure 6-46.

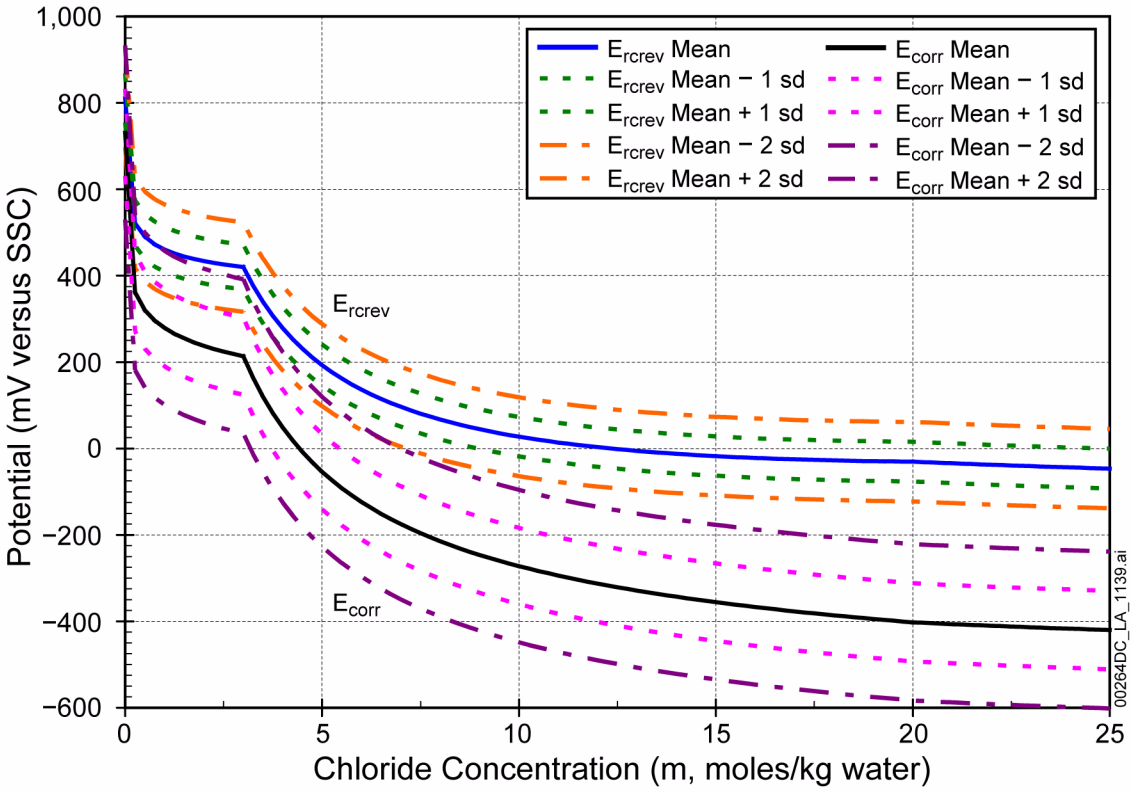

Figure 2.3.6-24. Alloy 22 Localized Corrosion Initiation Model Results as a Function of Chloride Concentration for 90°C, pH 7, and 3 *m* Nitrate

NOTE: Figure shows E_{rcrev} and E_{corr} versus chloride ion concentration for 3 *m* Nitrate, with a pH of 7, at 90°C. SD = standard deviation; SSC = saturated silver chloride electrode.

Source: SNL 2007c, Figure 6-47.

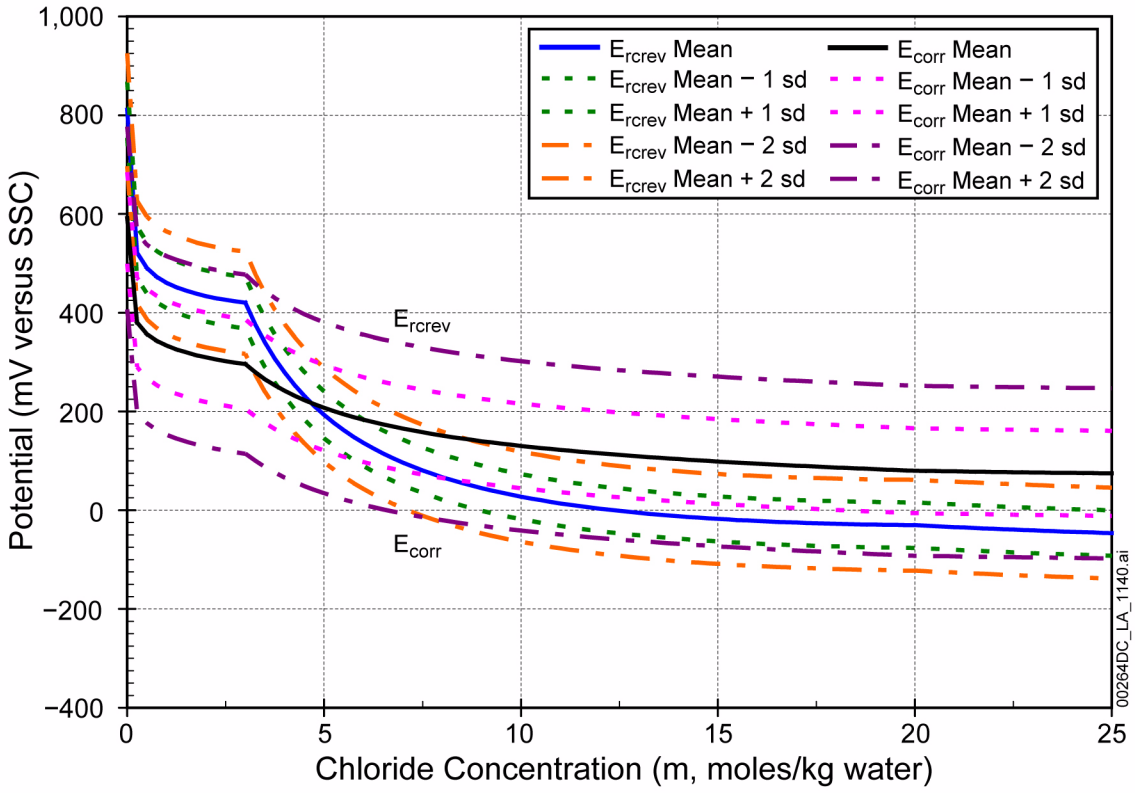

Figure 2.3.6-25. Alloy 22 Localized Corrosion Initiation Model Results as a Function of Chloride Concentration for 90°C, pH 4, and 3 *m* Nitrate

NOTE: Figure shows E_{rcrev} and E_{corr} versus chloride ion concentration for 3 *m* nitrate, with a pH of 4, at 90°C. SD = standard deviation; SSC = saturated silver chloride electrode.

Source: SNL 2007c, Figure 6-48.

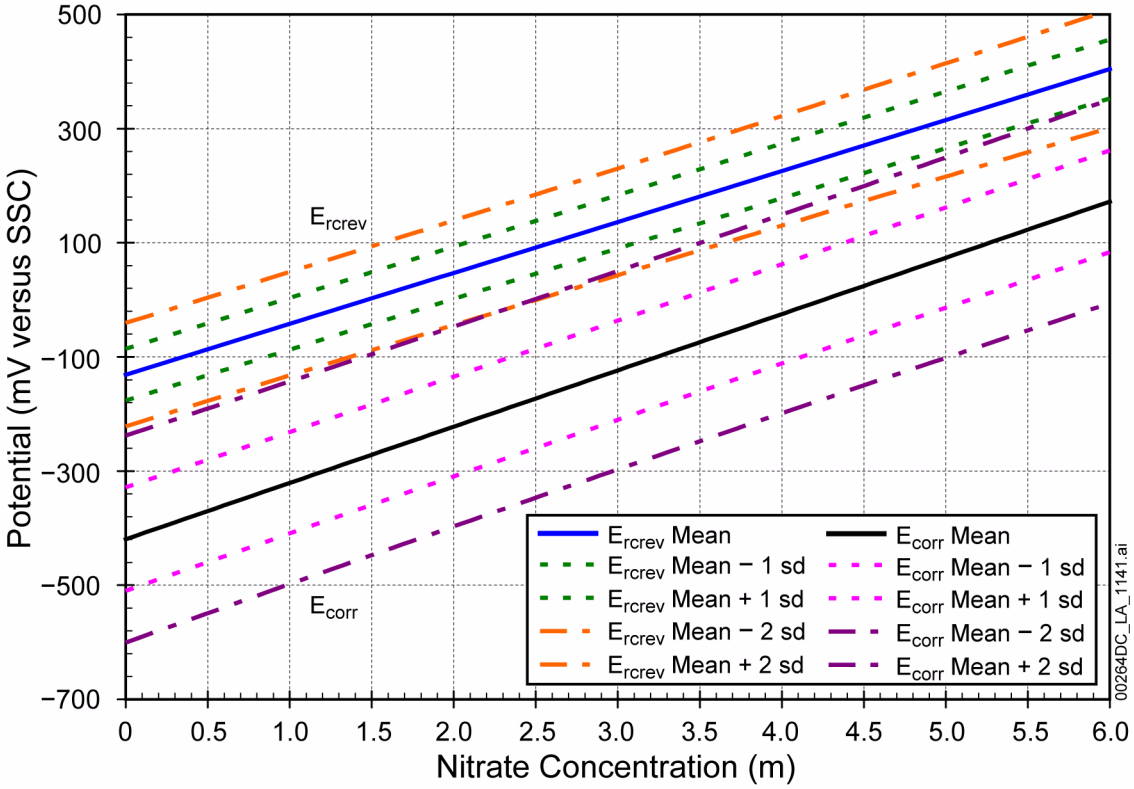

Figure 2.3.6-26. Alloy 22 Localized Corrosion Initiation Model Results as a Function of Nitrate Concentration for a pH of 7

NOTE: Figure shows E_{rcrev} and E_{corr} versus nitrate concentration for 6 *m* chloride, with a pH of 7 and a temperature of 90°C.
SD = standard deviation; SSC = saturated silver chloride electrode.

Source: SNL 2007c, Figure 6-51.

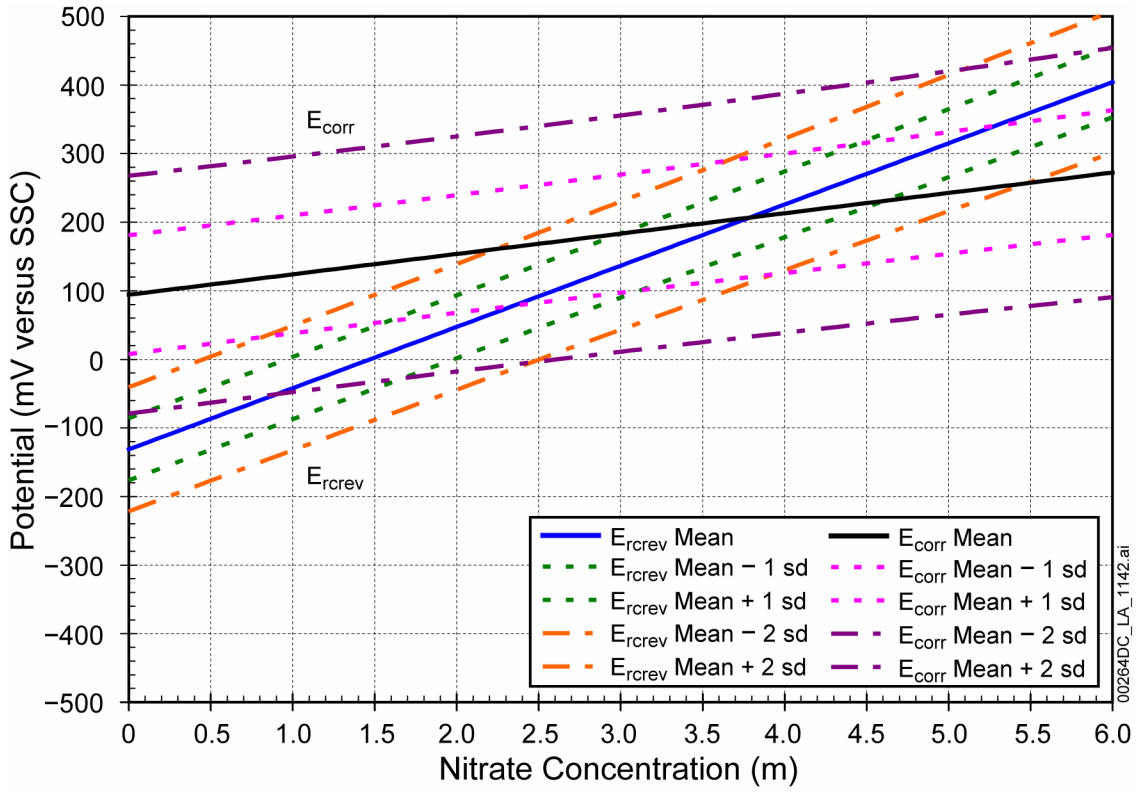

Figure 2.3.6-27. Alloy 22 Localized Corrosion Initiation Model Results as a Function of Nitrate Concentration for a pH of 4

NOTE: Figure shows E_{rcrev} and E_{corr} versus nitrate concentration for 6 *m* chloride, with a pH of 4 and a temperature of 90°C.
SD = standard deviation; SSC = saturated silver chloride electrode.

Source: SNL 2007c, Figure 6-52.

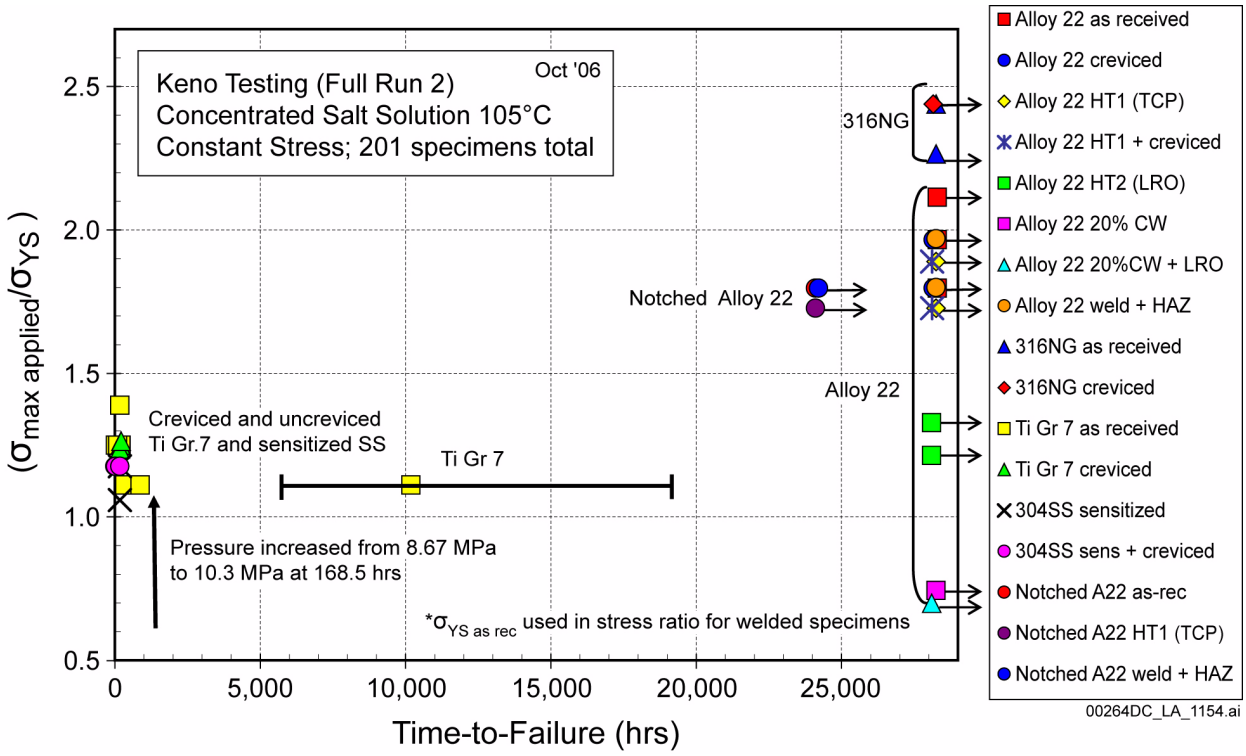

Figure 2.3.6-28. Time to Failure (or Time on Test) versus Applied Stress Ratio in 15% Basic Saturated Water Solution at 105°C

NOTE: A22 = Alloy 22; CW = cold worked; HT = heat treated; HAZ = heat affected zone; LRO = long-range ordering; SS = stainless steel; TCP = tetrahedrally close-packed.

Source: SNL 2007a, Figure 4-1.

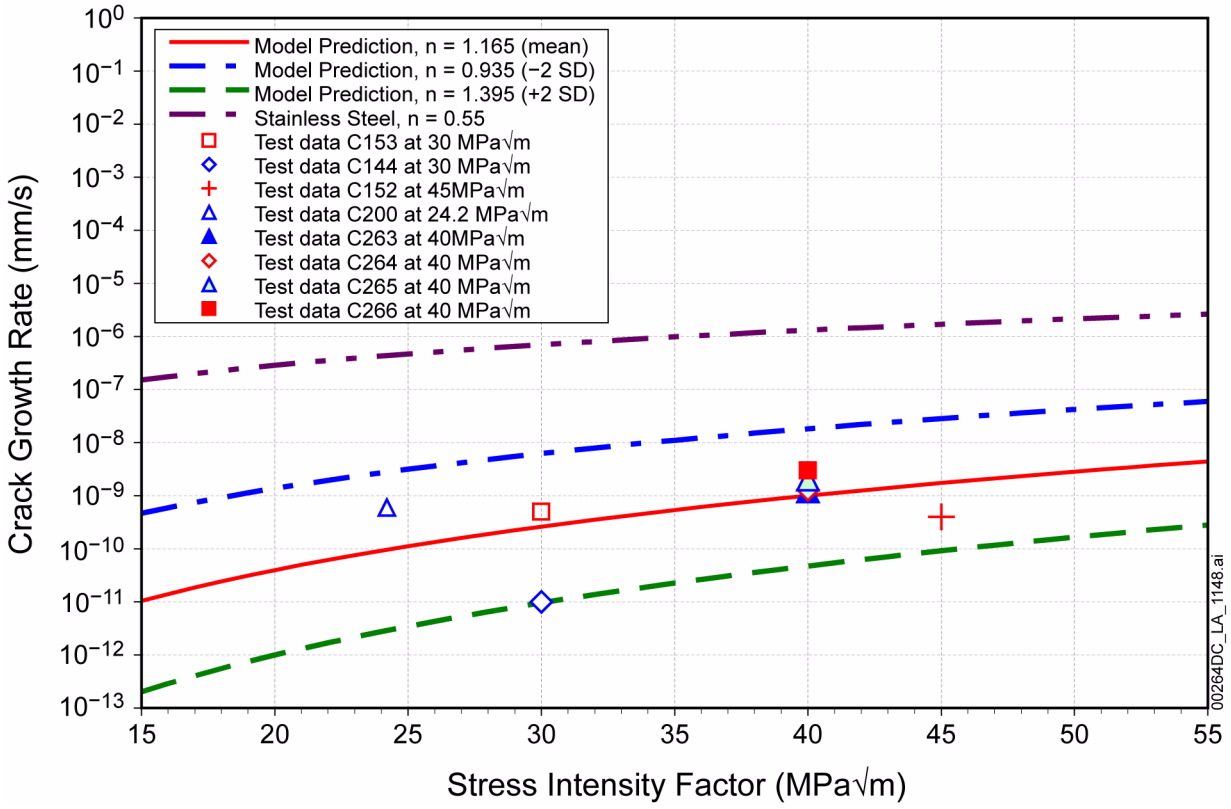

Figure 2.3.6-29. Predicted Crack Growth Rate for the Stress Corrosion Cracking of Alloy 22 in Basic Saturated Water at 110°C as a Function of Stress Intensity Factor for Bounding Values of the Repassivation Parameter

NOTE: *n* is a repassivation parameter.
SD = standard deviation.

Source: SNL 2007a, Figure 6-9.

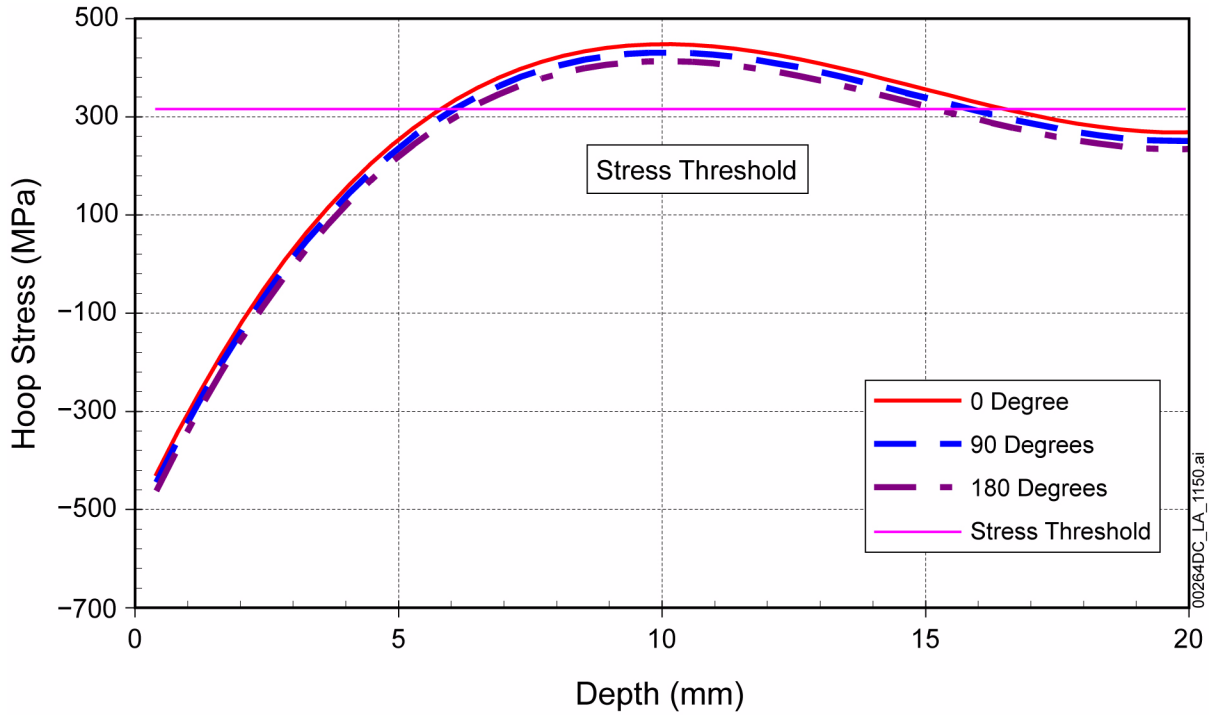

Figure 2.3.6-30. Hoop Stress versus Depth for Plasticity-Burnished Waste Package Outer Closure Lid with Variability as Function of Angle

Source: SNL 2007a, Figure 6-52.

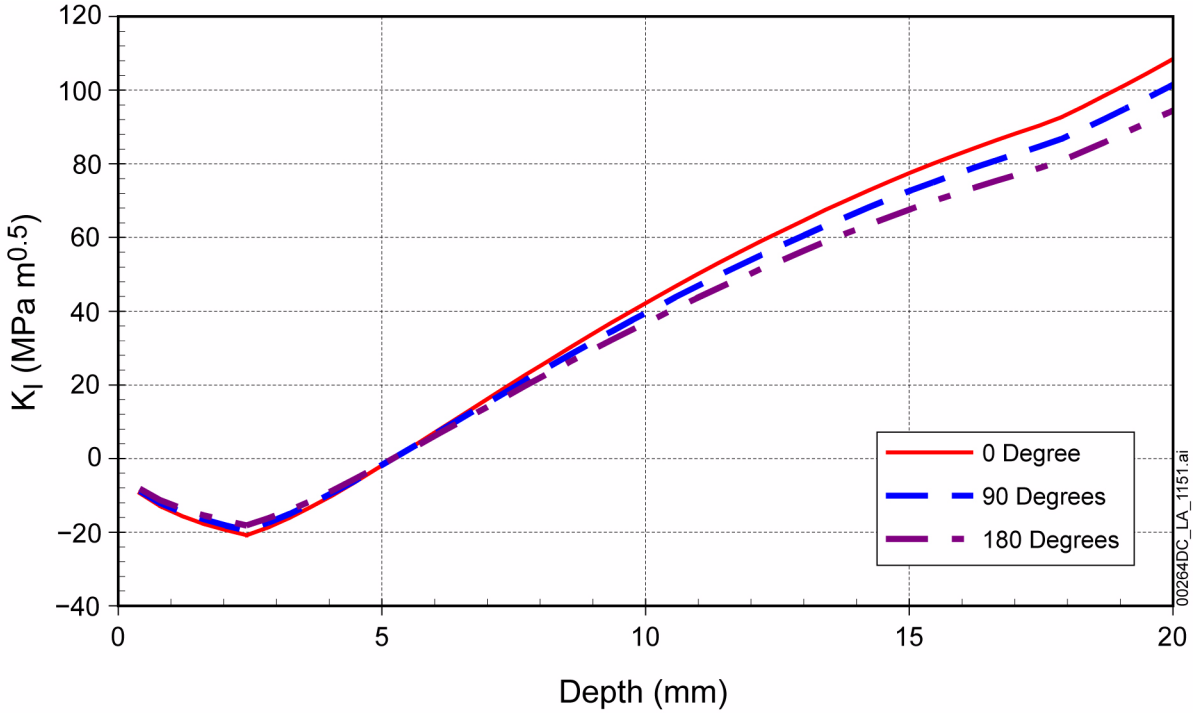

Figure 2.3.6-31. Stress Intensity Factor versus Depth for Plasticity-Burnished Waste Package Outer Closure Lid with Variability as Function of Angle

Source: SNL 2007a, Figure 6-54.

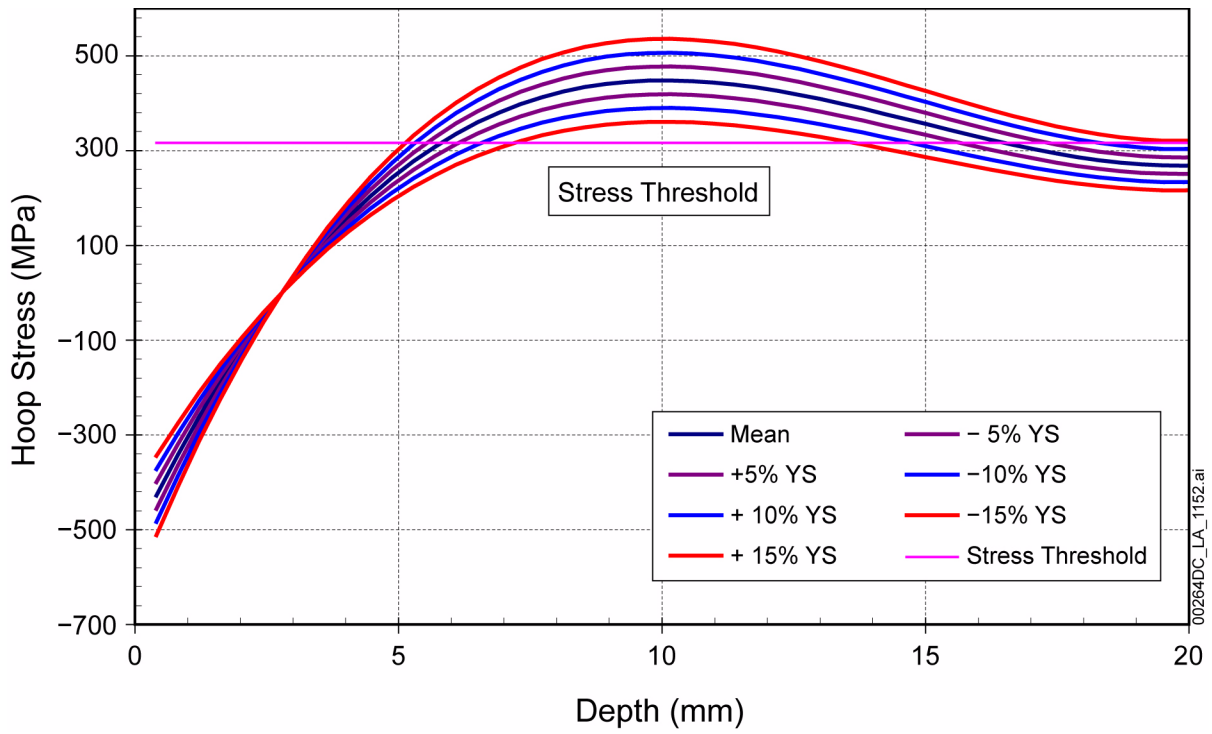

Figure 2.3.6-32. Hoop Stress ($\theta = 0$) versus Depth for Plasticity-Burnished Waste Package Outer Closure Lid with Uncertainty as Function of Yield Strength

NOTE: YS = yield strength.

Source: SNL 2007a, Figure 6-56.

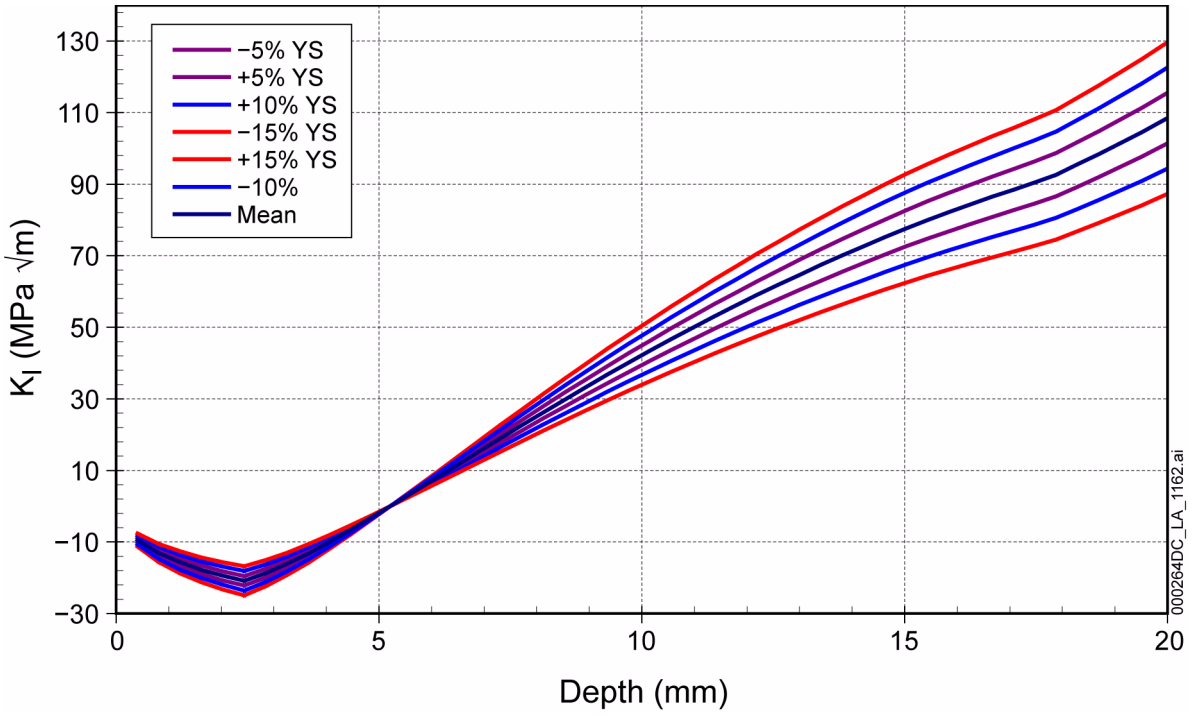

Figure 2.3.6-33. Stress Intensity Factor (θ = 0) versus Depth for Plasticity Burnished Waste Package Outer Closure Lid with Uncertainty as Function of Yield Strength

NOTE: YS = yield strength.

Source: SNL 2007a, Figure 6-58.

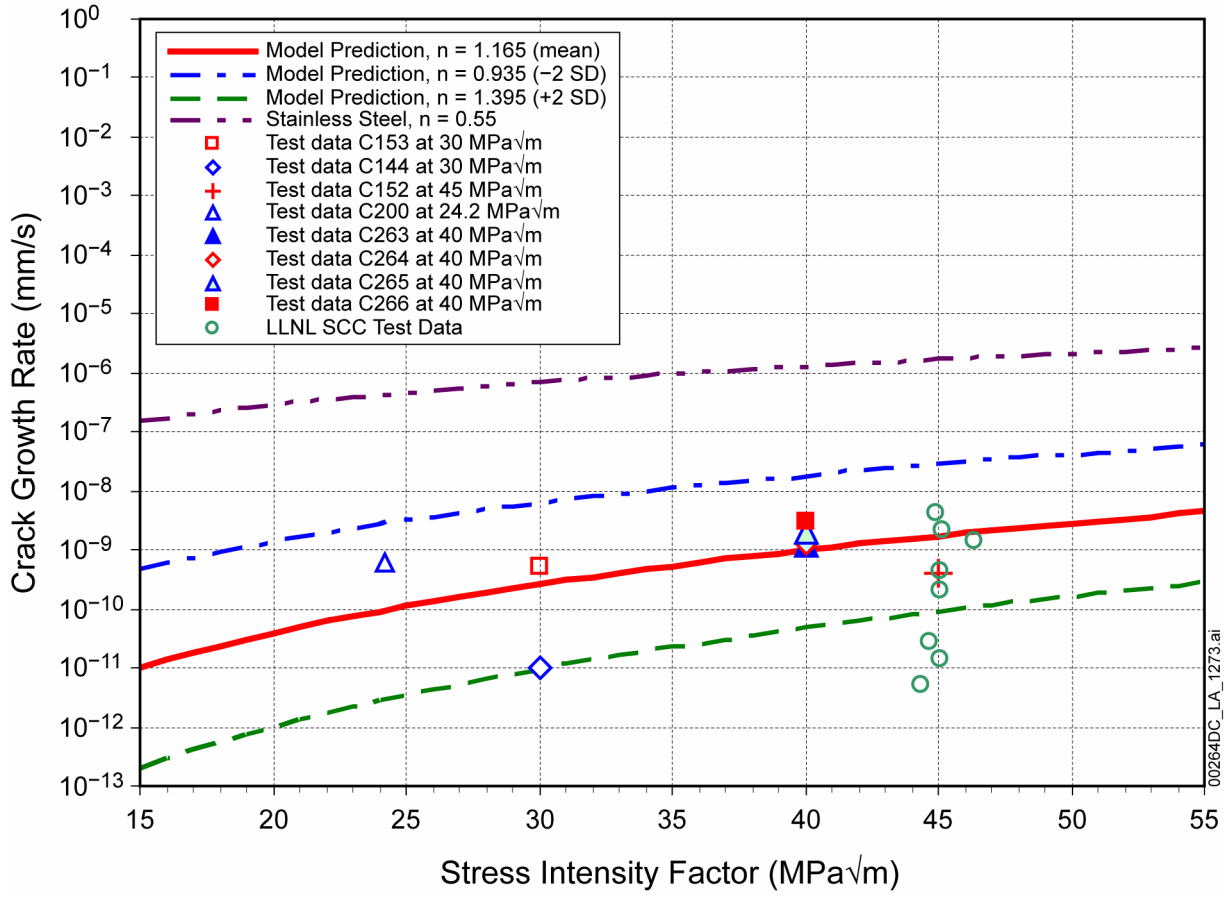

Figure 2.3.6-34. Modeled Crack Growth Rate for the Stress Corrosion Cracking of Alloy 22 in Basic Saturated Water at 110°C as a Function of Stress Intensity Factor Compared to Data not Used to Develop the Model

NOTE: LLNL = Lawrence Livermore National Laboratory; SD = standard deviation.

Source: SNL 2007a, Figure 7-2.

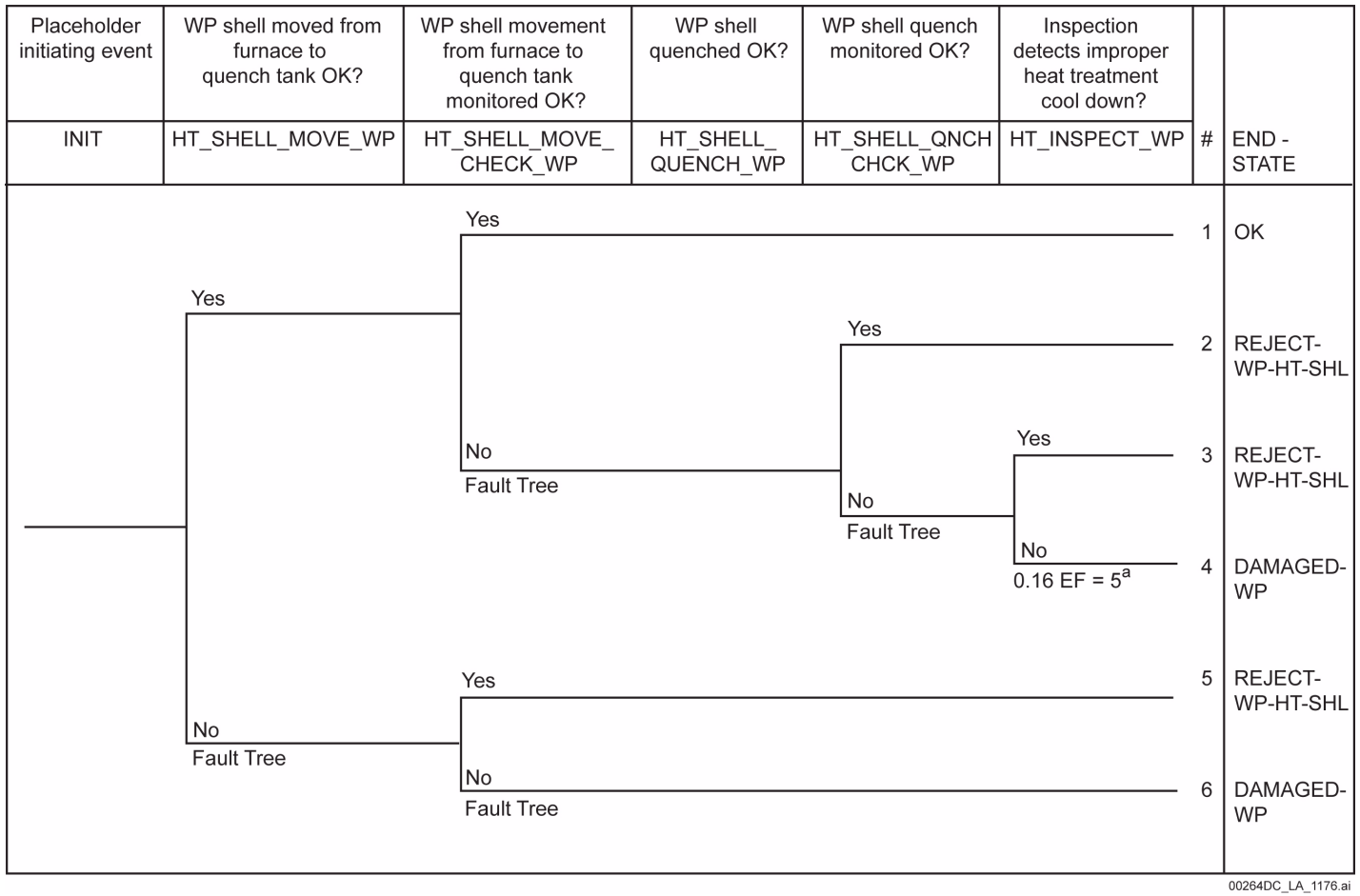

Figure 2.3.6-35. Example of Event Tree Used for Analyzing Early Failure

NOTE: [a]Table 2.3.6-22, Item 6.
In this example, only condition 6 would result in early failure. Item 1 is acceptable, and items 2 through 5 contain detected errors which would be repaired or rejected.
EF = error factor; WP = waste package.

Source: SNL 2007d, Figure 6-10.

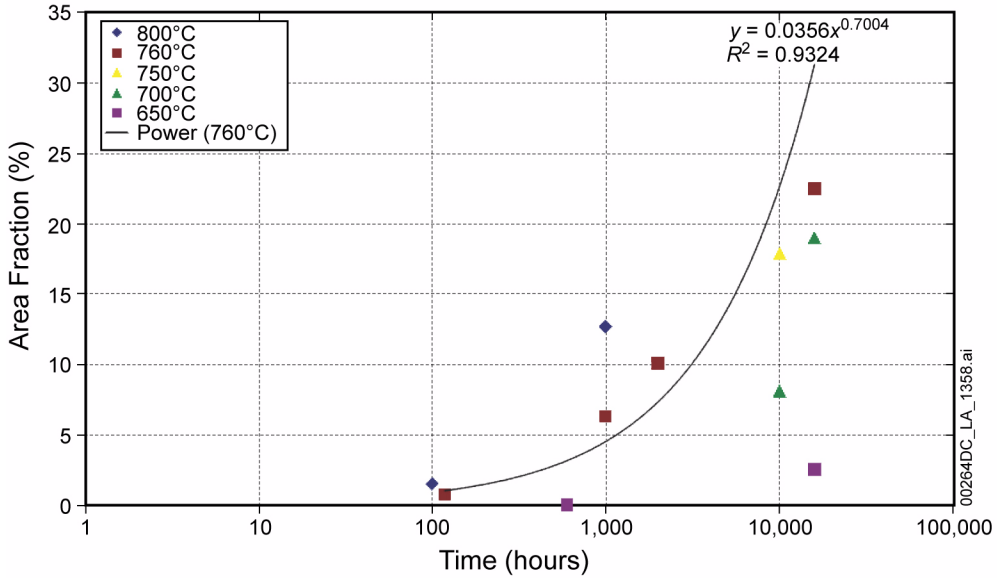

Figure 2.3.6-36. Precipitation of Tetrahedrally Close-Packed Phases in Alloy 22 Base Metal as a Function of Time and Temperature

Source: BSC 2004a, Figure 107.

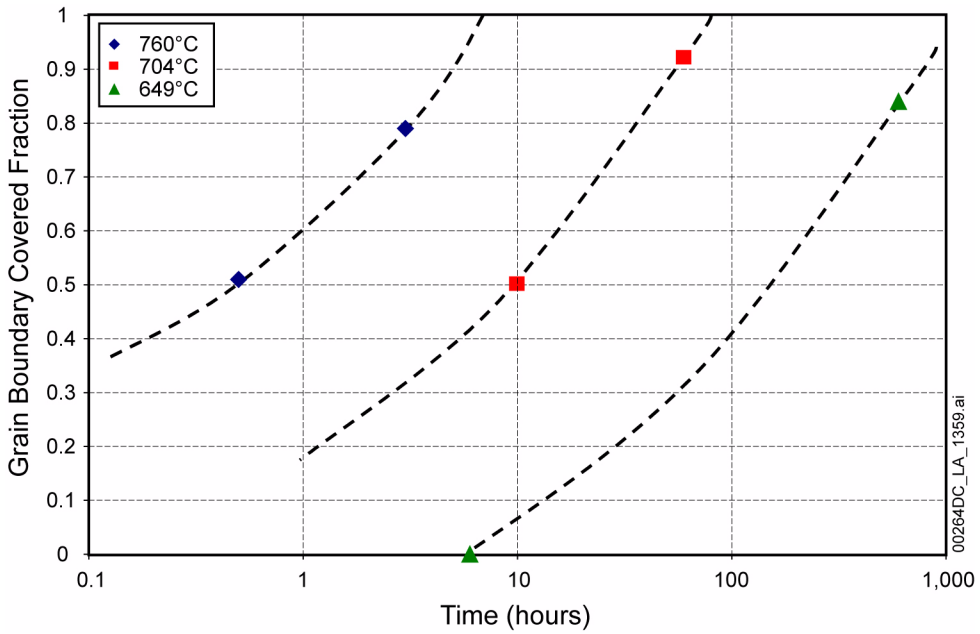

Figure 2.3.6-37. Precipitation of Tetrahedrally Close-Packed Phases at Alloy 22 Grain Boundaries as a Function of Time and Temperature

Source: BSC 2004a, Figure 91.

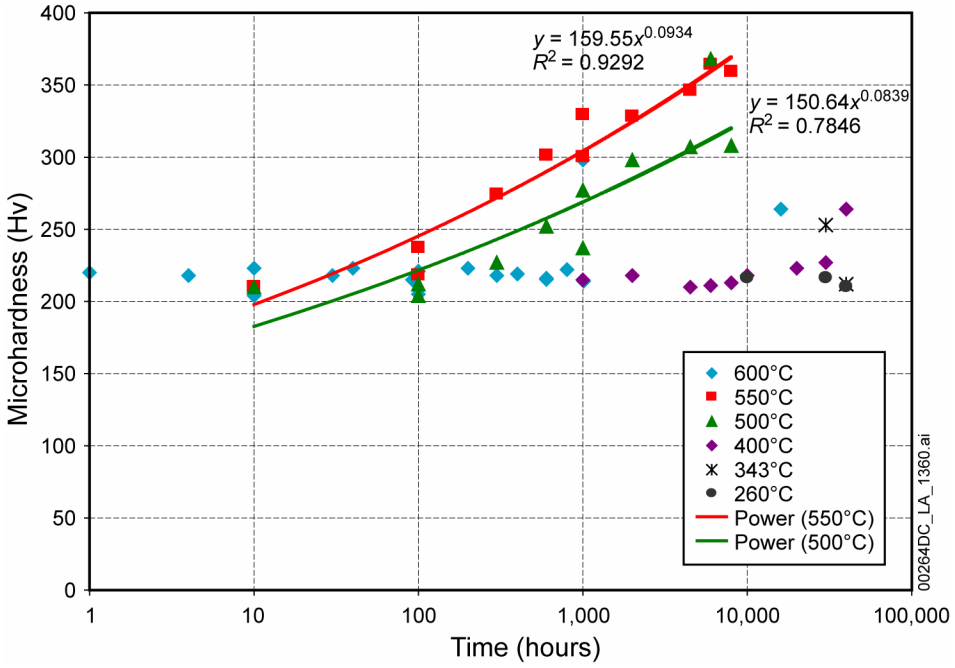

Figure 2.3.6-38. Microhardness Measurements on Aged Alloy 22 Base Metal Shown as a Function of Time and Temperature and Indicative of Long-Range Ordering

NOTE: Microhardness of "as-received" base metal is 217 Hv.

Source: BSC 2004a, Figure 110.

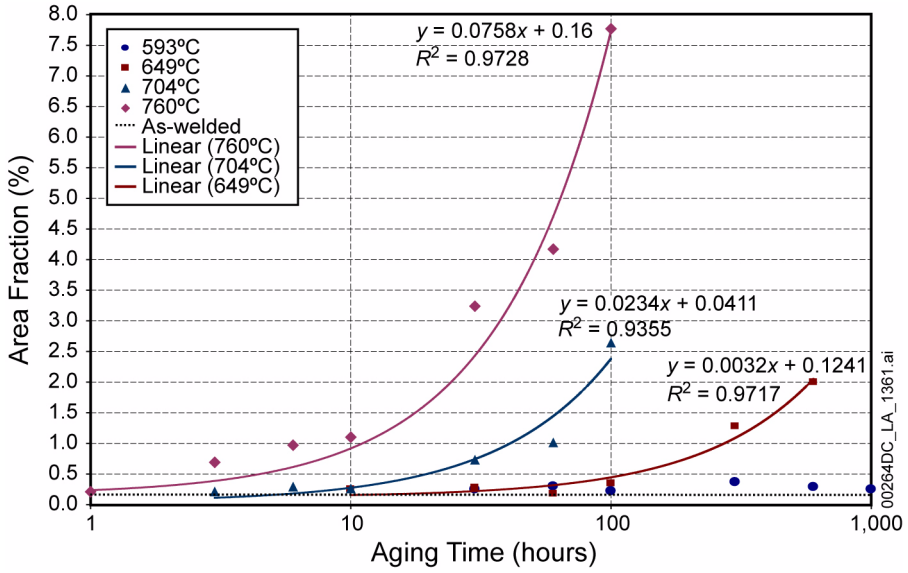

Figure 2.3.6-39. Tetrahedrally Close-Packed Phase Precipitation Kinetics for Alloy 22 Gas Tungsten Arc Weld as a Function of Time and Temperature

Source: BSC 2004a, Figure 93.

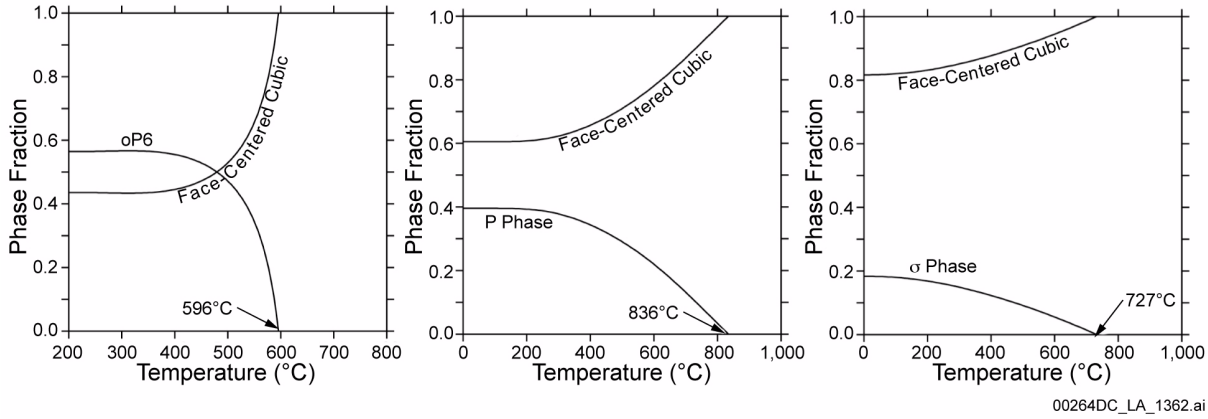

Figure 2.3.6-40. Property Diagram of Ni–21.1Cr–13.5Mo Alloy

NOTE: Ni–21.1Cr–13.5Mo (in wt %) alloy is a surrogate for Alloy 22. The face-centered cubic matrix and the oP6-ordered phase (left panel)—in this case, 7.5 wt % molybdenum—was considered instead of 13.5 wt % P phase (middle panel) and σ phase (right panel). All other phases are suspended during the calculations.

Source: BSC 2004a, Figure 87.

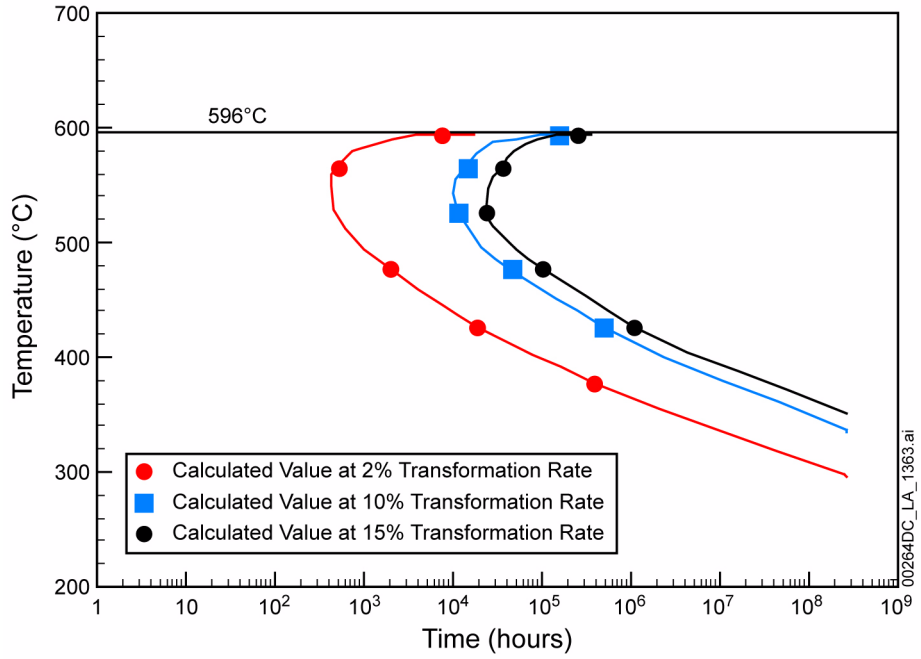

Figure 2.3.6-41. Calculated Isothermal Time-Temperature-Transformation for a Face-Centered Cubic Matrix of a Ternary Ni–21.1Cr–13.5Mo (in wt %) Alloy (Modeling Surrogate of Alloy 22) Transforming into the oP6-Ordered Phase for 2%, 10%, and 15% Transformation Rates

NOTE: At 596°C (Figure 2.3.6-40, left panel), the phase fraction of oP6-ordered phase drops to 0.

Source: BSC 2004a, Figure 88.

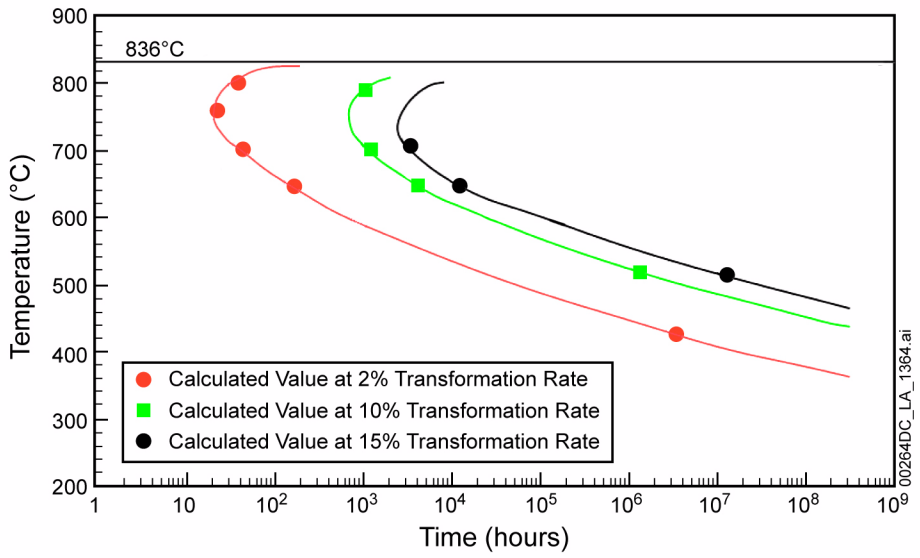

Figure 2.3.6-42. Calculated Isothermal Time-Temperature-Transformation for a Face-Centered Cubic Matrix of a Ternary Ni–21.1Cr–13.5Mo (in wt %) Alloy (Surrogate for Alloy 22) Transforming into the P Phase for 2%, 10%, and 15% Transformation Rates

NOTE: At 836°C (Figure 2.3.6-40, middle panel), the phase fraction of P phase drops to 0.

Source: BSC 2004a, Figure 89.

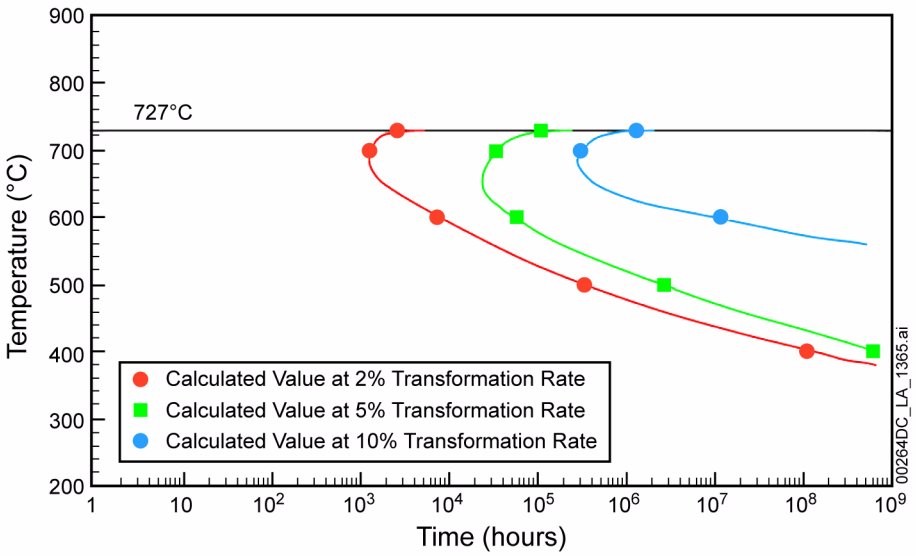

Figure 2.3.6-43. Calculated Isothermal Time-Temperature-Transformation for a Face-Centered Cubic Matrix of a Ternary Ni–21.1Cr–13.5Mo (in wt %) Alloy (Surrogate for Alloy 22) Transforming into the σ Phase for 2%, 5%, and 10% Transformation Rates

NOTE: At 727°C (Figure 2.3.6-40, right panel), the phase fraction of σ phase drops to 0.

Source: BSC 2004a, Figure 90.

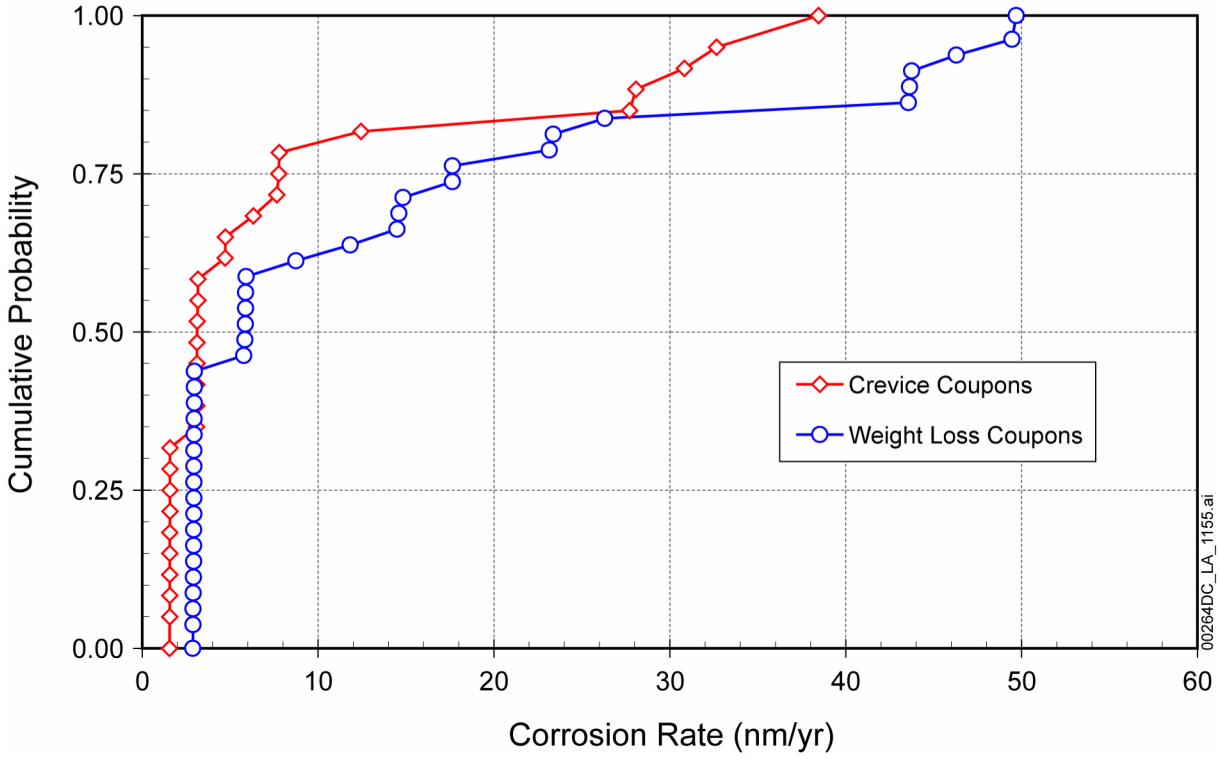

Figure 2.3.6-44. Cumulative Distribution Functions for Titanium Grade 7 Weight-Loss and Crevice Samples after 2.5-Year Exposure

NOTE: Zero and negative values are not shown.

Source: SNL 2007e, Figure 6-4[a].

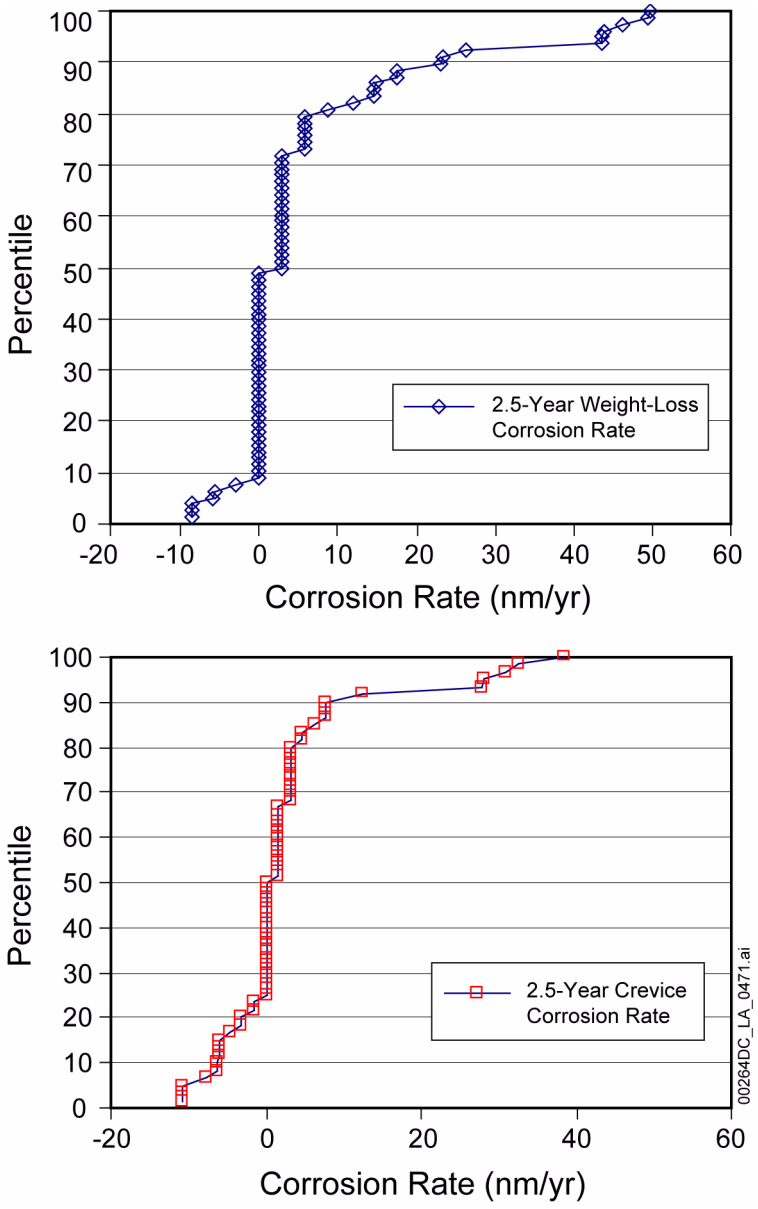

Figure 2.3.6-45. Corrosion Rate of Titanium Grade 7 (2.5-Year Data)

Source: SNL 2007e, Figure 26.

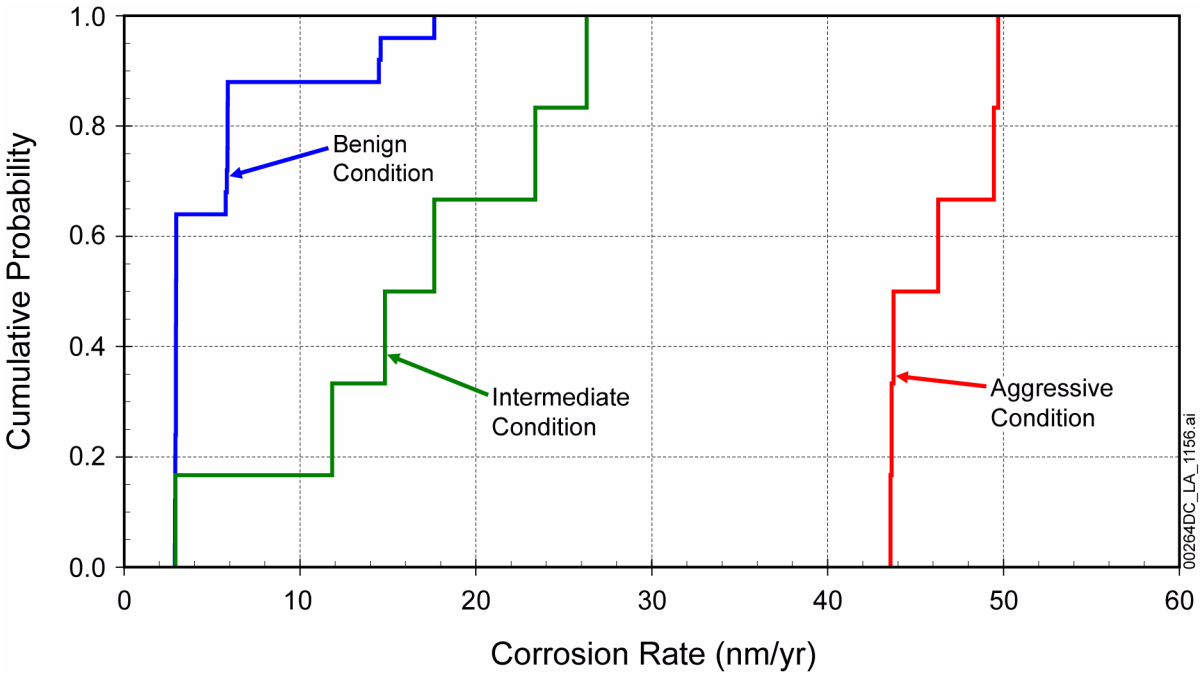

Figure 2.3.6-46. Cumulative Distribution Functions for General Corrosion Rates of Titanium Grade 7 Weight-Loss Samples for Different Exposure Conditions

Source: SNL 2007e, Figure 6-8[a].

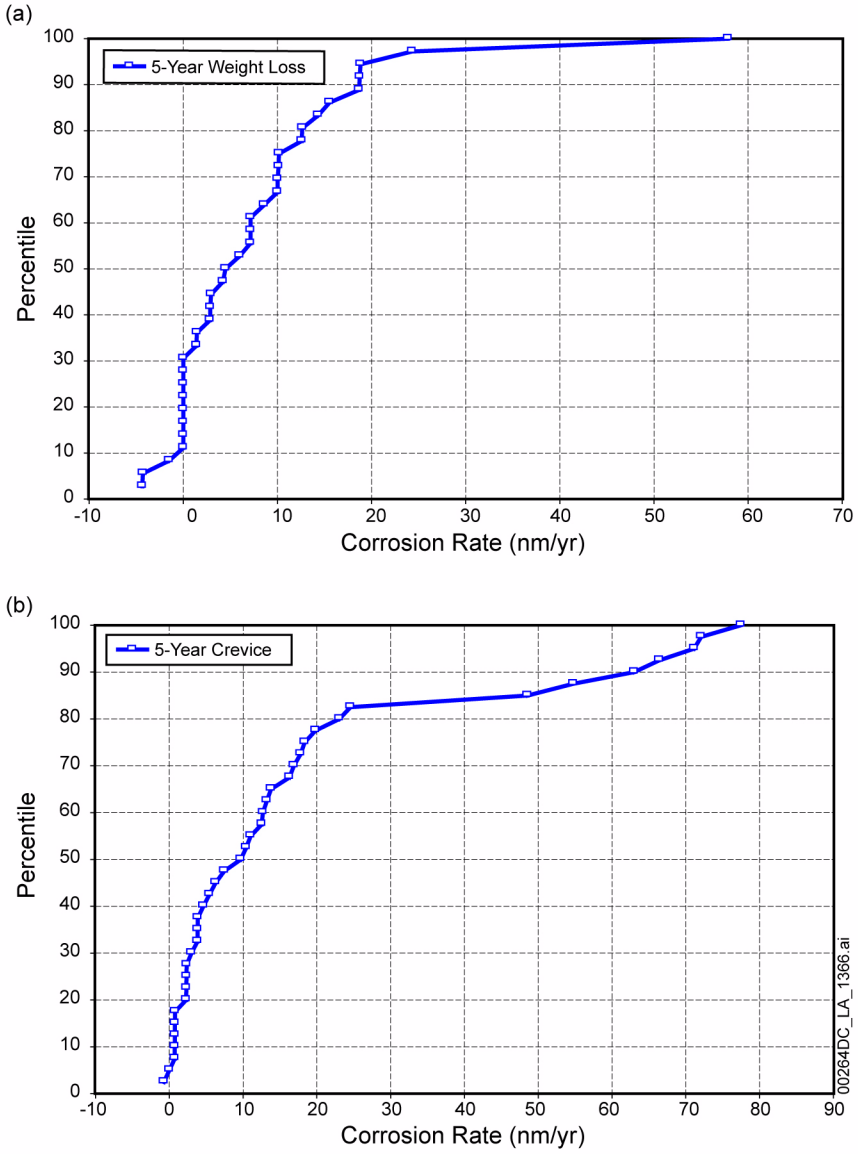

Figure 2.3.6-47. Distribution of General Corrosion Rates of Titanium Grade 16: (a) 5-Year Weight-Loss Samples and (b) 5-Year Crevice Samples

Source: SNL 2007e, Figures 22 and 23.

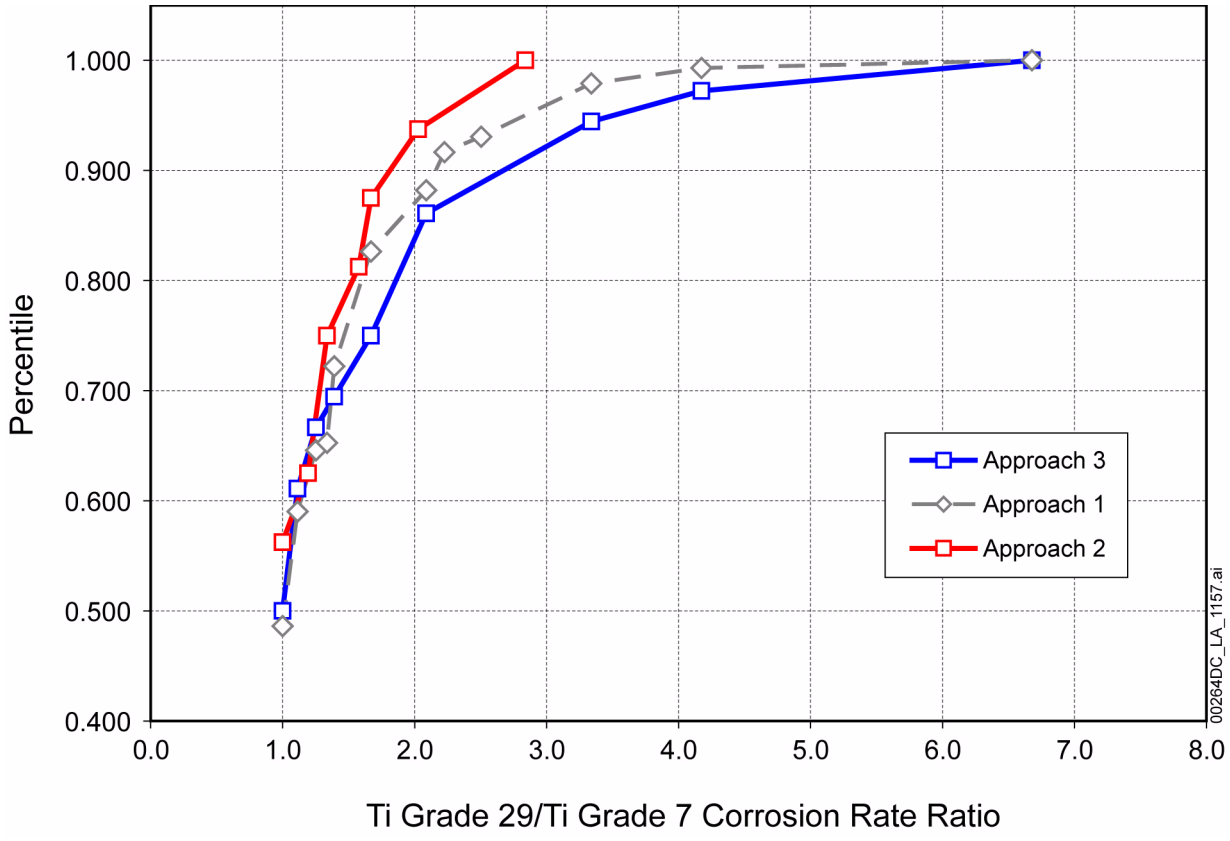

Figure 2.3.6-48. Titanium Grade 29/ Titanium Grade 7 Corrosion Rate Ratio

NOTE: Approach 3 is used for the ratio as it results in higher Titanium Grade 29 corrosion rates.

Source: SNL 2007e, Figure 6-20[a].

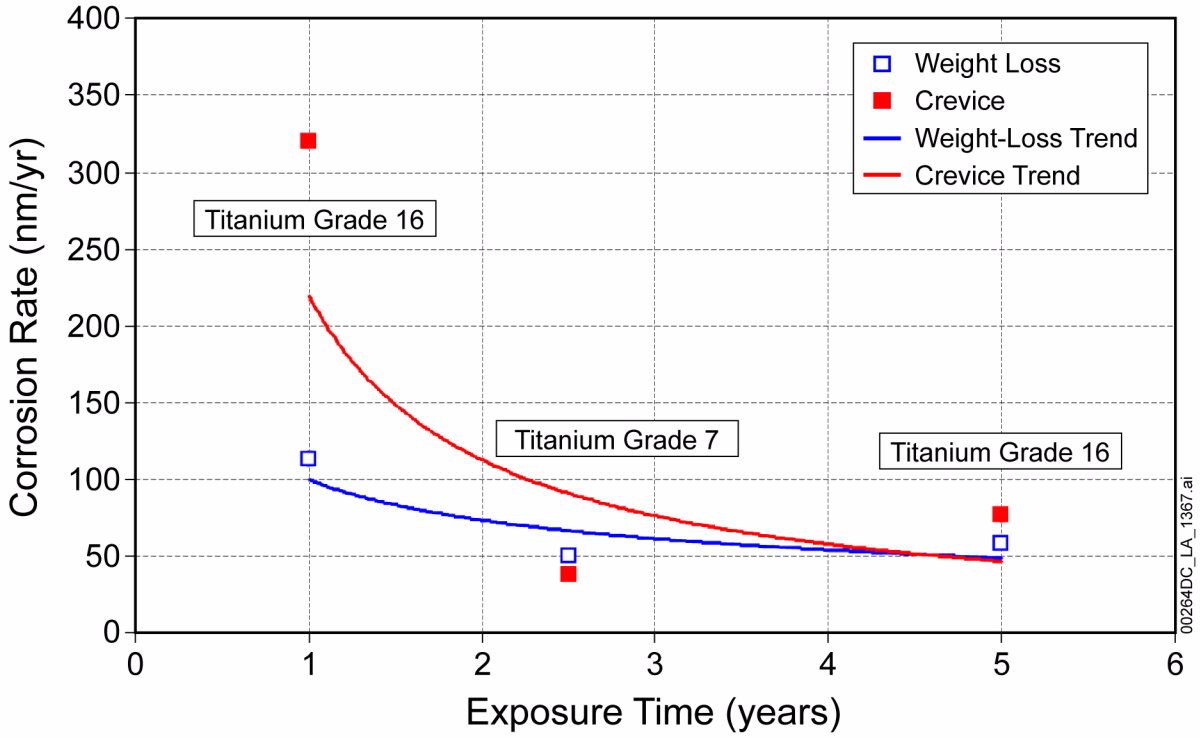

Figure 2.3.6-49. Comparison of 1-Year (Titanium Grade 16), 2.5-Year (Titanium Grade 7), and 5-Year (Titanium Grade 16) General Corrosion Rates Obtained from Weight-Loss Samples and Crevice Samples, Showing the Decreasing Trend in Corrosion Rate

Source: SNL 2007e, Figure 27.

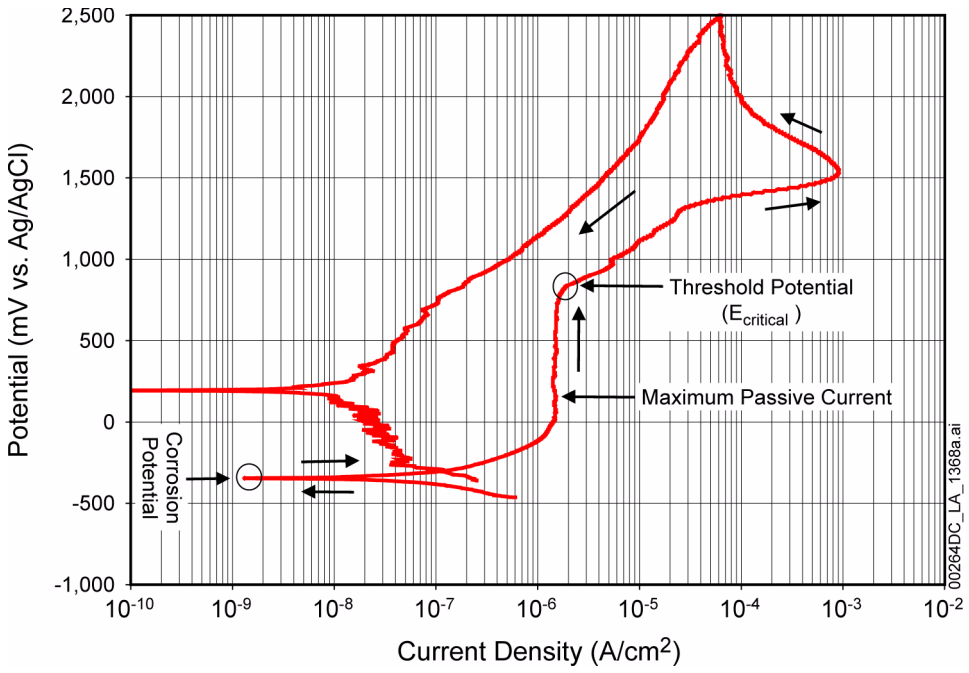

Figure 2.3.6-50. Titanium Grade 7 in Simulated Saturated Water at 120°C

NOTE: Negative hysteresis loop during reverse scan. No localized breakdown of passive film at reversal potential. No repassivation potential observed.

Source: SNL 2007e, Figure 14.

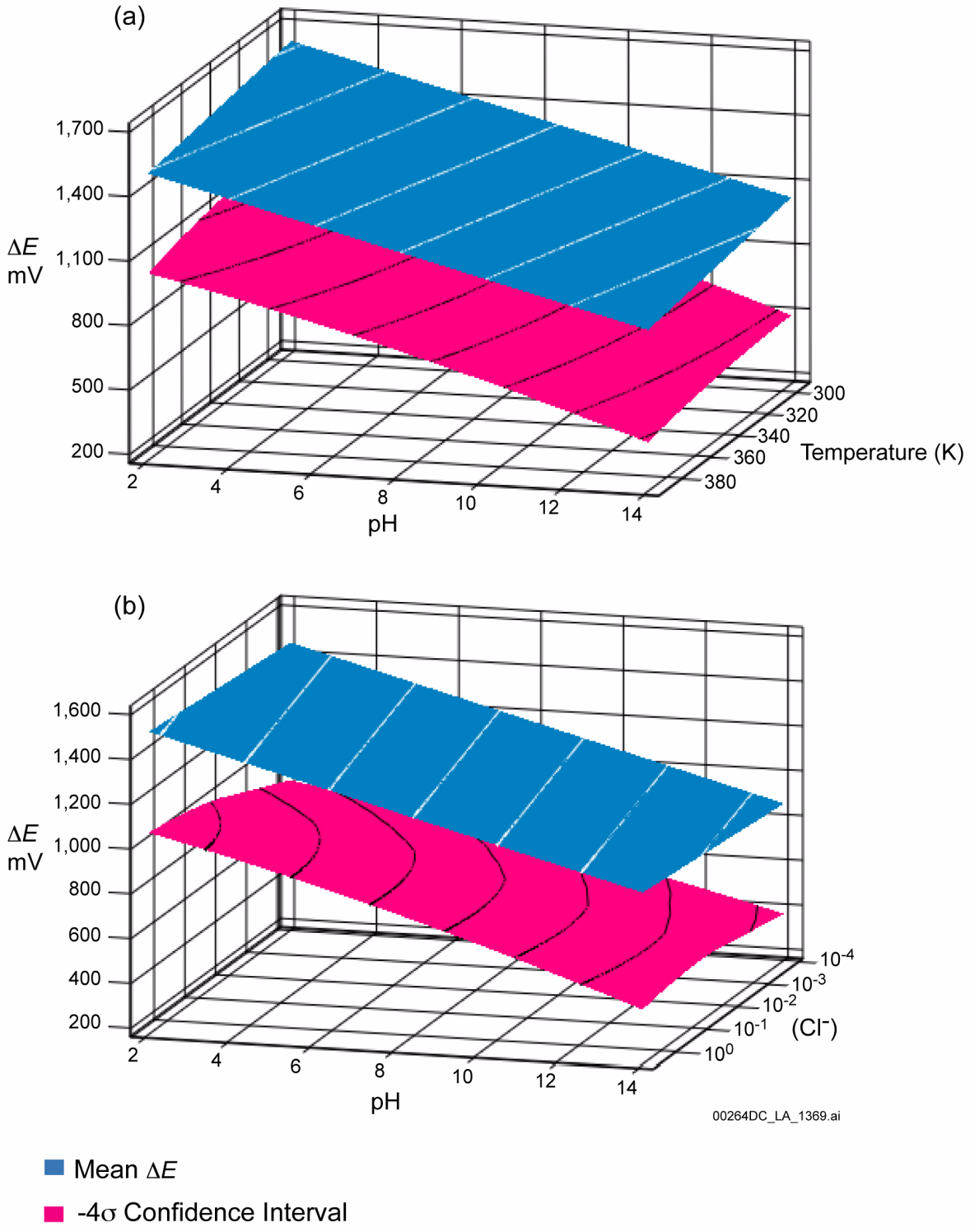

Figure 2.3.6-51. Plot of the Mean ΔE and -4σ Confidence Interval Surface (a) versus pH and Absolute Temperature at a Chloride Concentration of 3 mol/L and (b) versus pH and Logarithm of Chloride Ion Concentration for Titanium Grade 7 Using an Absolute Temperature of 400 K

Source: SNL 2007e, Figures 19 and 20.